MULTIPHASE REACTIVE TRANSPORT IN PLANETARY ICES

A Dissertation
Presented to
The Academic Faculty

By

Jacob Buffo

In Partial Fulfillment
Of the Requirements for the Degree
Doctor of Philosophy in Earth and Atmospheric Sciences

Georgia Institute of Technology

August, 2019

MULTIPHASE REACTIVE TRANSPORT IN PLANETARY ICES

Approved By:

Dr. Britney Schmidt
School of Earth and Atmospheric Sciences
Georgia Institute of Technology

Dr. Christian Huber
School of Earth, Environmental, and Planetary Sciences
Brown University

Dr. James Wray
School of Earth and Atmospheric Sciences
Georgia Institute of Technology

Dr. Chris Reinhard
School of Earth and Atmospheric Sciences
Georgia Institute of Technology

Dr. Alexander Robel
School of Earth and Atmospheric Sciences
Georgia Institute of Technology

Date Approved: July 7th, 2019

Water, water, every where,
Nor any drop to drink.

Samuel Taylor Coleridge
The Rime of the Ancient Mariner

TABLE OF CONTENTS

LIST OF TABLES

LIST OF FIGURES

LIST OF SYMBOLS

Symbol	Definition	Units	Value
α	1D Advection Coefficient	-	1.56×10^{-3}
$br^{\uparrow,\downarrow}$	Vertical Brine Transported	$m^3 s^{-1}$	Calculated
β	Density (Salinity) Coefficient	$kg\ ppt^{-1}$	5.836×10^{-4}
c	Heat Capacity	$J\ kg^{-1}\ K^{-1}$	Varies
c_{br}	Brine Heat Capacity	$J\ kg^{-1}\ K^{-1}$	3985
c_{ice}	Ice Heat Capacity	$J\ kg^{-1}\ K^{-1}$	2000
c_d	Drag Coefficient	-	2
c_0	Platelet Size Cutoff	m	0.1
dt	Time Discretization	s	50
dz	Spatial Discretization	m	0.01
D	Salt Diffusivity	$m^2\ s^{-1}$	Calculated
H	Enthalpy	$J\ kg^{-1}$	Calculated
H	Ice Shell Thickness	km	Varies
H_s	Enthalpy of Solid Cell	$J\ kg^{-1}$	Calculated
G	Acceleration Due to Gravity	$m\ s^{-2}$	9.8
H	Distance to Interface	m	Calculated
h	Mushy Layer Thickness	m	Varies
k	Heat Conductivity	$W\ m^{-1}\ K^{-1}$	Varies
k_{br}	Brine Heat Conductivity	$W\ m^{-1}\ K^{-1}$	0.6
k_{ice}	Ice Heat Conductivity	$W\ m^{-1}\ K^{-1}$	2
κ	Thermal Diffusivity	$m^2\ s^{-1}$	Varies
κ_{br}	Brine thermal diffusivity	$m^2\ s^{-1}$	Varies
κ_i	Ice Thermal diffusivity	$m^2\ s^{-1}$	Varies
L, L_f	Latent Heat of Fusion (Ice)	$J\ kg^{-1}$	334,774
λ	Coefficient Dependent on St	-	Calculated
λ_S	η_m for salt problem	-	Calculated
λ_T	η_m for thermal problem	-	Calculated
μ	Kinematic Viscosity	$m^2\ s^{-1}$	1.88×10^{-3}
η	Dimensionless length variable	-	Calculated
η_m	Dimensionless length at z^*_m	-	Calculated
ϕ	Liquid Fraction	-	Calculated
ϕ_c	Critical Porosity	-	0.7
P_s	Partition Coefficient	-	1/100
ρ	Density	$kg\ m^{-3}$	Calculated
ρ_{br}	Brine Density	$kg\ m^{-3}$	Varies
ρ_{ice}	Ice Density	$kg\ m^{-3}$	917
ρ_{sw}	Ocean/Reservoir Density	$kg\ m^{-3}$	Varies
Π	Permeability	m^2	Calculated
R	Radius	m	Varies
Ra	Rayleigh Number	-	Calculated
Ra_c	Critical Rayleigh Number	-	1.01
S	Salinity	ppt	Calculated

S_{lim}	Minimum Salinity	ppt	Varies
S_{oc}	Ocean/Reservoir Salinity	ppt	Varies
S_{tot}	Bulk Salinity/Total Salt	ppt	Calculated
S_{int}	Salinity at ice-mush interface	ppt	Calculated
St	Stefan Number	-	Calculated
T	Temperature	K	Calculated
T_0	Supercooled Temperature	K	Varies
T_1	Liquid Temperature	K	Varies
T_{oc}	Ocean Temperature	K	Varies
T_s	Surface Temperature	K	Varies
T_m	Melting Temperature	K	Calculated
t	Time	s	-
t^{adv}	Advection Timescale	s	Calculated
t^{diff}	Diffusion Timescale	s	Calculated
θ	Dimensionless salinity variable	-	Calculated
v	Platelet Velocity	m s^{-1}	Calculated
v_m	Freezing Front Velocity	m s^{-1}	Calculated
v_m	Mush-ocean interface velocity	m s^{-1}	Calculated
v^*_m	Ice-mush interface velocity	m s^{-1}	Calculated
w	Brine Velocity	m s^{-1}	Calculated
x_m	Freezing Front Position	m	Calculated
z	Vertical Coordinate	m	-
z_m	Mush-ocean interface position	m	Calculated
z^*_m	Ice-mush interface position	m	Calculated

SUMMARY

As an ice-ocean world itself, Earth provides a number of analog environments that can be used to better understand the dynamics of ice-ocean processes occurring on bodies like Europa [*Eicken*, 2002; *Gleeson et al.*, 2012; *Marion et al.*, 2003]. Natural and laboratory grown sea ice provides an accessible sample of ocean-derived ice, where the effects of the local thermochemical environment on ice formation rate, microstructure, and biogeochemistry can be studied in detail [*Wettlaufer*, 2010]. The remote environment of sub-ice shelf cavities provides an additional analog to the subsurface ocean of Europa. Devoid of sunlight, trapped beneath kilometers of overlying ice, and with limited contact to the open ocean these regions can aid in our understanding of the circulatory, biogeochemical, thermodynamic, and accretion/ablation processes that may occur beneath Europa's ice shell [*Lawrence et al.*, 2016]. Together, these possibilities motivate Chapter 2, which focuses on building a comprehensive model of the combined influence of temperature gradients, salinity, and ice nucleation within the water column on the properties of terrestrial ices.

Quantifying how environmental factors impact the dynamics and properties of terrestrial ices can then be extended to improve estimates of the characteristics and behavior of planetary ices subject to diverse thermochemical regimes [*Buffo et al.*, *in review; Buffo et al.*, 2019]. This ability to predict physicochemical properties of planetary ices informs numerical simulations of ice-ocean world geophysics, chemical cycling, and habitability and provides context for the synthesis and interpretation of spacecraft data. Our foundational and relatively extensive understanding of the terrestrial cryosphere provides

immense leverage when attempting to decipher the complex innerworkings of much less fully understood ice-ocean worlds and provides a benchmark for validating numerical models. In Chapter 3, the foundation provided by work in Chapter 2 is extended to accommodate the composition and dynamics of Europa's ice-ocean environment. The impacts of ocean composition and thermal regime on the state of the ice shell are explored. Fundamentally, this connects ocean properties to observable surface features via accretion and evolution of the ice shell that become accessible to future missions.

The physics of multiphase materials are applicable across a wide range of Earth and planetary problems; however the dynamics of reactive transport depend on the environmental and material properties of the system. The physical, thermal, and chemical properties of ice-ocean/brine systems in the solar system remain relatively unconstrained but likely span a substantial trade space. Moreover, the extent to which ice-ocean world environments can be assumed to be well described by known mushy layer physics has not been investigated as this area of study represents a relatively new element of planetary science. To that end, Chapter 4 explores the limits of the physics contained within this work, and comments on areas where new work and additional physics may be needed to realize a fully comprehensive systems understanding of Europa's and other worlds' ice shell(s).

There are certainly limitations to the applicability of Earth as an analog to other ice-ocean worlds and these must be identified and accounted for to ensure an appropriate use of the transitive strategies comparative planetology offers. For example, the chemistries of oceans and ices throughout the solar system may be quite diverse [*Kargel et al.*, 2000; *Neveu et al.*, 2017; *Zolotov*, 2007; *Zolotov and Shock*, 2001]. The addition of exotic salts

or ammonia to an ice-ocean system may alter its solidification dynamics and resultant ice properties [*Fortes*, 2000; *Hammond et al.*, 2018]. While laboratory experiments have begun to investigate the effects of these additives on ice properties [*Lorenz and Shandera*, 2001; *McCarthy et al.*, 2007], determining their impact on processes occurring at geophysical scales relies on theoretical predictions as no terrestrial analogue exits. The age and scale of many planetary ices also exceeds that of the oldest and thickest ice on Earth [*Fretwell et al.*, 2013]. Thus, while Earth provides an excellent, well-studied endmember for the dynamics and properties of planetary ices there may be as yet unseen deviations in the physical behavior and characteristics of ice-ocean systems under thermochemical pressures found only on other bodies in the solar system. In the concluding Chapter 5, I highlight accomplishments that have allowed this work to make significant steps towards best reconciling Earth and planetary ices, and comment on future directions and ongoing work that will enable me to continue to make progress. In particular, I discuss the future of incorporating biological elements into these models and benchmarking this relatively new work through laboratory and field programs. This multidisciplinary approach provides the greatest foundation by which the work described here can make a future impact on how we measure and understand ice-ocean worlds.

Chapter 1: Introduction

In recent decades the ubiquity of oceans and other water reservoirs within our solar system has become increasingly apparent [*Nimmo and Pappalardo*, 2016]. As a prerequisite for life as we know it [*Chaplin*, 2006; *Chaplin*, 2001; *Tait and Franks*, 1971], understanding the distribution, chemistry, thermal state, and longevity of these water masses is crucial in determining the evolution and habitability of such environments [*Priscu and Hand*, 2012]. While water is common to many bodies in the solar system, it typically resides beneath a thick icy shell or regolith [*Khurana et al.*, 1998; *Nimmo and Pappalardo*, 2016; *Porco et al.*, 2006; *Reynolds et al.*, 1983]. These icy strata act as both a barrier and conveyor of mass and energy between the surface and underlying water reservoir, ultimately dictating the thermochemical evolution, habitability and surface expression of the subsurface hydrosphere [*Buffo et al.*, *in review; Vance et al.*, 2016; *Vance et al.*, 2007]. The upper ice-atmosphere interface of planetary bodies is well documented in the literature [*Brown et al.*, 2006; *Fanale et al.*, 1999] and is primarily governed by depositional and radiolysis processes [*Consolmagno and Lewis*, 1978; *Jaumann et al.*, 2009]. Conversely, beyond Earth, the basal interfaces of planetary ice-ocean/brine systems remain largely unconstrained [*Prockter*, 2017]. These interfaces, characterized by multiphase regimes known as 'mushy layers', are composed of a solid ice matrix bathed in mobile interstitial brine and govern the formation and evolution of the overlying ice [*Buffo et al.*, 2018; *Buffo et al.*, *in review; Feltham et al.*, 2006; *Hunke et al.*, 2011]. Quantifying ice-ocean interactions and transport processes is crucial in constraining the role interior and ocean dynamics play in the evolution of ocean-derived ices, the entrainment and transport of endogenic material within the ice [*Buffo et al.*, *in review; Vance et al.*, 2016; *Vance et*

al., 2007], and our understanding of ice-ocean world geophysical processes [*Barr and McKinnon*, 2007; *Johnson et al.*, 2017b]. While there are currently no direct measurements of these elusive interfaces for other bodies within the solar system, Earth provides an excellent analog in sea ice [*Feltham et al.*, 2006; *Hunke et al.*, 2011] and is itself and ice-ocean world. Comparative planetology offers an opportunity to benchmark and validate both the theory and numerical simulation of these dynamic interfaces [*Buffo et al.*, 2018; *Buffo et al.*, *in review*]. Utilizing the foundational knowledge of reactive transport theory [*Berner*, 1980; *Feltham et al.*, 2006; *Steefel et al.*, 2005] and its historical success in simulating sea ice [*Griewank and Notz*, 2013; *Hunke et al.*, 2011; *Notz and Worster*, 2009; *Turner and Hunke*, 2015], one-dimensional finite difference models have been constructed which extend the representation of ice shelf adjacent sea ice and identify how spatiotemporal variations in ocean properties can be recorded in the physicochemical profiles of first year sea ice [*Buffo et al.*, 2018]. These models were extended to include the environmental properties of the Galilean satellite Europa and were implemented to produce physically realistic estimates of Europa's ice shell composition [*Buffo et al.*, *in review*]. Constitutive relationships between ocean chemistry, local thermal gradient at the ice-ocean interface, and resulting bulk ice composition have been identified and implemented to show their ability in predicting the thermochemical evolution of hydrological features within Europa's ice shell. These results highlight the crucial role multiphase physics play in governing the dynamics and evolution of ice-ocean/brine systems as they account for ocean derived impurity entrainment within the overlying ice, which dictates the thermodynamic, mechanical, and dielectric properties of the ice and provides a mechanism for both ocean-surface interactions conducive to sustaining a

habitable subsurface hydrosphere and endogenic surface expression. The numerical models constructed herein and their application to Earth and Europa are but two examples of the utility of multiphase reactive transport in describing ice-ocean systems and have been designed to provide an accessible foundation that can be extended to other ice-ocean/brine systems, modified to include additional physics, and tailored to answer specific questions.

1.1 Ice-Ocean Environments in the Solar System

While the Earth-Luna system is the only planet-satellite group that definitively resides within our sun's current habitable zone (regions of planetary systems where liquid water is stable on the surface), a number of solar system bodies are believed to have hosted hydrospheres in the past and others likely maintain contemporary subsurface liquid water reservoirs. Below, important potential environments where ice-ocean/brine dynamics are known or thought to impact system level evolution are summarized and their implications for habitability discussed.

1.1.1 Earth

By far the most accessible and well-studied ice-ocean world in our solar system is our own, Earth. With an active hydrological cycle that supports two dynamic and diverse polar regions, terrestrial ice-ocean environments play a crucial role in the climatic, oceanic, atmospheric, and biogeochemical components of the Earth system [*Aagaard and Carmack*, 1989; *Ebert and Curry*, 1993; *Holland and Bitz*, 2003; *Loose et al.*, 2011; *Pritchard et al.*, 2008]. Furthermore, they provide a natural laboratory to investigate the small-scale interfacial dynamics of these systems and determine the role these processes play in the

macroscale properties of our cryosphere [*Hunke et al.*, 2011; *Notz*, 2012; *Turner and Hunke*, 2015], which can then be extended to the ice-ocean environments of other bodies [*Buffo et al.*, *in review; Hammond et al.*, 2018; *Lipps and Rieboldt*, 2005].

1.1.1.1 Sea Ice

Likely the most ubiquitous and dynamic component of the cryosphere, sea ice forms directly from the ocean due to heat loss to the overlying atmosphere. Covering between fourteen and twenty-three million square kilometers of the planet at any given moment [*Cavalieri et al.*, 1997; *Weeks*, 2010] it forms a barrier between the ocean and atmosphere that governs energy and mass transport between the two reservoirs [*Bitz and Lipscomb*, 1999; *Loose et al.*, 2011]. In both the Arctic and Antarctic, it plays an imperative role in the local ecosystem and is harbinger of a changing climate due to its sensitivity to both oceanic and atmospheric forcing [*Bintanja et al.*, 2013; *Johannessen et al.*, 2004; *Shimada et al.*, 2006]. The *in situ*, top-down formation of sea ice from the ocean (as opposed to the depositional processes that create meteoric ice masses) makes it an ideal analog for other ice-ocean worlds whose icy shells and regolith likely originated from, and continue to interact with, an underlying parent liquid reservoir [*Barr and McKinnon*, 2007; *Hammond et al.*, 2018; *Prockter*, 2017; *Schubert et al.*, 2004; *Sotin and Tobie*, 2004]. The resulting ice preserves a record of its origin water mass and formation history, all the while acting as the transport medium between the surface and underlying ocean [*Allu Peddinti and McNamara*, 2015; *Barr and McKinnon*, 2007; *Kargel et al.*, 2000].

1.1.1.1.1 Climate

Sea ice coverage plays a crucial role in Earth's climate. As a high albedo material, it drastically affects the heat budget of the polar oceans by reflecting incoming solar radiation that would otherwise be absorbed by relatively low albedo seawater [*Curry et al.*, 1995]. Arctic sea ice maximum extents are currently decreasing at an unprecedented rate [*Cavalieri et al.*, 1997; *Stroeve et al.*, 2007; *Weeks*, 2010], raising concern for a potential runaway scenario of the positive ice-albedo feedback process [*Curry et al.*, 1995; *Winton*, 2008]. Conversely, sea ice maximum extents in the Southern Ocean have been gradually increasing [*Cavalieri and Parkinson*, 2008; *Cavalieri et al.*, 1997], however it has been suggested that this is a direct consequence of accelerated basal melting of adjacent meteoric ice shelves [*Bintanja et al.*, 2013; *Hellmer*, 2004], thinning and potentially increasing the susceptibility of these ice masses to retreat and/or collapse [*Paolo et al.*, 2015; *Rignot and Steffen*, 2008]. Additionally, the volume of multiyear fast ice around Antarctica's coastlines is decreasing [*Cavalieri et al.*, 2003], which could impact its ability to buttress the flow and breakup of ice shelves, and lead to the acceleration of mass loss from the continent [*Massom et al.*, 2018; *Miles et al.*, 2017].

As the barrier between the ocean and the atmosphere sea ice dictates the transport of gasses between these two reservoirs [*Loose et al.*, 2009; *Loose et al.*, 2011; *Rysgaard et al.*, 2007]. In a dynamic and changing climate understanding how and where greenhouse gases are stored in and transported to and from the ocean is imperative to determining the impacts of an evolving ocean-atmosphere system. Sea ice could provide a substantial sink for atmospheric carbon dioxide and methane and may act as a barrier preventing the acidification of the polar oceans [*Parmentier et al.*, 2013; *Rysgaard et al.*, 2007]. Understanding, quantifying, and predicting the numerous roles sea ice plays in governing

both polar and global climate systems depends on its accurate representation in Earth systems models [*Notz*, 2012]. As a deceivingly complex medium, this task is complicated by the multiphase and heterogeneous nature of sea ice [*Feltham et al.*, 2006; *Hunke et al.*, 2011; *Turner and Hunke*, 2015], however large-scale models have begun to successfully incorporate the nonlinear dynamics that govern its thermochemical and structural evolution and the associated interactions with both the ocean and atmosphere [*Hunke et al.*, 2011; *Notz*, 2012; *Turner and Hunke*, 2015].

1.1.1.1.2 Ocean

Sea ice formation and evolution is important for the generation and persistence of both polar and global ocean water masses [*Aagaard and Carmack*, 1989; *Grumbine*, 1991], which play a key role in the thermohaline circulation of the world's oceans [*Jacobs et al.*, 1979; *Orsi et al.*, 1999]. In the polar regions, when sea ice forms it rejects cold hypersaline brine into the upper ocean as salts are preferentially rejected from the growing crystalline ice lattice [*Lake and Lewis*, 1970]. This rejected brine mixes with the upper ocean forming a negatively buoyant water mass that leads to the formation of North Atlantic Deep Water (NADW) in the northern hemisphere [*Dickson and Brown*, 1994] and Antarctic Bottom Water (AABW) in the southern hemisphere [*Orsi et al.*, 1999]. These water masses drive circulation and act as conveyors of nutrients, oxygen, and carbon dioxide throughout the global oceans [*Goosse and Fichefet*, 1999; *Sarmiento et al.*, 2004]. In Antarctica, sea ice formation in wind driven coastal polynyas leads to the formation of High Salinity Shelf Water (HSSW) [*Zwally et al.*, 1985], a highly saline water mass that sinks and flows into ice shelf cavities leading to basal melting near the grounding line and the production of

fresh, buoyant Ice Shelf Water (ISW) plumes, which ascend oceanward along the underside of the ice shelf. This 'ice pump' mechanism [*Lewis and Perkin*, 1983] is responsible for the ablation of meteoric ice and the deposition of marine ice observed beneath Antarctic ice shelves [*Craven et al.*, 2009; *Fricker et al.*, 2001; *Galton-Fenzi et al.*, 2012]. This mass redistribution process has been suggested as a potential feedback mechanism by which thinning and fractured ice shelves could suture and arrest basal crevasses, preventing further destabilization [*Holland et al.*, 2009; *Khazendar et al.*, 2009; *McGRATH et al.*, 2012]. Additionally, ISW plumes that reach the ice shelf front modify the adjacent sea ice-ocean interface through the deposition of platelet ice, long, bladed ice crystals formed within the water column of the ascending plume due to adiabatic depressurization as the plume rises [*Robinson et al.*, 2014; *Smedsrud and Jenkins*, 2004]. This accretionary process affects the thickness and structural characteristics of the ice column, can affect large areas of sea ice and may explain the dichotomic behavior between the trends of Arctic and Antarctic sea ice extent [*Dempsey et al.*, 2010; *Langhorne et al.*, 2015]. Constraining the interactions between the cryosphere and ocean water masses is imperative to understanding and predicting the evolution of both and contemporary investigations have highlighted the delicate balance of this interdependent system [*Aagaard and Carmack*, 1989; *Bintanja et al.*, 2013].

1.1.1.1.3 Biogeochemistry

In the polar oceans the basal surface and internal microstructure of sea ice provides a substrate and refuge for ice algae and other microorganisms that serve as primary producers for polar food webs [*Loose et al.*, 2011; *Tedesco and Vichi*, 2014; *Vancoppenolle*

et al., 2013]. The biological component of sea ice plays a key role in governing the ocean-atmosphere fluxes of biogenic gases (O_2, CO_2, dimethyl sulfide), as their production, consumption, and transport through the permeable ice layer is affected by local ecology and biomass [*Loose et al.*, 2009; *Loose et al.*, 2011]. These resident organisms thrive by economizing the thermochemical gradients and porous medium provided by the formation of sea ice, frequently dwelling in the brine filled channels and pore spaces that characterize the lower skeletal layer of the ice cover [*Ackley and Sullivan*, 1994; *Eicken et al.*, 1998; *Thomas and Dieckmann*, 2008]. In addition to the more passive psychrophiles inhabiting these regions some organisms actively alter the ice structure to maintain local regions of liquid water [*Krembs et al.*, 2011]. Biogeochemical cycling and processes within sea ice play a key role in constraining carbon and gas cycling in the polar regions, influencing the microstructural and transport properties of the ice layer, and support an active algal community that provides the basis for under ice ecosystems. The field of sea ice biogeochemistry is relatively young and while the extent of this ecosystem and its role in sourcing some of the most nutrient rich waters on Earth make its importance to our planet undeniable our knowledge of these systems is still limited and it has only begun to be incorporated into models of sea ice [*Tedesco and Vichi*, 2014; *Vancoppenolle et al.*, 2013; *Vancoppenolle and Tedesco*, 2015]. Constraining the interdependence of ice biogeochemistry, the oceans, atmosphere, and climate are crucial to our understanding of this unique ecosystem and the role it plays in a changing Earth system. Additionally, our understanding of this psychrophilic/halophilic community has direct astrobiological implications, as understanding how microorganisms thrive in and modify the sea ice-ocean

interface is directly applicable to other ice-ocean/brine environments within the solar system [*Thomas and Dieckmann*, 2003; *Wettlaufer*, 2010].

1.1.1.1.4 Measurement

Measurements of sea ice thickness, characteristics, and extent date back to the late 1800's [*Mawson*, 1914; *Nansen*, 1897] and while vertical profiles of ice microstructure and thermochemical properties can be found as far back as 1927 [*Malmgren and Institutt*, 1927] prior to the 1960s historical sea ice data remains relatively sparse due to the remote and harsh nature of the polar regions, making *in situ* measurements a less than straightforward task. By the late 1970s improvements in polar exploration and transport coupled with the introduction of satellite measurements had drastically enriched the spatiotemporal observation of sea ice, providing us with a nearly continuous record of sea ice extent and an ever-expanding knowledge of sea ice thermodynamics and physicochemical properties [*Cavalieri et al.*, 2003; *Weeks and Ackley*, 1986]. By far the most common technique for sea ice observation is coring, wherein vertical sections of ice are extracted and can be partitioned to investigate the thermal, chemical, and structural properties of the ice pack [*Perovich et al.*, 2009; *Petrich and Eicken*, 2010; *Weeks and Ackley*, 1986]. Thermal measurements are typically carried out in the field while chemical and structural measurements can be completed in the field or in a laboratory after the cores have been frozen and shipped off site [*Eicken*, 1992; *Nakawo and Sinha*, 1981; *Schwerdtfecer*, 1963]. Chemical analysis is typically carried out by melting or crushing the ice and analyzing the resulting brine or gas to acquire bulk composition of the ice. Frequently polarized light microscopy is used to elucidate the crystallography and structural properties of various ice

fabrics [*Dempsey et al.*, 2010; *Gow et al.*, 1982; *Sinha*, 1977]. A number of experiments have investigated the growth and resulting properties of laboratory grown sea ice [*Cottier et al.*, 1999; *Eicken et al.*, 1998; *Golden et al.*, 2007; *Notz and Worster*, 2009]. While the scale of these experiments prevents a perfect analog to naturally grown sea ice, these controlled environments offer an exceptional setting to investigate the effect of thermochemical stressors on the evolution of ice dynamics and microstructure. Computed tomography imaging has revealed the complex multiphase evolution of brine pockets and channels occurring in the interior of these ices during thermal cycling [*Golden et al.*, 2007]. Quantifying the effects these heterogeneities have on the physical, thermodynamic, and dielectric properties of sea ice has important implications for predictive models. Sea ice dynamics occur on a wide range of scales, ranging from the microscopic to global, and understanding the evolution and interaction of these processes is key to constraining, and accurately simulating, the role of sea ice in the Earth system [*Notz*, 2012; *Turner and Hunke*, 2015].

1.1.1.2 Marine Ice

Beneath Antarctica's ice shelves there exists a unique type of ocean-derived ice. Marine ice accretion is a byproduct of the 'ice pump' mechanism wherein frazil ice crystals, formed in ascending ISW plumes due to adiabatic depressurization, buoyantly rise out of suspension and are deposited onto the underside of the shelf [*Lewis and Perkin*, 1983]. These crystals form a porous slurry of ice and interstitial seawater that evolves via compaction processes and thermodynamic heat loss to the overlying ice shelf [*Craven et al.*, 2009; *Holland et al.*, 2009]. These evolution processes occur at a much slower rate than

those of sea ice and the basal layer of marine ice that remains hydraulically connected to the underlying ocean can reach thicknesses up to ~70 m [*Craven et al.*, 2004; *Craven et al.*, 2009; *Craven et al.*, 2005]. This gradual formation leads to almost complete desalination of the ice and marine ice is typically clear, bubble free, and has bulk salinities < 1 ppt [*Wolfenbarger et al.*, 2018]. This exotic form of ocean-derived ice offers insight into unique accretion processes and provides constraints on the properties of ices that form under low thermal gradient conditions, likely akin to those experienced by the ice-ocean interfaces of icy moons today and throughout much of their formation history [*Moore*, 2000]. This additional ice type allows the investigation of how thermochemical properties of the environment effect the formation and evolution of the ice that forms, providing comparison and contrast with sea ice and strengthening our predictive capabilities when simulating the dynamics and evolution of ice-ocean systems on other worlds [*Buffo et al.*, *in review*].

Additionally, the dynamics and properties of marine ice accretion and ablation have important impacts on the stability of ice shelves and have critical interdependencies on the formation and circulation of multiple water masses in the Southern Ocean. It has been suggested that marine ice can infill and anneal basal fractures, curtailing their propagation and improving ice shelf stability [*Khazendar et al.*, 2009; *McGRATH et al.*, 2012]. The accretion of marine ice depends on the production of buoyant ISW plumes by melting near the grounding line induced by HSSW, a product of sea ice formation, and in turn contributes to the formation of AABW [*Grumbine*, 1991; *Robinson et al.*, 2014; *Smedsrud and Jenkins*, 2004]. Understanding these complex interactions between the cryosphere and

the oceans is imperative in understanding the future of both systems in a dramatically changing climate.

1.1.2 Mars

Mounting evidence suggests an active primordial water cycle existed on Mars, supporting a large ocean basin in the northern hemisphere and episodic glaciations [*Baker et al.*, 1991]. Fluvial features [*Carr*, 1987], spectral data [*Poulet et al.*, 2005; *Villanueva et al.*, 2015], and *in situ* rover observations (e.g. hematite spherules) [*Squyres et al.*, 2004] all support the persistence of a substantial surficial hydrosphere on ancient Mars. While Mars' current climate does not promote the stability of pure liquid water on the planet's surface, transient features near the equator suggest the presence of contemporary near-surface brine flow, likely in the form of concentrated perchlorate solutions [*Ojha et al.*, 2015]. Additionally, Mars supports polar ice caps composed of both water and CO_2 ices [*Douté et al.*, 2007] as well as extensive ground ice at an array of latitudes [*Byrne et al.*, 2009; *Mustard et al.*, 2001]. It has been theorized that contemporary subsurface aquifers or subglacial lakes may persist [*Gaidos*, 2001; *Orosei et al.*, 2018]. With a relatively mild climate, by planetary standards, and an ongoing interest in the potential habitability of the red planet understanding the distribution, chemical properties, and interactions of Mars' water, brine, and ice have implications for both planetary protection and exploration as well as further understanding the role water and ice have played in Mars' evolution.

1.1.3 Ceres

The Dawn spacecraft has provided an exceptional view into the dwarf planet Ceres and a number of observations revealed the small body harbors a substantial water ice component and may currently possess subsurface liquid water reservoirs [*Russell et al.*, 2016]. Ceres' ice rich crust supports the idea that during the bodies partial differentiation it likely maintained a substantial near surface ocean, a remnant of which may still be present between its rocky core and icy mantle [*Castillo-Rogez and McCord*, 2010; *Hand*, 2015]. Remote observations of Ceres' surface shows evidence of recent resurfacing in the form of extrusive, lobate flow [*Schmidt et al.*, 2017b], and depositional features [*Schenk et al.*, 2019]. Ahuna Mons has been suggested as a hydrologically driven extrusive feature [*Ruesch et al.*, 2016]. A plethora of flow like features resembling glacial processes on Earth have been documented in the literature [*Buczkowski et al.*, 2016; *Schmidt et al.*, 2017b]. Possibly Ceres' most striking feature, Occator crater may house a remnant impact induced melt chamber beneath it surface, evidenced by recent flows, fractures, and the deposition of the likely endogenic sodium carbonate dominated facula [*Hesse and Castillo-Rogez*, 2019; *Quick et al.*, 2019; *Scully et al.*, 2019].

1.1.4 Ice-Ocean Worlds

Since the discovery of Europa's ocean by the Galileo spacecraft [*Carr et al.*, 1998; *Khurana et al.*, 1998; *Kivelson et al.*, 2000] the list of solar system bodies that likely possess contemporary, large subsurface reservoirs of liquid water has been steadily growing [*Nimmo and Pappalardo*, 2016]. With the unique role water plays in facilitating life as we know it [*Chaplin*, 2006; *Chaplin*, 2001; *Tait and Franks*, 1971] this is an exciting prospect for the potential existence of life elsewhere in the solar system [*Mottl et al.*, 2007].

With each ice-ocean system offering a unique physical, thermal, and chemical environment understanding the potential processes and dynamics that control each is crucial in constraining their habitability and will inform both planetary exploration and protection as well as the design, implementation, and analysis of future spacecraft observations.

The satellites of the outer solar system make up the overwhelming majority of known ice-ocean worlds [*Nimmo and Pappalardo*, 2016]. Beyond the solar system's frost line temperatures during formation were sufficiently cool to allow the stable accretion of substantial volatiles into the giant planets and their moons [*Canup and Ward*, 2002; *Lewis*, 1971; *Prockter*, 2005]. The resulting composition of these moons facilitate the formation of volatile rich hydrospheres during their accretion. The persistence and longevity of these water reservoirs depends on internal radiogenic heating as well as tidally induced heating from parent planets and resonance with companion satellites [*Hussmann et al.*, 2006; *Hussmann et al.*, 2002; *Reynolds et al.*, 1987].

The Jupiter system harbors three such ocean worlds in the Galilean satellites Europa, Ganymede, and Callisto. Europa, Jupiter's second closest moon, provides an archetype for potentially habitable ice-ocean worlds. A fully differentiated body, Europa is believed to harbor an ~100 km thick global ocean, in contact with a silicate mantle below and overlain by an ~15-30 km thick ice shell above. Europa's ocean is maintained by a Laplace resonance with Io and Ganymede, which tidally heats Europa's ice shell and interior [*Anderson et al.*, 1998; *Schubert et al.*, 2004]. The ocean-silicate interface may support serpentinization reactions and hydrothermal activity that, when coupled with the putative overturn and recycling of the ice shell, could produce gradient rich environments and an ocean chemistry favorable for the origination and persistence of life [*Hand et al.*,

2009; *Vance et al.*, 2016; *Vance et al.*, 2007]. Ganymede, the solar system's largest moon, is differentiated and additionally possesses its own intrinsic magnetic field [*Schubert et al.*, 2004], the only moon to do so. With a substantial volatile content, Ganymede's upper ~800 km is believed to consist of ocean layers separated by different phases of ice. This stratigraphy can support high-pressure ices at depth and may produce a dynamic environment where heat and mass can be transported between layers by a number of fluid dynamic, solid state convection, multiphase, and depositional processes [*Vance et al.*, 2014]. Callisto, the outermost Galilean moon, is likely highly undifferentiated [*Anderson et al.*, 1997; *Schubert et al.*, 2004]. Callisto is believed to house an ~150-200 km thick global ocean beneath an ~80-150 km thick icy shell [*Khurana et al.*, 1998]. Callisto's undifferentiated mantle likely consists of mixtures of silicates and high-pressure ices [*Kuskov and Kronrod*, 2005; *Nagel et al.*, 2004].

The Saturn system houses many potential ice-ocean worlds, with two confirmed in Enceladus and Titan. Enceladus is a small (~500 km in diameter) moon in Saturn's inner group. Despite its size, Enceladus shows evidence of extensive past and ongoing geologic activity [*Porco et al.*, 2006]. Enceladus possesses both heavily cratered, older terrain and crater poor terrain indicative of recent surface activity [*Collins and Goodman*, 2007; *Plescia and Boyce*, 1983; *Schenk and McKinnon*, 2009]. Possibly the most iconic feature of Enceladus is its active south polar terrain, which houses the linear fracture features dubbed 'Tiger Stripes'. These fracture features have been identified as the source of persistent plumes that send icy particles out into space and ultimately form Saturn's E-ring [*Dougherty et al.*, 2006; *Porco et al.*, 2006]. Ongoing plume activity [*Postberg et al.*, 2009], coupled with evidence of recent surface processes [*Parkinson et al.*, 2008], and

gravimetric data [*Čadek et al.*, 2016] support the existence of a subsurface ocean on Enceladus. Originally thought to be localized in the south polar region recent evidence suggests Enceladus' ice shell is decoupled from its likely rocky interior implying a global subsurface water reservoir [*Thomas et al.*, 2016]. The small size of Enceladus may additionally permit fluid flow throughout its potentially porous interior [*Choblet et al.*, 2017]. In 2005 the Cassini spacecraft directly sampled the plume, revealing a primarily water vapor dominated chemistry alongside traces of methane, nitrogen, and CO_2 [*Waite et al.*, 2006]. Further measurements revealed that organic hydrocarbons were also present within the plume ejecta [*Glein et al.*, 2015; *Matson et al.*, 2007]. The presence of an active and contemporary liquid ocean in contact with a silicate interior and the potential for ongoing surface-ocean interaction has made Enceladus a primary target for astrobiological investigation [*Glein and Shock*, 2010; *Parkinson et al.*, 2008; *Vance et al.*, 2018; *Waite et al.*, 2017]. Titan, Saturn's largest moon, is the only body in the solar system, besides Earth, that possesses an active hydrologic cycle [*Lunine and Atreya*, 2008]. Both methane and ethane are stable in their liquid forms on the surface of Titan [*Brown et al.*, 2008; *Lunine et al.*, 1983; *Mitri et al.*, 2007]. Titan's solid surface is primarily composed of ice 1h, and akin to Callisto likely possesses deeper layers of high-pressure ices overlying a hydrated, partially differentiated, silicate core. It has been suggested that Titan's interior has likely remained warm enough to sustain a contemporary liquid water or ammonia-water ocean between the ice 1h surface and lower layers of high-pressure ices [*Castillo-Rogez and Lunine*, 2010; *Hussmann et al.*, 2006; *Sohl et al.*, 2003]. The promise of a subsurface water reservoir combined with the moon's abundance of organic hydrocarbons, the presence of

liquid solvents on its surface, and a stable atmosphere makes Titan a priority target for astrobiological investigation [*Board and Council*, 2012; *Fortes*, 2000; *Imanaka*, 2019].

A number of satellites of Uranus and Neptune as well as the dwarf planet Pluto may house contemporary subsurface oceans, however with limited observations of these bodies much of the evidence supporting this remains theoretical and/or speculative [*Hussmann et al.*, 2006; *Nimmo et al.*, 2016; *Vance et al.*, 2007]. One exception is Neptune's moon Triton. By far the largest of Neptune's satellites, Triton is comprised of nitrogen-water-CO_2 ice outer shell overlying a primarily water ice mantle and rocky metal core. Triton shows signs of active surface recycling by extrusive, eruptive, and tectonic processes, suggesting the presence of a subsurface water reservoir [*Bauer et al.*, 2010; *Brown et al.*, 1990; *Cruikshank*, 2005; *Gaeman et al.*, 2012]. The largest moons of Uranus (Titania and Oberon) may harbor present day liquid water layers between their rocky cores and outer ice shells [*Hussmann et al.*, 2006]. Pluto may possess a subsurface water ocean sustained either by internal heating or as a result of the large impact that produced Sputnik Planitia [*Johnson et al.*, 2016; *Nimmo et al.*, 2016; *Robuchon and Nimmo*, 2011].

1.1.5 Europa

The hypothesized internal structure of Europa coupled with its active geophysical processing, young surface, and relative proximity to Earth have garnered it a pole position in the list of high priority astrobiology targets [*Chyba and Phillips*, 2001; *Hand et al.*, 2009; *Hand et al.*, 2007; *Pappalardo et al.*, 1998; *Vance et al.*, 2016]. An archetypal ice-ocean world, coupling theoretical modeling with both spacecraft and ground based observations of Europa has provided insight into how these dynamic bodies behave and evolve.

However, much still remains to be understood, and NASA has prioritized the exploration and observation of these worlds to better understand their formation, structure, geodynamics, and potential habitability [*Board and Council*, 2012; *Des Marais et al.*, 2008]. This directive has resulted in the selection of Europa Clipper as a NASA Flagship Mission [*Phillips and Pappalardo*, 2014]. Slated to launch in the early to mid 2020s, assessing the current state of knowledge regarding Europa while continuing to pointedly investigate its ice-ocean system in a way that integrates with and facilitates mission objectives is key to optimizing the mission's scientific return.

1.1.5.1 Geophysics

1.1.5.1.1 Surface

One of the most iconic and striking features of Europa is its surface. Mottled, crosscut, ridged, and sometimes completely destroyed, the moon's outer icy crust hints at a dynamic subsurface that results in the active recycling of the ice shell [*Greeley et al.*, 2004; *Lucchitta and Soderblom*, 1982]. As the transport medium for both energy and mass between the ocean and surface as well as the substrate for observable surface features, the ice shell plays a crucial role in governing Europa's thermochemical evolution, and will affect interpretations of nearly all spacecraft observations. Europa is home to a menagerie of diverse geological features, including ridges, extensional and compressional fractures, faults, subsumption/subduction regions, extrusive resurfacing features, pits, domes, and chaos terrain [*Greeley et al.*, 2004; *Greeley et al.*, 1998b; *Pappalardo et al.*, 1998; *Sotin and Prieur*, 2007].

Ridged terrain provides the backdrop for nearly all other surface features, present at all latitudes and longitudes on Europa and constituting both the oldest terrain and some of the youngest features on the surface, ridges appear to be a persistent byproduct of Europa's geodynamics [*Head et al.*, 1999]. Characterized by closely spaced peak and trough patterns with topographic relief on the order of 10s to 100s of meters ridges can be linear, arcuate, or tortuous and can extend for 10s to 1000s of km across Europa's surface [*Greeley et al.*, 2004; *Greeley et al.*, 1998b]. A definitive mechanism for the formation of ridges has yet to be identified but current theories include cyclic tidal deformation, fluid injection and ice wedging [*Dombard et al.*, 2013; *Fagents et al.*, 2000; *Head et al.*, 1999; *Hoppa et al.*, 1999; *Nimmo and Gaidos*, 2002]. While each proposed formation method successfully addresses certain aspects of ridge geomorphology no model can account for all of the observed ridge properties. As the most ubiquitous feature on Europa's surface and a potential mechanism for ocean-surface exchange, understanding the formation and evolution of these feature has both geological and astrobiological implications [*Figueredo et al.*, 2003; *Howell and Pappalardo*, 2018].

Numerous fractures can be found across the surface of Europa, in regions undergoing both extensional and compressive tidal forcing [*Helfenstein and Parmentier*, 1983]. These fractures may be the first step in the formation of bands [*Dombard et al.*, 2013]. Faults are another common feature on Europa's surface, and akin to their terrestrial counterparts, exhibit slip-like motions indicated by the offset of features that cross the faults [*Hoppa et al.*, 2000; *Hoppa et al.*, 1999; *Nimmo and Schenk*, 2006]. Another tectonic process identified on Europa is the subduction and subsumption of the moon's brittle icy lithosphere (upper few km) into the underlying more ductile portion of the ice shell

[*Johnson et al.*, 2017b; *Kattenhorn and Prockter*, 2014]. This process could provide a mechanism for surface recycling, where endogenic ice is exposed at dilational bands and subsumed back into the shell in subduction/subsumption zones, delivering ocean derived reductants to the surface and oxidants produced by radiolysis processes on the surface back into the ocean [*Doggett et al.*, 2009; *Howell and Pappalardo*, 2018; 2019]. This redox cycling could facilitate an ocean-surface geochemical overturn that may promote an ocean composition favorable for life [*Chyba and Phillips*, 2001; *Vance et al.*, 2016; *Vance et al.*, 2018].

A number of features on Europa's surface suggest the presence of and/or interaction with near surface water reservoirs. Pits and domes, small (~10 km), circular to oblate depressions and uplifts have been suggested as the topographic relief caused by the presence of near subsurface lenses or sills [*Collins and Nimmo*, 2009; *Head et al.*, 1997; *Manga and Michaut*, 2017; *Michaut and Manga*, 2014]. Some of these features exhibit blocky/mélange textures that are consistent with the collapse or breakup of the overlying ice, and direct exposure and subsequent solidification of the underlying fluid. Part of the class of 'chaotic' terrain on Europa, these mélange-like regions have larger counterparts in features like Thrace and Thera Macula and Murias Chaos. Large chaos regions all exhibit geological features which suggest recent interaction with near surface liquid water reservoirs [*Schmidt et al.*, 2011a; *Spaun et al.*, 1998]. In this light, understanding the thermochemical evolution of these near surface water bodies, and the extent to which they interact with both the surface and underlying ocean, will aid in constraining their longevity, habitability and the role they may play in ocean-surface exchange processes, all of which have direct implications for both planetary exploration and protection.

1.1.5.1.2 Mantle

The ice shell of Europa is believed to contain two distinct regions, a cold, thin (~3-5 km), brittle lithospheric layer and a thicker (~10-30 km), more temperate and ductile mantle layer [*Ojakangas and Stevenson*, 1989]. This dichotomy is believed to be the byproduct of solid-state convection within the ice shell. As Europa cooled and its ice shell thickened a thermal, and possibly compositional, density instability would have been created – cold, dense ice near the surface would be negatively buoyant relative to deeper and warmer ice [*Barr and McKinnon*, 2007; *McKinnon*, 1999]. Given viscosity estimates for planetary ices, the thickness of a growing ice shell where convective processes begin to dominate is ~ 10 km [*McKinnon*, 1999]. At the extreme temperatures experienced at Europa's surface the viscosity of ice 1h is comparable to that of rock and would not undergo solid state convection, suggesting the formation of a stagnant lid convection regime [*Barr and McKinnon*, 2007; *Mitri and Showman*, 2005].

The prospect of convection in the mantle region of the ice shell brings with it the potential for geologically rapid transport of heat and mass to and from the ocean and has been linked to a number of geophysical processes and related surface features [*Allu Peddinti and McNamara*, 2015; *McKinnon*, 1999; *Mitri and Showman*, 2005; *Pappalardo and Barr*, 2004; *Travis et al.*, 2012]. Convective motions and diapirism have been proposed as a mechanism that could drive the spreading of dilational bands and the formation of suduction/subsumption regions, mirroring the mid ocean ridges and subduction zones of terrestrial tectonics [*Head et al.*, 1997; *Howell and Pappalardo*, 2018; 2019]. Thermal upwellings in the ductile region could provide temperature anomalies large enough that if

they impinged upon chemically enriched eutectic regions within the shell may produce *in situ* melting. This has been proposed as a mechanism for the formation of lenses near the lithosphere-mantle transition, which could provide a near surface water reservoir for the production of lenticulae, pits, domes, and chaos terrain [*Schmidt et al.*, 2011a]. Europa's youthful surface suggests active ice shell overturn [*Carr et al.*, 1998]. Exposure of endogenic ices likely carry with them entrained impurities from and information about the parent water body from which the ice formed [*Howell and Pappalardo*, 2018]. Impurity entrainment and transport has important implications for the chemical evolution of the subsurface ocean [*Vance et al.*, 2016; *Vance et al.*, 2018], has been linked to a number of geophysical processes within the ice shell [*Pappalardo and Barr*, 2004], and may provide a mechanism for the expression of Europa's endogenic properties in surface regions containing newly exposed ice [*Howell and Pappalardo*, 2018; *Soderlund et al.*, 2014].

1.1.5.1.3 Ocean and Silicate Interior

Europa's ocean is likely ~100 km thick and separates the moon's silicate interior from the overlying ice shell [*Kuskov and Kronrod*, 2005; *Prockter*, 2017; *Schubert et al.*, 2004]. The measurement of an induced magnetic field by the Galileo magnetometer provided the initial evidence for a subsurface ocean on Europa. Its conductive nature indicates the presence of ions, likely salts [*Khurana et al.*, 1998; *Kivelson et al.*, 2000]. Although the exact composition of the ocean is unknown, theoretical estimates based on the aqueous differentiation of Europa's carbonaceous chondrite constitutive material and spectral observations of likely endogenic surface features suggest an ocean containing substantial levels of sodium, magnesium, chloride, and sulfate salts [*Fanale et al.*, 1999;

Kargel et al., 2000; *Zolotov and Shock*, 2001]. Numerical modeling of the ocean predicts a zonal current structure as a result of Europa's synchronous rotation with Jupiter, sustaining current speeds of (~250 cm/s). Hadley cell like circulation may facilitate thermal downwelling near the poles and upwelling at mid latitudes (~3 cm/s) and has been suggested as a potential driver of an ice pump mechanism akin to that seen beneath terrestrial ice shelves, globally redistributing mass at the ice-ocean interface [*Soderlund et al.*, 2014]. It is likely that Europa's ocean is well mixed and as such will efficiently homogenize thermochemical anomalies produced at the seafloor and ice-ocean interface boundaries [*Soderlund et al.*, 2014; *Thomson and Delaney*, 2001].

While there exist no measurements of Europa's seafloor, theoretical investigation coupled with our knowledge of the analogous terrestrial interface predict an evolving, porous, silicate region [*Vance et al.*, 2016; *Vance et al.*, 2007]. It has been predicted that continuous cooling of Europa's interior and tidal forces drive the progressive fracture of the subsea lithology, allowing for continued infiltration of seawater and serpentinization of the surrounding rock [*Vance et al.*, 2016]. This process, along with hypothesized hydrothermalism [*Barge and White*, 2017; *Lowell and DuBose*, 2005; *Vance et al.*, 2007], has been proposed as a potential source of reductants, which when coupled with surface delivered oxidants could provide crucial metabolites for any potential organisms [*Vance et al.*, 2018].

1.1.5.2 Habitability

Possessing many of the components considered necessary for the origin and sustenance of life, Europa has long been lauded as one of the most favorable locales for

potential organisms [*Des Marais et al.*, 2008]. Alongside a long-lived and contemporary global ocean, Europa's ice-ocean-silicate stratigraphy, continued tidal heating, ongoing geophysical activity, and putative thermochemical cycling constitute a dynamic system that promotes the formation of potentially habitable environments [*Sotin and Prieur*, 2007; *Vance et al.*, 2018]. The geochemical byproducts of serpentinization reactions and hydrothermalism have been considered favorable components when determining the habitability of water-rock environments. The global hydrogen fluxes associated with these seafloor process, when coupled with the potential oxidant flux from ice shell overturn, influences the chemical disequilibria, pH, water activity, and redox potential of the ocean – characteristics directly linked to habitability [*Barge and White*, 2017; *Lowell and DuBose*, 2005; *Vance et al.*, 2016; *Vance et al.*, 2007; *Vance et al.*, 2018]. The thermal and chemical gradients provided by interfacial environments, both water-rock and water-ice, may provide habitable niches for life, akin to the flourishing ecosystems of the terrestrial benthos and algal communities found at the sea ice-ocean interface [*Barge and White*, 2017; *Lowell and DuBose*, 2005; *Wettlaufer*, 2010]. A geophysically active ice shell may promote ocean-surface interaction, delivering ocean sourced reductants to the surface through convective or fracture processes and potentially exposing entrained biosignatures in regions of recently upwelled ice [*Figueredo et al.*, 2003; *Howell and Pappalardo*, 2018], and transporting radiolitic oxidants back into the ice shell and ocean through subduction/subsumption processes [*Johnson et al.*, 2017b; *Kattenhorn and Prockter*, 2014; *Vance et al.*, 2018]. Constraining estimates of Europa's biogeochemical reservoir and their interaction with the moon's geophysical processes is crucial to estimating its habitability

and identifying potentially habitable environments in the ocean and ice shell, a key goal of the upcoming Europa Clipper mission [*Phillips and Pappalardo*, 2014].

1.1.5.3 Measurements

1.1.5.3.1 Past

Past measurements of Europa have included space and ground based telescopic observation as well as spacecraft observation. Mauna Kea's Keck observatory has been used to take spectral measurements of Europa's surface. Used to identify surface composition, observations identified signatures of water ice and hydrated mineral components, particularly sodium chloride [*Brown and Hand*, 2013; *Fischer et al.*, 2015]. The Hubble Space Telescope has been used to identify recurring plumes emanating from the moon [*Sparks et al.*, 2016]. Voyager 1 and 2 provided the first spacecraft-based observations of Europa, revealing a colorful, active and fractured icy surface [*Buratti and Veverka*, 1983; *Lucchitta and Soderblom*, 1982; *Pieri*, 1981; *Spencer*, 1987]. The overwhelming majority of the information we have about Europa was provided by the Galileo mission. In orbit around Jupiter for nearly 8 years Galileo was outfitted with spectrometric, imaging, magnetometer, plasma, and particle detecting instrumentation. Galileo observations revealed the diversity of Europa's geology, helped constrain its composition, and aided in the identification of its subsurface ocean [*Anderson et al.*, 1998; *Fanale et al.*, 1999; *Greeley et al.*, 1998b; *Head et al.*, 1999; *Kivelson et al.*, 2000]. The overarching success of this mission in expanding our knowledge and understanding of ice-ocean worlds, the Jupiter system, and particularly Europa has encouraged further exploration and inspired additional missions in the Juno spacecraft, the Jupiter Icy Moons

Explorer (JUICE) [*Grasset et al.*, 2013], and the Europa Clipper [*Phillips and Pappalardo*, 2014].

1.1.5.3.2 Future

Both JUICE and Europa Clipper are slated to begin their journey to the Jupiter system in 2022. The JUICE mission's primary target is Ganymede and will perform complimentary measurements of Callisto and Europa to investigate and characterize the geology, interior structure, magnetic fields, assess the potential habitability of these ice-ocean worlds [*Grasset et al.*, 2013]. The Europa Clipper mission is a targeted investigation of Europa and is designed to assess the moons habitability by focusing on identifying the components necessary for life: water, favorable chemistry, and energy. Utilizing a suite of instruments (ice penetrating radar, imagers, spectrometers, plasma instruments, magnetometers, particle detectors) during ~45 scheduled flybys Europa Clipper aims to: characterize the ice shell by constraining the presence of any liquid water features and identify any potential ocean-surface transport processes it may facilitate, determine the composition of the ice shell and underlying ocean, and identify dynamic and geological sources of potential thermochemical energy [*Pappalardo et al.*, 2017; *Phillips and Pappalardo*, 2014]. If successful, these missions promise to greatly extend our understanding of ice-ocean worlds and provide an unparalleled data set that will facilitate the assessment of these moon's habitability, pushing us closer to answering the question of 'Is life unique to Earth?' and informing future exploration of these ice-ocean systems.

1.2 The Purpose of this Thesis

Comparative planetology, the study of natural processes, their similarities, and differences across multiple bodies in the solar system, provides a strategy for identifying the physical limits of these processes and devises methods for accurately extending terrestrial analog studies to other planetary and satellite systems.

1.2.1 Ice as a Multiphase Reactive Porous Medium

A unique characteristic of ocean derived ices, and more generally the solidification of multicomponent solutions, is the production of a multiphase boundary layer at the solid-liquid interface characterized by a crystalline ice lattice bathed in concentrated interstitial brine. This dynamic, two-phase region referred to as a 'mushy layer', is capable of diffusive and convective heat and mass transport and is well described by the physics of reactive transport in a porous medium [*Feltham et al.*, 2006; *Hunke et al.*, 2011]. As the exchange interface between the ocean and overlying ice the dynamics of this boundary govern the thermal and chemical fluxes between these two masses, and in turn the growth rate and physicochemical properties of the forming ice [*Buffo et al.*, *in review; Loose et al.*, 2009; *Loose et al.*, 2011; *Turner and Hunke*, 2015]. This has important implications for the evolution and material properties of both terrestrial and planetary ices as the disparate thermal characteristics of ice and brine, alongside the propensity for fluid transport, means the efficiency with which a mushy layer can transport heat to and from the ice and ocean is starkly different than that of a smooth non-porous interface [*Feltham et al.*, 2006; *Hunke et al.*, 2011; *Worster*, 1997; *Worster and Rees Jones*, 2015]. Additionally, the rejection of impurities from the forming crystalline lattice into concentrated brine pockets and channels and the ensuing diffusive and advective solutal transport will determine the chemical

composition of the forming ice [*Buffo et al.*, *in review; Turner and Hunke*, 2015]. Impurities alter the density, eutectic point, dielectric properties, mechanical strength, and rheology of ice [*Galley et al.*, 2009; *Johnson et al.*, 2017b; *Kalousová et al.*, 2017; *Kargel et al.*, 2000; *Moore*, 2000]. With these properties governing the geophysics and observational interpretation of both terrestrial and planetary ices, quantifying the relationships between environmental pressures (e.g. thermal forcing, ocean chemistry) and ice composition has important implications for numerical modelling applications and empirical investigations.

1.2.1.1 Theoretical Approach

While it has long been documented that there exist impurities within terrestrial ices [*Eicken*, 1992; *Malmgren and Institutt*, 1927], the use of reactive transport theory to describe and simulate the dynamics and evolution of these systems is a relatively recent advance [*Feltham et al.*, 2006; *Notz and Worster*, 2009; *Worster*, 1997; *Worster and Rees Jones*, 2015]. However, the success with which it can describe the physical and thermochemical processes within ocean derived ices has led to its use in the construction of one- and two-dimensional models of sea ice, as well as large-scale Earth systems models of the cryosphere [*Griewank and Notz*, 2013; *Hunke et al.*, 2011; *Notz*, 2012; *Notz and Worster*, 2009; *Oertling and Watts*, 2004; *Turner and Hunke*, 2015; *Wells et al.*, 2019].

The central architecture of these models as well as how they differ from and improve upon their predecessors generally takes the following theoretical approach. When seawater is cooled below its salinity dependent liquidus point pure solid ice crystals form in the solution, rejecting solutes into the residual liquid, altering the composition and

thermochemical properties of the concentrated brine. This two-phase slurry of ice and brine is thermodynamically stable as the latent heat of fusion, salt rejection, and salinity dependent freezing point of the pore fluid interact to maintain a thermal profile within the mushy layer that lies on the salinity dependent liquidus curve for seawater. Heat transport within the layer can occur through diffusion in the ice and pore fluid as well as advective transport in the liquid portion of the mush. Additionally, heat can be generated or consumed by phase change. Solute transport can occur through diffusion and advection in the liquid component of the mushy layer, and by the rejection or dissolution of salt by freezing or melting ice, respectively [*Feltham et al.*, 2006; *Hunke et al.*, 2011].

Mushy layer thermal and molecular diffusivities are typically represented as volume averages of ice and brine diffusivities (i.e. for liquid fraction ϕ, ice diffusivity D_i, and brine diffusivity D_{br}, the volume averaged diffusivity would be $\overline{D} = \phi D_{br} + (1 - \phi) D_i$). Molecular diffusivity in the ice phase is typically assumed to be zero [*Feltham et al.*, 2006; *Hunke et al.*, 2011]. One of the unique features of mushy layers is the propensity for advective transport of the interstitial pore fluid through the evolving porous medium. In the top-down solidification of sea ice as the interstitial brine becomes more saline a density instability is created between the concentrated pore fluid and the underlying ocean. When this instability reaches the critical limit for convective overturn the interstitial brine down wells, and along its way melts a brine channel into the ice [*Wells et al.*, 2019]. This process has analogues in hydrological, metallurgical, and magmatic systems [*Berner*, 1980; *Fowler*, 1987; *Worster*, 1997; *Worster et al.*, 1990]. Convective patterns are setup in mushy layers that have reached a critical thickness, and the circulation of seawater into the ice and dense pore fluid into the underlying ocean, referred to as gravity drainage, has been

shown to be the primary desalinization mechanism for sea ice [*Griewank and Notz*, 2013]. This convective overturn is frequently parameterized using properties of the mushy layer (e.g. thickness, pore fluid density anomaly, gravity) and has successfully been incorporated into a number of sea ice models [*Griewank and Notz*, 2013; *Notz and Worster*, 2009; *Wells et al.*, 2011].

Numerical models simulating the two-phase nature of ocean derived ices and the fluid dynamics that govern its physical and thermochemical evolution more accurately predict the growth rate, salt content, microstructure, thermodynamics, and material properties of sea ice than do models that only implement conductive heat transport and/or parameterize salt entrainment within growing ice [*Griewank and Notz*, 2013; *Notz and Worster*, 2009; *Turner and Hunke*, 2015; *Turner et al.*, 2013]. These results demonstrate the utility of the reactive transport treatment of ocean derived ices and highlights its ability to predict the thermodynamic evolution and material properties of these ices. This field of study has only just begun, and while contemporary models have begun to include additional physics such as biogeochemical and depositional processes [*Buffo et al.*, 2018; *Dempsey et al.*, 2010; *Tedesco and Vichi*, 2014; *Vancoppenolle et al.*, 2013; *Vancoppenolle and Tedesco*, 2015], the opportunities provided by this approach to extend our understanding of the terrestrial cryosphere and ice-ocean worlds throughout the solar system are only beginning to be realized.

1.2.1.2 Implications: Impurities and Material Properties

Physicochemical heterogeneities within ice can drastically affect its material properties, impacting its dynamics and observational signatures. Salts constitute a major

portion of the impurities in ocean-derived ice and alter its density [*Buffo et al.*, *in review; Johnson et al.*, 2017b], eutectic point [*McCarthy et al.*, 2007], rheology [*Kauffeld et al.*, 2005], material strength [*Assur*, 1958], and dielectric properties [*Weeks*, 2010; *Weeks and Ackley*, 1986]. For sea ice this impacts estimates of ice thickness, both through buoyancy and electromagnetic induction measurements, melt dynamics, and fracture mechanics [*Abdalati et al.*, 2010; *Assur*, 1958; *Haas et al.*, 1997; *Laxon et al.*, 2013; *Mellor*, 1986; *Turner and Hunke*, 2015]. Structural characteristics of the ice cover, especially near the ice-ocean interface, determine the efficiency of ocean-atmosphere heat and mass exchange, quantifying the thermal and chemical insulating/buffering abilities of sea ice [*Feltham et al.*, 2006; *Golden et al.*, 2007; *Goosse and Fichefet*, 1999; *Hunke et al.*, 2011; *Loose et al.*, 2011]. In a changing climate, where the reservoirs of multiyear and first year sea ice are in flux [*Cavalieri et al.*, 2003], and both are subject to accelerating ocean and atmosphere anomalies understanding the complex interdependencies of these systems, assessing the best way to monitor them, and determining the impact they have on the Earth system is crucial to protecting our polar regions.

In the Europa system physical and chemical variations in the ice shell have been linked to a number of geophysical processes. Lateral heterogeneities in salt content of lithospheric slabs have been suggested as a potential mechanism for driving the subduction/subsumption seen on Europa's surface [*Johnson et al.*, 2017b]. The presence of salts in the ductile region of the ice shell can either aid or hinder thermochemically driven solid-state convection [*Barr and McKinnon*, 2007; *Pappalardo and Barr*, 2004]. Localized enhancements of salts near the brittle-ductile transition of the ice shell could produce eutectic regions susceptible to melting under the influence of thermal diapirs,

producing perched lenses that could drive the formation of chaos terrain and other surface features [*Schmidt et al.*, 2011a]. Both grain size and the presence of salts have been proposed as key factors in determining the rheological and mechanical properties of Europa's ice, influencing the dynamics of solid-state convection and fracture processes operating within the shell [*Barr and McKinnon*, 2007; *McKinnon*, 1999]. Akin to sea ice, measurements of the ice shell that depend on the dielectric properties of the ice will depend critically on the chemical composition of the ice [*Galley et al.*, 2009; *Kalousová et al.*, 2017; *Moore*, 2000]. The ice penetrating radars RIME (JUICE) and REASON (Europa Clipper) are particularly susceptible to these effects as they will utilize dielectric contrasts within the ice to determine the ice shell's properties and identify any subsurface liquid water reservoirs [*Grasset et al.*, 2013; *Pappalardo et al.*, 2017; *Phillips and Pappalardo*, 2014]. Constraining the expected physicochemical composition of planetary ices and how this impacts the material properties of ice shells is crucial in predicting the geophysical and transport processes they can support and in interpreting future spacecraft data products.

1.2.1.3 Implications: Impurities as a Record of the Origin Water Mass

As ocean water (or brine) solidifies and is incorporated into the overlying ice cover it carries with it a record of the water reservoir that sourced it and the thermodynamic conditions under which it formed [*Allu Peddinti and McNamara*, 2015; *Buffo et al.*, *in review; Buffo et al.*, 2019; *Kargel et al.*, 2000]. Analogous to the depositional and diagenetic processes which govern meteoric ice and terrestrial sediments [*Berner*, 1980], the resulting characteristics and stratigraphy provides a glimpse into the environment under which the ice formed. This entrainment/imprint of chemical and thermodynamic

information is applicable and important to both terrestrial and planetary ice-ocean environments. While certainly more accessible than the subsurface ocean of Europa, Earth's sub-ice oceanic environments remain difficult to observe due to their remoteness and dynamic ice covers. Easier to access due to the relative thinness of the ice, sub-sea ice ocean environments and their interaction with the overlying ice have been well documented in the literature [*Dempsey et al.*, 2010; *Langhorne et al.*, 2015; *Nakawo and Sinha*, 1981; *Robinson et al.*, 2014; *Weeks*, 2010; *Weeks and Ackley*, 1986]. Nevertheless, the yearly formation and breakup of much of the sea ice cover make collecting continuous, high resolution observations difficult, resulting in a relatively sparse spatiotemporal dataset. Extracting and analyzing sea ice cores provides a method of filling in these discontinuities as the physicochemical profile of the ice core contains a record of the formation history of the ice cover [*Dempsey et al.*, 2010; *Eicken*, 1992; *Nakawo and Sinha*, 1981]. Constitutive relationships between thermochemical ocean dynamics and associated ice characteristics enable the reconstruction of ocean properties from the stratigraphy of the ice core, removing the need for continuous *in situ* measurements of the underlying ocean [*Buffo et al.*, 2018; *Buffo et al.*, *in review*]. There exist limitations to this method insofar as there may exist non-unique relationships between ocean thermochemical dynamics and ice core properties, however the ability to reconstruct a season of ocean variability from ice core analysis provides a powerful tool for both empiricists and modelers.

The cavities beneath Antarctica's ice shelves are even more remote and difficult to access, and as such have remained largely unexplored. There have been a handful of projects that have drilled through these thick ice layers to reach and measure properties of the deep ice and underlying ocean, and fewer still that have installed moorings to capture

the temporal variability of the water masses that lie within these unique ocean zones [*Craven et al.*, 2004; *Craven et al.*, 2009; *Craven et al.*, 2005; *Fricker et al.*, 2001; *Holland et al.*, 2009; *Wolfenbarger et al.*, 2018; *Zotikov et al.*, 1980]. However, Antarctic's ice shelves cover over 1,500,000 square kilometers [*Depoorter et al.*, 2013] and nearly everything that lies beneath them has never been directly measured. Understanding the circulation, water mass properties, accretion/ablation, and ecology of these cavities has broad implications across multiple disciplines including oceanography, climatology, cryospheric sciences, and astrobiology. Thus, devising techniques to investigate and quantify the properties of these regions, both directly and indirectly, is of great interest. One such method is measuring the properties of ISW plumes emanating from the front of ice shelves. These water masses, formed within the ice shelf cavities, carry with them information about the dynamics and processes they have been subject to from the time of their generation near the grounding line [*Robinson et al.*, 2014; *Smedsrud and Jenkins*, 2004]. As these plumes flow out from beneath their parent ice shelves they continue to ascend and interact with ice shelf adjacent sea ice through the deposition of platelet ice. A byproduct of the ice pump mechanism, crystals nucleate and grow in the water column of the plume due to depressurization induced supercooling [*Lewis and Perkin*, 1983]. As these crystals float out of suspension and are buoyantly deposited on the sea ice-ocean interface they produce an unconsolidated highly porous layer of crystals [*Dempsey et al.*, 2010; *Langhorne et al.*, 2015; *Robinson et al.*, 2014]. The volume of this layer is associated with spatiotemporal properties of the plume as both the level of supercooling and the plumes variability determine the production rate of platelet ice [*Buffo et al.*, 2018; *Robinson et al.*, 2014]. Thus, variations recorded in the characteristics of the sub-ice platelet layer beneath

ice shelf adjacent sea ice acts as a proxy for the dynamics, evolution, and properties of ISW plumes. These variations can be observed by *in situ* measurement [*Dempsey et al.*, 2010; *Langhorne et al.*, 2015; *Robinson et al.*, 2014] and are also preserved in ice cores as the sub ice platelet layer is incorporated into the growing sea ice [*Buffo et al.*, 2018; *Dempsey et al.*, 2010]. Both techniques provide an indirect measurement of sub-ice shelf cavity processes and water mass characteristics that have been recorded in the adjacent sea ice column, highlighting the ability of ocean derived ices to preserve information about their thermochemical environment at the time of formation and parent water reservoir.

It stands to reason that planetary ices formed in analogous ice-ocean environments would similarly retain signatures of interfacial thermochemical properties and origin water masses. In the case of Europa this could provide a mechanism by which ocean materials could become entrained within the ice shell, and ultimately be transported to the surface, providing observable signatures of subsurface ocean characteristics [*Figueredo et al.*, 2003; *Howell and Pappalardo*, 2018]. To accurately relate measurements of potentially endogenic surface material to the properties of the ocean the dynamics of impurity entrainment at the ice-ocean interface must be constrained [*Buffo et al.*, *in review*]. Additionally, on its putative journey through the ice shell any entrained material may be subject to additional processing in the form of freeze/melt cycling, ongoing chemical reactions, and mechanical stresses. What is expressed at the surface will be a record of the cumulative thermodynamic and physicochemical processes the ice, and any material it contains, has been subject to since the time of its formation and incorporation into the ice shell at the ice-ocean interface [*Buffo and Schmidt*, 2017; *Buffo et al.*, *in review; Schmidt et al.*, 2017a]. With a dynamic and continuously recycled surface containing numerous

features indicative of recently exposed endogenic material (e.g. chaos, dilational bands) there exists an accessible spatiotemporal record of Europa's contemporary interior processes and characteristics [*Figueredo et al.*, 2003; *Howell and Pappalardo*, 2018]. Deciphering these records critically depends on extending our knowledge of planetary ice-ocean interactions and ice shell processes through numerical modeling, spacecraft and Earth analog investigations. Devising a strategy to quantitatively link ocean and ice shell properties and processes to measurables on the surface has substantial implications for understanding ice-ocean world geophysics, assessing the habitability of moons like Europa, and interpreting spacecraft data.

1.2.2 Summary of the Thesis

As an ice-ocean world itself, Earth provides a number of analog environments that can be used to better understand the dynamics of ice-ocean processes occurring on bodies like Europa [*Eicken*, 2002; *Gleeson et al.*, 2012; *Marion et al.*, 2003]. Natural and laboratory grown sea ice provides an accessible sample of ocean-derived ice, where the effects of the local thermochemical environment on ice formation rate, microstructure, and biogeochemistry can be studied in detail [*Wettlaufer*, 2010]. The remote environment of sub-ice shelf cavities provides an additional analog to the subsurface ocean of Europa. Devoid of sunlight, trapped beneath kilometers of overlying ice, and with limited contact to the open ocean these regions can aid in our understanding of the circulatory, biogeochemical, thermodynamic, and accretion/ablation processes that may occur beneath Europa's ice shell [*Lawrence et al.*, 2016]. Together, these possibilities motivate Chapter 2, which focuses on building a comprehensive model of the combined influence of

temperature gradients, salinity, and ice nucleation within the water column on the properties of terrestrial ices.

Quantifying how environmental factors impact the dynamics and properties of terrestrial ices can then be extended to improve estimates of the characteristics and behavior of planetary ices subject to diverse thermochemical regimes [*Buffo et al.*, *in review; Buffo et al.*, 2019]. This ability to predict physicochemical properties of planetary ices informs numerical simulations of ice-ocean world geophysics, chemical cycling, and habitability and provides context for the synthesis and interpretation of spacecraft data. Our foundational and relatively extensive understanding of the terrestrial cryosphere provides immense leverage when attempting to decipher the complex innerworkings of much less fully understood ice-ocean worlds and provides a benchmark for validating numerical models. In Chapter 3, the foundation provided by work in Chapter 2 is extended to accommodate the composition and dynamics of Europa's ice-ocean environment. The impacts of ocean composition and thermal regime on the state of the ice shell are explored. Fundamentally, this connects ocean properties to observable surface features via accretion and evolution of the ice shell that become accessible to future missions.

The physics of multiphase materials are applicable across a wide range of Earth and planetary problems, however the dynamics of reactive transport depend on the environmental and material properties of the system. The physical, thermal, and chemical properties of ice-ocean/brine systems in the solar system remain relatively unconstrained but likely span a substantial trade space. Moreover, the extent to which ice-ocean world environments can be assumed to be well described by known mushy layer physics has not been investigated as this area of study represents a relatively new element of planetary

science. To that end, Chapter 4 explores the limits of the physics contained within this work, and comments on areas where new work and additional physics may be needed to realize a fully comprehensive systems understanding of Europa's and other worlds' ice shell(s).

There are certainly limitations to the applicability of Earth as an analog to other ice-ocean worlds and these must be identified and accounted for to ensure an appropriate use of the transitive strategies comparative planetology offers. For example, the chemistries of oceans and ices throughout the solar system may be quite diverse [*Kargel et al.*, 2000; *Neveu et al.*, 2017; *Zolotov*, 2007; *Zolotov and Shock*, 2001]. The addition of exotic salts or ammonia to an ice-ocean system may alter its solidification dynamics and resultant ice properties [*Fortes*, 2000; *Hammond et al.*, 2018]. While laboratory experiments have begun to investigate the effects of these additives on ice properties [*Lorenz and Shandera*, 2001; *McCarthy et al.*, 2007], determining their impact on processes occurring at geophysical scales relies on theoretical predictions as no terrestrial analogue exits. The age and scale of many planetary ices also exceeds that of the oldest and thickest ice on Earth [*Fretwell et al.*, 2013]. Thus, while Earth provides an excellent, well-studied endmember for the dynamics and properties of planetary ices there may be as yet unseen deviations in the physical behavior and characteristics of ice-ocean systems under thermochemical pressures found only on other bodies in the solar system. In the concluding Chapter 5, I highlight accomplishments that have allowed this work to make significant steps towards best reconciling Earth and planetary ices, and comment on future directions and ongoing work that will enable me to continue to make progress. In particular, I discuss the future of incorporating biological elements into these models and benchmarking this relatively

new work through laboratory and field programs. This multidisciplinary approach provides the greatest foundation by which the work described here can make a future impact on how we measure and understand ice-ocean worlds.

Chapter 2: Multiphase Reactive Transport and Platelet Ice Accretion in the Sea Ice of McMurdo Sound, Antarctica

A compact version of this chapter is published in the Journal of Geophysical Research: Oceans [Buffo et al., 2018]. The goal of this work was to construct a stand-alone one-dimensional finite difference model capable of simulating the multiphase reactive transport processes that govern the formation and evolution of sea ice. The motivation for including the physics of buoyancy driven platelet ice accretion was twofold. First and foremost, was to devise an efficient method of simulating platelet ice accretion and its effects on the structural and thermochemical properties of ice shelf-adjacent sea ice. The ability to relate environmental characteristics (e.g. ocean chemistry, atmospheric forcing, supercooling) to observable ice core properties provides a method to reconstruct the spatiotemporal evolution of the ice-ocean interface from the thermochemical signatures recorded in the stratigraphy of the overlying ice. In regard to platelet ice accretion, this has direct implications for identifying the presence and evolution of sub-ice shelf water masses and their interactions with the global oceans, atmosphere and cryosphere – an imperative interrelation to understand in a rapidly changing climate. The second purpose was to demonstrate the versatility of such an approach to accommodate the physics of diverse environments. In the long term, this verification of the model against terrestrial analogues with substantial empirical observations bolsters the model's applicability to more exotic ice-ocean environments in the solar system.

Abstract

Sea ice seasonally to interannually forms a thermal, chemical, and physical boundary between the atmosphere and hydrosphere over tens of millions of square kilometers of ocean. Its presence affects both local and global climate and ocean dynamics, ice shelf processes, and biological communities. Accurate incorporation of sea ice growth and decay, and its associated thermal and physiochemical processes, is underrepresented in large-scale models due to the complex physics that dictate oceanic ice formation and evolution. Two phenomena complicate sea ice simulation, particularly in the Antarctic: the multiphase behavior brought about by the inhomogeneous solidification of seawater, and the buoyancy driven accretion of platelet ice formed by supercooled ice shelf water onto the basal surface of the overlying ice. Here a one-dimensional finite difference model capable of simulating both processes is developed and tested against ice core data. Temperature, salinity, liquid fraction, fluid velocity, total salt content, and ice structure are computed during model runs. The model results agree well with empirical observations and simulations highlight the effect platelet ice accretion has on overall ice thickness and characteristics. Results from sensitivity studies emphasize the need to further constrain sea ice microstructure and the associated physics, particularly permeability-porosity relationships, if a complete model of sea ice evolution is to be obtained. Additionally, implications for terrestrial ice shelves and icy moons in the solar system are discussed.

2.1 Introduction

Sea ice is a ubiquitous feature of the Earth's polar regions and, as the boundary between the hydrosphere and atmosphere, it plays a critical role in both local and global climatic, oceanic, and biological processes [*Thomas*, 2017]. With north polar sea ice

maximums decreasing at unprecedented rates [*Thomas*, 2017], it is imperative to understand and quantify the physical, thermal, and chemical processes that affect the evolution of sea ice. Sea ice plays an important role in facilitating Arctic and Antarctic water mass formation that in turn affects global ocean circulation [*Meredith and Brandon*, 2017]. It sources high salinity shelf water, crucial in controlling basal melt rates and the stability of floating ice shelves, affecting mass loss of the Antarctic and Greenland ice sheets [*Joughin and Alley*, 2011]. It provides a refuge for ice algae, a key primary producer in the polar oceans, along with other micro- and macro-fauna in its lower layers [*Loose et al.*, 2011; *Vancoppenolle et al.*, 2013]. Understanding how these organisms persist within the ice can help elucidate their survival mechanisms and has potential astrobiological application to putative ice-ocean interfaces elsewhere in the solar system [*Greeley et al.*, 1998a; *Soderlund et al.*, 2014; *Thomas and Dieckmann*, 2008; *Wettlaufer*, 2010].

Compared to freshwater ice, sea ice is dynamic and complex, due primarily to the inherent impurities of seawater. When a solution, such as seawater, is cooled below its freezing point the solvent (water) begins to solidify while the solute (salt) is preferentially rejected from the crystalline lattice increasing the concentration (salinity) of the remaining liquid fraction [*Feltham et al.*, 2006; *Wettlaufer et al.*, 1997a]. A similar process dictates the fractional crystallization of magmas and metal alloys [*Emms and Fowler*, 1994; *Wettlaufer et al.*, 1997a; *Worster*, 1992; *Worster*, 1991; 1997; *Worster et al.*, 1990], although in a vastly different temperature regime. In the case of ocean water, the result is a porous crystalline ice matrix flush with brine-filled pockets and channels. The two-phase nature of this system determines the thermal, chemical, and mechanical properties of the ice and allows for fluid and solute transport [*Petrich and Eicken*, 2017]. The physics

governing the formation and reactive transport processes affecting sea ice are well summarized by mushy layer theory, which treats ice as a multiphase reactive porous media [*Feltham et al.*, 2006; *Hunke et al.*, 2011].

The fact that there exist impurities within sea ice has been known for nigh on a century [*Malmgren and Institutt*, 1927], and documentation of its heterogeneities, as well as the impact they have on the mechanical and thermal properties of the ice, has been carried out ever since [*Cox and Weeks*, 1974; *Eicken*, 1992; 2003; *Schwerdtfecer*, 1963]. [[*Worster and Rees Jones*, 2015] provide a comprehensive review of the laboratory experiments (i.e. [*Huppert and Worster*, 1985]), and theoretical work [*Feltham et al.*, 2006; *Huppert and Worster*, 1985; *Worster*, 1991], that has led to contemporary models of sea ice [*Griewank and Notz*, 2015; *Griewank and Notz*, 2013; *Hunke et al.*, 2011; *Rees Jones and Worster*, 2013; 2014; *Turner and Hunke*, 2015; *Turner et al.*, 2013; *Vancoppenolle et al.*, 2007; *Vancoppenolle and Tedesco*, 2015; *Wells et al.*, 2011; *Wells et al.*, 2019]. While these models have improved drastically over the years and have greatly increased our understanding of the small-scale physics that dictate the formation and evolution of sea ice, there remain numerically unconstrained processes and others that need refinement [*Petrich and Eicken*, 2017].

Sea ice near the termini of ice shelves is subject to an additional phenomenon known as platelet ice accretion. Here, a buoyant plume of supercooled water (below its *in situ* freezing point) created by pressure melting at the basal surface of the abutting ice shelf upwells from the ice shelf cavity and bathes the underside of the sea ice. As the plume rises, and the *in situ* freezing point increases, small ice crystals (platelets) begin to nucleate in the water column to relieve the thermodynamically unstable supercooling. The crystals

continue to grow until buoyant forces lead them to rise upward, where they accrete onto the basal surface of the sea ice [*Dempsey et al.*, 2010; *Gough et al.*, 2012; *Leonard et al.*, 2006]. These floating crystals modify the ice-ocean interface, creating a highly porous layer of platelet ice with notably different crystal geometry and texture than the typical granular or columnar ice produced by the direct freezing of ocean water onto the sea ice-ocean interface [*Dempsey and Langhorne*, 2012; *Dempsey et al.*, 2010]. The addition of platelet ice crystals to the sea ice layer can modify the thermal and mechanical properties of the ice as well as contribute meters of consolidated platelets to the overall ice thickness (with maximums near ice shelf fronts reaching ~10m) [*Eicken and Lange*, 1989; *Hellmer*, 2004; *Hoppmann et al.*, 2015; *Hunkeler et al.*, 2016]. Quantifying this interaction between sea ice and ice shelves and incorporating it into numerical simulations of platelet-affected ice would improve the fidelity and predictions of such models, increasing our understanding of polar ice-ocean interactions.

Platelet ice was first recorded in the literature a half century ago [*Dayton et al.*, 1969], and while a number of observations have documented the existence, structure, ecology, and regional abundance of platelet ice [*Arrigo et al.*, 1995; *Dempsey et al.*, 2010; *Gough et al.*, 2012; *Jeffries and Weeks*, 1993; *Leonard et al.*, 2006; *Smith et al.*, 2001], nearly all numerical models exclude it from their treatment of sea ice - with notable exceptions [*Dempsey*, 2008; *Dempsey et al.*, 2010; *Kawano and Ohashi*, 2008; *Ohashi*, 2004; 2007]. The most extensive and complete model of platelet ice accretion to date is the work of [*Wongpan et al.*, 2015], wherein the authors simulate platelet ice rise dynamics as well as diffusive heat and salt transport within the sub-ice platelet layer. The result is an extremely high-fidelity three-dimensional simulation of a small portion (10 cm x 10 cm x

10 cm) of the advancing sea ice-ocean interface. The model excludes fluid dynamics such as advection and convection but does artificially increase the thermal and chemical diffusion constants in an attempt to remedy this. Different model techniques have their own benefits and limitations. Purely mechanical models can simulate larger domains but cannot accurately recreate the thermal and chemical physics occurring in the forming layer. These physics are partially captured in the models of [*Kawano and Ohashi*, 2008] and [*Wongpan et al.*, 2015] but the computational expense of these models limits them to much smaller spatial scales.

Formation of ice crystals in a supercooled water column also occurs beneath ice shelves and in rivers (See [*Martin*, 1981]). [*Daly*, 1984] provides a comprehensive background on the subject, covering the formation, evolution, dynamics, and size distribution of frazil ice. Modeling efforts have sought to simulate the physical and thermal evolution of these ice-laden waters [*Holland and Feltham*, 2005; *Jenkins and Bombosch*, 1995; *Smedsrud and Jenkins*, 2004; *Svensson and Omstedt*, 1994] as well as the ensuing accretion and ablation cycles [*Galton-Fenzi et al.*, 2012].

While the importance of sea ice in many of the Earth systems is widely accepted [*Aagaard and Carmack*, 1989; *Barry et al.*, 1993; *Notz and Bitz*, 2017], predictive models that capture the full suite of physics occurring within the ice are uncommon and are often traded for simpler parameterizations of its properties. Although computationally less expensive, excluding the microscale processes that in turn shape the macroscale properties of the sea ice layer can drastically reduce the accuracy of these models [*Petrich and Eicken*, 2010; 2017] and prevent effective representation of sea ice in larger Earth systems models [*Notz*, 2012]. Here a one-dimensional, finite difference model of sea ice that includes the

multiphase physics described by mushy layer theory as well as a mechanical, energy-conserving model of platelet ice accretion is presented. What follows is a description of the one-dimensional numerical model, results from the model's application to sea ice under various oceanic and atmospheric conditions to reproduce field observations, and a discussion of the utility of such an approach in simulating an array of Earth and planetary ice-ocean environments.

2.2 Numerical Model

Sea ice growth is treated as a reactive transport model where water/ice mass, energy and salinity are conserved in a multiphase framework. The growth of sea ice also accounts for accretion at the ice-seawater interface. An overview of the different aspects of the model is given below.

2.2.1 Advection-Reaction-Diffusion Multiphase Model

The model discussed herein utilizes mushy layer theory to simulate the ice-ocean system. This approach uses continuum mechanics to approximate the properties of representative elementary volumes [*Feltham et al.*, 2006; *Hunke et al.*, 2011] and has been implemented in several contemporary sea ice models [*Griewank and Notz*, 2013; *Turner and Hunke*, 2015; *Turner et al.*, 2013].

The equations of mushy layer theory ensure the conservation of heat (eq. 1) and mass (eq. 2 & 3):

$$\overline{\rho c}\frac{\partial T}{\partial t} = -\rho_{br} c_{br} w \frac{\partial T}{\partial z} + \frac{\partial}{\partial z}\left(\bar{k}\frac{\partial T}{\partial z}\right) - \rho_{ice} L \frac{\partial \phi}{\partial t} + Q \qquad (1)$$

$$\phi \frac{\partial S_{br}}{\partial t} = -w \frac{\partial S_{br}}{\partial z} + \frac{\partial}{\partial z}\left(\bar{D} \frac{\partial S_{br}}{\partial z}\right) - \frac{\rho_{ice}}{\rho_{br}} P_S S_{br} \frac{\partial \phi}{\partial t} \quad (2)$$

$$\frac{\partial w}{\partial z} = \left(\frac{\rho_{ice}}{\rho_{br}} - 1\right) \frac{\partial \phi}{\partial t} \quad (3)$$

where ρ is density, c is specific heat capacity, T is temperature, t is time, w is brine velocity, z is the vertical coordinate, k is heat conductivity, L is the latent heat of fusion for the water to ice phase transformation, ϕ is liquid fraction, Q is any external heat sources such as solar radiation, S is salinity, D is salt diffusivity, and P_S is a partition coefficient used to simulate the incorporation of salt into the solid phase (ice) via precipitation and fractional crystallization. Subscripts *ice* and *br* refer to characteristics of the ice and brine components of the cell, respectively, and variables with the over bar are volumetrically averaged quantities (i.e. for a characteristic y, $\bar{y} = \phi y_{br} + (1 - \phi) y_{ice}$).

Equations (1-3) contain four unknowns and the system of partial differential equations still needs to be closed. The present model employs an enthalpy method [*Huber et al.*, 2008] to iteratively calculate the liquid fraction of a given unit cell. This is done using the following two equations:

$$H = c_{ice} T + L\phi \quad (4)$$

$$\phi = \begin{matrix} 0 \\ (H - H_s)/L \\ 1 \end{matrix} \quad -if- \quad \begin{matrix} H < H_s = c_{ice} T_m \\ H_s \leq H \leq H_s + L \\ H > H_s + L \end{matrix} \quad (5)$$

where H is enthalpy, T_m is the melting temperature, and H_s is the enthalpy if the cell was completely frozen out (enthalpy of solid ice) given its current salinity. The melting temperature is calculated via a linearization of the freezing point depression:

$$T_m = 273.15 - \Delta T = 273.15 - 1.853 * \frac{S}{28} \quad (6)$$

This system of equations is solved using the following discretization schemes: for a given set of initial conditions first enthalpy and liquid fraction are solved for explicitly, the liquid fraction is used to solve for the brine velocity using an upwind scheme with a no-slip boundary condition at the top boundary, temperature and salinity are then solved for using implicit temporal and centered spatial discretization. This process is repeated until convergence to a specified tolerance is reached for each of the unknown variables before moving to the next time step, using the resultant values for the new initial conditions.

Salt diffusivity is modeled using Archie's law which describes ion flow in consolidated porous media [*Glover et al.*, 2000] and can be written as:

$$D' = D\phi^m \quad (7)$$

where D' is salt diffusivity including the effects of porosity, D is salt diffusivity in water, ϕ is porosity, and m is a cementation exponent which accounts for the reduction of ion diffusivity with decreasing porosity and will always be greater than 1. Throughout the current work a cementation exponent of 2 has been used.

There are a number of assumptions implied with the definition of the model. First, the model neglects external heat sources (Q), such as solar radiation. Second, thermal conductivities (k), salt diffusivities (D), and specific heats (c) are taken to be approximately constant for both ice and brine allowing for their removal to outside of the spatial derivatives in the equations for heat and mass conservation. Additionally, the partition coefficient (P_S) is set to a constant. These simplifications were made to accelerate the development process, and upon validation of the utility of the model full expressions for these variables will be included. Finally, we assume that the discretization cells are in local thermodynamic equilibrium, which is shown to be appropriate for sea ice [*Feltham et al.*, 2006]. The one-dimensional model can then produce spatially and temporally varying profiles of temperature, salinity, brine velocity, liquid fraction, precipitated/fractionally crystallized salt, and total salt content.

2.2.2 One-Dimensional Density Driven Convection Parameterization

Due to the reduced ability of crystalline ice to incorporate salt into its lattice, as a volume of sea ice solidifies its interstitial brine becomes increasingly saline. With a temperature gradient present from the ice-atmosphere interface to the ice-ocean interface, there inevitably forms a similar gradient in salinity of the interstitial brine (based on the liquidus relationship of seawater and the assumption of local thermodynamic equilibrium). This gradient produces a density instability that results in convection through the porous portion of the ice, leading to desalination of the ice column.

In the one-dimensional regime, the phase change-driven brine velocity of the model outlined above is insufficient to expel enough salt to match field and experimental

observations. This leads to supersalination of the upper ice layers and ultimately unphysical numerical simulations. One-dimensional models cannot explicitly simulate the gravity driven convection that occurs in the porous layers of the forming ice as it is an inherently multi-dimensional process. This process has been shown to be the primary mode of sea ice desalinization aside from surface flushing [*Notz and Worster*, 2009]. Thus, a parameterization of density driven convection is implemented. These types of parameterizations have been investigated before [*Griewank and Notz*, 2013; *Turner et al.*, 2013] and the model presented in [*Griewank and Notz*, 2013] (From here on GN2013) is closely followed here.

To parameterize convection in the one-dimensional model a local Rayleigh number, describing the propensity for convection to occur, is defined as follows (for a vertical layer *j*):

$$Ra_j = \frac{t_j^{diff}}{t_j^{adv}} = \frac{g\rho_{sw}\beta\Delta S_j \widetilde{\Pi}_j h_j}{\kappa\mu} \tag{8}$$

where Ra_j is the Rayleigh number of the *j*th layer, t_j^{diff} is the diffusion timescale, t_j^{adv} is the advection timescale, g is acceleration due to gravity, ρ_{sw} is the density of seawater, β is a density coefficient describing the relationship between density and salinity, ΔS_j is the difference in salinity of the brine from ambient seawater, h_j is the height of the *j*th layer above the basal surface of the ice, κ is the thermal diffusivity of seawater, μ is the kinematic viscosity of seawater, and $\widetilde{\Pi}_j$ is the minimum permeability of any layer between the *j*th layer and the basal ice surface, where permeability is defined as:

$$\Pi = 10^{-17} * (10^3 * \phi)^{3.1} \quad (9)$$

following GN2013. Use of the minimum permeability ensures that thick sea ice, with central regions characterized by low liquid fraction and reduced permeability, ceases to expel brine via convective overturn when porosities drop below a critical level (here $\phi < 0.05$ [*Golden et al.*, 2007]). There is disagreement in the literature as to whether such a porosity cutoff exists for sea ice [*Golden et al.*, 2007; *Griewank and Notz*, 2013; *Oertling and Watts*, 2004], and additional permeability-porosity relationships are investigated in Section 2.4.3.

The one-dimensional parameterization represents convection through brine channels as a linear function of the local Rayleigh numbers. [*Wells et al.*, 2010] used calculus of variations to maximize the solute flux out of simulated sea ice containing brine channels and found a linear relationship between the local Rayleigh number and solute flux. [*Rees Jones and Worster*, 2013] independently produce a similar linear relationship between solute flux and Rayleigh number for parameter space relevant to sea ice. These approaches are founded on the idea that a physical system tends to minimize its overall potential energy. GN2013 gives the mass of brine transported from layer *j*, via convection, back to the ocean as:

$$br_j^{\downarrow} = \alpha\left(Ra_j - Ra_c\right) dz^3\, dt = \alpha\left(\frac{g\rho_{sw}\beta\Delta S_j\widetilde{\Pi}_j h_j}{\kappa\mu} - Ra_c\right) dz^3\, dt \quad (10)$$

where α is a constant of proportionality optimized by GN2013 using the Levenberg-Marquardt algorithm to be 1.56*10^-3 kg/(m^3 s), Ra_c is the critical Rayleigh number, and *dz* and *dt* are the spatial and temporal discretization sizes, respectively.

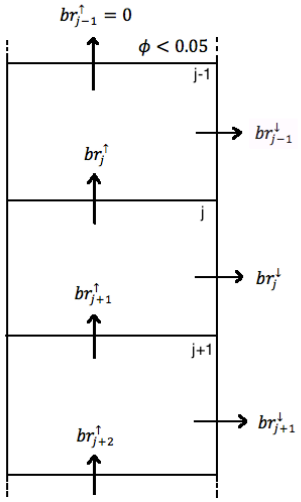

Figure 2.1 – **Schematic representation of the gravity drainage parameterization.** The brine channel is to the right and the arrows represent the brine fluxes between cells, guaranteeing mass conservation. (Modified from GN2013)

To conserve mass, for a downward transport of brine from a given cell *j*, an equal amount of brine must be transported upward from the cell below it. A simple schematic is shown in Figure 2.1. In this scenario, the element *j*-1 is the uppermost 'active' layer. Above this layer, where the liquid fraction is below the critical porosity for gravity drainage, fluid flow due to convective overturn will not occur. Therefore, the only flow in element *j*-1 is downward transport through brine channels ($br_{j-1}^{\downarrow}$) and incoming brine flow from layer *j* ($br_j^{\uparrow}$). Using an upwind strategy all the incoming and outgoing brine flows can be calculated (i.e. $br_{j+1}^{\uparrow} = br_j^{\downarrow} + br_j^{\uparrow}$, $br_{j+2}^{\uparrow} = br_{j+1}^{\downarrow} + br_{j+1}^{\uparrow}$, etc.).

Heat and salt are transported via these brine flows. Thus, alongside the one-dimensional advection-reaction-dispersion model, for every time step, the heat and salt transported via the density driven convection parameterization is calculated using the brine flows, producing a heat and salt sink/source term for each layer *j*. The heat and salt sink/source terms are utilized in equations (1) and (2), respectively, to simulate the evolution of the forming ice with the inclusion of one-dimensional parameterized density driven convection. Equations (1) and (2) now become:

$$\overline{\rho c}\frac{\partial T}{\partial t} = -\rho_{br} c_{br} w \frac{\partial T}{\partial z} + \frac{\partial}{\partial z}\left(\bar{k}\frac{\partial T}{\partial z}\right) - \rho_{ice} L \frac{\partial \phi}{\partial t} + Q_{source} \tag{11}$$

$$\phi \frac{\partial S_{br}}{\partial t} = -w \frac{\partial S_{br}}{\partial z} + \frac{\partial}{\partial z}\left(\overline{D}\frac{\partial S_{br}}{\partial z}\right) - \frac{\rho_{ice}}{\rho_{br}} P_S S_{br} \frac{\partial \phi}{\partial t} + S_{source} \tag{12}$$

where the *source* terms are calculated using the previous time step's liquid fraction, temperature, and salinity values. These new source terms account for the one-dimensional advection terms' inability to simulate convection.

2.2.3 Platelet Ice Accretion

The accretion of frazil and platelets once again alters the ice-ocean interface. In order to test the sensitivity of floating ice evolution to variations in platelet ice characteristics and the impact of variable supercooling on ice and platelet layer thickness, a method for parameterizing platelet ice accretion was developed that can be used in a continuum scale representation of sea ice formation. The model calculates an accretion rate

in two steps. First, the enthalpy method described above is utilized to predict the frazil/platelet production rate in the water column (this step is thermodynamically independent of the reactive transport model described in Section 2.2 and is used solely to predict the volume of ice nucleated and grown in the water column due to supercooling). Second, for a given platelet ice crystal size distribution, a vertical mass flux is calculated based on a force balance of rising frazil/platelets (for a 1 cm [radius] platelet with a rise velocity of ~0.02 m/s the Reynolds number is ~114).

For a given amount of supercooling (e.g. 40 mK for the upper water column of McMurdo Sound [*Hughes et al.*, 2014; *Robinson et al.*, 2014]) and a given time discretization (e.g. dt=50 s) the enthalpy method is used to calculate the change in ice volume fraction over a specified spatial grid node (e.g. dz=1 cm). Next a prescribed probability distribution is used to represent the sizes of the platelets present in this layer. This is a parameter space that will be varied as the actual population distribution of platelet sizes may be broad and is not well constrained [*McFarlane et al.*, 2014] (See Section 2.4.3.1). Using an inverse exponential probability distribution:

$$P(R) = a\exp(-bR) \tag{13}$$

where a and b are constants, and R is the platelet radius. The constant b is chosen ahead of time, while the constant a is calculated based on the total volume of platelet ice that is formed due to supercooling (calculated using the enthalpy method). The range of R has been limited to be between 0-10cm (variations in maximum radii have been explored in Section 2.4.3.1). An example of the pre-weighted probability distribution can be seen in

Figure 2.2. To calculate a volume flux (and then accretion rate) of rising platelet ice the constant *a* must be chosen so that the total amount of platelet ice in the layer (the integral area of the probability distribution) is equal to the solid fraction calculated using the enthalpy method. This is easily done using the equality:

$$a = \frac{1 - \phi_{En}}{\int_0^{0.1} \exp(-bR)} \tag{14}$$

where ϕ_{En} is the liquid fraction remaining in the layer subject to supercooling after a time step *dt*. This can be translated to a volume distribution using the density of ice and the size of the layer (*dz*). The next step in acquiring an accretion rate is calculating the rise velocity of the suspended platelets. This is done by balancing the buoyancy force and the drag force on a given platelet, assuming platelets do not interact hydrodynamically with each other, and solving for velocity:

$$\vec{F}_B = \vec{g}(\rho_{sw} - \rho_{ice})\pi R^2 h = \frac{1}{2}\rho_{sw} v^2 c_d A = \vec{F}_D \tag{15}$$

where $\vec{F}_B$ is the buoyancy force, $\vec{F}_D$ is the drag force, *R* is the platelet radius, *h* is the platelet height, *v* is the rise velocity, c_d is the drag coefficient, and *A* is the platelet cross sectional area. To rewrite the solution in terms of the platelet radius, *R,* an aspect ratio, $a_s = h/R$, is introduced that assumes the platelets exist as flattened cylinders. This is done for simplicity, as the complex and unique geometry of the suspended ice crystals will undoubtedly result in associated complex rise dynamics [*McFarlane et al.*, 2014]. The

aspect ratio and drag coefficient are variable parameters that are not well constrained by observations. Sensitivity analysis was conducted to investigate the feasible limits of platelet dynamics and accretion, and the effects of platelet properties on the overlying ice evolution (See Section 2.4.3.1). Substituting the aspect ratio into equation (15) and solving for velocity gives:

$$\vec{v} = \sqrt{\frac{2\vec{g}(\rho_{sw} - \rho_{ice})a_s R}{\rho_{sw} c_d}} \tag{16}$$

An example of the platelet size dependent rise velocity can be seen in Figure 2.2. Multiplication of the rise velocity distribution by the population distribution produces a platelet flux distribution that, when integrated, will give the solid fraction flux passing through a horizontal plane in the water column (Figure 2.2). This solid fraction flux is used as the buoyancy driven accretion rate. During a simulation, for a given time step *dt*, the advection-reaction-diffusion model and the one-dimensional convection model are allowed to stabilize, then an amount of solid ice, equal to the accretion rate times the time step *dt*, is added to the lowest multiphase layer. The only exception to this is when the bottom multiphase layer is below a pre-set critical porosity, ϕ_c (i.e. the combined solid fraction [congelation ice formed via heat loss to the atmosphere + accreted platelet ice] at the ice-seawater interfacial node is greater than (1-ϕ_c)). In this case the ice is added to the liquid layer below it. This ensures that the simulated sub-ice platelet layer does not exceed observed solid fractions by accretion alone (typically anything less than $\phi \cong 0.7$).

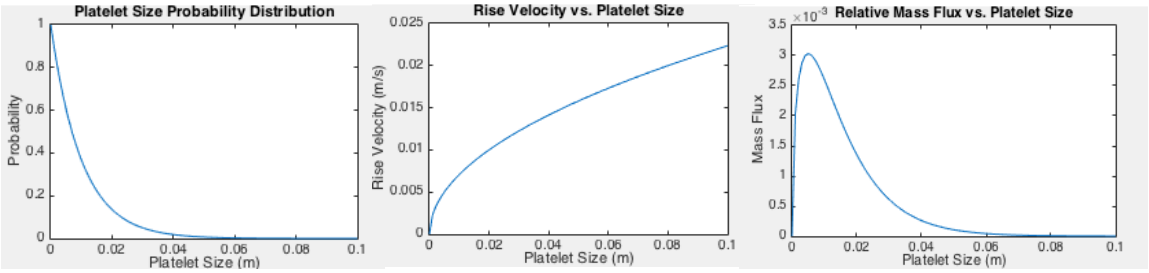

Figure 2.2 - The platelet size probability distribution (left), platelet rise velocity distribution (middle), and relative mass flux (right) used to determine platelet ice accretion dynamics in the model were constructed using equations 13-16. It is assumed that smaller platelets dominate the size distribution. The buoyancy-drag force balance dictates that larger plate will sediment out of the water column more rapidly, resulting in the mass flux distribution seen at right.

2.3 Results

In addition to the simulation of realistic sea ice cores (Section 2.3.2) the model was run under simplified conditions to simulate the dynamics of pure substance melting (The Stefan Problem) to validate its accuracy against the known analytical solution (Section 2.3.1). The numerical model produced melting front propagations and liquid fraction profiles that agree well with the analytical solution. Additionally, sensitivity studies were performed to test the capability of the model to handle a wide range of parameter space and to investigate the effects observationally unconstrained parameters may have on the properties and evolution of forming sea ice (Section 2.4.3). Modifying the population distribution and variables governing the dynamics of forming and accreting platelet ice appreciably affected the growth rate of the forming sea ice. Varying the relationship coefficient (α) dictating the efficiency of brine expulsion from the growing sea ice impacted both growth rates and overall salt content of the forming ice. The permeability-

porosity relationship utilized is shown to drastically effects the chemical characteristics of growing sea ice. Finally, changing values of the partition coefficient (P_S) minimally affected the salt content in the simulated ice.

2.3.1 Validation Using a Stefan Problem

To ensure the accuracy and capabilities of the model it was tested against a simplified melting scenario with a known analytical solution; a Stefan problem. The classic Stefan problem describes the temperature and phase change evolution of a pure substance with isotropic and homogeneous diffusivity when a thermal boundary condition induces either solidification or melting of the substance. Stefan problems are well documented in the literature [*Rubinšteĭn*, 2000] and for a detailed description of the formulation used here the reader is directed to [*Huber et al.*, 2008]. In this case, we simulate a one-dimensional column of fresh water ice initially at its melting temperature (T_m) and then apply an increased temperature to the upper boundary (T_{top}). The result is the propagation of a melting front driven solely by thermal diffusion and the latent heat of fusion. The time dependent position of the ice-water interface for this simulation has the analytical solution:

$$x_m(t) = 2\lambda\sqrt{\kappa t} \qquad (17)$$

$$\lambda \exp(\lambda^2)\,\mathrm{erf}(\lambda) = \frac{St}{\sqrt{\pi}} \qquad (18)$$

where $x_m(t)$ is the location of the ice-water interface at time *t*, κ is the thermal diffusivity of ice, and λ is solved for using the Stefan number, *St*, defined as $St = c(T_{top} - T_m)/L$, where *c* is the specific heat of ice and *L* is the latent heat of fusion for the ice-water phase

transition. Both the model output and the analytical solution can be seen in Figure 2.3. The simulated results are in excellent agreement with theory which allows for a confident application of the model to more complex freezing and melting problems that lack an analytical solution.

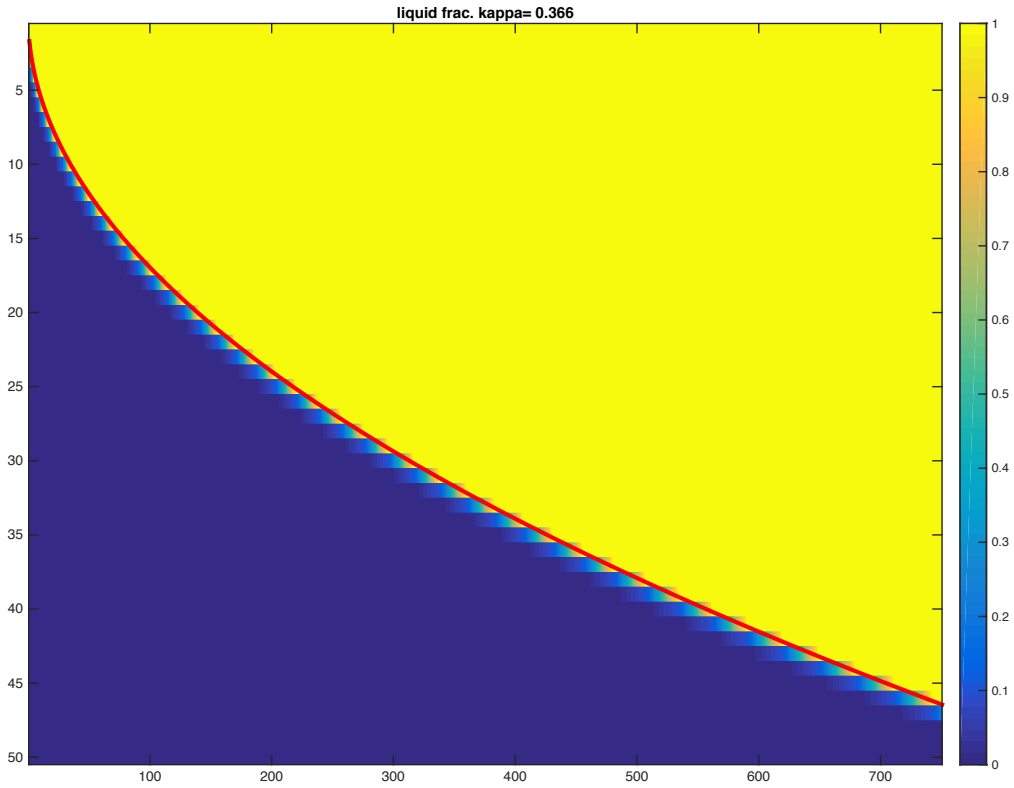

Figure 2.3 – **Model results validated against the analytic solution to the Stefan problem.** Density plot showing the results of the numerical model (blue-yellow corresponding to pure solid-pure liquid), along with the analytical solution to the Stefan problem (red line) for a thermal diffusivity, $\boldsymbol{\kappa = 0.366}$. The x- and y-axis represent de-dimensionalized time and length scales, respectively.

2.3.2 Sea Ice Core Simulations

The model was used to simulate sea ice growth under realistic environmental conditions for the McMurdo Sound (Antarctica) to both test the model, and to investigate

the role of platelet accretion in sea ice growth. The McMurdo runs implemented environmental conditions described by [*Dempsey et al.*, 2010] (from here on D10) to reproduce three ice cores extracted and analyzed in the Austral summer of 2007. D10 extracted a total of six sea ice cores from a west to east transect just north of the McMurdo Ice Shelf terminus, an area heavily influenced by a supercooled ice shelf water plume [*Dempsey et al.*, 2010; *Robinson et al.*, 2014]. The cores were analyzed for structural and compositional properties, resulting in profiles of ice texture (columnar, granular, and incorporated platelet ice) and salinity. Here we focus on three distinct cores, (using the vernacular from D10, see Figure 2.4) W1, W3, and E-type (E1-E3), chosen for the theorized disparate conditions under which they formed. The western cores are thought to have formed in a region more heavily influenced by the buoyant ice shelf water plume, resulting in a higher degree of localized supercooling in the underlying water column, producing the greater relative platelet ice abundance observed in their respective ice cores. The three core types also display unique predicted freeze over dates, constrained by satellite data, allowing for investigation of how surface temperature impacts sea ice characteristics.

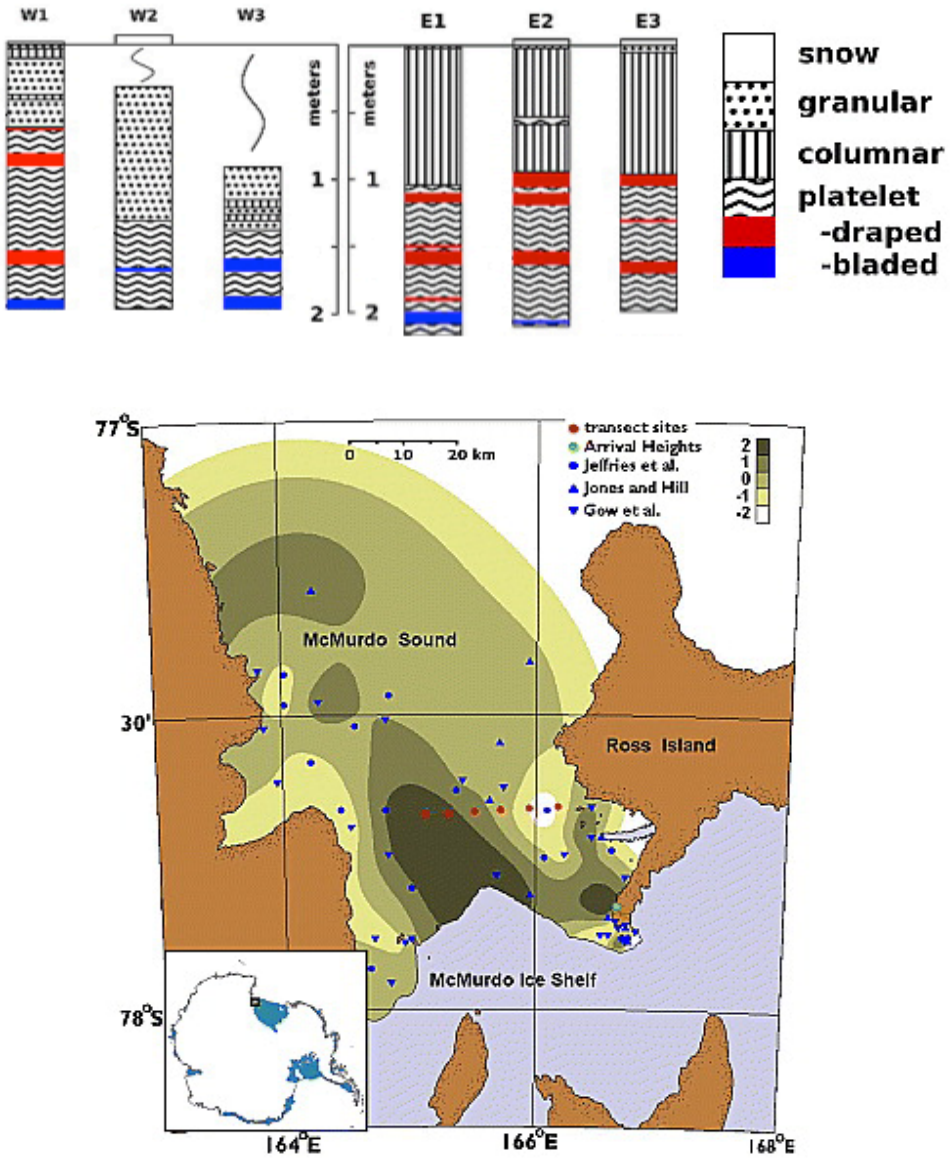

Figure 2.4 – **Platelet ice contribution to the sea ice cover in McMurdo Sound, Antarctica is influenced by local ocean conditions.** Adapted from [*Dempsey et al.*, 2010]. Top – Depiction of the results of the structural analysis carried out on the extracted sea ice cores, highlighting variations in crystal texture with depth. Bottom – Geographical representation of the study location. The cores analyzed by D10 are shown in red, and progress from left to right in line with the above ice core structure diagram. The white to brown shading of the sound is a measurement of relative platelet ice abundance utilizing the D10 results and other historical studies. This can be used as a proxy for the geometry and intensity of the ice shelf water plume.

2.3.2.1 Initial and Boundary Conditions

For each run a one-dimensional column of seawater (34 ppt, 100% liquid fraction, fluid at rest) just above its freezing point (-1.9 °C) is simulated. From this point forward the bottom boundary is refreshed to this ambient seawater temperature and salinity. The top boundary is subject to a simplification of a seasonally varying atmospheric temperature (Dirichlet boundary condition, see Figure 2.5). Each core's predicted freeze over date acts as the initial surface temperature and it then progresses per the temperatures given in Figure 2.5. Throughout the run the top surface is simulated as being in contact with an atmosphere containing no liquid fraction at the given surface temperature. The bottom boundary is simulated as a free slip surface in contact with ambient seawater (34 ppt, 100% liquid fraction, -1.9 °C, no fluid velocity) that can exchange heat, salt, and fluid into and out of the model domain.

Vertical transport of solid ice through the model domain is not modeled, therefore, to simulate platelet formation and transport in the water column an additional thermal profile tracking supercooling is kept separately. This ensures that immobile solid fraction does not form throughout the water column during simulations but is utilized alongside the enthalpy method to calculate the platelet ice accretion rate (eq. 13-16) at each time step. The oceanic boundary is forced by a simple spatially and temporally varying amount of supercooling, simulating an ice shelf water plume impinging upon the base of the sea ice. The seasonal supercooling for the W1, W3, and E-type ice cores can be seen in Figure 2.5, where the cores are subject to an ambient supercooling of 17.5 mK until the central portion of the sound begins to freeze over at which point the supercooling is amplified in line with the relative platelet ice abundance presented in D10 (See Figure 2.4). The supercooling in

the central portion of the plume is set to 50 mK (in agreement with maximal supercooling values measured in the area [*Hughes et al.*, 2014; *Robinson et al.*, 2014]), falling off to 40 mK by the W3 core, and finally 25 mK for the E-type cores. Here we take advantage of the model's ability to accommodate variable supercooling to demonstrate the effects it has on ice core structure. Improvements to plume geometry and temporal variability and their effects on sea ice evolution are left for future development.

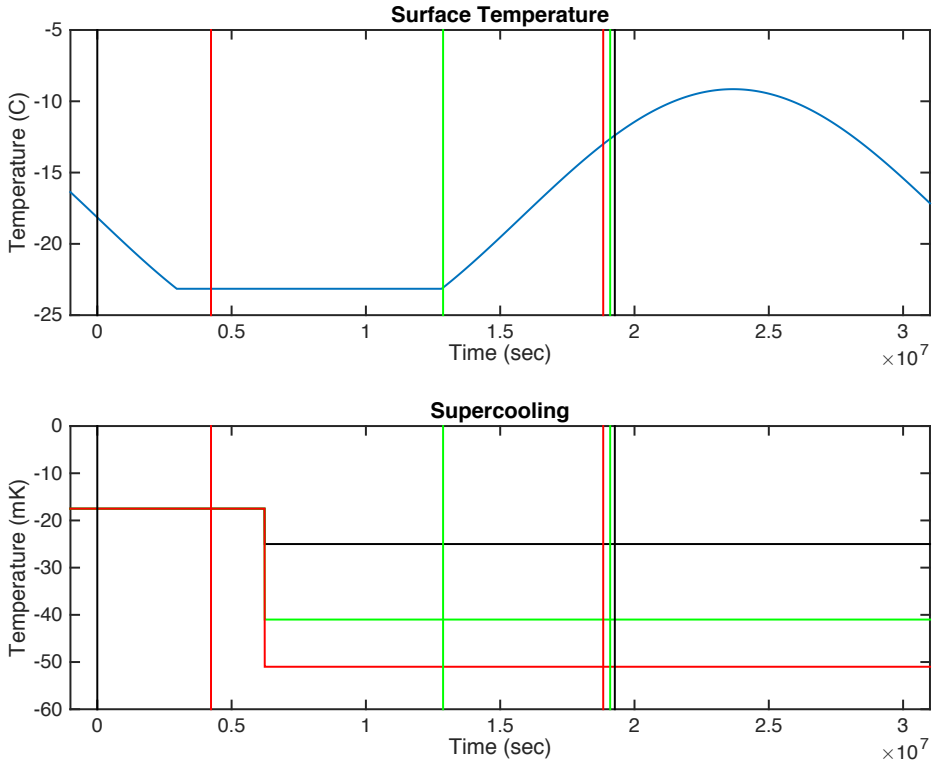

Figure 2.5 - Boundary conditions used during the model runs. Top – Surface temperatures used for the no-slip upper boundary (blue). E-type, W1, and W3 ice core start and stop times can be seen in black, red, and green, respectively. Bottom – Supercooling values used to force the formation and accretion of platelet ice throughout the model runs. Color coded as above, vertical lines represent start and stop times and the variable supercooling can be seen after ~6x10^6 sec.

2.3.2.2 Simulated Ice Cores

Model runs for each core type were carried out utilizing the estimated freeze over dates, simulation durations, and supercooling values listed in Table 2.1 (also listed are the range of freeze over dates predicted by D10 and the dates the cores were extracted). Color density plots of the physical, chemical, and thermodynamic profiles produced by the model are shown in Figure 2.6, which displays the entire numerical simulation of the W3 ice core. These profiles allow for high temporal (dt=50 s) and spatial (dz=1 cm) resolution of the evolution and dynamics occurring during the formation of congelation sea ice affected by platelet ice accretion. The model can accurately simulate variable boundary and initial conditions, the realistic reactive transport phenomenon observed in natural sea ice, and the inclusion of platelet ice accretion. A comparison of the vertical properties of the ice cores simulated during the model runs to the observations made by D10 is given in Figure 2.7. Layers demarcated as 'platelet ice' have more than 10% of their volume fraction made up by accreted platelet ice, in line with the ice core structure characterization used by D10. Throughout the simulations the only parameters that differ between the three core types are the level of supercooling in the underlying water column and the freeze over/extraction dates, all other free parameters (drag coefficient, convection parameterization coefficient, platelet aspect ratio, etc.) are chosen *a priori* using values in the median of realistic parameter space and are held constant for all runs. The model results are in excellent agreement with the observations of D10, utilizing conditions well within the predicted range for McMurdo Sound [*Dempsey et al.*, 2010; *Hughes et al.*, 2014; *Robinson et al.*, 2014]. Temporally varying ice core profiles of temperature, salinity, liquid fraction, and total salt content can be extracted to easily visualize the year-long evolution of the ice at each location (W1, W3, E-type), examples of which can be seen in Figures 2.8.1-2.8.3. The

thermal, chemical (salinity, total salt content), and structural (liquid fraction, ice texture – congelation vs. platelet ice) profiles are in good agreement with both observation and theory: these reveal a primarily conductive temperature profile, a low but non-zero porosity ice structure with a highly porous basal layer, and a progressively desalinating 'c-shape' total salinity profile [*Malmgren and Institutt*, 1927].

Table 2.1 – Comparison of Simulated Ice Cores and Field Observations: Summary of boundary conditions, model results, and empirical observations of ice core structure

Ice Core	W1	W3	E-type
Supercooling (Model) (mK)	17.5-50	17.5-40	17.5-25
Congelation-Platelet Transition (D10) (cm)	60	46	94-104
Congelation-Platelet Transition (Model) (cm)	61	48	102
Total Core Length (D10) (cm)	197	105	199-218
Total Core Length (Model) (cm)	192	105	196
Total Run Duration (Model) (day)	169	72	223
Total Freeze Duration (D10) (day)	113-169	55-72	150-260

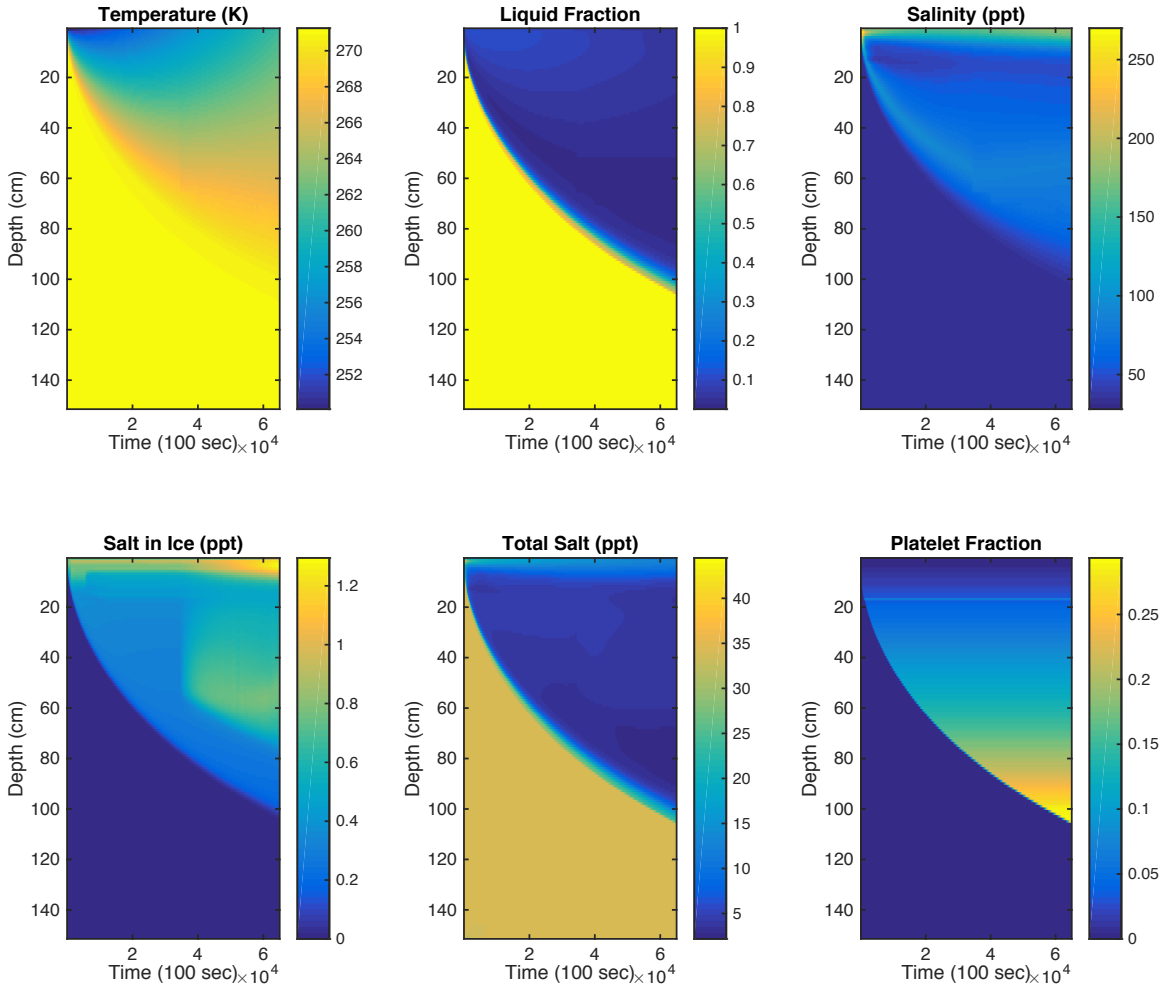

Figure 2.6 – Density plots displaying the entire numerical simulation of the W3 ice core reveal its spatiotemporal evolution through the freezing season. The notable jump in the 'Salt in Ice' is associated with the minimum permeability cutoff imposed in the gravity drainage parameterization, which effectively traps salt in pockets where it precipitates out of solution. The brief jump in the 'Platelet Fraction' at ~18cm is associated with the onset of convection as it briefly impedes the propagation of the freezing front. This onset can be seen in the ice 'Salinity' as well, represented by a decrease in salinity when the sea ice reaches this critical thickness.

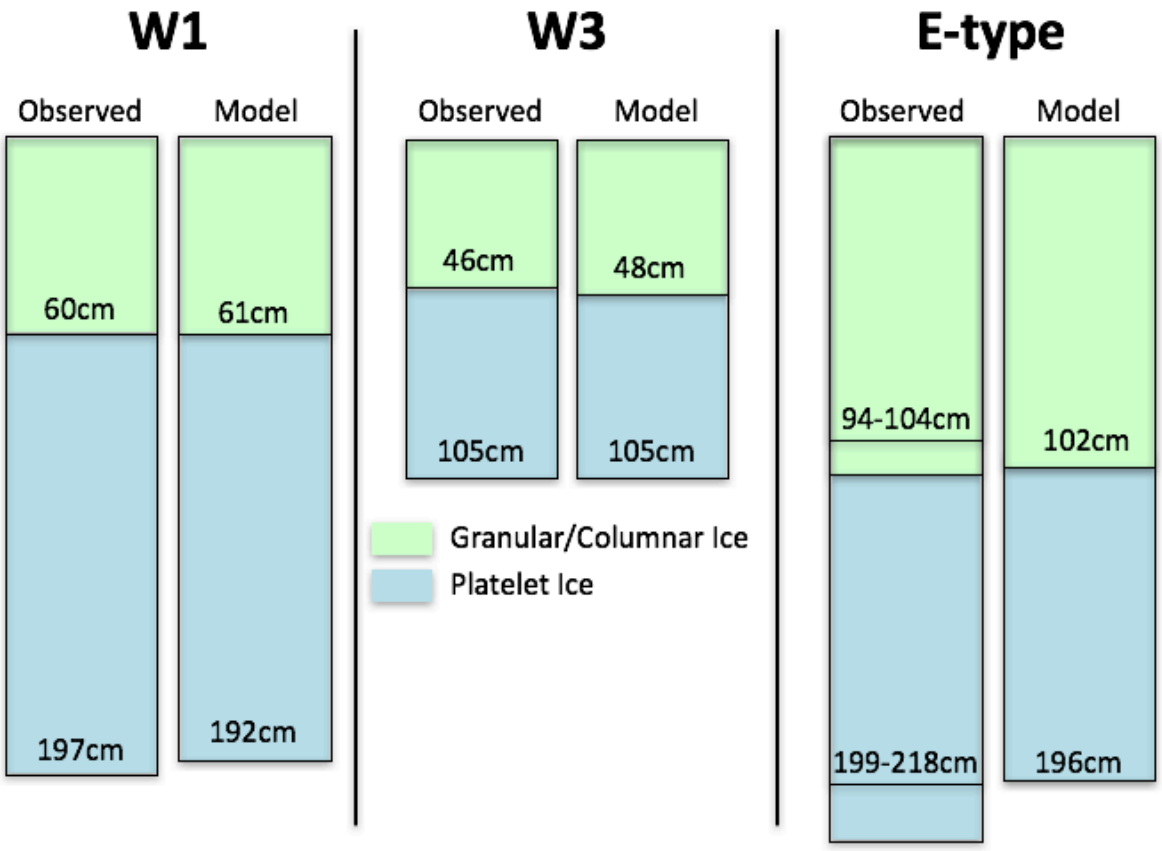

Figure 2.7 – **Modeled ice profiles depicted in Figures 2.8.1-2.8.3 are able to match the E-type, W1, and W3 cores described by [*Dempsey et al.*, 2010]**. Platelet ice is defined as ice with a platelet ice fraction greater than 10%, following [*Dempsey et al.*, 2010].

2.4 Discussion

2.4.1 Comparison to Field Observations

The profiles produced by the numerical simulation agree well with the observations made by D10. In nearly all cases, the qualitative structure of the salt content, temperature, and porosity profiles, as well as their simulated values, are in line with those seen in the

actual cores extracted during the D10 study (or theory and comparable studies for properties not measured in D10). In the case where the quantitative values do not mirror those seen empirically, namely total salt content, modifying free parameters in the numerical model can remedy the minimal discrepancy (See Section 2.4.3).

2.4.1.1 Structure and Temperature Profiles

The simulated ice core stratigraphies both qualitatively and quantitatively agree with the structural properties seen by D10. A layer of congelation ice is formed early in the season when temperature gradients at the basal surface of the ice are high. Even in the presence of a supercooled water column the advancing ice-ocean interface propagates at a rate that quickly consumes any accumulating platelets, leaving a granular or columnar texture as the dominant crystal fabric. This can be seen in Figures 2.6, 2.7, & 2.8.1-2.8.3 where a low platelet fraction persists throughout the upper portion of the ice. Later in the season, when surface temperatures have begun to increase and the sea ice growth from heat loss to the atmosphere slows, the crystal fabric becomes dominated by incorporated platelet ice. This occurs in situations with variable supercooling (as in cores W1 and E-type, where an amplification in supercooling is initiated at a preset date) and with constant supercooling (as in core W3, that was subject to 40 mK of supercooling throughout its formation). During the spring-summer season, when the ice cores were extracted, the temperature gradients at the basal surface of the ice were at their lowest and if sufficient supercooling persists, a sub-ice platelet layer forms.

A sub-ice platelet layer can be seen beginning to form for the W1 core in Figure 2.8.2. This core has the highest supercooling (50 mK) and thus has the highest propensity

for forming this layer. It is characterized in the numerical model output by the sharp downward propagation of an ice layer with a porosity equal to the pre-set critical porosity, ϕ_c, demarcated by the dashed line in Figure 2.8.2. There are some instances where simulated ice cores have total lengths and/or congelation-platelet ice transitions that minimally vary from observations. These variations are only a few centimeters and modifying the environmental parameters (e.g. surface temperature, supercooling, freeze duration, platelet size distribution, etc.) could quickly remove any discrepancies (See Section 2.4.3).

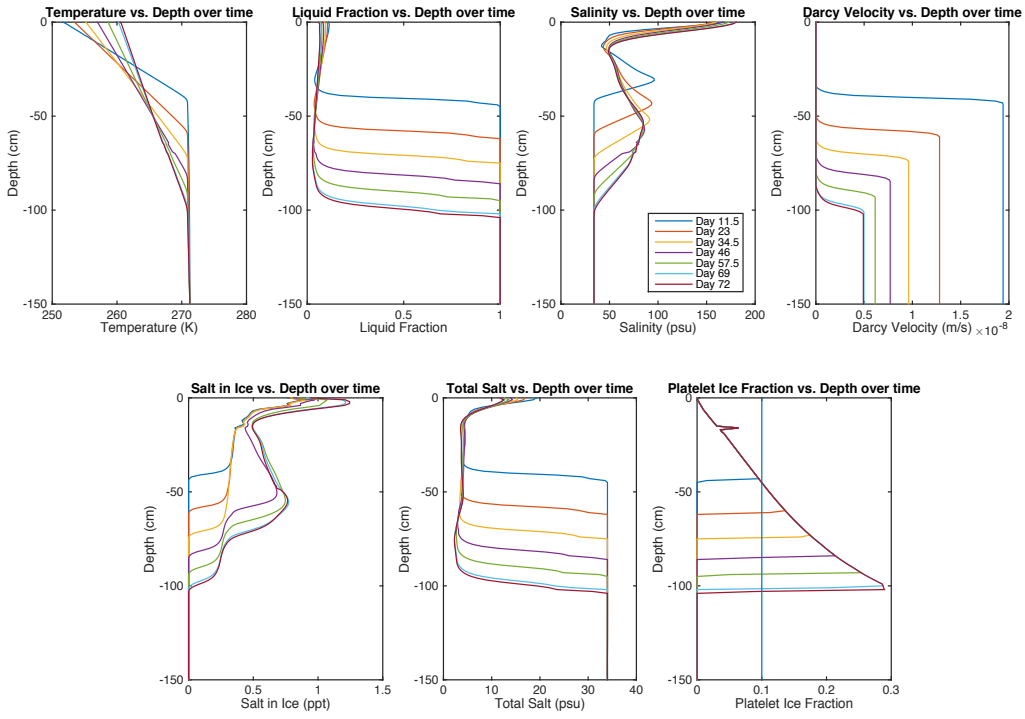

Figure 2.8.1 - Temporally varying vertical profiles produced by the model for the W3 ice core. Vertical line in the Platelet Ice Fraction plot represents 10% volume fraction of platelet ice.

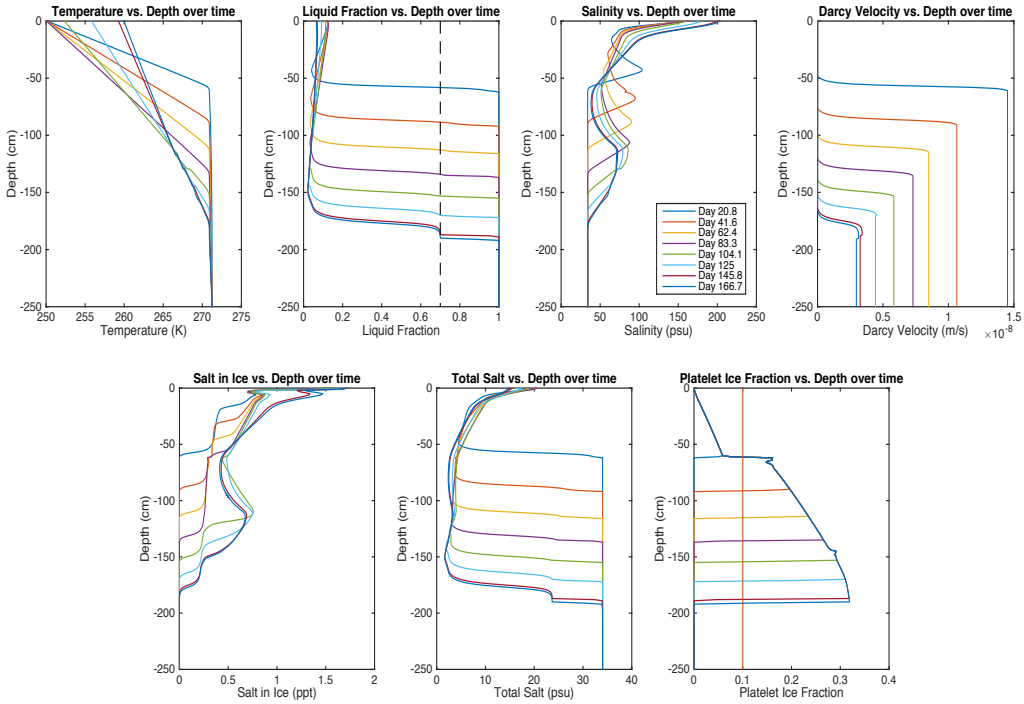

Figure 2.8.2 - Temporally varying simulated vertical profiles for the W1 ice core. The dotted line in the liquid fraction plot denotes the critical porosity of 0.7 set for the accreting platelet ice. Vertical line in the Platelet Ice Fraction plot represents 10% volume fraction of platelet ice.

Simulated temperature profiles agree with thermodynamic predictions as well as field measurements using thermistor arrays frozen into growing sea ice [*Perovich et al.*, 1997; *Petrich and Eicken*, 2010; *Thomas*, 2017; *Thomas and Dieckmann*, 2008]. An equilibrated conductive profile is expected due to the high thermal conductivity of ice (compared to brine or seawater). This allows the ice layer to reach thermodynamic equilibrium at a faster rate than the ice-ocean interface propagates, leading to a linear temperature profile between the surface and the ambient ocean. The agreement between the model and both theory and observations is shown in the temperature profiles of Figures 2.8.1-2.8.3.

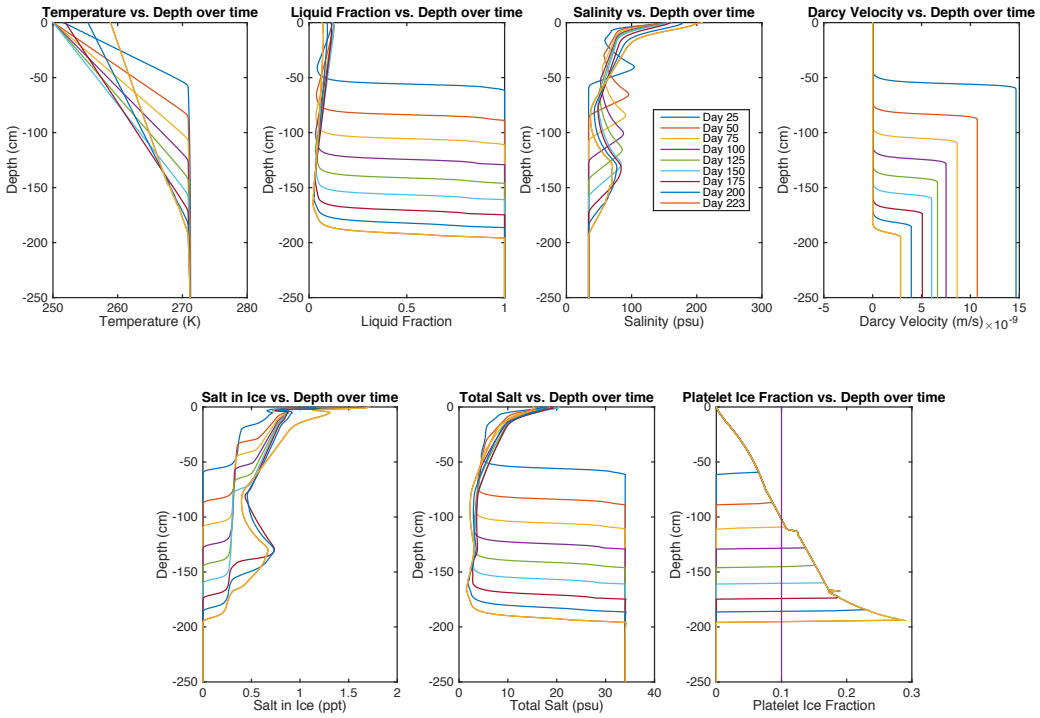

Figure 2.8.3 - Temporally varying simulated vertical profiles for the E-type ice core. Vertical line in the Platelet Ice Fraction plot represents 10% volume fraction of platelet ice.

2.4.1.2 Salt in Sea Ice

The total salt profile in young first year sea ice (before surface melting initiates) typically has a 'c-shape' profile with increased salt concentrations at the ice-atmosphere and ice-ocean interfaces. While this has been well documented by field observations for nearly a century (see [*Malmgren and Institutt*, 1927]), numerical models of sea ice struggle to reproduce total salt values without assuming an *a priori* salt distribution, and frequently underestimate the bulk salinity of sea ice [*Turner and Hunke*, 2015]. The models utilizing *a priori* salt distribution parameterizations can more closely reproduce total salt content values for some ice cores, but inevitably not for others, as they take no account of how the environment affects the salt distribution within the ice. Sensitivity analyses reveal that the

local environment and the ensuing ice dynamics uniquely determines the chemical profile of the ice that forms (See Section 2.4.3, Figures 2.10 & 2.11). The goal of successfully incorporating sea ice models into Earth systems models relies on the interaction between the ice, the ocean, and the atmosphere, thus in this model we choose to forego *a priori* assumptions and utilize environmental conditions and conservation equations to determine the total salt profiles. The model results produce the characteristic 'c-shape' profiles quite well, but suffer from an underestimation of total salt, with average bulk salinities 1.63-3.27 ppt below those measured by D10 (likely due to the lack of constraint on a number of variable parameters – See Section 2.4.3). Most importantly, these results highlight the need to constrain the dynamics that dictate brine motion throughout the ice, namely gravity drainage. Heterogeneous brine pocket/channel distribution, dead-end conduits, capillary forces, and permeability-porosity relationship errors are all factors that could reduce brine flux out of the forming ice, and in turn increase total salt content relative to the idealized case modeled here.

2.4.2 Implications of Platelet Ice Accretion

The ice core simulations help constrain which conditions are capable of producing the ice stratification observed in the D10 study, allowing us to better understand ice shelf-ocean-sea ice interactions. In addition to the model's predictive capabilities regarding the simulation of sea ice thickness and properties under the influence of known environmental forcing, including platelet accretion due to oceanic supercooling, it can be implemented to reconstruct atmospheric and oceanic conditions during the time of freezing. The ability to link observable ice core properties to historic variations in ocean and atmosphere forcing

provides a method to reconstruct the spatiotemporal evolution of remote and unique water masses that are difficult to continuously instrument. In the case of McMurdo sound, the stratigraphy of sea ice cores extracted during the Austral summer provides a proxy for the spatiotemporal evolution of ice shelf water plumes emanating from the McMurdo ice shelf – a water mass indicative of basal ablation and ice shelf mass flux. Additionally, the model includes the full suite of multiphase physics occurring within the ice layer, which is imperative in accurately capturing the microscale physics, and in turn the macroscale properties, of sea ice.

Large-scale sea ice models typically do not include the effects of supercooled waters and platelet ice, yet a large portion of fast ice around Antarctica is likely affected by these processes. The platelet abundance map of [*Dempsey et al.*, 2010] (seen in Figure 2.4) suggests that the ice shelf water plume emanating from beneath the McMurdo Ice Shelf likely impacts sea ice up to 80 kilometers from the ice shelf front, meaning thousands of square kilometers of sea ice in McMurdo Sound alone are potentially modified by platelet ice accretion. To test the role of platelet ice accretion in stimulating sea ice growth, ice growing under identical conditions but subject to *no* supercooling was simulated and compared to the supercooling case. These results are shown in Figure 2.9. The discrepancy between the two scenarios amounts to a 15 cm difference in sea ice thickness, a ~14% variability. This comparison shows that platelet ice accretion has the potential to drastically alter the thickness and mass balance estimates of an extensive area of sea ice. These modified estimates have the potential to improve the accuracy of not only sea ice models,

but also large-scale models of the cryosphere, ocean, and climate that hope to incorporate the dynamics and effects of sea ice.

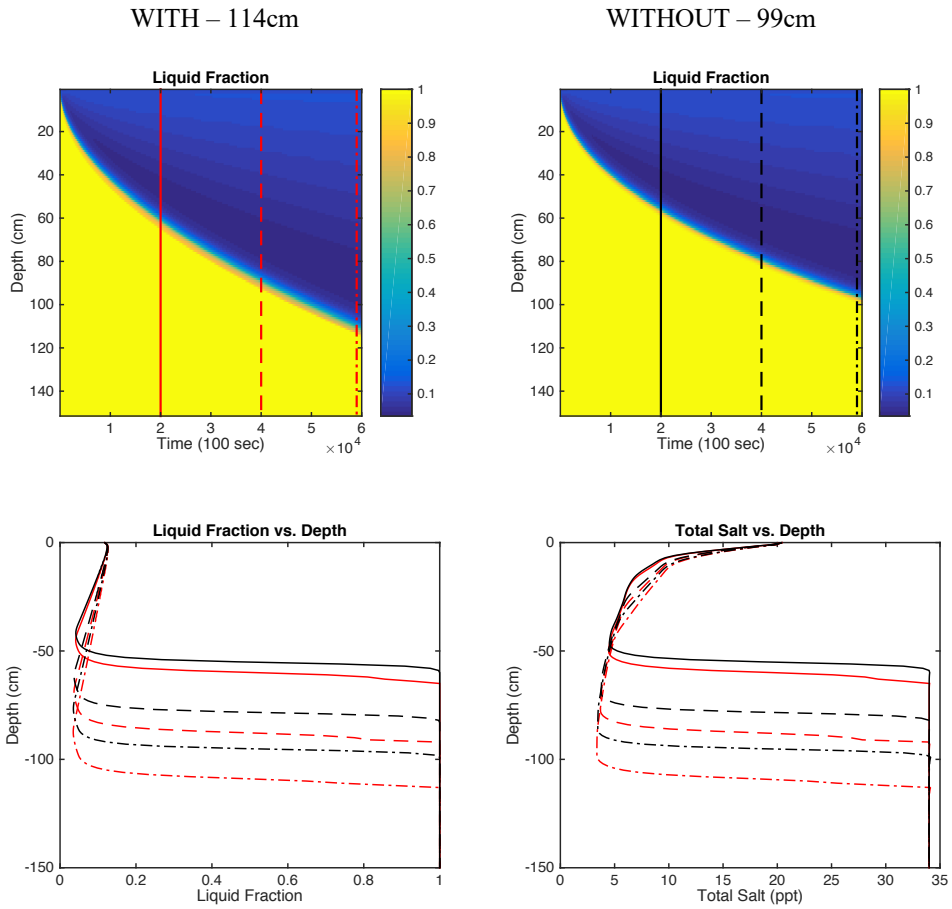

Figure 2.9 – The influence of ocean conditions and platelet ice on the properties of sea ice. (Top) Density plots showing the output of two identical model runs, save for the application of a 40 mK supercooled water layer to the lower portion of the *left* plot. (Bottom Plots) Liquid fraction and bulk salinity evolution for both scenarios (line varieties correspond to vertical lines in the density plots).

Using this approach, the brine flux out of the growing ice layer can be tracked. This influx of hypersaline water into the ocean is a catalyst for the production of high salinity shelf water and also affects buoyancy driven circulation of the Southern Ocean (e.g. [*Goosse and Fichefet*, 1999]). An increasing number of ocean simulations include this

source of dense, saline water in their model architecture. The multiphase platelet ice model presented here could provide accurate source terms for these ocean models and improve the sea ice component of coupled ice-ocean models.

While these simulations focus on the high thermal gradient conditions in sea ice, the same approach can be used to simulate dynamics occurring beneath Antarctic ice shelves. Marine ice forms through a similar accretion process, although with reduced supercooling values due to the slow ascension of melt water along the underside of the shelves [*Galton-Fenzi et al.*, 2012; *Khazendar and Jenkins*, 2003]. The model can easily accommodate low temperature gradients at the basal surface of ice shelves and can be used to reproduce multiple years of marine ice accretion and ensuing dynamics. While models exist that simulate the basal accretion and ablation of ice shelves, these models do not simulate the multiphase processes within the accreting marine ice, which could better constrain its properties (thermal, chemical, and physical) and will dictate the solute flux into the top layer of the water column. Understanding the formation and evolution of marine ice is crucial to understanding the mass redistribution of ice shelves, the impact it may have on stabilizing these floating ice masses, how marine ice may impact sea ice formation, and the effects a changing climate has on our world's meteoric ice budget.

2.4.3 Sensitivity Analysis

Several variables can potentially affect the output of the simulation, given the complexities considered here. Additionally, due to limited observational data the values of many relevant variables are not well constrained. Here key variables are discussed, and

sensitivity studies are presented that demonstrate the impact these variables have on the evolution of the overlying ice.

2.4.3.1 Platelet Ice Dynamics

Likely the least constrained portion of the model is the production and evolution of frazil/platelet ice crystals in the water column and their accretion onto the basal surface of the sea ice. The enthalpy method guarantees conservation of energy and thus accurately accounts for the mass of ice produced, however how this ice mass is distributed among platelet shapes and sizes in the water column is largely unconstrained. Crystals have been documented to range from millimeters to centimeters, possessing 'high' aspect ratios (proposed ratios range from 1:10-1:100) [*McGuinness et al.*, 2009], and the overall size distribution has at most been qualitatively documented. All of these properties can influence the overall ice flux onto the overlying ice and thus the overall ice thickness. The drag coefficient of the rising platelets (eq. 15) is an additional unconstrained parameter, although it likely varies over a much smaller magnitude. Finally, the packing efficiency of the rising crystals, governed by ϕ_c, can influence the thickness of the sub-ice platelet layer, the overall sea ice thickness, and sets the liquid fraction of the forming platelet layer, in turn determining its volume averaged quantities. Measuring this packing efficiency amounts to measuring the porosity of the newly accreted sub-ice platelet layer, thus far *in situ* measurement of this quantity has proven difficult, as the layer is difficult to access, fragile and cannot be sampled with coring.

Sensitivity studies were carried out wherein identical initial and boundary conditions were utilized while one of the aforementioned variables was altered from its

baseline value. The results can be seen in Figure 2.10. It is evident that a number of variables substantially affect the evolution of the simulated sea ice, most notably its growth rate. Most modifications to the baseline values result in logical model outputs. Reducing the drag coefficient and considering a linear platelet size distribution, which more heavily favors larger platelets than does the baseline decreasing exponential distribution, both produce increased growth rates, while decreasing the maximum platelet size or increasing the aspect ratio of the platelets decreases growth rates. There are some properties of the platelet model that, at least on short time scales, do not affect the overall ice evolution. Both a modified critical Rayleigh number and various critical porosities determining incoming platelet packing efficiency negligibly affected the simulated ice layer. These runs were carried out for relatively short total times (2×10^6 seconds). Therefore, some variables that did not noticeably affect the ice during these runs could very well affect older, more slowly forming ice. Runs simulating thicker ice during the summer season explicitly showed a critical porosity cutoff where platelet ice accretion became the dominant growth mechanism, as opposed to the congelation dominated growth of young, thin ice subject to much colder atmospheric conditions. In the late season the critical porosity uniquely determined the solid fraction of the lowest layer of the forming ice (See Section 2.4.1.1 and Figure 2.8.2).

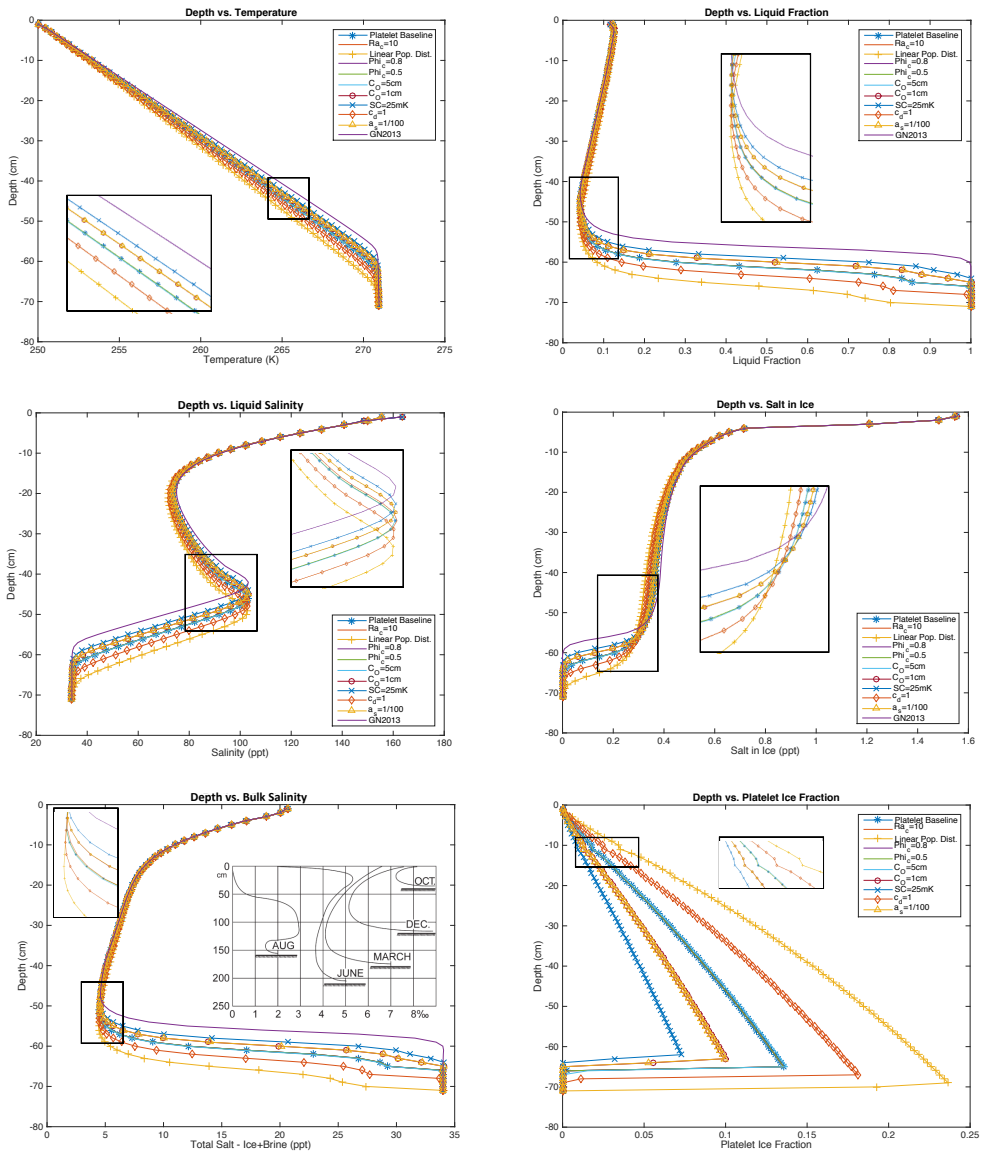

Figure 2.10 - Sensitivity analysis carried out by varying free parameters that dictate the dynamics of platelet ice accretion and parameterized gravity drainage (as seen in the legend: Platelet Baseline – control run, Ra_c – critical Rayleigh number, Phi_c - critical porosity for platelet accretion, c_0 – platelet size cutoff for population distribution, SC – supercooling, c_d - drag coefficient, a_s – platelet aspect ratio). Results are from 2.0x10^6 s (~23 days) model runs. All other parameters are held constant during the simulations. Lines without symbols produce results that vary negligibly from the 'Platelet Baseline' run. The inset from [*Malmgren and Institutt*, 1927] shows the qualitative agreement between the numerical model and observations for total salt content in young sea ice.

2.4.3.2 Salt Distribution

Two processes that can drastically affect sea ice salinity but remain 'tunable' parameters, if they are even included in models, are gravity drainage via convection and precipitated salt content. First, the convective desalination of the lower layer of forming sea ice, described in Section 2.2.2, is the primary means of expelling salt during ice growth. The quantity of salt expelled, and thus also the final ice salinity, depends on the efficiency of the convective process. In the numerical model outlined here the primary control of this efficiency is the linear relationship assumed between the local Rayleigh number and the downward flow of brine through channels, and the associated relationship coefficient α. The default value utilized for α is based on the work of [*Wells et al.*, 2010; 2011] wherein brine channels are spaced such that potential energy is minimized and brine drainage is maximized. In reality, brine channel spacing, heterogeneous porosity, and other environmental factors could lead to less than optimal brine drainage. A number of sensitivity studies were carried out utilizing various values for α to simulate less than ideal brine drainage (Figure 2.11).

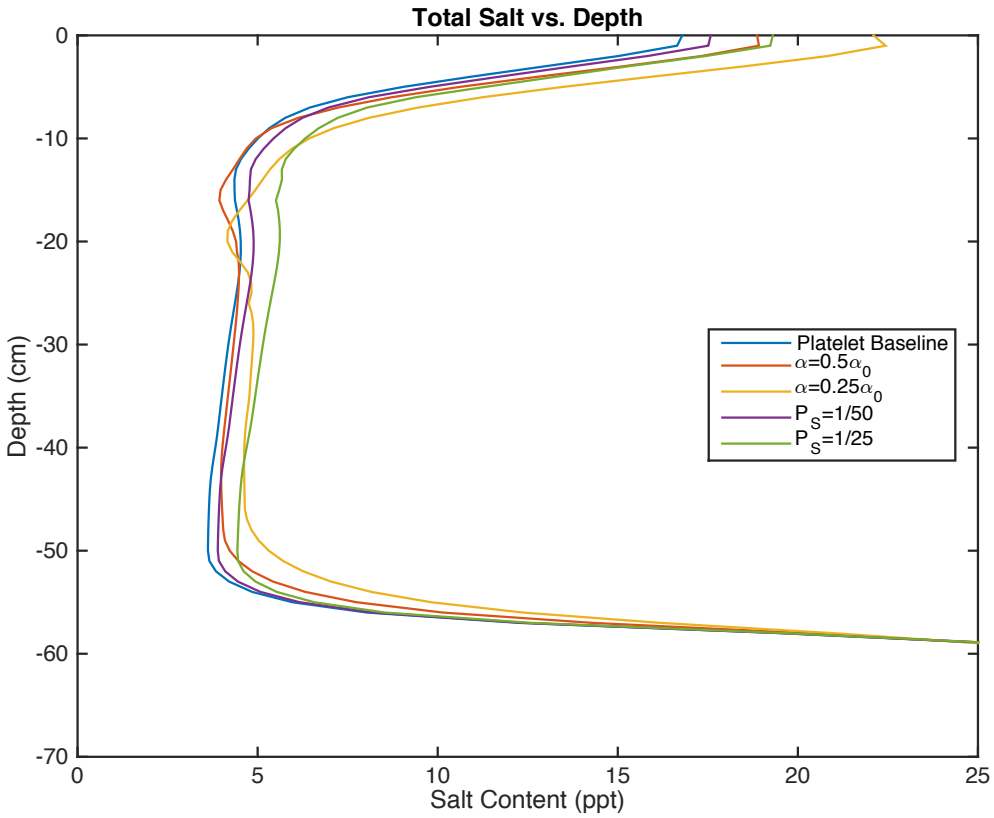

Figure 2.11 - Sensitivity of sea ice growth to variations in parameters affecting the gravity drainage (linear relationship coefficient (α)) and partition coefficient (P_S) and the impact they have on the total salt content of growing sea ice. All runs were carried out for 2.0x10^6 s (~23 days) using the identical seasonally varying surface temperatures of Figure 2.5.

The second factor affecting sea ice salinity is the quantity of salt precipitated out of the salt water solution contained in pockets and channels within the ice. As the temperature of seawater is depressed a variety of solid salts begin to precipitate. Due to the presence of sulfate in standard ocean water (~8% of 'sea salts') mirabilite ($H_2SO_4 \cdot 10H_2O$) begins to form at temperatures below approximately -8 °C. Mirabilite is a hydrated salt and its precipitation in brine pockets and tubes of first year sea ice has been observed by [*Light et al.*, 2003]. When temperatures drop below -23 °C the hydrated salt hydrohalite ($NaCl \cdot$

$2H_2O$) begins to precipitate [*Carns et al.*, 2015; *Light et al.*, 2003]. Precipitation of these hydrated salts has the potential to increase the overall salt content of the ice. Formation of solid salt crystals in highly concentrated, heavily cooled brine pockets and tubes prevents their expulsion back to the underlying ocean. In the current model the complex dynamics that determine precipitation rates and their dependence on temperature and salinity has been crudely represented via the partition coefficient P_S. While currently included as a tunable constant, the partition coefficient could be replaced with a complete implementation of salinity and temperature dependent salt precipitation, which will be included in future renditions of the model. Here the partition coefficient, and thus the precipitation rate, is varied to investigate its effect on the overall salt content of forming ice. The results can be seen in Figures 2.11 and 2.12.

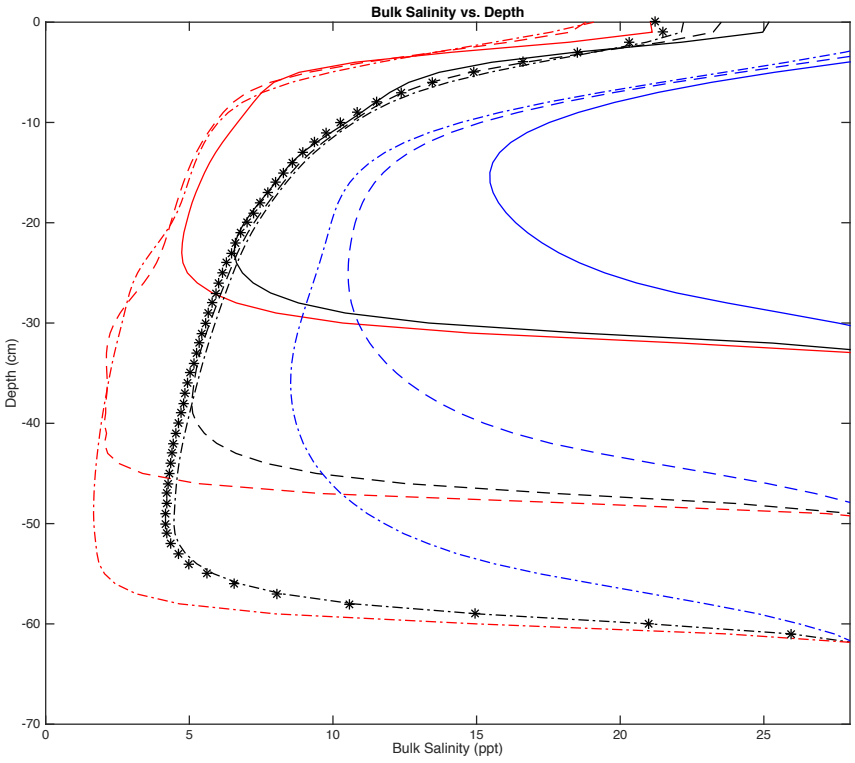

Figure 2.12 - The effects of removing the critical porosity cutoff ($\phi < 0.05$), varying the permeability-porosity relationship ($\Pi = \Pi(\phi)$), and removing the partition coefficient (P_S) on the evolution of sea ice bulk salinity. All runs were carried out for 2.0x10^6 s (~23 days) using a constant surface temperature of -23.15 ℃. Solid lines, dashed lines, and dash-dot lines correspond to 7 days, 15 days, and 23 days after the simulation is initiated, respectively. Black lines represent model runs with $P_S = 1/100$, a porosity cutoff for $\phi < 0.05$, and the permeability-porosity relationship of GN2013 $\Pi = 10^{-17} * (10^3 * \phi)^{3.1}$. Red lines represent model runs with $P_S = 0$, no porosity cutoff, and the permeability-porosity relationship of GN2013. Blue lines represent model runs with $P_S = 0$, no porosity cutoff, and a modified Kozeny-Carman equation for the permeability-porosity relationship $\Pi = \left(0.5 + \frac{1}{\pi}\arctan\left[100(0.5 - \phi)\right]\right) * (5 * 10^{-10}) * \left(\frac{\phi^3}{(1-\phi)^2}\right)$, similar to that used by [*Oertling and Watts*, 2004]. Black stars correspond to a model simulation identical to that of the black lines except $P_S = 0$ (results shown only for 23 days after initiation).

An additional difficulty, common to many simulations of porous media flow, is determining an accurate permeability-porosity relationship. A wide range of such relationships have been proposed for sea ice [*Freitag*, 1999; *Golden et al.*, 2007; *Griewank and Notz*, 2013; *Wells et al.*, 2010]. The default permeability-porosity relationship implemented in the current model is the same as that used by GN2013, and is based on the empirical results of [*Freitag*, 1999]. A critical porosity cutoff is implemented in the model, akin to that of [*Golden et al.*, 2007], however others have suggested that it may be unphysical and that a finite permeability may persist even for very low porosity ice [*Griewank and Notz*, 2013; *Petrich and Eicken*, 2010]. To investigate the effects of a critical porosity cutoff and various permeability-porosity relationships on the characteristics of growing sea ice sensitivity studies were carried out. The results can be seen in Figure 2.12, where the default model, utilizing the permeability-porosity relationship of GN2013 with a porosity cutoff of $\phi < 0.05$ and a partition coefficient, P_S,

of 1/100, is compared to simulations without porosity cutoffs or partition coefficients ($P_S = 0$), and another which utilizes an alternate permeability-porosity relationship.

The sensitivity studies clearly show that the efficiency of brine drainage as well as the partition coefficient influence the quantity of salt retained by the forming sea ice. The simulated ice grew to a depth of 62 cm in all cases (the bottom of the domain is not included in Figure 2.11 or 2.12 to highlight the variations in salt content within the ice). The depth averaged salt content of the 'Platelet Baseline' run (Figure 2.11) is 6.82 ppt, while that for $P_S = 1/25$ is 7.89 ppt. Thus, by increasing the partition coefficient by a factor of four the depth-averaged salt content increased by 1.07 ppt, equivalent to a 16% increase. For small, and likely realistic, values of the partition coefficient, assuming instead $P_S = 0$ has a negligible effect on the overall salinity of the forming ice, as can be seen in Figure 2.12. The depth-averaged salt content of the default model subject to a constant surface temperature (black lines in Figure 2.12) after 23 days is 8.73 ppt, while that of the model utilizing a modified Kozeny-Carman permeability-porosity relationship (blue lines in Figure 2.12) is 13.86 ppt, a 59% increase. This result suggests that, for sea ice, salt precipitation is unlikely to significantly contribute to the overall bulk salinity. Conversely, the results highlight the substantial impact permeability has on convective processes that ultimately determine the overall properties of forming sea ice and, therefore, the importance of identifying improved constraints on permeability-porosity correlations.

2.5 Conclusion

Sea ice is a major component of the cryosphere, yet its chemical and thermal dynamics are typically underrepresented in large scale Earth systems models. Complex

multiphase processes that dictate the formation and evolution of sea ice have been difficult to accurately simulate, but they play a crucial role in determining energy and chemical fluxes to and from both the atmosphere and the ocean. Sea ice is relevant to the formation of water masses affecting the evolution of nearby ice shelves, exhibits unique characteristics influenced by ice shelf evolution, provides a habitat for an immense biomass crucial to the polar ocean ecosystem, and acts as an analog for ice-ocean environments elsewhere in the solar system. Numerical modeling of sea ice formation and evolution can shine light on the complex dynamics occurring in sea ice, and how these microscale physics affect the macroscale properties of the ice.

The one-dimensional, multiphase reactive transport model for sea ice, incorporating mushy layer theory, gravity drainage and an energy conserving model of platelet ice formation and accretion, allows for a realistic treatment of sea ice near ice shelves, which can be dramatically affected by supercooled ice shelf water plumes. The inclusion of a multi-faceted approach results in accurate simulation of the structural, thermal, and chemical properties observed or theorized for sea ice, as evidenced by the successful reproduction of the McMurdo Sound sea ice cores analyzed by D10. We demonstrate that minor underestimation in total salt content results from an idealized gravity drainage parameterization, which provides insight into the role that heterogeneous ice structure and non-optimized drainage processes may play in sea ice evolution. Additionally, it was shown that platelet accretion can drastically affect the thickness (up to ~15%) and properties of forming sea ice, which has implications for sea ice duration and evolution in larger scale Earth systems models.

The platelet ice accretion parameterization constitutes a novel tool for future multiphase sea ice models and offers a strategy for incorporating the ice shelf driven process of platelet ice dynamics into larger systems models. Together with the multiphase reactive transport model and gravity drainage parameterization it constitutes a numerical method with predictive abilities capable of forecasting ice structure, thickness, and characteristics in diverse ice-ocean environments. Future work will focus on utilizing the model in such a capacity.

Chapter 3: Entrainment and dynamics of ocean-derived impurities within Europa's ice shell

A compact version of this chapter has been submitted to Science Advances [Buffo et al., in review]. The goal of this work was to understand the likely composition of the ice shell of Europa by constructing a stand-alone one-dimensional finite difference model capable of simulating the multiphase reactive transport processes and diverse thermochemical environments that govern the formation and evolution of planetary ices. These affects have previously never been incorporated in ice shell models. The numerical model of sea ice described in Chapter 2 was extended to accommodate putative Europan ocean compositions and a wide range of potential ice-ocean interface thermal gradients. The motivation for constructing such a model was to provide a physically realistic simulation of planetary ice-ocean interfaces capable of predicting the physical and thermochemical properties of ices formed under environments relevant to ice-ocean worlds. For while heterogeneities in ice characteristics have been invoked as a potential driver of ice shell geophysical processes, the thermochemical structure of the ice shell remains largely unconstrained. Based on terrestrial examples, impurity entrainment at the ice-ocean interface likely influences ocean-surface material transport, which has been lauded as a crucial control on the moon's habitability. The adapted model was used to derive constitutive relationships between ocean chemistry, ice-ocean interface thermal gradients, and ice composition – providing a method to quantify the thermochemical evolution of Europa's ice shell and hydrological features contained within. Moreover, this work links observable ice characteristics to properties of its parent water body and thermal

environment at the time of formation. These results have direct implications for geophysical and biogeochemical models of Europa, as well as interpreting upcoming spacecraft observations. The model was designed to be accessible and easily adapted to accommodate the diverse thermal and physicochemical environments of ocean worlds throughout the solar system with the intent of creating a useful tool for both the terrestrial and planetary science communities.

Abstract

Geologic features and areas of irradiation on the icy surface of Jupiter's moon Europa are often dark and red in color, produced by locally high salt content within the ice. Compositional heterogeneities within Europa's ice shell can arise from and facilitate geologic processes, providing a pathway for potential expression of ocean-derived materials at the moon's surface. The detailed chemistry and transport of these solutes play an imperative role in the dynamics and habitability of the ice and subsurface ocean, but the total inventory and distribution of impurities within Europa's ice shell is unknown. In sea ice on Earth, the local thermochemical environment at the ice-ocean interface governs impurity entrainment into the ice, which has been successfully reproduced by multiphase reactive transport models that capture the physics occurring at this dynamic boundary. Here, we report constraints on the total impurity load and bulk salinity profile of the Europan ice shell derived from constitutive relationships between impurity entrainment and local thermal gradient for a variety of ocean compositions, resulting in bulk ice shell salinities that range from 1.053-14.72 ppt. These models show that the upper ice shell freezes rapidly with high salt content down to ~250 meters and place a permeability

dependent upper limit on impurity entrainment into Europa's ice of 5% of the ocean composition for the bulk of the ice shell over most of Europa's history. We apply these new constraints to geologic features of interest; fractures derived from the ice-ocean interface and shallow lenses within the shell. Our results show that water-filled fractures refreeze rapidly, producing high salt content along fracture walls that could promote future sliding. Finally, we show that impurity rejection during the solidification of perched water within the ice shell produces highly concentrated salt layers, over 2 m thick for a 2 km deep lens. These results demonstrate how ocean materials are entrained and processed within Europa's ice shell, which has important implications for the formation of geologic terrain on Europa and other icy satellites, as well as the interpretation of a broad swath of observations to be made by future spacecraft.

3.1 Introduction

Europa's ocean was the first detected beyond Earth [*Khurana et al.*, 1998; *Kivelson et al.*, 2000]. Studies [*Cassen et al.*, 1979; *Pappalardo et al.*, 1999; *Ross and Schubert*, 1987; *Squyres et al.*, 1983] indicate that Europa's internal structure hosts a thick global ocean bounded by a silicate mantle below and a water ice shell above. These findings have fueled interest in the moon's interior dynamics that might constitute environments suitable for life [*Board and Council*, 2012; *Chyba and Phillips*, 2001; *Des Marais et al.*, 2008; *Reynolds et al.*, 1983; *Russell et al.*, 2017]. As both a barrier and conveyer between the ocean and surface, Europa's ice shell plays a crucial role in the moon's dynamics and evolution. Because most of the data available for Europa is derived from remote sensing techniques, the ice shell is a primary medium through which the properties of the ocean

and interior can be understood, as the ice expresses how the body has evolved through its geology and composition. However, at present many of the ice shell's properties are not well constrained, including ice thickness, ice chemistry, and the distribution of shallow water [*Billings and Kattenhorn*, 2005; *Schmidt et al.*, 2011b; *Walker and Schmidt*, 2015; *Zolotov and Shock*, 2001]. Locating potentially habitable niches, understanding the transport processes supporting them, investigating their connectivity, and constraining characteristics of the Europan environment are planned objectives of the Europa Clipper mission currently under development by NASA [*Phillips and Pappalardo*, 2014]. As such, quantifying the physical, thermal, chemical, and mechanical properties of the ice shell is imperative to understanding Europa's geophysical and material transport processes that control its habitability.

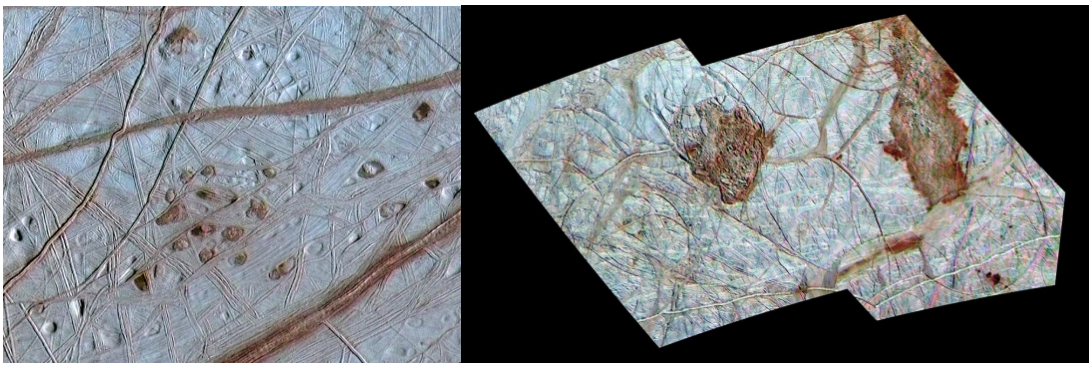

Figure 3.1 – Europa's geological features. Impurity rich geological features are found across the surface of Europa, indicated by their dark and red coloration. (Left) Dark red material associated with the most recently emplaced Lenticulae and Lineae (Image Credit: NASA/JPL/University of Arizona/University of Colorado – PIA03878) (Right) Similar concentrations of dark material is present at Thera and Thrace Macula, two regions of chaos terrain thought to be some of the most recently active regions on the moon (Image Credit: NASA/JPL/University of Arizona – PIA02099).

Heterogeneities in the ice shell have been linked to a number of dynamic processes: solid state convection in the lower ice shell [*Han and Showman*, 2005; *Howell and Pappalardo*, 2018; *McKinnon*, 1999], subduction or subsumption of surface material [*Johnson et al.*, 2017a; *Kattenhorn*, 2018; *Kattenhorn and Prockter*, 2014], eutectic melting that may lead to the formation of chaos and lenticulae [*Manga and Michaut*, 2017; *Michaut and Manga*, 2014; *Schmidt et al.*, 2011b], formation and sustenance of water bodies within the shell [*Kargel et al.*, 2000; *Zolotov and Kargel*, 2009]. Furthermore, observations reveal that young, active terrain is richer in non-ice material than the average ice [*McCord et al.*, 2002] (Figure 3.1), suggesting recent interaction with subsurface water reservoirs enriched with salts [*Manga and Michaut*, 2017; *Michaut and Manga*, 2014; *Schmidt et al.*, 2011b]. Yet the process by and rate at which impurities are entrained within the ice remain poorly constrained, and while current models implement a range of potential impurity loads to test model sensitivity to variations in ice composition [*Han and Showman*, 2005; *Johnson et al.*, 2017b; *Pappalardo and Barr*, 2004] they do not predict ice composition directly.

When ice forms in an aqueous environment, it preserves a thermochemical record of the water from which it formed [*Feltham et al.*, 2006; *Hunke et al.*, 2011; *Turner and Hunke*, 2015]. For Europa, the ice shell grew from the freezing of, and is thus a window into, the ocean, as well as the primary media through which the surface and ocean communicate. With a geologically young surface ($<10^8$ yr [*Carr et al.*, 1998]) suggesting active ice shell overturn, dynamic regions of Europa's surface (e.g. bands and chaos) may harbor 'fossil ocean material' entrained in the ice shell as recently as 1Mya [*Howell and Pappalardo*, 2018]. This could provide an accessible sample of the contemporary ocean,

as it is highly likely that Europa's ice, much like sea ice and marine ice on Earth, contains pockets and channels filled with brine, salts, gasses, and other impurities derived from the dynamics of freezing at the ice-ocean interface [*Eicken*, 2003; *Pappalardo and Barr*, 2004; *Zolotov and Kargel*, 2009; *Zotikov et al.*, 1980] (Figure 3.2). On Earth, sea ice captures such a record of the thermochemical processes in the upper ocean during its formation [*Buffo et al.*, 2018]. As the ocean solidifies, dissolved solutes are rejected as crystalline ice forms and a porous water-ice matrix filled with hypersaline interstitial fluid is produced [*Buffo et al.*, 2018; *Feltham et al.*, 2006; *Hunke et al.*, 2011; *Turner and Hunke*, 2015]. This process produces a compositionally-driven gravitational instability in the newly formed porous ice layer that results in buoyancy-driven convection of the denser pore fluid into the underlying liquid reservoir. Referred to as gravity drainage, this process has been observed to be the primary method of desalination during sea ice formation and has been successfully incorporated into a number of numerical models [*Buffo et al.*, 2018; *Griewank and Notz*, 2013; *Turner and Hunke*, 2015; *Wells et al.*, 2011]. Quantifying the relationship between Europa's ice composition and interfacial thermochemistry at the time of formation would provide a technique for linking observed ice properties to characteristics of its origin liquid water reservoir (a 'frozen fingerprint' of the source water) and forecasting the properties of ice produced under diverse thermal and chemical conditions – informing the synthesis of future mission data and geodynamic models. Impurities and structural heterogeneities within ice alter its thermal, physicochemical, and dielectric properties [*Feltham et al.*, 2006; *Hunke et al.*, 2011; *Weeks and Ackley*, 1986]. Thus, beyond the ice shell's chemistry, the dynamics of impurity entrainment will affect the potentially appreciable, and ongoing, hydrological activity within Europa's ice shell in the form of

perched water lenses, fractures, dikes, and sills [*Manga and Michaut*, 2017; *Michaut and Manga*, 2014; *Schmidt et al.*, 2011b; *Walker and Schmidt*, 2015]. Moreover, interpretation of measurements taken by Europa Clipper's ice penetrating radar, REASON, depend critically on ice composition and dielectric properties [*Kalousová et al.*, 2017; *Weeks and Ackley*, 1986].

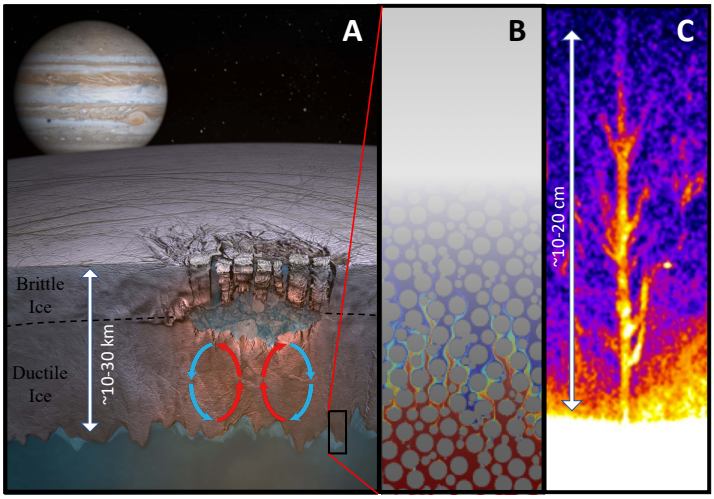

Figure 3.2 – The Europa ice-ocean system. A) A brittle ice lithosphere overlies a ductile ice mantle (dashed line) in contact with a subsurface ocean. A diapir generated perched water lens is an example of a putative hydrological feature within the ice shell that may facilitate the surface expression of recently entrained ocean material. B) Akin to terrestrial environments, the ice-ocean interface of Europa will likely be characterized by a two-phase ice-brine system, allowing solutes and other ocean material to be trapped within pore spaces. C) Brine channels in terrestrial sea ice. (Image Credit: A – Adapted from Britney Schmidt/Dead Pixel FX, UT Austin. B – Adapted from Joaquín Jiménez-Martínez http://petrelharp. github.io/asn_2016/asn-2016-talk.html C – Adapted from [*Worster and Rees Jones*, 2015])

To constrain the impurity load within Europa's ice shell and investigate the possible dynamics associated with the presence of salt in the ice shell, we constructed a one-

dimensional reactive transport model adapted from the sea ice model of [*Buffo et al.*, 2018] for the Europa environment. We performed simulations of the formation and evolution of Europa's ice shell, validated against empirical observations of sea ice and marine ice growth rates and composition. The simulations include fluid and solute transport and the associated impurity entrainment that occurs at ice-ocean/brine interfaces. The model actively tracks the dynamic ice-ocean/brine interface as it propagates and catalogs the composition of the ice as it becomes impermeable and traps solutes within the ice. Since the ice composition derives from the initial ocean, we test an array of putative Europan ocean chemistries and thermal regimes and derive constitutive relationships between entrainment rates and the local thermal and chemical environment.

3.2 Numerical Model

The growth and evolution of the ice-ocean/brine interface is treated using an adapted version of the one-dimensional, two-phase, reactive transport model of sea ice described by [*Buffo et al.*, 2018]. Water/ice mass, energy, and salinity are conserved using a coupled set of equations that combines mushy layer theory and the enthalpy method. The governing equations are:

$$\overline{\rho c}\frac{\partial T}{\partial t} = \left(\bar{k}\frac{\partial^2 T}{\partial z^2}\right) - \rho_{ice} L \frac{\partial \phi}{\partial t} \tag{3.1}$$

$$\phi \frac{\partial S_{br}}{\partial t} = \left(\bar{D}\frac{\partial^2 S_{br}}{\partial z^2}\right) - \frac{\rho_{ice}}{\rho_{br}} S_{br} \frac{\partial \phi}{\partial t} \tag{3.2}$$

$$H = c_{ice}T + L\phi \tag{3.3}$$

$$\phi = \begin{cases} 0 & H < H_s = c_{ice}T_m \\ (H - H_s)/L & -\ if\ - \quad H_s \leq H \leq H_s + L \\ 1 & H > H_s + L \end{cases} \tag{3.4}$$

where ρ is density, c is specific heat capacity, T is temperature, t is time, z is the vertical coordinate, k is heat conductivity, L is the latent heat of fusion for the water to ice phase transformation, ϕ is liquid fraction, S is salinity, D is salt diffusivity, H is enthalpy, H_s is the enthalpy of a discretization cell consisting of only solid ice, and T_m is melting/freezing temperature. Subscripts *ice* and *br* refer to characteristics of the ice and brine components of the two-phase mixture, respectively, and variables carrying an over bar are volumetrically averaged quantities (i.e. $\bar{y} = \phi y_{br} + (1 + \phi)y_{ice}$). Equations 1 and 2 ensure conservation of heat and mass, respectively, and equations 3 and 4, combined, make up the enthalpy method.

The desalination of forming ice is governed by brine expulsion and gravity drainage. Brine expulsion refers to the phase change driven flux of hypersaline brine within the porous ice matrix into the underlying liquid reservoir. As a volume containing both ice and brine components continues to solidify, assuming incompressible flow, conservation of mass requires that brine must be expelled from the volume. This is due to the density difference between ice and water. Given the unidirectional solidification scenarios considered here, the brine will move downward into the ambient ocean/brine. Gravity drainage refers to the buoyancy-driven convective overturn of brine within the permeable

multiphase layer. This latter process is the result of salt rejection during the growth of crystalline ice, concentrating interstitial pore fluid which ultimately migrates downward forming tubular void spaces known as brine channels as it flows into the underlying ocean [*Cottier et al.*, 1999; *Wells et al.*, 2010; 2011; *Wells et al.*, 2019; *Worster and Rees Jones*, 2015].

With minimal loss of accuracy, we forego simulating phase change driven Darcy flow in the porous ice and opt to use the one-dimensional gravity drainage parameterization of [*Griewank and Notz*, 2013] to represent fluid transport. This parameterization represents the process of gravity drainage through brine channels as a linear function of the local Rayleigh number, and is widely used for solving multiphase melting/solidification problems [*Griewank and Notz*, 2013; *Turner and Hunke*, 2015; *Turner et al.*, 2013; *Wells et al.*, 2011]. Both effects were considered by the model of [*Buffo et al.*, 2018]; however, in line with previous research [*Griewank and Notz*, 2013; *Wells et al.*, 2011], gravity drainage was shown to be the primary mode of desalination. As such, to optimize the current model, brine expulsion was excluded.

Following [*Griewank and Notz*, 2013] we define the mass of brine transported out of a multiphase layer *j* as:

$$br_j^{\downarrow} = \alpha\left(Ra_j - Ra_c\right)dz^3dt = \alpha\left(\frac{g\rho_{sw}\beta\Delta S_j\widetilde{\Pi}h_j}{\kappa\mu} - Ra_c\right)dz^3dt \qquad (3.4)$$

where α is a constant of proportionality, Ra_j is the Rayleigh number of the *j*th layer, Ra_c is the critical Rayleigh number, *dz* and *dt* are the spatial and temporal discretization sizes, respectively, g is acceleration due to gravity, ρ_{sw} is the density of the ambient reservoir

fluid (ocean/brine), β is a density coefficient describing the relationship between density and salinity, ΔS_j is the difference in salinity of the brine from ambient fluid, h_j is the height of the *j*th layer above the basal surface of the ice, κ is the thermal diffusivity of seawater, μ is the kinematic viscosity of seawater, and $\widetilde{\Pi}_j$ is the minimum permeability of any layer between the *j*th layer and the basal ice surface. The permeability function given by [*Griewank and Notz*, 2013] is utilized, and a critical porosity cutoff is implemented to prevent drainage from layers containing low liquid fractions (here $\phi < 0.05$ [*Golden et al.*, 2007] results in a layer's fluid transport being shut off). Heat and salt are transported out of the model domain by this convective process and the equations of mushy layer theory (Eq. 3.1 & 3.2) are modified accordingly [*Buffo et al.*, 2018].

3.3 The Stefan Problem: Deriving the Constitutive Equations

The interpolation of results used to derive the constitutive relationships between ice characteristics and the thermochemical environment hinges on the ability to fit the simulated data to a predefined function. The form of this function should be representative of the physical processes occurring within the simulation. As the equations governing the multiphase reactive transport model do not lend themselves to an analytical solution, it is logical to seek a simplified system that does. To investigate the evolution of dissolved salt in an ice-ocean environment we make a number of simplifying assumptions and solve Equation 3.2 analytically. The resulting solution provides the functional forms of the constitutive equations relating bulk salinity to depth within the ice shell and local thermal gradient.

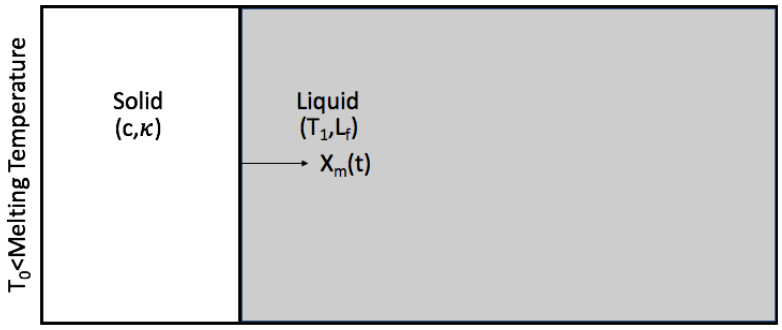

Figure 3.3 – The geometry and physical properties involved in the Stefan problem. The liquid at temperature T_1 loses heat through the solid whose left end is subject to a constant supercooling set to $T_0 < T_m$, leading to a propagating freezing front at position $x_m(t)$.

The classic Stefan problem describes the dynamics and evolution of pure substance melting/solidification and is well documented in the literature [*Huber et al.*, 2008; *Michaut and Manga*, 2014; *Rubinšteĭn*, 2000]. The basic geometry of the problem can be seen in Figure 3.3. In 1860 Carl Neumann found the analytical solution of the thermal profile in the solid and the time dependent solidification front to be [*Huber et al.*, 2008]:

$$T(x,t) = T_0 - (T_0 - T_1)\frac{\operatorname{erf}\left(\frac{x}{2\sqrt{\kappa t}}\right)}{\operatorname{erf}(\lambda)} \tag{3.5}$$

$$x_m(t) = 2\lambda\sqrt{\kappa t} \tag{3.6}$$

$$\lambda \exp(\lambda^2)\operatorname{erf}(\lambda) = \frac{St}{\sqrt{\pi}} = \frac{c(T_0 - T_1)}{L_f\sqrt{\pi}} \tag{3.7}$$

where $T(x,t)$ is the temperature within the solid at position x and time t, T_0 is the temperature at the undercooled surface and is lower than the melting temperature of the solid, T_1 is the temperature of the liquid, κ is the thermal diffusivity of the solid, x_m is the position of the solidification front, λ is a coefficient depending on St, erf is the error function, St is the Stefan number defined as $St = c(T_0 - T_1)/L_f$, c is the specific heat of the solid, and L_f is the latent heat of fusion for the water-ice phase transition.

While the Stefan problem represents a simpler system than that of our reactive transport model, the underlying physics governing solidification are the same and similar behavior is to be expected. It has been suggested that the amount of impurities entrained in forming ice is related to the rate at which the ice forms [*Nakawo and Sinha*, 1984; *Weeks and Ackley*, 1986; *Zolotov and Kargel*, 2009]. Equations 3.5-3.7 can be utilized to investigate the relationships between the rate of ice formation and both the freezing front position and local thermal gradient. First, differentiating Equation 3.6 with respect to time gives:

$$v_m(t) = \dot{x}_m(t) = \frac{\lambda\kappa}{\sqrt{\kappa t}} = \frac{2\lambda^2\kappa}{x_m(t)} \tag{3.8}$$

$$\Rightarrow \quad v_m(t) \propto \frac{1}{x_m(t)} \tag{3.9}$$

where $v_m(t)$ is the solidification front velocity, which is equivalent to the rate of ice formation. This suggests that the rate of ice formation is inversely proportional to the

position of the solidification front. Second, differentiating Equation 3.5 with respect to position gives:

$$\frac{\partial T(x,t)}{\partial x} = -\frac{(T_0 - T_1)}{\mathrm{erf}(\lambda)} \frac{1}{\sqrt{\pi \kappa t}} \exp\left(-x^2/4\kappa t\right) \qquad (3.10)$$

At the position of the solidification front, $x_m(t) = 2\lambda\sqrt{\kappa t}$, Equation 3.10 becomes:

$$\frac{\partial T(x_m,t)}{\partial x} = -\frac{(T_0 - T_1)}{\mathrm{erf}(\lambda)} \frac{1}{\sqrt{\pi \kappa t}} \exp\left(-\lambda^2\right) \qquad (3.11)$$

From Equation 3.8 we see that $\sqrt{\kappa t} = \lambda\kappa / v_m(t)$. Substituting this result into Equation 3.11 gives:

$$\frac{\partial T(x_m,t)}{\partial x} = -\frac{(T_0 - T_1)}{\mathrm{erf}(\lambda)} \frac{1}{\sqrt{\pi}\lambda\kappa} \exp\left(-\lambda^2\right) v_m(t) \qquad (3.12)$$

$$\Rightarrow \quad \frac{\partial T(x_m,t)}{\partial x} \propto v_m(t) \qquad (3.13)$$

Suggesting that the rate of ice formation is directly proportional to the local thermal gradient at the solidification front. The relationships derived in Equations 3.9 & 3.13 provide insight into the spatiotemporal evolution of the Stefan problem and its dependence on the local thermal environment. These results will be utilized below, where a modified

Stefan problem (inclusion of a solute and fluid dynamics) is described and an analytical solution is derived. This solution describes the spatial and temporal distribution of the solute and provides the functional form of the constitutive equations used throughout the text.

To investigate the evolution of dissolved salt in an ice-ocean environment we make a number of simplifying assumptions and solve Equation 3.2 analytically. Assuming top-down unidirectional solidification of a salty ocean (e.g. sea ice, Europan ocean solidification) the evolution of salt in the system can be described by the equations of reactive transport (Equation 3.2 including the gravity drainage parameterization, with *br* subscripts dropped from *S* terms for simplicity):

$$\phi \frac{\partial S}{\partial t} = \left(\overline{D} \frac{\partial^2 S}{\partial z^2} \right) - \frac{\rho_{ice}}{\rho_{br}} S \frac{\partial \phi}{\partial t} + br_j^{\downarrow} \frac{\partial S}{\partial z} \qquad (3.14)$$

where $br_j^{\downarrow}$ is the brine velocity in the *j*th layer described by the one-dimensional gravity drainage parameterization. Introducing a new coordinate, ξ, such that $\xi = z - z_m(t)$, places the origin at the ice-ocean interface and constitutes a moving coordinate system. In this new coordinate system Equation 3.14 can be written as:

$$\phi \frac{\partial S}{\partial \xi} \frac{\partial \xi}{\partial t} = \overline{D} \left[\frac{\partial^2 S}{\partial \xi^2} \left(\frac{\partial \xi}{\partial z} \right)^2 + \frac{\partial S}{\partial \xi} \frac{\partial^2 \xi}{\partial z^2} \right] - \frac{\rho_{ice}}{\rho_{br}} S \frac{\partial \phi}{\partial \xi} \frac{\partial \xi}{\partial t} + br_j^{\downarrow} \frac{\partial S}{\partial \xi} \frac{\partial \xi}{\partial z} \qquad (3.15)$$

Rearranging Equation 3.15:

$$-\overline{D}\left[\frac{\partial^2 S}{\partial \xi^2}\left(\frac{\partial \xi}{\partial z}\right)^2 + \frac{\partial S}{\partial \xi}\frac{\partial^2 \xi}{\partial z^2}\right] - br_j^{\downarrow}\frac{\partial S}{\partial \xi}\frac{\partial \xi}{\partial z} + \phi\frac{\partial S}{\partial \xi}\frac{\partial \xi}{\partial t} = -\frac{\rho_{ice}}{\rho_{br}}S\frac{\partial \phi}{\partial \xi}\frac{\partial \xi}{\partial t} \qquad (3.16)$$

Taking the appropriate spatial and temporal derivatives of ξ and substituting their values into Equation 3.16 gives:

$$-\overline{D}\frac{\partial^2 S}{\partial \xi^2} - \left(br_j^{\downarrow} + \phi v_m(t)\right)\frac{\partial S}{\partial \xi} = v_m(t)\frac{\rho_{ice}}{\rho_{br}}S\frac{\partial \phi}{\partial \xi} \qquad (3.17)$$

For simplicity, we assume that $\phi(\xi) = H(\xi)$, where $H(\xi)$ is the Heaviside step function. While this is indeed a simplification, as it represents the mushy layer as an infinitesimally thin regime, the general liquid fraction profile of evolving sea ice demonstrates similar structure (See Figures 5-7 of [*Buffo et al.*, 2018]). Substituting $\phi(\xi) = H(\xi)$ into Equation 3.17 results in a simplified conservation of mass equation in the moving coordinate system:

$$-\overline{D}\frac{\partial^2 S}{\partial \xi^2} - \left(br_j^{\downarrow} + \phi v_m(t)\right)\frac{\partial S}{\partial \xi} = v_m(t)\frac{\rho_{ice}}{\rho_{br}}S\delta(\xi) \qquad (3.18)$$

where $\delta(\xi)$ is the delta function. Equation 3.18 can be solved using Fourier transforms. Let the transform variable be χ, such that:

$$S(\chi) = \mathcal{FT}[S(\xi)] = \int_{-\infty}^{\infty} S(\xi)\exp(-i2\pi\chi\xi)\,d\xi \qquad (3.19)$$

$$S(\xi) = \mathcal{FT}^{-1}[S(\chi)] = \int_{-\infty}^{\infty} S(\chi)\exp(i2\pi\chi\xi)\,d\chi \qquad (3.20)$$

Applying the Fourier transform to Equation 3.18 gives:

$$4\pi^2\chi^2\overline{D}\,S(\chi) - i2\pi\chi\left(br_j^{\downarrow} + \phi v_m(t)\right)S(\chi) = v_m(t)\frac{\rho_{ice}}{\rho_{br}}S(\xi = 0, t) \qquad (3.21)$$

Equation 3.21 has the solution:

$$S(\chi) = S(\chi, t) = \frac{v_m(t)\frac{\rho_{ice}}{\rho_{br}}S(\xi = 0, t)}{4\pi^2\chi^2\overline{D} - i2\pi\chi\left(br_j^{\downarrow} + \phi v_m(t)\right)} \qquad (3.22)$$

Taking the inverse Fourier transform of Equation 3.22 gives:

$$S(\xi, t) = \int_{-\infty}^{\infty}\left[\frac{v_m(t)\frac{\rho_{ice}}{\rho_{br}}S(\xi = 0, t)}{4\pi^2\chi^2\overline{D} - i2\pi\chi\left(br_j^{\downarrow} + \phi v_m(t)\right)}\right]\exp(i2\,\pi\chi\xi)\,d\chi \qquad (3.23)$$

$$= \frac{v_m(t)\frac{\rho_{ice}}{\rho_{br}}S(\xi = 0, t)}{\left(br_j^{\downarrow} + \phi v_m(t)\right)}\left[\pm 1 \mp \exp\left(\frac{-\pi\xi\left(br_j^{\downarrow} + \phi v_m(t)\right)}{\overline{D}}\right)\right] \qquad (3.24)$$

Throughout this work we seek constitutive equations that relate the amount of salt entrained in forming ice to depth and local thermal gradient. Using the relationships of Equations 3.9 & 3.13, the definition of $\xi = z - z_m(t)$, and assuming in the active mushy layer near the

ice-ocean interface, where reactive transport is possible, $z \sim z_m(t)$, we can rewrite Equation 3.24 in two forms:

$$S(z_m, t) \propto \frac{1}{z_m}[1 - \exp(-z_m)] \tag{3.25}$$

$$S\left(\frac{\partial T}{\partial z}, t\right) \propto \frac{\frac{\partial T}{\partial z}}{1 + \frac{\partial T}{\partial z}}\left[1 - \exp\left(-1/\frac{\partial T}{\partial z}\right)\right] \tag{3.26}$$

where the first term on the right-hand side of each equation is a diffusion term which dominates at later times (deeper depths, lower thermal gradients) and the second term is an advection-reaction term which dominates at early times (shallower depths, larger thermal gradients). Together, Equations 3.25 & 3.26 provide the functional forms for the constitutive equations produced throughout the remainder of the text.

3.4 Results

3.4.1 Salt Entrainment on Earth

Two types of ice present on Earth provide the best end-member analogs for Europa's ice shell: sea ice and marine ice. While both ices form via the directional solidification of seawater, and thus undergo the same dynamics during their formation, they form under different thermal regimes, resulting in unique compositional and physical structure. Sea ice provides the upper limit of impurity entrainment and an ideal analog for ice formed along steep thermal gradients near Europa's surface, as its formation is driven by rapid heat loss to the cold polar atmosphere. Fortunately, there exists nigh on a century's

worth of observations and quantitative measurements regarding vertical heterogeneities in the thermal, chemical, and microstructural properties of sea ice [*Malmgren and Institutt*, 1927]. With the proximity of the 100 K surface, a young, thin Europan ice shell (tens to hundreds of meters thick) as well as any newly emplaced shallow liquid water features within the contemporary ice shell will experience similarly high thermal gradients, suggesting high impurity uptake akin to that of sea ice. We have previously modeled the annual growth of sea ice to study its thermochemical evolution and ability to record variations in ocean characteristics through the reproduction of ice core properties [*Buffo et al.*, 2018]. This model was adapted to actively track the advancing ice-ocean interface and accommodate the Europa environment. In Figure 3.4, we present model results for sea ice and compare these to empirical measurements of depth dependent sea ice bulk salinity [*Nakawo and Sinha*, 1981; *Notz and Worster*, 2009]. Actively tracking the evolution of the ice-ocean interface and simulating small-scale solute transport within the porous ice produces bulk salinity profiles that agree well with observations. We achieve salinity profiles that exhibit the characteristic 'c-shape' typical of first-year sea ice, represented by the 'MARCH' profile of Figure 3.4b [*Malmgren and Institutt*, 1927], and reproduce the bulk salinity values observed in the field. Based on the constitutive relationship between depth and bulk salinity (Methods), we use an inverse fit to the simulated values to extend the profile to the upper portion of the ice where extreme temperature gradients affect numerical stability when using a Neumann boundary condition. Thus, our model captures the physical processes that occur during ice formation in high thermal gradient environments, which will govern the formation of ice near Europa's surface.

Conversely, as thermal gradients decrease, ice composition approaches an asymptotic lower limit governed by the critical porosity of the active layer when it is in diffusive equilibrium with the underlying ocean. Much of Europa's deeper ice shell, below about 1 km, will have formed under these conditions. A similar environment exists at the base of deep ice on Earth, called marine ice [*Zotikov et al.*, 1980]. This unique, and less studied, variety of ocean-derived ice forms on the basal surface of terrestrial ice shelves due to much lower thermal gradients than typical open ocean sea ice (e.g. ~10 K/m for surficial sea ice; ~0.08 K/m for marine ice [*Zotikov et al.*, 1980]) leading to greatly reduced growth rates (~2 cm/yr [*Zotikov et al.*, 1980]). While the thermal gradients present in the marine ice system (~0.08 K/m) exceed the upper estimates for a thin (5-10 km) Europan ice shell (~0.02 K/m) [*McKinnon*, 1999; *Mitri and Showman*, 2005], they represent the best terrestrial analog of basally accreting ice in this thermal regime, and it can be shown that impurity entrainment has already approached its lower limit – characterized by asymptotic bulk salinity profiles (Figure 3.4c). Adopting a critical porosity of $\phi_c = 0.05$, based on observations of sea ice permeability [*Golden et al.*, 1998; *Golden et al.*, 2007], and assuming an ocean salinity, $S_{oc} = 34\ ppt$, the theoretical lower limit for salt entrainment into terrestrial ice (diffusive equilibrium when impermeability is reached) is given by $S_{lim} = \phi_c S_{oc} = 1.70\ ppt$. The average bulk salinity of the 'asymptotic region' seen in Figure 3.4c is 2.32 ppt. Utilizing the constitutive equation for bulk salinity versus thermal gradient derived in the next section for terrestrial seawater in the diffusive regime (dT/dz = 0.08 K/m), a bulk salinity of 1.95 ppt is predicted. The difference of 0.37 ppt between the observed and predicted bulk salinity values translates to a 16% error, attributed to small variations in unconstrained parameters, such as critical porosity and permeability-porosity

relationships (both of which can appreciably affect impurity entrainment rates [*Buffo et al.*, 2018]). The efficiency of brine migration through the porous ice lattice and the threshold at which percolation is possible are poorly constrained [*Golden et al.*, 1998; *Golden et al.*, 2007; *Wells et al.*, 2011] but govern the dynamics of multiphase flow, brine retention in the ice, and ultimately ice composition. At the ice-ocean/brine interface, reduced permeability or a larger critical porosity would lead to more salt being entrained in the ice. Alternately, enhanced permeability or a smaller critical porosity would result in less salt entrainment. Nevertheless, our model closely reproduces observations of sea ice, and the same multiphase reactive transport physics applied in low-thermal gradient conditions match observations of marine ice composition, which capture broadly the two thermochemical regimes that ice on Europa is expected to occupy.

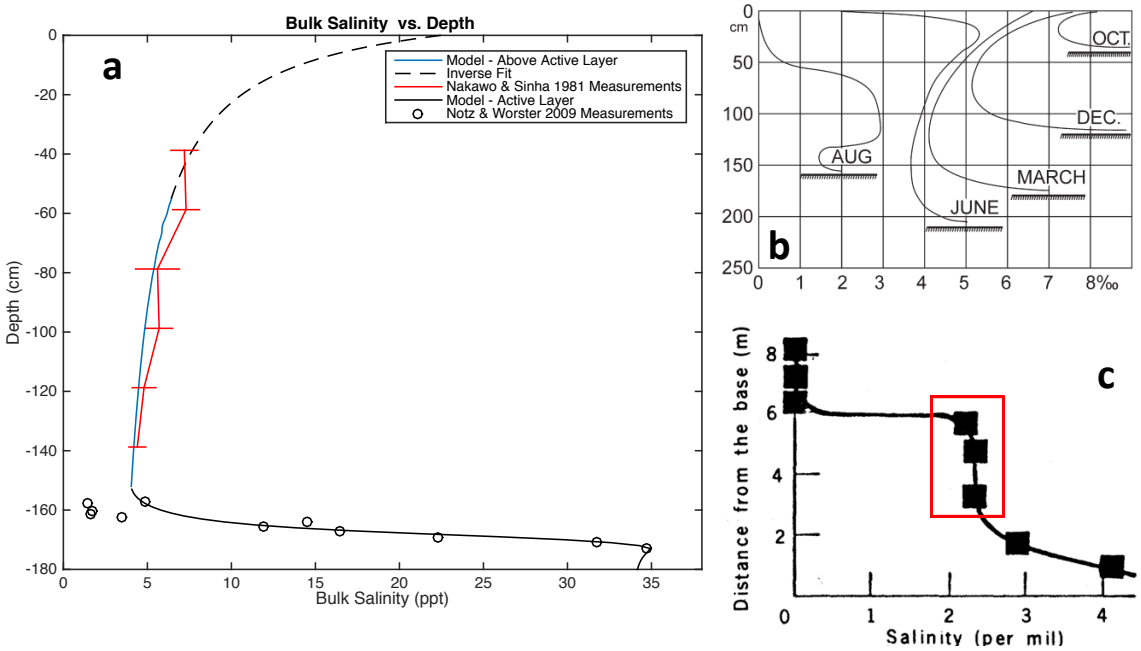

Figure 3.4: Salinity profiles within observed and modeled marine and sea ice. a) Modeled (blue and black solid lines), empirical (red line [*Nakawo and Sinha*, 1981] and black circles [*Notz and Worster*, 2009]),

and interpolated (black dashed line) bulk salinity profiles of sea ice. The numerical model assumes a preexisting 50 cm thick layer of sea ice in conductive equilibrium (linear temperature profile) with an atmospheric temperature of 250K and an ocean temperature of 271.5K. A conductive heat flux is maintained throughout the simulation at the upper boundary. The model was run for $1.5x10^7$ sec (~174 days, a typical sea ice annual cycle) with a time step of 100 sec. The dashed line is the product of a Levenberg-Marquardt algorithm fit to the function S(z)=a+b/(c-z), where S is bulk salinity, z is depth, and a, b, and c are constants, applied to the modeled bulk salinities above the active layer (blue solid line). **b)** Typical first-year sea ice salinity profiles have a characteristic 'c' shape where the bulk salinity evolves over the season due to material transport and ice growth (from [*Malmgren and Institutt*, 1927]). **c)** Bulk salinity measurements from the bottom 8 m of an ice core extracted from the Ross Ice Shelf by [*Zotikov et al.*, 1980]. The bottom 6 m is accreted marine ice, with the 'asymptotic region' outlined in red approaching diffusive equilibrium during ice formation.

3.4.2 The Role of Thermal Gradients and Ocean Chemistry

Aside from the different surface temperature (<110 K vs ~250 K), gravity (1.32 vs 9.81 m/s^2) and potential compositional characteristics between Europa and Earth, one of the largest differences is sheer scale of the ice. While the majority of sea ice exhibits a maximum thickness of <10 m [*Kurtz and Markus*, 2012; *Laxon et al.*, 2013] (ice drafts have been known to exceed 25 m and reach up to 47 m beneath pressure ridges [*Davis and Wadhams*, 1995; *Lyon*, 1961]) and marine ice accretion occurs at depths <1.5 km [*Craven et al.*, 2009; *Galton‐Fenzi et al.*, 2012; *Zotikov et al.*, 1980], Europa's ice shell is likely 10-30 km thick [*Billings and Kattenhorn*, 2005; *Nimmo et al.*, 2003; *Tobie et al.*, 2003]. It is important to note, however, that despite differences in ice thickness, all ice-ocean interfaces will remain at or near their pressure melting point, which for a 1.5 km thick terrestrial ice shelf is comparable to an ~11.1 km thick Europan ice shell. Modeling the entire ice shell thickness and lifespan at the resolution needed to capture the reactive

transport dynamics occurring near the ice-ocean/brine interface is computationally intractable. To overcome these difficulties, we modified our model [*Buffo et al.*, 2018] such that it actively tracks only the permeable or 'active' region of the ice shell, determined by the critical porosity where fluid flow ceases [*Golden et al.*, 1998; *Golden et al.*, 2007]. In the top-down solidification scenarios modeled, when the fluid fraction of a discretized layer drops below the critical porosity it is removed from the active domain and its properties are cataloged, along with all the cells above it, and an equal number of replacement layers are added to the bottom of the domain with ambient ocean/brine characteristics ($T_{oc}, S_{oc}, \rho_{sw}$). Model runs are initiated with the domain completely filled by one of the ocean chemistries investigated at a temperature just above its freezing point (Supplementary Section S3). The top boundary is governed by a Neumann boundary condition with a no-flux condition set for salt and it is assumed that the overlying ice is in conductive thermal equilibrium [*McKinnon*, 1999] (i.e. $dT/dz = (T_{oc} - T_S)/H$). The bottom boundary is governed by a Dirichlet boundary condition and is simulated as being in contact with an infinite ambient ocean/brine reservoir ($T_{oc}, S_{oc}, \rho_{sw}$) (for additional information on code functionality see [*Buffo et al.*, 2018] and Methods). To construct the full ice shell from discrete model runs, several simulations at various depths (solidification front locations) run in parallel, and the results are combined to produce the constitutive relationships that relate ice composition to its thermochemical environment at the time of formation.

Table 3.1 – Possible Europan ocean compositions. List of ion species and relative abundances for terrestrial seawater and the proposed Europan ocean chemistry of Zolotov and Shock (2001).

Species	Terrestrial Seawater (mol/kg)	Europan Ocean (mol/kg)
Na^+	4.69×10^{-1}	4.91×10^{-2}
K^+	1.02×10^{-2}	1.96×10^{-3}
Ca^{2+}	1.03×10^{-2}	9.64×10^{-3}
Mg^{2+}	5.28×10^{-2}	6.27×10^{-2}
Cl^-	5.46×10^{-1}	2.09×10^{-2}
SO_4^{2-}	2.82×10^{-2}	8.74×10^{-2}
Total Salt (ppt)	34	12.3

Composition of the ocean is critical to ice formation because of the relationship between the salinity of water and its freezing point. The conductive nature of Europa's ocean [*Khurana et al.*, 1998; *Kivelson et al.*, 2000], as well as spectrographic measurements [*McCord et al.*, 1999], suggests the presence of dissolved salts, but nearly all of its intrinsic properties (thickness, composition, structure) remain poorly constrained. Potential Europan ocean chemistries have been explored in a number of studies [*Vance et al.*, 2016; *Zolotov and Kargel*, 2009; *Zolotov and Shock*, 2001]. Here we implement the chemistry proposed by [*Zolotov and Shock*, 2001] (Table 3.1), who assumed that Europa's ocean formed during its differentiation via partial aqueous extraction from bulk rock with the composition of CV carbonaceous chondrites. Alternate formation materials (e.g. CI chondrites [*Zolotov and Kargel*, 2009]) will alter the predicted ionic composition of the ocean, and variable molecular diffusivities, atomic masses, and v'ant Hoff factors may affect impurity entrainment rates in associated ocean-derived ices. For comparison, we also considered an ocean composition identical to terrestrial seawater (Table 3.1). Well-known liquidus curves exist for terrestrial seawater [*Commission*, 2010]. However, the freezing

behavior of potentially more exotic Europan ocean compositions is comparatively less well known, so we constructed a new software package, Liquidus 1.0, to derive quadratic liquidus curves for any chemistry supported by the equilibrium chemistry package FREZCHEM 6.2, which includes a wide range of material properties for the expected non-ice components of brines. A given aqueous solution is simulated at an array of temperatures and concentrations and the mole fraction of solid ice, under each condition, is tracked. For each concentration, the midpoint between the warmest temperature where any solid ice is present and the next warmest temperature is calculated. A quadratic fit is applied to these midpoints, and this is taken to be the liquidus curve for the solution. An example can be seen in Figure 3.5. Liquidus 1.0 and its associated documentation can be found at: https://github.com/jbuffo/Liquidus-1.0/releases/tag/v1.0.

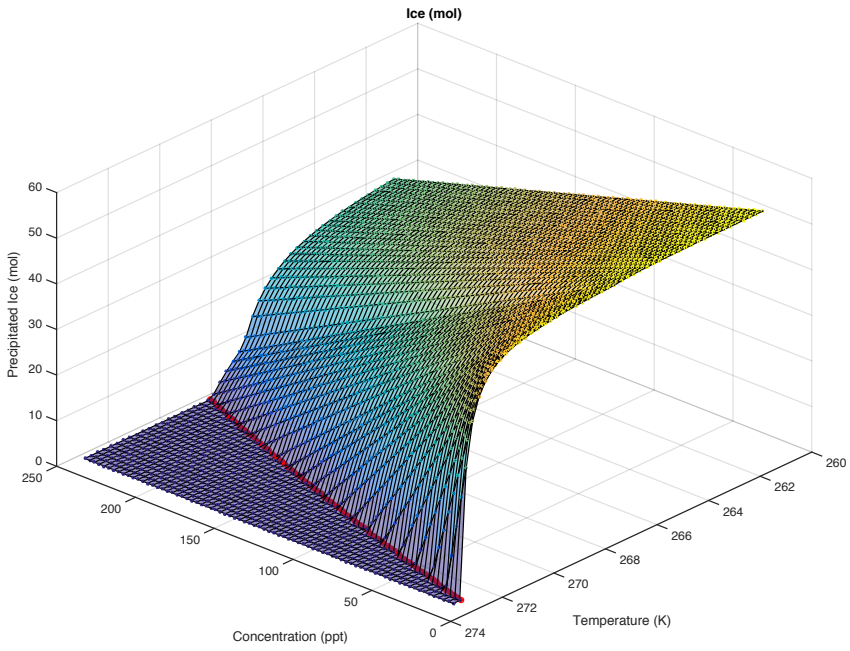

Figure 3.5 – Calculating the Europan ocean liquidus curve. Temperature and concentration dependent ice precipitation for the Europan ocean chemistry of [*Zolotov and Shock*, 2001]. From this a quadratic liquidus curve is derived using Liquidus 1.0. (Precipitated ice – gridded surface, quadratic fit liquidus curve – red line)

We simulated Europa's ice shell growth at eight discrete ice thicknesses (10 m, 50 m, 75 m, 100 m, 150 m, 200 m, 250 m, and 300 m), for four different hypothetical ocean compositions (Europan Ocean 12.3 ppt/100 ppt/282 ppt and Terrestrial Seawater 34 ppt). By the time the ice shell reaches 300 m in thickness the thermal gradient at the ice-ocean interface is shallow enough that the bulk salinity curve becomes asymptotic and variations in the salt entrainment rate will be minimal at all greater depths. This asymptotic lower limit is set by the ocean composition and critical porosity ($S_{lim} = \phi_c S_{oc}$). Simulations of larger ice thicknesses (>300 m) were therefore excluded, given the predicted ice composition below 300 m would vary by <1 ppt (see the first row of Table 3.2 and the following paragraph). Europan ocean concentrations were selected to bound the best estimates available from theory and observation: the most comprehensive estimate provided from theoretical calculations is 12.3 ppt [*Zolotov and Shock*, 2001], while the saturation point of the same fluid would reach an ocean salinity of 282 ppt, and the upper limit based on the Galileo magnetometer data estimates a salinity of 100 ppt [*Hand and Chyba*, 2007]. The results for all ocean compositions can be seen in Figures 3.6 and 3.7. The results are depth-dependent and thermal gradient-dependent bulk salinity profiles, which are then interpolated using a Levenberg-Marquardt algorithm fit to the constitutive equations, the explicit form of which, including the coefficients needed to accommodate stretches and translations, are shown in Table 3.2.

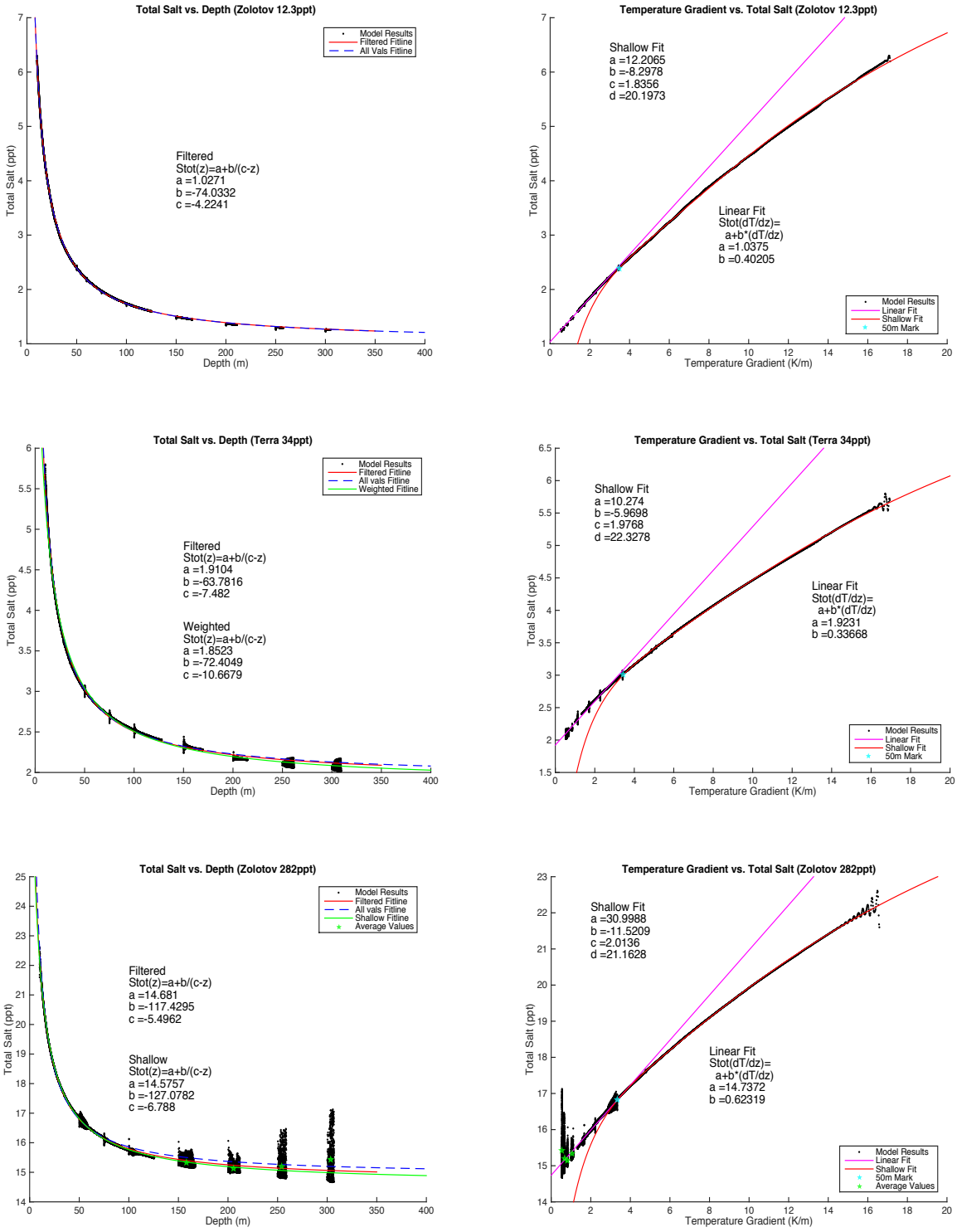

Figure 3.6: Simulations of depth dependent and thermal gradient dependent bulk salinity for three different ocean chemistries (100 ppt simulation is presented in Figure 3.7) Relationships are fit by the constitutive equations of Table 3.2. **Left Column,** Model results [black dots] (numerical dispersion at the

onset of each run has been removed) and original (all values), filtered (numerical dispersion at run onset removed), weighted (where applicable – weighted by data density), and shallow (where applicable – fitting model results from 10-200 m runs) fit lines [blue dashed line, red line, and green lines, respectively]. **Right Column,** Simulated results [black dots] as well as linear and 'Shallow' (See Table 3.2) fit lines [pink and red lines, respectively]. Green stars represent average bulk salinity for an entire run at a given depth – highlighting that the majority of the simulated data lies near the fit lines, even when scatter is present. Blue stars identify the thermal gradient associated with a 50 m depth within an equilibrated conductive ice shell, which is the transition point between the diffusive and advective-reactive regimes.

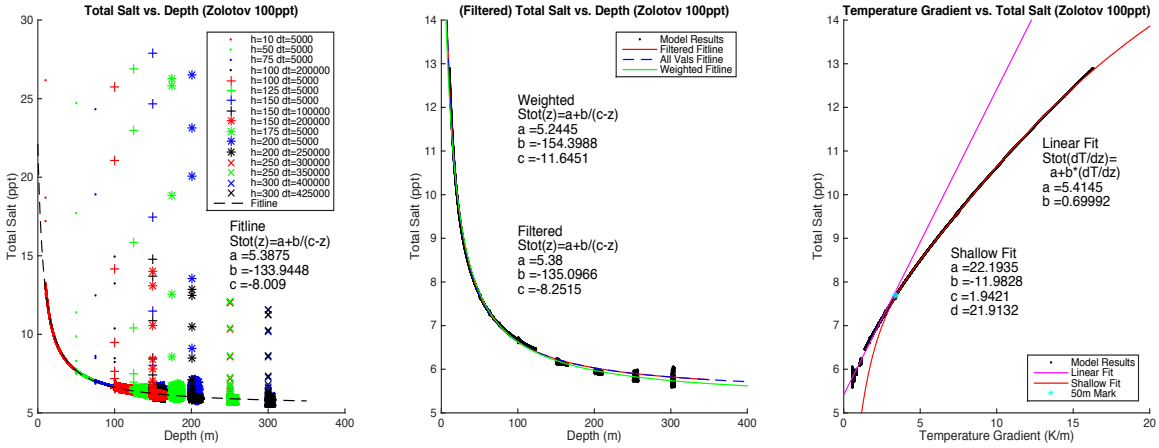

Figure 3.7 – Ice bulk salinity vs. depth and thermal gradient (100 ppt). Simulation results and constitutive equation fit lines for a hypothetical 100 ppt Europan ocean utilizing the chemistry given in Table 3.1. In addition to the two panels depicted for similar runs in the main text, a panel depicting the 'raw' simulation results is included. This includes values produced at the onset of simulations that are plagued by numerical dispersion, as well as results for an array of temporal discretizations to investigate the effect this variance has on model output.

Table 3.2: Constitutive Equations. The reactive transport model results are fit by constitutive equations relating bulk salinity to shell depth and temperature gradient for each of the ocean compositions, column 1, and their associated coefficients, a-d. Subscripts 12.3, 100, 282, and 34 refer to Europan ocean compositions with concentrations of 12.3 ppt, 100 ppt, 282 ppt, and terrestrial seawater with a concentration of 34 ppt, respectively. These equations provide a parameterization of Europa's ice shell composition's dependence on the local thermal environment at the time of ice formation, which can be utilized to provide efficient first order estimates of the properties of ice formed in a variety of chemical and thermal environments without the need for explicit simulation.

Constitutive Equation	**a**	**b**	**c**	**d**
$S_{tot}(z) = a + \frac{b}{(c-z)}$	$a_{12.3}$=1.0271 a_{100}=5.38 a_{282}=14.681 a_{34}=1.8523	$b_{12.3}$=-74.0332 b_{100}=-135.096 b_{282}=-117.429 b_{34}=-72.4049	$c_{12.3}$=-4.2241 c_{100}=-8.2515 c_{282}=-5.4962 c_{34}=-10.6679	
$S_{tot}\left(\frac{\partial T}{\partial z}\right) = a + b\frac{\partial T}{\partial z}$	$a_{12.3}$=1.0375 a_{100}=5.4145 a_{282}=14.737 a_{34}=1.9231	$b_{12.3}$=0.40205 b_{100}=0.69992 b_{282}=0.62319 b_{34}=0.33668		
(Shallow Fit Line) $S_{tot}\left(\frac{\partial T}{\partial z}\right) = a + \frac{b\left(\frac{\partial T}{\partial z} + c\right)}{1 + \frac{\partial T}{\partial z}}\left[1 - exp\left(\frac{-d}{\partial T/\partial z}\right)\right]$	$a_{12.3}$=12.21 a_{100}=22.19 a_{282}=31.00 a_{34}=10.27	$b_{12.3}$=-8.30 b_{100}=-11.98 b_{282}=-11.52 b_{34}=-5.97	$c_{12.3}$=1.836 c_{100}=1.942 c_{282}=2.014 c_{34}=1.977	$d_{12.3}$=20.20 d_{100}=21.91 d_{282}=21.16 d_{34}=22.33

The translation of the model from the Earth system to Europa hinges on the observation that as thermal gradients near the ice-ocean/brine interface decrease ice bulk salinity asymptotically approaches a lower limit governed by equilibration of the pore fluid with the underlying ocean (Figure 3.4c & 3.9). The result of this is twofold. First, the ice shell will experience ice-ocean interface thermal gradients below those found on Earth during much of its formation. This suggests a relatively homogeneous ice layer (formed in the asymptotic regime) underlying a thin (~1 km), compositionally distinct surficial layer (formed under steep thermal gradients). This stratification would produce variations in the thermochemical and mechanical properties of these layers, potentially introducing a

boundary along which rheological transitions (e.g. brittle lid vs. ductile mantle) and transport regimes (conduction vs. convection) may be promoted. Second, the lower portion of the contemporary ice shell is believed to be ductile enough to undergo solid state convection [*Barr and McKinnon*, 2007; *Han and Showman*, 2005; *McKinnon*, 1999; *Tobie et al.*, 2003], providing a mechanism that would homogenize this region of the shell, both thermally and chemically. An isothermal profile in this ductile region suggests an ice-ocean interface subject to very low thermal gradients [*Mitri and Showman*, 2005], implying that accreted ice salinities would be at or near their lower limit, irrespective of ice thickness. Thus, the ductile region of the contemporary ice shell should have a bulk composition at or near the lower limit set by the critical porosity. Such a compositional profile varies negligibly from those predicted by the unidirectional solidification scenarios we simulate here (below 1 km predicted salinities vary by <150 ppm from the theoretical lower limit). Any heterogeneities in impurity entrainment would require associated ice-ocean heat flux variations (e.g., ocean driven heating of the ice shell [*Soderlund et al.*, 2014], thermochemical diapirism [*Pappalardo and Barr*, 2004], spatiotemporal variations in basal heat flux due to downwelling cold ice and/or the evolution of tidal heating within the ice shell [*Tobie et al.*, 2003]) with amplitudes large enough to appreciably affect entrainment rate. Notably, this implies that for much of the ice shell it is not the thermal regime of the ice but rather its critical porosity and permeability which will determine ice composition.

In general, the bulk salinity profiles and their corresponding relationships to depth within the ice shell and local temperature gradients are well-represented by our derived constitutive equations, suggesting that their functional forms (Equations 3.25 & 3.26) capture much of the reactive transport physics that govern how ice forms in the presence

of dissolved materials, and the movement of this material via advection and diffusion while the ice is still permeable. The division of impurity entrainment rate into two distinct thermal regimes, diffusive (low) and advective-reactive (high), is well accommodated and justified by the terrestrial benchmarks above. While there exist uncertainties in the limit of extreme thermal gradients ($\gg 20\ K/m$) and large salinities (e.g. scatter observed for the 282 ppt ocean at low thermal gradients), the high thermal conductivity of ice relative to water quickly diffuses such thermal anomalies, and the results demonstrate that, as expected, the bulk salinity in the ice approaches the diffusive equilibrium limit under low thermal gradients. Thus, as perhaps the first quantitative estimate of impurity content, the constitutive equations derived here allow us to investigate the properties and evolution of Europa's ice shell and hydrological features contained therein.

3.4.3 The Material Properties of Ice

Many of ice's material properties are thermally, chemically, and structurally dependent. Ice density is affected by temperature, porosity, and salt content [*Barr and McKinnon*, 2007; *Johnson et al.*, 2017b]. Its rheology is dependent on grain size, liquid fraction, and temperature [*Barr and McKinnon*, 2007] and its specific heat, thermal conductivity, and dielectric properties are all affected by local thermochemistry [*Kalousová et al.*, 2017; *Weeks and Ackley*, 1986]. As such, the properties and dynamics of Europa's ice shell will be dictated by these complex dependencies. This directly impacts buoyancy estimates, predicted ice shell thermodynamics, and the synthesis of future mission data [*Grima et al.*, 2016; *Johnson et al.*, 2017b; *McKinnon*, 1999; *Phillips and Pappalardo*, 2014]. A full foray into the implications of these dependencies on our current

results is beyond the scope of this work, however the general applicability of the constitutive equations allows straightforward integration of more complex material properties, as demonstrated by the following example.

For ice, thermal conductivity is commonly described as varying inversely with temperature (e.g. [*Johnson et al.*, 2017b] utilize the relationship $k = 651/T$ W/m, where k is thermal conductivity and T is temperature). An ice shell of thickness H, with ocean temperature T_{oc}, and surface temperature T_S, supports conductive equilibrium temperature profiles of the form:

$$T(z) = T_S \left(\frac{T_{oc}}{T_S}\right)^{z/H} \tag{3.27}$$

Where z is depth beneath the surface. The resulting thermal gradient at the ice-ocean interface and its dependence on ice shell thickness can be seen in Figure 3.8. Implementing an inverse relationship between thermal conductivity and temperature leads to amplified thermal gradients at the base of the ice shell. The constitutive equations relating bulk salinity to thermal gradient (Table 3.2) can then be utilized to investigate the resulting variance in ice shell composition induced by the modified thermal conductivity (Figure 3.8). At all depths an increase in bulk salinity is observed due to the amplified thermal gradients at the ice-ocean interface. These new bulk salinities will in turn increase near surface density values, alter electrical permittivity estimates, and affect predictions of other material properties. The overall salt content in the ice shell will increase by ~0.3%. This example demonstrates the versatility and applicability of the constitutive equations, which can easily be implemented to account for the effects of impurities on a given ice shell

process. Future work will utilize the current results (one-dimensional reactive transport model and constitutive equations) to investigate the effects of entrainment rate and ice composition on a broader class of geophysical processes, on a number of ice-ocean worlds, in greater detail.

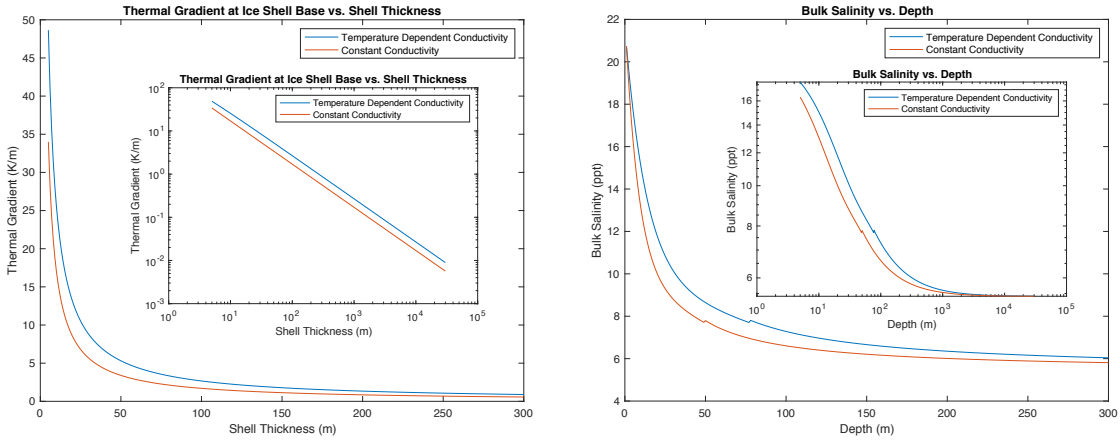

Figure 3.8 – Investigating the effects of temperature dependent thermal conductivity on impurity entrainment. (Left) Thermal gradients at the ice-ocean interface for a given ice shell thickness (5-300 m) utilizing a constant thermal conductivity (Red Line) and a thermal conductivity inversely related to ice temperature (Blue Line). Thermal gradients are calculated assuming equilibrium thermal states in the overlying ice, linear for constant thermal conductivity, and the thermal profile given by Equation 3.27 for the inversely dependent thermal conductivity. (Inset) Log-log plot of thermal gradient at ice-ocean interface vs. ice shell thickness for 5-30,000 m. (Right) The associated bulk salinity profiles calculated using the thermal gradients of the left plot and the constitutive equations of Table 3.2. (Inset) Log-log plot of bulk salinity vs. depth for 5-30,000 m. The slight jump is due to the transition between the linear and 'Shallow Fit Line' of Table 3.2.

3.5 The Evolution of Europa's Ice Shell

3.5.1 Total Salt

The constitutive equations derived above can be used to estimate the total salt content of Europa's ice shell prior to the onset of solid-state convection, producing an upper limit on the total impurity load of the ice shell. For these calculations, we assume a 25 km thick ice shell with an inner radius of 1,535 km and an outer radius of 1,560 km. The total salt content for a given ocean composition can be calculated by integrating the constitutive equation over the volume of the ice shell given the coefficients in Table 3.2. For an ice shell with inner radius R_1 and outer radius R_2, the total salt contained in the ice shell can be acquired by volumetrically integrating the constitutive equation relating bulk salinity to depth in the ice shell:

$$Total\ Salt\ in\ Shell = \frac{\rho_{ice}}{1000}\int_V S_{tot}(z)dV \qquad (3.28)$$

where ρ_{ice} is the density of ice, V is the volume of the ice shell, and $S_{tot}(z)$ is the constitutive equation relating bulk salinity and depth. Rewriting z in terms of the spherical coordinate r, gives:

$$Total\ Salt\ in\ Shell = \frac{\rho_{ice}}{1000}\int_{R_1}^{R_2}\int_0^{2\pi}\int_0^{\pi}\left[a + \frac{b}{(c-(R_2-r))}\right]r^2 \sin\varphi\, dr\, d\theta\, d\varphi \qquad (3.29)$$

where a, b, and c are coefficients from the ocean/brine specific constitutive equation and (r, θ, φ) represent a spherical coordinate system.

The total volume of the 25 km thick Europan ice shell is ~7.5235 x 10^{17} m^3, while the approximate collective volume of Earth's oceans is ~1.332 x 10^{18} m^3 [*Charette and*

Smith, 2010]. For the Europan ocean composition (Table 3.1), with concentrations of 12.3 ppt, 100 ppt, and 282 ppt the total salt entrained in a 25 km shell is 7.2894 x 10^{17} kg, 3.6633 x 10^{18} kg, and 1.0189 x 10^{19} kg, respectively. This corresponds to average ice shell salinities (total salt/ice shell mass) of 1.0565 ppt, 5.3099 ppt, and 14.769 ppt, respectively. For a terrestrial ocean composition with a concentration of 34 ppt the total salt entrained in a 25 km shell is 1.2978 x 10^{18} kg, corresponding to an average ice shell salinity of 1.8811 ppt. For comparison, Earth's oceans contain ~4.5288 x 10^{19} kg of salt.

Crucial in driving any potential solid-state convection on Europa, compositional buoyancy due to density variations may either help or hinder large scale, thermally driven convective overturn in the ice shell. Horizontal density gradients have also been proposed as a potential driver of observed subduction/subsumption on Europa's surface [*Johnson et al.*, 2017a; *Kattenhorn*, 2018]. Mirroring the profiles of bulk salinity, there exists a rapid and asymptotic decrease in ice density with depth for all ocean chemistries (Figure 3.9), and subsequently throughout much of the shell the density is nearly homogeneous (e.g. for a 100 ppt Europan ocean chemistry ρ_{500m}=922.54 kg/m^3 and ρ_{25km}=922.25 kg/m^3). Our results demonstrate that, apart from a geophysically thin surface layer, significant variations in density with depth are unlikely to form as the ice shell freezes out. However, the physical, thermal, and chemical characteristics of the ice shell likely act in concert to control Europa's dynamics, as the material properties of ice are structurally, thermally, and chemically dependent (Section 3.4.3). The expected salinity profile, along with the total impurity load, provides context on the nature of liquid and solid phases within the ice shell. Combined with thermal variations due to convection, tidal heating, or heat transfer from the ocean [*Howell and Pappalardo*, 2018; *Mitri and Showman*, 2005] and variations in

physical properties such as porosity and viscosity [*Barr and McKinnon*, 2007; *Johnson et al.*, 2017b], more explicit constraints on the thermophysical formation of many of Europa's surface features are thus possible.

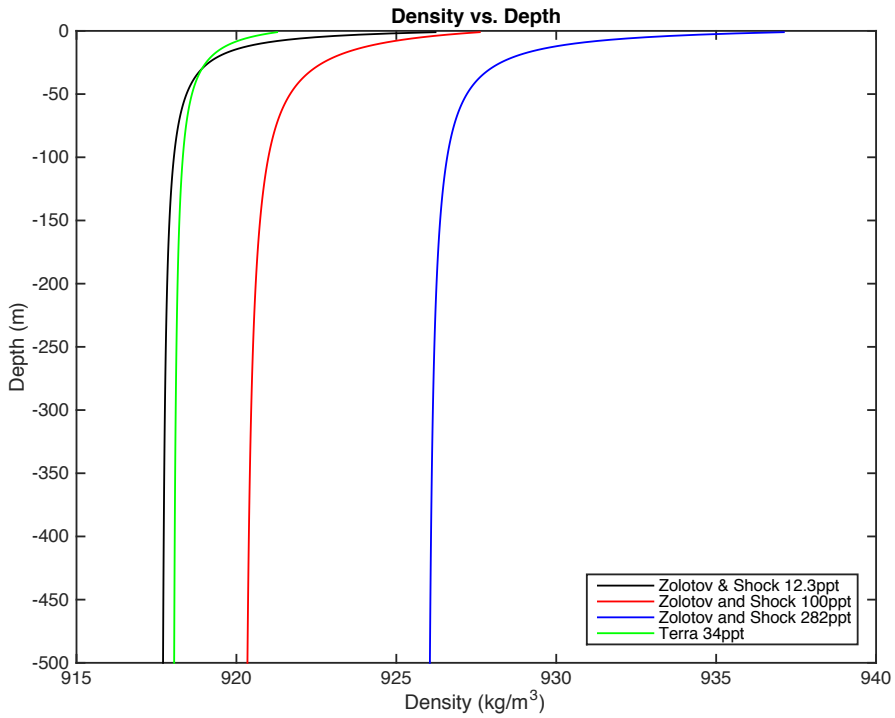

Figure 3.9 – Density profiles in the shallow subsurface of Europa's ice shell. Ice density variation with depth for the four ocean chemistries investigated. Depths greater than 500 m have been excluded as density variations below this point vary negligibly.

3.5.2 Basal Fractures

3.5.2.1 Composition Upon Refreeze

The fundamental processes that occur during the freezing of ice are not only applicable to the ocean, but to any water within the ice shell. We adapted our approach to accommodate the geometry of simple basal fractures to investigate their composition upon re-freezing. Akin to the basal fractures of terrestrial ice shelves, fractures at the ice-ocean

or other ice-liquid interface of Europa could either locally stabilize or destabilize the ice shell; they have the potential to suture the shell back together with newly frozen oceanic material [*Khazendar et al.*, 2009], or to propagate further, potentially penetrating to the surface [*Bassis and Walker*, 2011]. Such fractures appear within Europa's chaos terrain [*Walker and Schmidt*, 2015], a potential indicator of near-surface water reservoirs [*Schmidt et al.*, 2011b] and a potential pathway for shallow water to make it to the surface in the form of plumes [*Sparks et al.*, 2017].

To apply the model to basal fractures, we adapt the model by assuming the fractures have a characteristic basal width and penetration depth and altering the gravity drainage parameterization to account for the new geometry of the active layer (Figure 3.10). The fracture width and penetration depth are determined using a linear elastic fracture mechanics (LEFM) model. Fracture mechanics theory is based upon the assumption that all materials contain defects that affect their load-bearing capacity. LEFM, specifically, is a simplified approach that models the propagation of initial starter cracks or flaws in an elastic layer by assessing stress concentration near the crack tip. In reality, ice is not a linear elastic material, as its deformation is best described by a viscoelastic rheology. However, on short timescales such as that of fracture propagation, it behaves elastically. As such, LEFM is an adequate approximation to study fracture propagation in Europa's ice shell. It has been widely used in terrestrial ice systems to determine surface and basal fracture penetration depth (e.g., [*Van der Veen*, 1998a; b]), as well as in planetary surface fracture applications (e.g., [*Rudolph and Manga*, 2009]). Full details and analysis regarding the application to basal planetary fractures can be found in [*Walker et al.*, (in revision)]; in essence, the height to which basal fractures propagate is controlled primarily by the

tectonic stress field in which the fracture starts, overburden pressure at depth, and water pressure at the base. These stresses are additive at the crack tip, and the fracture propagates until this combined stress falls below the tensile strength of ice. We have conducted analyses using a tensile strength of 0.1 MPa $m^{1/2}$, a value representative of natural ice sheets [*Manga and Wang*, 2007; *Rist et al.*, 1999]. For this application, we have assumed the base of the ice shell or ice lid is at hydrostatic equilibrium, i.e., basal water pressure is equal to the overburden pressure. We apply a range of tectonic (far-field) stresses to determine heights to which fractures propagate and their associated basal widths. Model results for a 25 km thick ice shell and a 3 km ice lid overlaying a perched water lens can be seen in Figure 3.11. Using these heights and widths, we produce simple basal fracture geometries; although fracture geometries are almost certainly more complex in reality, this simplified triangle ideal is also used in terrestrial studies (e.g., [*Luckman et al.*, 2012]).

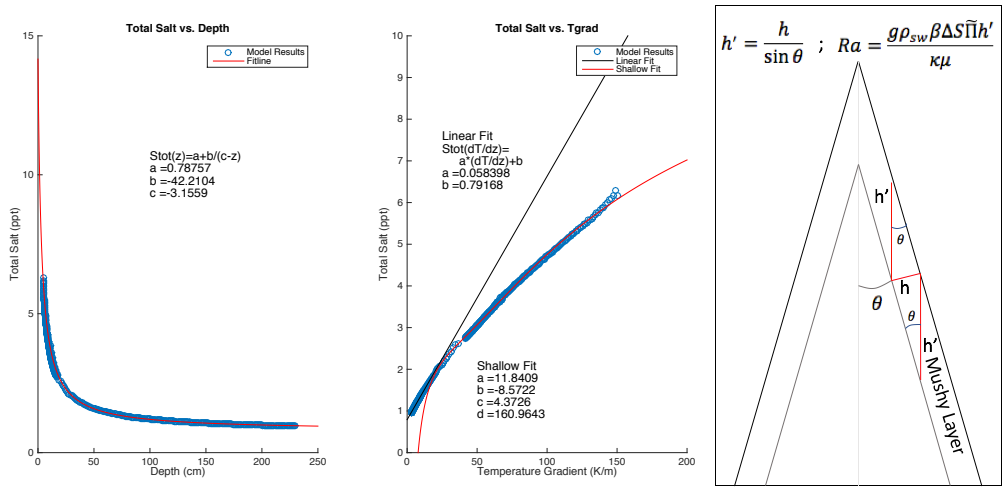

Figure 3.10 – Basal fracture geometry and constitutive relationships. (Left and Center) Model results (blue circles) and associated constitutive equations (red and black lines) for a hypothetical ice-ocean interface basal fracture (1.125 km penetration depth, 11.34 m basal width – associated with a 0.1 MPa stress). (Right) Basal fracture geometry, highlighting features that are used to modify the gravity drainage parameterization.

New constitutive equations are produced for each fracture geometry and ocean/brine composition combination (an example can be seen in Figure 3.10). We modeled basal fractures at both Europa's ice-ocean interface and a hypothetical ice-lens interface (Figure 3.12). The fractures are filled with fluid from the underlying reservoir (ocean or lens) and the fluid is assumed to remain well mixed during the simulations since the advective timescale for rejected brine with a density 1 kg m^{-3} greater than the ambient fluid through a 25 km fracture is <1 day (equating gravitational and viscous drag forces for a parcel of brine near the crack tip of width $\mathcal{O}(1)$, $v \sim \Delta\rho g/\eta$). Due to the high aspect ratio of the basal fractures (penetration depth/basal width) we modeled them as solidifying horizontally inward, akin to how terrestrial magmatic dikes form, forced by the conductive profile of the ice shell into which the fracture is emplaced (Section 3.4.4.2.2). The injection of water into the ice shell produces regions of very high thermal gradients between the relatively warmer water and cold ice. As a result, fractures refreeze to form ice wedges with chemically gradated composition, due to the amplified solidification rates at the fracture's edges and tip. While these simulations do not completely capture all of the inherently two-dimensional structure of the fracture (especially near the crack tip) these results provide the most realistic evaluation of basal fracture physicochemical evolution. The results suggest that basal fractures are geologically short-lived, at least in the upper shell, due to their high aspect ratios and rapid heat loss to the surrounding ice. At depth their lifetime may be extended by deformation processes brought about by tidal forces [*Nimmo and Gaidos*, 2002] or the presence of a warmer ductile ice layer [*Barr and McKinnon*, 2007; *Tobie et al.*, 2003]. While it is unlikely that fractures in the shallow shell

contain liquid water for long, we show that the rapid injection and refreezing of saline fluid within a colder ice shell produces local chemical heterogeneities along the fracture walls that could preserve the fracture. Two important implications arise: the high salinity regions along the fracture walls produce a gradient in mechanical properties, potentially weakening the center of the fracture or concentrating stress here, while at the same time these regions could be more easily melted during reactivation of the fracture even in the absence of water from the ocean. Both of these provide mechanisms by which features can remain active even once they refreeze.

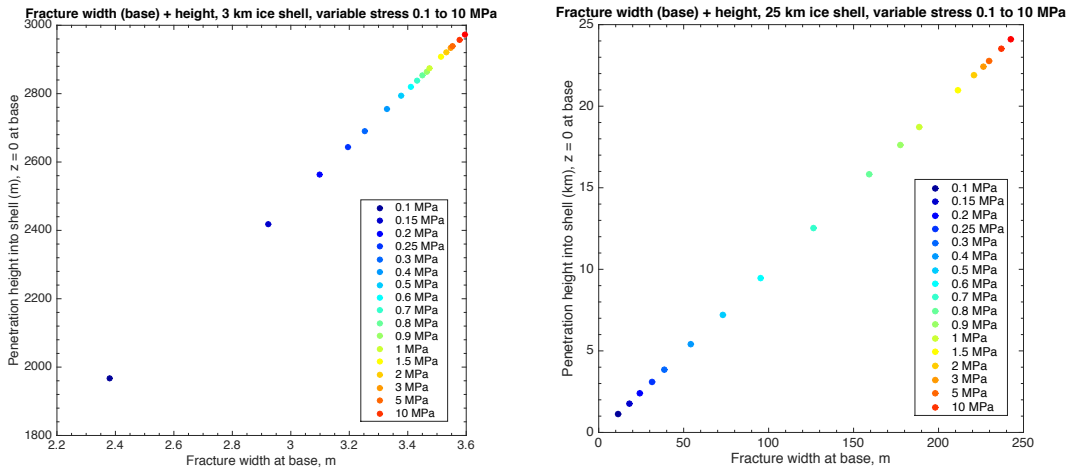

Figure 3.11 – Basal fracture geometry variations with induced stress. Plots modified from [*Walker et al.*, (in revision)]. (Left) Fracture widths and penetration depths under variable stress conditions for a 3 km ice lid (e.g. overlaying a hypothetical perched water lens). (Right) Fracture widths and penetration depths under variable stress conditions for a 25 km ice shell.

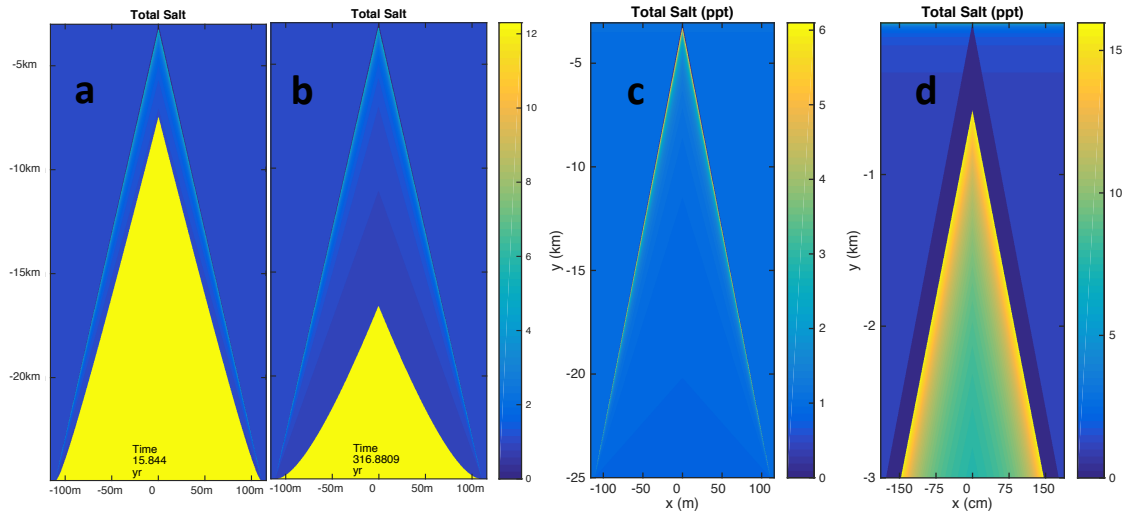

Figure 3.12: **Basal ice fractures refreeze to produce a gradient in salinity.** Temporal evolution of a hypothetical basal fracture, **a-b** shows that rapid refreezing occurs, down to 5km within 15 years if the fracture can be held open over this timeframe. Profiles for deep fractures from the ice-ocean interface, **c** (due to 2 MPa stress in a 25 km shell; Depth – 21.925 km, Width – 220.9 m), and fractures from shallow lens interfaces, **d** (due to 2 MPa stress in a 3 km lid, Depth – 2.922 km, Width – 3.53 m), show similar patterns of high salt content along the fracture wall and toward the tip, and lower salinity toward the interior and base. These results show that gradients in mechanical properties are likely toward the surface where tidally modulated activity is more likely. For fractures from the ocean, the majority of the ice formed in the interior of the fracture, however, will have a salinity that is nearly indistinguishable from the bulk Europa ice. This suggests that fractures are likely to be regions of local discontinuities in ice shell properties, and potentially regions of weakness within the ice shell created by interfaces between salt and ice grains.

3.5.2.2 Solidification Rates

The solidification rate of a 2 MPa stress induced, ice-ocean interface, basal fracture is investigated by implementing the fracture geometry (Depth – 21.925 km, Width – 220.9 m) and utilizing the multiphase reactive transport model to simulate the evolution of the ice-ocean interface along the fracture walls. This process is carried out for a range of

thermal gradients, and the associated solidification front propagation velocities can be obtained by:

$$v_m(t) = \dot{x}_m(t) \tag{3.30}$$

where v_m is the solidification front propagation velocity, and $\dot{x}_m$ is the time derivative of the solidification front position. The relationship between thermal gradient and ice-ocean interface propagation velocity can be seen in Figure 3.13. A linear fit, representing ice-ocean interface growth rate as a function of local thermal gradient, is produced (setting the y-intercept to zero, guaranteeing $v_m(t)$=0 for $\partial T/\partial z$=0 [See Figure 3.13]).

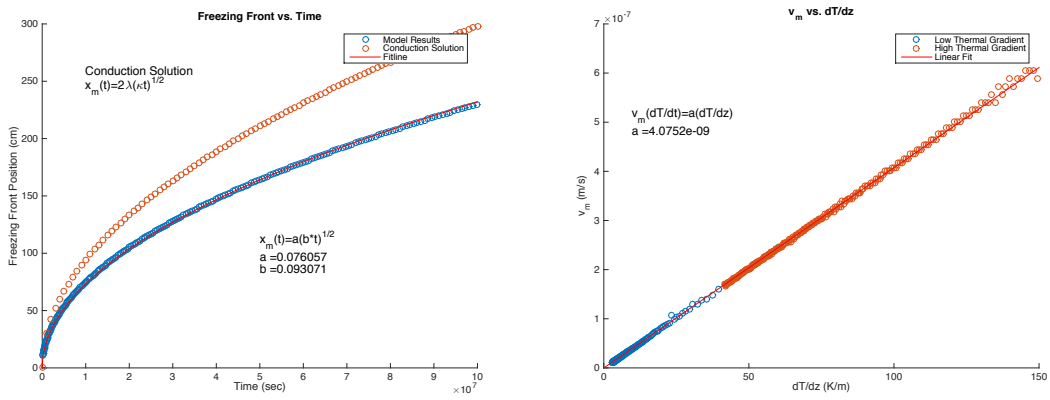

Figure 3.13 – Basal fracture ice-ocean interface evolution. Spatiotemporal evolution of the freezing front for a simulated basal fracture (Left) and the relationship between ice-ocean interface growth rate and local thermal gradient (Right) for a 12.3 ppt Europan ocean within a 2 MPa induced basal fracture (25 km ice shell). (Left - Conduction solution included to highlight the impact multiphase reactive transport processes have on ice-ocean interface dynamics)

The relationship derived between solidification front propagation speed and local thermal gradients within a simulated basal fracture in a 25 km thick Europan ice shell agree with intuition. In regions with high thermal gradients (large undercooling) the solidification front propagates quickly, entraining larger amounts of impurities in the ice. Conversely, in regions with lower thermal gradients the freezing front propagates more slowly, allowing for expulsion of impurities out of the ice, and into the underlying/adjacent ocean. This results in the rapid solidification of the upper and edge regions of the fracture, where high bulk salinities can be seen. Meanwhile, in the lower portion of the fracture a longer-lived remnant of the fracture slowly diminishes, forming nearly pure ice as it freezes out. Unfortunately, to our knowledge, there exists no detailed measurements of the thermochemical evolution of potential fracture refreeze analogs in the terrestrial cryosphere (e.g. solidification of sea ice leads, infilling and solidification of basal ice shelf fractures). However, the solidification of mafic dikes and binary metal alloys frequently display similar thermal gradient dependent compositional structures [*Chistyakova and Latypov*, 2010; *Martorano et al.*, 2011]. While this example of thermally driven fracture closure is an oversimplification, neglecting mechanics/movement of the ice shell, fluid flow within the fracture, evolving fracture geometry, and infilling of the fracture due to marine ice accretion, it demonstrates the first order properties expected in these environments.

3.5.3 Brines within the Ice

Knowing the composition of the ice provides the chance to evaluate the formation, evolution, and longevity of water or brine systems within Europa's ice shell. For example,

shallow lenses of liquid water are suggested to form *in situ* via melting of the ice shell [*Schmidt et al.*, 2011b] (Figure 3.2) or by injection through diking processes [*Manga and Michaut*, 2017; *Michaut and Manga*, 2014]. For such a lens, assuming the ice shell derived from a 34 ppt terrestrial ocean chemistry, letting the diffusive limit govern ice bulk salinity as shown above ($S_{lim} = \phi_c S_{oc}$) and tracking the evolving lens salinity, upon top down refreeze a 2 km thick lens located 1 km beneath a 100 K surface will produce ice compositions ranging from 0.0946 to 14.10 ppt. Additionally, upon complete refreeze, impurity rejection leads to the precipitation of an approximately 2.23 m layer of pure salt, assuming a saturation limit of 282 ppt (Figure 3.14). Thus, impurity entrainment and rejection during freezing produce compositional heterogeneities within the ice shell and introduce a concentration process capable of producing layers within the shell that have highly distinct mechanical, thermal, and dielectric properties. The ability to predict compositional variations around putative hydrological features in Europa's shell will both constrain how these features form and inform spacecraft observations [*Blankenship et al.*, 2009; *Kalousová et al.*, 2017].

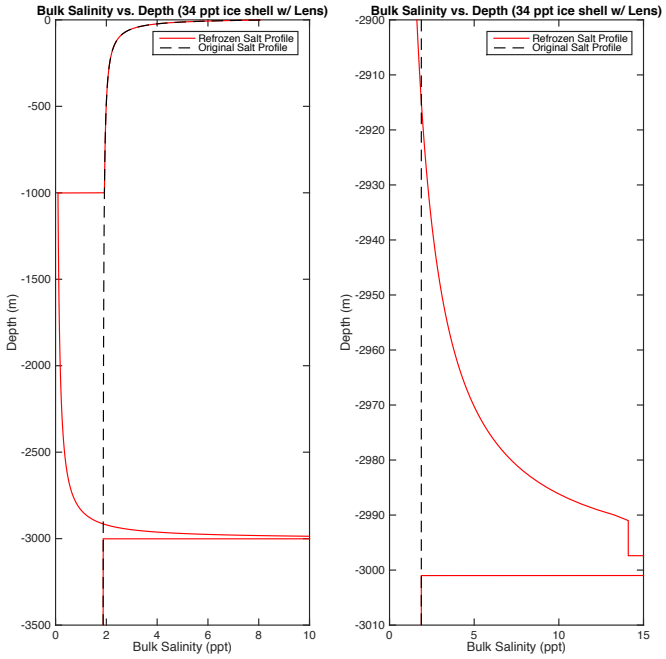

Figure 3.14: Bulk salinity profile of a perched water lens upon re-solidification. Left) A 2 km thick lens is assumed to form via the *in situ* melting of a preexisting ice shell, whose original composition is given by the black dashed line. Initially the lens salinity is less than that of the original ocean, but upon top down solidification salt is concentrated in the remaining liquid phase, leading to an increase in ice bulk salinity [red line] near the base of the refrozen lens as well as ~2.23 m of precipitated salt on the lens floor (1000 ppt values excluded from plot). **Right)** A magnified view of ice bulk salinity near the bottom of the lens (2.90 – 3.01 km). The lens saturates (282 ppt) when the ice reaches 2991 m, resulting in salt precipitation (2997.77 – 3000 m).

3.6 Conclusion

The impurity load and distribution of entrained ocean materials within Europa's ice shell impacts the evolution of the ice shell, Europa's geology, and interactions between the surface and the ocean. Salts affect the rheological properties of the ice, especially relative to pure water ice, which impacts its mechanical behavior [*Durham et al.*, 2010]. We explicitly quantify the overall impurity content of Europa's ice shell, suggesting an average

composition (total salt/ice shell mass) of between 1.053 and 14.72 ppt of non-ice material (depending on ocean composition), which can be included in more realistic models of geophysical evolution of the ice shell. These results also demonstrate regions of high material contrast within the ice shell that could promote or extend geologic activity. Compositional heterogeneities can either aid or prevent buoyancy driven convection in the ductile region of the ice shell, which is important for constraining the rates of subduction and surface recycling [*Johnson et al.*, 2017a; *Kattenhorn*, 2018]. Determining the lifetime of liquid water features within the ice shell is of profound importance in considering whether such reservoirs could be putative habitats; relevant for both planetary exploration and planetary protection. While our models suggest that shallow subsurface water in a conductive ice shell is short lived, the warmer, isothermal regime of an ice shell undergoing convection may provide an environment where hydrological features could persist for much longer. New constraints on the average density and composition of the ice feeds forward into the putative reductant-oxidant cycle associated with ocean-surface interaction [*Vance et al.*, 2016], by which ice shell overturn delivers surface-generated oxidants and ice-shell derived chemical species as potential energy sources to the ocean. Compositional profiles of the bulk ice shell and geologic features effectively capture the thermal and physicochemical nature of the ice that can be observed by Europa Clipper's remote sensing and radar instruments: the spatial distribution of impurities on the surface and the dielectric properties of the ice and water within the shell carry with them an accessible fingerprint of ice shell dynamics and the ocean below.

Chapter 4: Ice-Ocean Interfaces as Mushy Layers

The goal of this chapter is to further investigate the structure and evolution of ice-ocean interfaces and the implications their presence and characteristics have on the geophysics and habitability of ice-ocean worlds. The dependence of mushy layer geometry and evolution on environmental parameters is explored by analytically solving for the thickness of a simplified ice-ocean mushy layer system. Two dynamic regimes are investigated, one driven by molecular diffusion and one driven by convection of brine within the mushy layer. The impact of gravity, thermal gradient, and ocean composition on the thickness of mushy layers is explored. Additionally, perturbation analysis is carried out to investigate the stability of mushy layers. It is shown that there exist stable equilibrium mushy layer thicknesses, suggesting that mushy layers are likely persistent and common features of ice-ocean worlds. Understanding the potential diversity of these multiphase layers across solar system bodies provides insight into the potential rates and mechanisms of heat and solute transport between their respective oceans and ice shells. Variations in mushy layer properties may drive diverse geophysical processes unique to individual bodies or that may vary regionally on an individual icy world. Current limitations to numerical models of multiphase reactive transport in planetary ices are discussed, highlighting the important roles critical porosity and permeability-porosity relationships play in the dynamics and evolution of ice-ocean interfaces. Contemporary models exploring the two-dimensional heterogeneities produced during the solidification of sea ice are reviewed as are the diagenetic and biogeochemical processes that characterize a number of terrestrial ice-ocean environments. The potential geophysical and astrobiological implications of

analogous processes and heterogeneities occurring on icy satellites is discussed, drawing parallels to the advances made by reactive transport modelling in our understanding of the Earth system.

4.1 Introduction

In a rapidly changing Earth system, understanding and quantifying the interdependencies of the cryosphere, hydrosphere, atmosphere, and biosphere are imperative in constraining their interactions and constructing accurate predictive models [*Notz*, 2012; *Notz and Bitz*, 2017]. Likewise, constraining the exchange of energy and mass between the oceans and ice shells of icy satellites in our solar system is crucial to understanding their geophysical evolution and assessing their habitability [*Jaumann et al.*, 2009; *Sotin and Tobie*, 2004; *Vance et al.*, 2018]. In either case, the physics occurring near the ice-ocean interface play a disproportionate role. When ice forms from an aqueous solution, such as an ocean, rather than forming a monocrystalline solid the ice-liquid interface is characterized by a porous matrix of dendritic ice crystals bathed in interstitial brine. Frequently referred to as a 'mushy layer', this two-phase regime forms a dynamic boundary between the ocean and overlying ice, whose evolution is best described by the equations of reactive transport in porous media, which account for the diffusive and advective transport of both heat and mass alongside thermochemical reactions [*Feltham et al.*, 2006; *Hunke et al.*, 2011]. This complex and dynamic multiphase boundary layer plays a crucial role in governing the evolution and properties of both the overlying ice and underlying water reservoir [*Buffo et al.*, 2018; *Buffo et al.*, *in review; Grumbine*, 1991; *Lake and Lewis*, 1970; *Lewis and Perkin*, 1983; *Turner and Hunke*, 2015]. The most

ubiquitous and well observed example of such an ice-ocean mushy layer is sea ice. While it has long been known that sea ice is a heterogeneous medium [*Malmgren and Institutt*, 1927], only recently have the dynamics and effects of these physicochemical heterogeneities begun to be understood, quantified, and incorporated into numerical models. For sea ice, the mushy layer can comprise a substantial amount of the ice cover and determines the heat and mass transport to and from both the ocean and atmosphere [*Aagaard and Carmack*, 1989; *Bitz and Lipscomb*, 1999; *Buffo et al.*, 2018; *Eicken et al.*, 2002; *Freitag*, 1999; *Griewank and Notz*, 2013; *Loose et al.*, 2009; *Loose et al.*, 2011; *Turner and Hunke*, 2015]. It provides an ecological niche for a diverse and important group of primary producers and grazers in the polar oceans [*Loose et al.*, 2011; *Tedesco and Vichi*, 2014; *Thomas and Dieckmann*, 2003; *Vancoppenolle et al.*, 2013; *Vancoppenolle and Tedesco*, 2015], plays a fundamental role in the formation of global ocean water masses [*Dickson and Brown*, 1994; *Grumbine*, 1991; *Hughes et al.*, 2014; *Robinson et al.*, 2014], and governs the properties and evolution of the overlying sea ice [*Cottier et al.*, 1999; *Cox and Weeks*, 1974; *Eicken*, 1992; *Griewank and Notz*, 2015; *Kawano and Ohashi*, 2008; *Nakawo and Sinha*, 1981; *Ohashi*, 2007]. Consequently, models which include the physics of multiphase reactive transport provide the most accurate simulations of sea ice growth, dynamics and material properties [*Bitz and Lipscomb*, 1999; *Griewank and Notz*, 2015; *Griewank and Notz*, 2013; *Wells et al.*, 2011; *Wells et al.*, 2019; *Wettlaufer et al.*, 1997a; *Worster and Rees Jones*, 2015].

Ice-ocean/brine interfaces are likely not a feature unique to Earth, as a number of other solar system bodies likely harbor substantial liquid water reservoirs [*Čadek et al.*, 2016; *Carr*, 1987; *Carr et al.*, 1998; *Kivelson et al.*, 2000; *Kuskov and Kronrod*, 2005;

Nimmo and Pappalardo, 2016; *Porco et al.*, 2006; *Sohl et al.*, 2003; *Vance et al.*, 2014]. The putative structure of many of these ice-ocean worlds is a thick (2-80+ km) ice shell overlaying a subsurface ocean from which the ice shell likely formed [*Schubert et al.*, 2004]. A unique feature of a number of these ice-ocean worlds (Europa, Triton, Enceladus) is the presence of youthful surface terrain, suggesting recent geological activity [*Greeley et al.*, 2004; *Kattenhorn and Prockter*, 2014; *Sotin and Prieur*, 2007], potential ocean-surface interaction [*Howell and Pappalardo*, 2018; 2019], and possible near surface hydrological features [*Manga and Michaut*, 2017; *Manga and Wang*, 2007; *Michaut and Manga*, 2014; *Schmidt et al.*, 2011a; *Sotin and Tobie*, 2004]. Ongoing energy production within the interior of these bodies (radiogenic, tidal) may promote such contemporary geophysical processes [*Hussmann et al.*, 2006; *Hussmann and Spohn*, 2004; *Hussmann et al.*, 2002; *Vance et al.*, 2007]. Other ice-ocean worlds (e.g. Callisto, Ganymede) may possess subsurface oceans thick enough to maintain layers of high-pressure ices separating their silicate interiors and liquid water reservoirs [*Fortes*, 2000; *Kuskov and Kronrod*, 2005; *Nagel et al.*, 2004; *Sohl et al.*, 2003; *Vance et al.*, 2014]. Triton and Pluto possess more exotic ices (e.g. ammonia, nitrogen) that may be in contact with subsurface oceans [*Gaeman et al.*, 2012; *Hammond et al.*, 2018; *Johnson et al.*, 2016; *Nimmo et al.*, 2016; *Robuchon and Nimmo*, 2011], while Ceres likely possesses a water-rich silicate crust and potentially a deep brine reservoir [*Castillo-Rogez and McCord*, 2010; *Ruesch et al.*, 2016] as well as localized near surface hydrological features beneath recent impact craters [*De Sanctis et al.*, 2016; *Hesse and Castillo-Rogez*, 2019; *Ruesch et al.*, 2016; *Schenk et al.*, 2019; *Scully et al.*, 2019].

A common, and likely important, feature that distinguishes the ice on all of these worlds from sea ice on Earth is its spatiotemporal scale. While thicker and older multiyear sea ice exits, the overwhelming majority of sea ice is first year ice [*Korosov et al.*, 2018]. Regardless, both exhibit ages and thickness that pale in comparison to those of planetary ices, which may be millions to billions of years old and are typically kilometers to tens of kilometers thick [*Hussmann et al.*, 2002; *Prockter*, 2017; *Schubert et al.*, 2004]. The orders of magnitude disparity between the spatial and temporal scales of these ices likely subjects them to unique thermal and physicochemical processes that cannot be simulated wholescale in the laboratory or observed in natural terrestrial ices. It has been suggested that these ancient, thick planetary ice layers may exhibit geophysical processes and stratigraphy akin to that of Earth's interior [*Barr and McKinnon*, 2007; *Head et al.*, 1997; *Kattenhorn and Hurford*, 2009; *Kattenhorn and Prockter*, 2014; *McKinnon*, 1999]. When the exterior ice shells of these worlds reach a critical thickness, they are thought to undergo solid state convection, forming stratigraphic layers that mirror the terrestrial lithosphere-mantle-outer core system [*Barr and McKinnon*, 2007; *Foley and Becker*, 2009; *Head et al.*, 1997; *McKinnon*, 1999; *Mitri and Showman*, 2005]. The Galilean satellite Europa provides an archetype example of such a system, exhibiting surface geology indicative of a dynamic, layered ice shell [*McKinnon*, 1999]. This would consist of a brittle upper ice lithosphere (~2-6 km) [*Pappalardo and Coon*, 1996], a relatively isothermal, ductile ice mantle undergoing solid state convection, overlaying a liquid water ocean (here, akin to Earth's outer core) [*Barr and McKinnon*, 2007; *McKinnon*, 1999; *Mitri and Showman*, 2005]. There exist regions where the icy lithosphere has likely been subducted/subsumed into the moon's interior [*Kattenhorn and Prockter*, 2014], surface features that suggest

interaction with near surface water [*Manga and Michaut*, 2017; *Michaut and Manga*, 2014; *Schmidt et al.*, 2011a], evidence of resurfacing [*Fagents et al.*, 2000; *Manga and Wang*, 2007], and dilational bands that mimic terrestrial mid-ocean ridges [*Head et al.*, 1999; *Howell and Pappalardo*, 2018; 2019; *Manga and Sinton*, 2004; *Prockter et al.*, 2002]. Moreover, the mottled texture and coloration of Europa's surface suggests there exist compositional and phase heterogeneities within the moon's ice shell [*Fanale et al.*, 1999; *Pappalardo and Barr*, 2004; *Zolotov and Shock*, 2001]. Much like the terrestrial rock cycle it is likely that physical and thermochemical variations within the ice shell play a crucial role in governing its material properties, dynamics and evolution [*Barr and McKinnon*, 2007; *Foley and Becker*, 2009; *Lyubetskaya and Korenaga*, 2007; *Steefel et al.*, 2005].

In Earth's mantle and lithosphere such mushy layers govern the thermochemical evolution of magma bodies [*Fowler*, 1987; *McKenzie*, 1984; *Reiners*, 1998; *Worster et al.*, 1990] and the process of fractional crystallization can be extended to ice-ocean systems to understand the chemical evolution of interstitial brines. In the magmatic analog, melt transport and evolution, physicochemical heterogeneities, and regions of phase change are all important factors governing the interior geodynamics of Earth and the other terrestrial planets [*Foley and Becker*, 2009; *Lyubetskaya and Korenaga*, 2007; *McKenzie*, 1984; *Nakagawa and Tackley*, 2004; *Reiners*, 1998; *Zhong et al.*, 2008]. Inclusion of the physics associated with these processes has revolutionized geophysical models and drastically improved our understanding of Earth's interior and the surface expression of these subterranean dynamics [*Braun*, 2010; *McKenzie*, 1984; *Steefel et al.*, 2005]. While ice-ocean worlds appear to undergo similar processing and exhibit a number of surface features consistent with a multiphase and hydrologically active lithosphere-mantle-ocean system,

in this case represented by the ice shell [*Fagents et al.*, 2000; *Greeley et al.*, 2004; *Howell and Pappalardo*, 2018; *Kargel et al.*, 2000; *Kattenhorn and Prockter*, 2014; *Kuskov and Kronrod*, 2005; *Manga and Michaut*, 2017; *McKinnon*, 1999; *Michaut and Manga*, 2014; *Schmidt et al.*, 2011a], the physical and thermochemical structure of these planetary ice layers remain largely unconstrained [*Buffo et al.*, *in review; Kargel et al.*, 2000]. A number of ice-ocean world geophysical models have highlighted the importance that impurities, heterogeneity, and melts may play in driving tectonism [*Howell and Pappalardo*, 2018; 2019; *Johnson et al.*, 2017b], hydrological feature generation and evolution [*Manga and Michaut*, 2017; *Michaut and Manga*, 2014; *Schmidt et al.*, 2011a], thermo-compositional convection in the ductile mantle [*Barr and McKinnon*, 2007], and the formation of geological features [*Head et al.*, 1999], however the majority of these models implement *a priori* heterogeneous distributions of salts and other impurities and do not incorporate the thermochemical evolution of multiphase systems explicitly. Conversely, recent work, e.g. [*Buffo et al.*, *in review; Hammond et al.*, 2018; *Hesse and Castillo-Rogez*, 2019; *Kalousová et al.*, 2014; 2016] has begun to demonstrate the crucial role reactive transport processes and properties of multiphase regions play in the dynamics and evolution of ice-ocean worlds. What has become clear is that planetary ices are likely not homogenous and inert, but rather contain structural and chemical heterogeneities that determine their material properties and in turn govern the characteristic geophysics of ice-ocean worlds.

The terrestrial core-mantle boundary (CMB or D" region) is likely a molten mushy layer whose structure, topography, and dynamics may drive a number of global geophysical processes including plate tectonics, mantle plumes, and the geodynamo [*Burke et al.*, 2008; *Lay et al.*, 2008; *Maruyama et al.*, 2007; *Nakagawa and Tackley*, 2004; *Olson*

et al., 1987; *Olson et al.*, 2010]. This global solid-liquid interface likely exhibits density driven fluid processes and pressure dependent phase structure akin to the brine rejection and pressure induced basal accretion/ablation cycling of growing and evolving ice shells [*Buffo et al.*, *in review; Soderlund et al.*, 2014]. Thus, the analogous ice-ocean interface may play a similar role in driving the geodynamics of ice-ocean systems.

A fundamentally important component in all of the systems outlined above is the multiphase boundary layer (mushy layer) between regions of solid and regions of melt. On icy worlds, ice-ocean/brine interfaces will likely dictate the physical and thermochemical properties and evolution of both the ice and parent liquid reservoir, while providing a dynamic, gradient rich substrate that could, like the ice-ocean interface of sea ice, provide a habitable environment for organisms. With the crucial role multiphase mushy layers play in terrestrial geophysical processes and their likely analogous counterparts on ice-ocean worlds it is instructive to investigate the characteristics and evolution of these boundary layers and the effects environmental variables have on their structure, stability, and thermochemical transport capabilities. Here, two such investigations are presented, described in further detail, and their implications for ice-ocean worlds discussed; the thickness and stability of mushy layers in diverse environments, and the effects of small-scale multi-dimensional processes and heterogeneities on the evolution of mushy layers.

4.2 Mushy Layer Thickness and Stability

The presence and dynamics of mushy layers determines the thermal and chemical fluxes across the ice-ocean/brine interface, thus it is important to understand what determines the stability and properties of this boundary. Quantifying the interdependence

of mushy layer characteristics and local environmental pressures can aid in predicting the structure and dynamics of the potentially diverse mushy layers that may exist throughout the solar system, and how these variations could promote or constrain distinct geophysical processes. To investigate the thickness and stability of mushy layers a simplified ice-mush-ocean system is assumed (Figure 4.1) such that analytical solutions of the evolving mushy layer geometry can be sought. The effects of gravity, ocean concentration, and thermal gradient on equilibrium mushy layer thickness are investigated. Perturbation stability analysis is carried out, demonstrating that these equilibrium thicknesses are indeed stable. Finally, potential implications of variable mushy layer thicknesses on the habitability, geophysics, and future spacecraft observations of ice-ocean worlds are discussed.

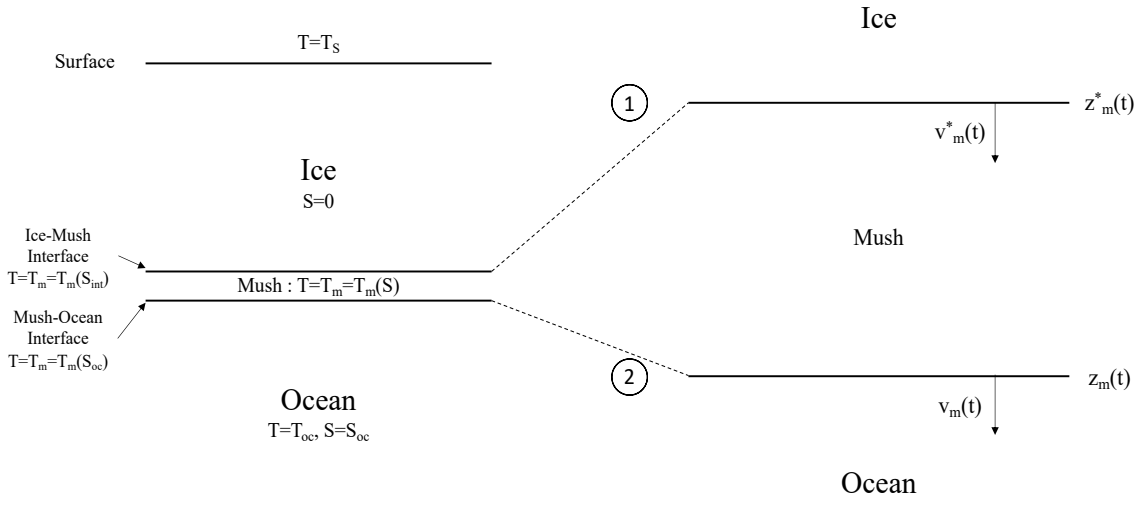

Figure 4.1 – Geometry and dynamics of the mushy layer. (Left) Schematic showing the simplified geometry of the ice-mush-ocean system as well as relevant boundary condition values. **(Right)** A magnified view of the mushy layer highlighting the ice-mush (1) and mush-ocean (2) interfaces and their respective propagation velocities.

4.2.1 Equilibrium Mushy Layer Thickness

Given the geometry presented in Figure 4.1, the mushy layer thickness will be defined by two boundaries, the ice-mush interface (1) and the mush-ocean interface (2). It is assumed that when the respective velocities of these two boundaries are equal an 'equilibrium' mushy layer of thickness *h* will form. Symbolically, there exist velocities that characterize equilibrium mushy layers of thickness *h* determined by environmental parameters such that:

$$v_m(t) = \dot{z}_m(t) = \dot{z}_m^*(t) = v_m^*(t) \qquad (4.1)$$

The velocities of these interfaces can be solved for assuming the evolution of the interfaces can be represented by Stefan problems, one dictated by heat transport, the other by mass (salt) transport. Such an approach is valid because at the mush-ocean interface, a high liquid fraction regime, a small change in liquid fraction (ice formation) will produce a certain amount of latent heat that needs to be removed from the interface before continued freezing can occur, while the resultant increase in salinity due to salt rejection from the forming ice will negligibly affect the freezing front propagation (i.e. at large liquid fractions the freezing point depression due to salinity increase will be small). Conversely, at the ice-mush interface, a low liquid fraction regime, an equal amount of latent heat will be produced by the same change in liquid fraction, but a much larger increase in salinity will occur. Thus, the freezing point depression due to salinity increase will be large and for continued freezing to occur salt must be transported away from the interface. While certainly a simplification, such a system lends itself to analytical solutions that bound the general evolution of the mushy layer. The strategy presented herein for solving these types

of problems follows closely the heat transfer and Stefan problem solutions presented in [*Turcotte and Schubert*, 2014].

It is assumed that the mush-ocean interface (interface 2, $z_m(t)$) propagation is dictated by conductive heat transport away from the interface upwards through the overlying ice. This is the classic Stefan problem and has the solution [*Huber et al.*, 2008]:

$$z_m(t) = 2\lambda_T\sqrt{\kappa_i t} \tag{4.2}$$

$$\lambda_T \exp(\lambda_T^2)\,\mathrm{erf}(\lambda_T) = \frac{c_i(T_{oc} - T_S)}{L\sqrt{\pi}} \tag{4.3}$$

$$T(z,t) = T_S - (T_S - T_{oc})\frac{\mathrm{erf}\left(\dfrac{z}{2\sqrt{\kappa_i t}}\right)}{\mathrm{erf}(\lambda_T)} \tag{4.4}$$

We investigate the evolution of the ice-mush interface (interface 1, $z_m^*(t)$) in two mass transport regimes, an advective regime when brine drainage is the dominant mechanism of salt transport and a diffusive regime when molecular diffusion is the dominant mechanism of salt transport. These two regimes provide endmember scenarios for mushy layer evolution in high and low thermal gradient environments. The advective regime will dominate the interface evolution of thin ice and ice-ocean/brine interfaces subject to large thermal gradients, while the diffusive regime will dictate the interface dynamics of thick and temperate ice. In either case, we will assume that there is no salt in the ice phase, and that the system is governed by the boundary conditions:

$$S(z = \infty, t) = S_{oc} \tag{4.5}$$

$$S(z = z_m^*(t), t) = S_{int} \tag{4.6}$$

$$S(z, t = 0) = S_{oc} \tag{4.7}$$

Introducing the dimensionless salinity ratio:

$$\theta = \frac{S - S_{oc}}{S_{int} - S_{oc}} \tag{4.8}$$

We see that the boundary conditions on θ are:

$$\theta(z = \infty, t) = 0 \tag{4.9}$$

$$\theta(z = z_m^*(t), t) = 1 \tag{4.10}$$

$$\theta(z, t = 0) = 0 \tag{4.11}$$

4.2.1.1 Diffusion Regime

We solve for the interfacial velocity (and ultimately the mushy layer thickness) in the diffusive regime first. In this case the evolution of salinity in the system is governed by:

$$\frac{\partial S}{\partial t} = D\frac{\partial^2 S}{\partial z^2} \tag{4.12}$$

And we introduce the dimensionless variable:

$$\eta = \frac{z}{2\sqrt{Dt}} \tag{4.13}$$

In a similar fashion as before we can show that in terms of θ and η the diffusion equation can be written as:

$$-\eta\frac{\partial \theta}{\partial \eta} = \frac{1}{2}\frac{\partial^2 \theta}{\partial \eta^2} \tag{4.14}$$

And boundary conditions necessitate that for both $z = \infty$ and $t = 0$, $\eta = \infty$ and for $z = z_m$, $\eta_m = \frac{z_m}{2\sqrt{Dt}} = \lambda_S$. So,

$$\theta(\eta = \infty) = 0 \tag{4.15}$$

$$\theta(\eta = \lambda_S) = 1 \tag{4.16}$$

Let

$$\phi = \frac{\partial \theta}{\partial \eta} \tag{4.17}$$

The diffusion equation can be solved to produce:

$$\theta = c_1 \int_0^{\eta} \exp(-\eta'^2)\, d\eta' + c_2 \tag{4.18}$$

Utilizing the boundary conditions to solve for c_1 and c_2:

$$\theta = \frac{1}{erfc(\lambda_S)} - \frac{\text{erf}\,(\eta)}{erfc(\lambda_S)} \tag{4.19}$$

Writing in terms of the original variables *S, z* and *t*:

$$S = S_{oc} + (S_{int} - S_{oc})\left(\frac{1}{erfc(\lambda_S)} - \frac{\text{erf}\,(z/2\sqrt{Dt})}{erfc(\lambda_S)}\right) \tag{4.20}$$

The Stefan condition for this problem can be garnered from the equation for conservation of salt:

$$\int_{z_m^*(t)}^{\infty} S(z,t)dz = cnst. \tag{4.21}$$

Taking the temporal derivative of this equation and applying the Leibniz integral rule:

$$-S(z_m^*, t)\frac{dz_m^*}{dt} + \int_{z_m^*(t)}^{\infty} \frac{\partial S}{\partial t} dz = 0 \qquad (4.22)$$

Substituting $\frac{\partial S}{\partial t} = D\frac{\partial^2 S}{\partial z^2}$, noting $S(z_m^*, t) = S_{int}$ and carrying out the integral gives:

$$S_{int}\frac{dz_m^*}{dt} = -D\frac{\partial S(z = z_m^*)}{\partial z} \qquad (4.23)$$

The derivatives are:

$$\frac{dz_m^*}{dt} = \frac{\lambda_S\sqrt{D}}{\sqrt{t}} \qquad (4.24)$$

And

$$\frac{\partial S(z = z_m^*)}{\partial z} = \frac{-(S_{int} - S_{oc})}{erfc(\lambda_S)}\frac{\exp(-\lambda_S^2)}{\sqrt{\pi D t}} \qquad (4.25)$$

Substituting,

$$S_{int}\sqrt{\pi} = \frac{(S_{int} - S_{oc})}{\lambda_S erfc(\lambda_S)}\exp(-\lambda_S^2) \qquad (4.26)$$

Or, rearranging

$$\lambda_S erfc(\lambda_S)\exp(\lambda_S^2) = \frac{(S_{int} - S_{oc})}{S_{int}\sqrt{\pi}} \qquad (4.27)$$

Substituting the value of S_{int} and setting the interface velocities equal produces two equations:

$$\lambda_S = \frac{\lambda_T\sqrt{\kappa_i}}{\sqrt{D}} \qquad (4.28)$$

And

$$15.1106\left(T_{mp} - \left(T_S + (H-h)\frac{(T_{oc}-T_S)}{H}\right)\right)\sqrt{\pi} = \frac{15.1106\left(T_{mp} - \left(T_S + (H-h)\frac{(T_{oc}-T_S)}{H}\right)\right) - S_{oc}}{\lambda_S erfc(\lambda_S)}\exp(-\lambda_S^2) \qquad (4.29)$$

Which can be solved for *h*. The equation is linear in *h*, so has one solution.

Archie's law is employed to estimate the molecular diffusion in a porous medium and it is assumed that the ice-mush interface porosity is equal to a critical porosity (ϕ_c) which relates to the percolation threshold of ice [*Buffo et al.*, 2018; *Buffo et al.*, *in review; Golden et al.*, 2007]:

$$D = k_S\phi_c^m \qquad (4.30)$$

Where k_S is the molecular diffusivity of salt in water and *m* is a cementation exponent, here=2, which describes how ion transport is limited by porosity. Lastly the permeability-porosity relationship utilized is that of [*Griewank and Notz*, 2013]:

$$\Pi(\phi_c) = 10^{-17}(10^3\phi_c)^{3.1} \qquad (4.31)$$

In the diffusion regime equilibrium mushy layer thicknesses always exceed the total ice thickness. This is an impossible mushy layer thickness and implies that there does not exist stable mushy layer thicknesses driven by diffusion of salt from the ice-mush interface. This is a reasonable result for the simplified system considered here as the molecular diffusivity of salt is much less than the thermal diffusivity of ice and salinity has been handcuffed to temperature by the linear liquidus relationship, therefore large salinity gradients in the absence of large thermal gradients cannot be produced (which could potentially offset the difference between D and κ_i).

In reality, there exist ice-ocean interfacial systems which *are* governed by diffusive processes (e.g. marine ice beneath terrestrial ice shelves [*Wolfenbarger et al.*, 2018; *Zotikov et al.*, 1980], and likely the majority of Europa's deep ice shell [*Buffo et al.*, *in review*]). This suggests that the detailed microphysics governing the evolution of these dynamic layers plays a crucial role in governing the transport processes and resultant ice physicochemical properties. Furthermore, the analytical solutions provided herein account for more physics than the standard partition coefficient approach (e.g. [*Weeks and Lofgren*, 1967]) yet still fail to capture all of the dynamics occurring at this interface. This highlights the need to identify the environmental pressures and physical characteristics that constrain the dynamics governing mushy layer evolution and reinforces the necessity of including multiphase reactive transport processes in models simulating these interfaces. Below we identify a number of current limitations in our understanding of relevant microphysical

processes and emphasize the important role constraining mushy layer properties such as critical porosity and permeability will play in improving our predictions of planetary ice material properties, biogeochemistry, and ice-ocean world geophysics.

4.2.1.2 Advection Regime

In this case the evolution of salinity in the system is governed by:

$$\frac{\partial S}{\partial t} = -br_j^{\downarrow} \frac{\partial S}{\partial z} \tag{4.32}$$

Where $br_j^{\downarrow}$ is brine velocity out of the interfacial layer as calculated by the linear relationship presented in [*Griewank and Notz*, 2013] (See Section 2.2.2). In dimensionless form θ:

$$\frac{\partial \theta}{\partial t} = -br_j^{\downarrow} \frac{\partial \theta}{\partial z} \tag{4.33}$$

We introduce the dimensionless length scale:

$$\eta = \frac{z}{br_j^{\downarrow} t} \tag{4.34}$$

And it follows that at the interface, z_m^*, the dimensionless variable can be written:

$$\eta_m = \frac{z_m^*}{br_j^{\downarrow} t} \tag{4.35}$$

Rewriting the advection equation components in terms of η:

$$\frac{\partial \theta}{\partial t} = \frac{\partial \theta}{\partial \eta}\frac{\partial \eta}{\partial t} = \frac{\partial \theta}{\partial \eta}\frac{-z}{br_j^{\downarrow} t^2} = -\frac{\eta}{t}\frac{\partial \theta}{\partial \eta} \tag{4.36}$$

$$\frac{\partial \theta}{\partial z} = \frac{\partial \theta}{\partial \eta}\frac{\partial \eta}{\partial z} = \frac{1}{br_j^{\downarrow} t}\frac{\partial \theta}{\partial \eta} \tag{4.37}$$

$$\implies \eta\frac{\partial \theta}{\partial \eta} = \frac{\partial \theta}{\partial \eta} \tag{4.38}$$

Therefore $\eta = \eta_m = 1$. Which implies that:

$$z_m^* = br_j^{\downarrow} t \tag{4.39}$$

Demonstrating that the interface will propagate as fast as salt can be advected away from it. Setting the two velocities equal to each other ($\dot{z}_m(t) = \dot{z}_m^*(t)$) and solving for *h,* we make use of the gravity drainage parameterization (Equation 2.10) and the relationship between thermal gradient and freezing front propagation velocity (Equation 3.12). $\dot{z}_m^*(t) = br_j^{\downarrow} = v_m(t) = \dot{z}_m(t)$, from Equation 3.12:

$$v_m(t) = -\frac{\partial T}{\partial z}\frac{\mathrm{erf}(\lambda_T)\sqrt{\pi}\lambda_T\kappa_i \exp(\lambda_T^2)}{(T_S - T_{oc})} \qquad (4.40)$$

And from equation 2.10:

$$br_j^{\downarrow} = \alpha\left(\frac{g\rho_{sw}\beta\Delta S_j\widetilde{\Pi}h}{\kappa\mu} - Ra_c\right) \qquad (4.41)$$

Assuming a conductive (linear) thermal profile in the ice shell, $\partial T/\partial z = (T_{oc} - T_S)/H$, we have:

$$\alpha\left(\frac{g\rho_{sw}\beta\Delta S_j\widetilde{\Pi}h}{\kappa_{br}\mu} - Ra_c\right) = \frac{\mathrm{erf}(\lambda_T)\sqrt{\pi}\lambda_T\kappa_i \exp(\lambda_T^2)}{H} \qquad (4.42)$$

The term ΔS_j is the difference in salinity between the interface and the ocean, $S_{int} - S_{oc}$, and we assume that the interface is at its melting temperature, T_f, which we take as a linear function of salinity $T_f = T_{mp} - 0.066178S$, where T_{mp} is the melting temperature of pure ice. Solving for *S* and letting T_f lie on the conductive thermal profile at a depth *H-h*. We have:

$$S_{int} = 15.1106\left(T_{mp} - T_f\right) = 15.1106\left(T_{mp} - \left(T_S + (H-h)\frac{(T_{oc} - T_S)}{H}\right)\right) \qquad (4.43)$$

Substituting into ΔS_j:

$$\alpha\left(\frac{g\rho_{sw}\beta(15.1106\left(T_{mp}-\left(T_S+(H-h)\frac{(T_{oc}-T_S)}{H}\right)\right)-S_{oc})\widetilde{\Pi}h}{\kappa\mu}-Ra_c\right)=\frac{\mathrm{erf}(\lambda_T)\sqrt{\pi}\lambda_T\kappa_i\exp(\lambda_T^2)}{H} \quad (4.44)$$

Algebraic manipulation reveals this equality produces a quadratic equation in h with one positive root and one negative root (which can be ignored, as a negative mushy layer thickness is not physically meaningful).

The ability to solve for the expected mushy layer thickness, to first order, under given environmental conditions provides a method to predict and compare the general characteristics and evolution of multiphase interfaces across different ice-ocean worlds in the solar system. Mushy layer thickness has direct implications for the rate and method of heat and mass transport across the ice-ocean interface as the extent of hydraulic conductivity near the base of the ice will dictate the spatiotemporal evolution of the pore fluid flow, governing solidification rates and ultimately the composition of the overlying ice [*Buffo et al.*, *in review*]. This is especially true in the advective regime, where gravity drainage provides the primary mechanism for ice desalination [*Griewank and Notz*, 2013]. As a gateway for material and energy transport between the ocean and ice shell determining whether certain environmental parameters can act to catalyze or buffer material entrainment and/or heat transport at the ice-ocean interface has implications for ocean-surface material transport estimates, basally driven geodynamic processes, surface expression of potential ocean-derived biosignatures, as well as ice shell composition and material properties.

4.2.1.3 The Effects of Environmental Parameters on Mushy Layer Thickness

To investigate the influence of a number of environmental parameters on the equilibrium thickness of mushy layers Equation 4.44 is solved under variable gravity, ocean concentrations, and thermal forcing. The intention of these solutions is to understand the range of potential mushy layer properties and corresponding dynamics that may arise across the diverse ice-ocean worlds that populate our solar system. These same techniques may be applied to even more exotic ice-ocean worlds beyond the reaches of our own planetary system.

4.2.1.3.1 Validation Under Terrestrial Conditions

It is instructive to validate the mushy layer equilibrium thicknesses predicted by Equation 4.44 for the terrestrial ice-ocean system as there exist laboratory and field measurements against which the results can be compared. A terrestrial ocean composition is assumed (See Table 3.1), and three surface temperatures are investigated; 230 K, 255 K, and 265 K, while an ocean temperature of 270.90 K is utilized. The relationship between ice thickness (H) and mushy layer equilibrium thickness (h) for all three surface temperatures can be seen in Figure 4.2, which demonstrates that colder surface temperatures promote thinner equilibrium mushy layer thicknesses than do more temperate surface temperatures. Mushy layer equilibrium thicknesses range between 0-10 cm. These thicknesses agree well with values measured in both laboratory experiments of sea ice growth [*Wettlaufer et al.*, 1997a; b] and empirical observation of natural sea ice [*Notz and Worster*, 2008], which typically find mushy layer thicknesses ~10 cm or less, with maximums reaching ~20 cm. Sea ice is relatively thin and thus supports substantial thermal

gradients [~10 K/m] (when compared to those near the base of terrestrial ice shelves [~0.08 K/m [*Zotikov et al.*, 1980]] and those expected at the base of planetary ice shells [~0.02 K/m [*McKinnon*, 1999; *Mitri and Showman*, 2005]]), resulting in relatively thin equilibrium mushy layer thicknesses. Thicker ice with lower interfacial thermal gradients should support thicker mushy layers, and indeed columnar ice accreted 410 m beneath the Ross Ice Shelf was observed to be hydraulically connected to the underlying ocean multiple meters above the ice ocean interface [*Zotikov et al.*, 1980].

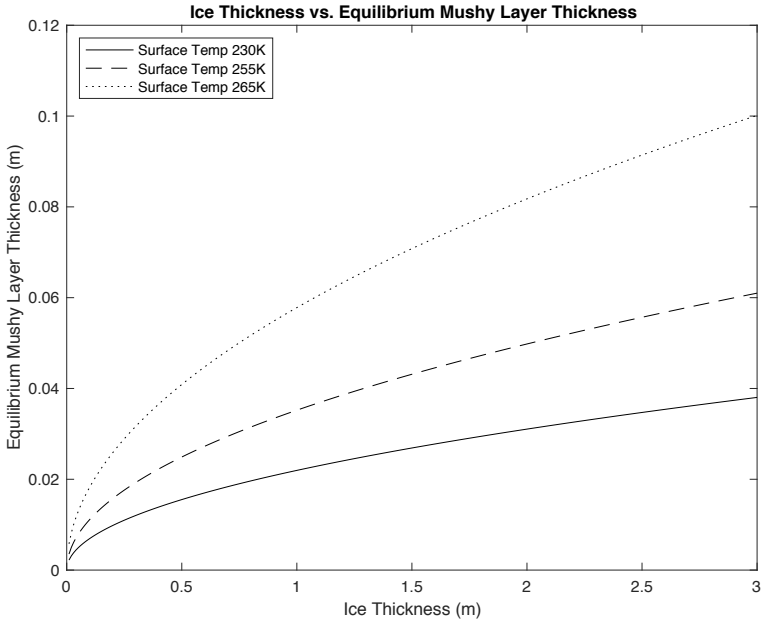

Figure 4.2 – Mushy layer equilibrium thicknesses under terrestrial conditions. As ice-ocean interface thermal gradients decrease equilibrium mushy layer thickness increases. These results match empirical observations of terrestrial ices, both qualitatively and quantitatively, as newly formed ice typically supports thin mushy layers that thicken with growth of the ice cover – reaching thicknesses ~10 cm.

4.2.1.3.2 Gravity

To investigate the effects of gravity on mushy layer equilibrium thickness Equation 4.44 was solved using conditions for Earth ($9.8\,m/s^2$), Europa ($1.315\,m/s^2$), and

Enceladus ($0.113\ m/s^2$). A terrestrial ocean composition is assumed (See Table 3.1), a surface temperature of 100 K and an ocean temperature of 270.91 K is utilized. The relationship between ice shell thickness (H) and mushy layer equilibrium thickness (h) for all three gravities can be seen in Figure 4.3, which shows that ice-ocean worlds with lower gravity can support much thicker mushy layers. Variations in mushy layer thickness will impact the rate and method of heat and solute transport to and from the underlying ocean, affecting the buffering ability of the multiphase boundary as well as the thermochemical characteristics and evolution of the ice it forms. Additionally, the stable thickness of the mushy layer will determine the depth of hydraulic conductivity within the lower layer of the ice shell. Quantifying the properties and fluxes associated with this boundary will inform models of ice shell geophysics and ocean-surface biogeochemical transport.

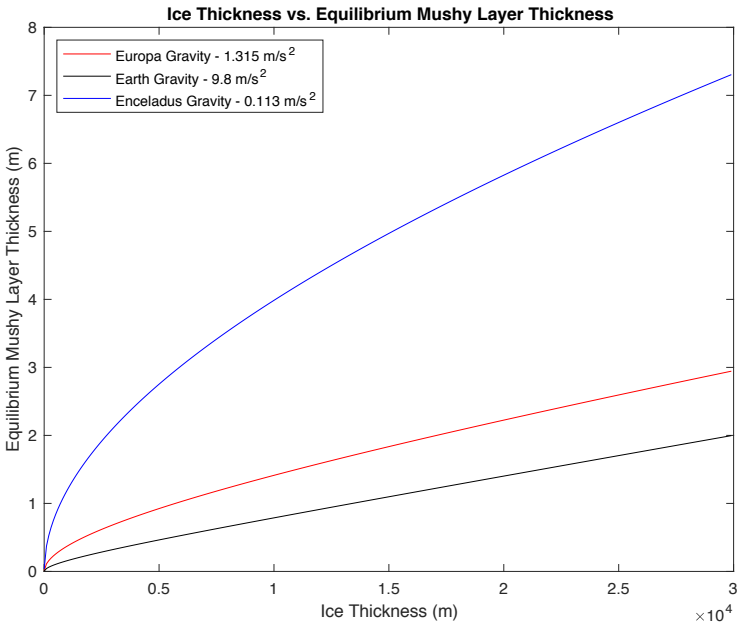

Figure 4.3 – Mushy layer equilibrium thickness vs. ice shell thickness under variable gravity. Bodies with lower gravity support mushy layers of greater thickness. This is a direct consequence of the dependence of pore fluid convection on local density instabilities. Substantial mushy layers on smaller bodies (e.g.

Enceladus) may promote ice-ocean heat and solute transport dynamics that differ from those of their larger counterparts (e.g. Earth, Europa).

4.2.1.3.3 Ocean Salinity

To investigate the effects of ocean salinity on the equilibrium thickness of the mushy layers Equation 4.44 was solved using four ocean concentrations; 12 ppt, 34 ppt, 100 ppt, and 250 ppt. A terrestrial ocean composition is assumed (Table 3.1), a surface temperature of 100 K and an ocean temperature at the salinity dependent freezing point of the respective ocean is utilized (See Section 4.2.1.2). The relationship between ice shell thickness (H) and mushy layer equilibrium thickness (h) for all four ocean concentrations can be seen in Figure 4.4. While increased ocean salinities result in slightly thinner mushy layer equilibrium thicknesses the variance is relatively minimal. That the equilibrium mushy layer thins with increasing salinity follows logically, as amplified ocean salinities will rapidly concentrate interstitial pore fluid and enhance gravity drainage of the concentrated brine into the underlying ocean, whereas lower ocean salinities will require longer evolution and thickening of the mushy layer to reach density instabilities that are sufficient to drive convection in the multiphase region.

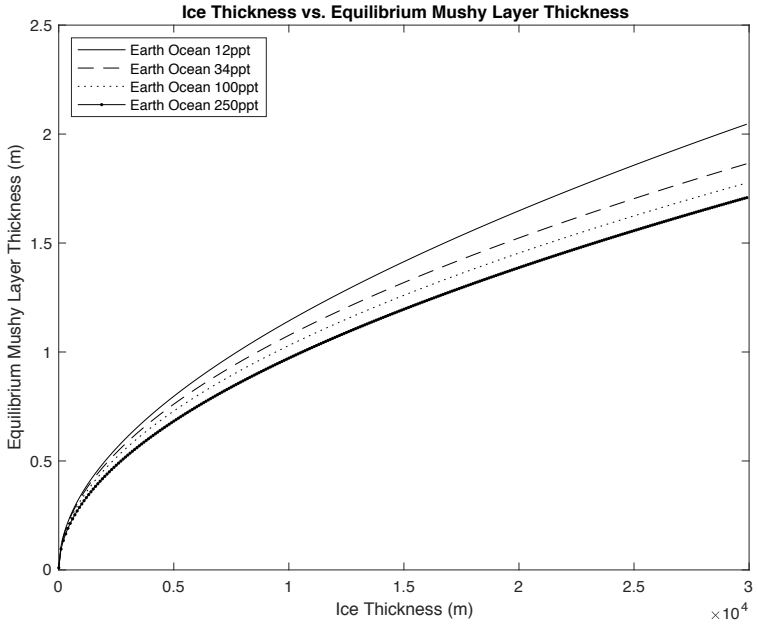

Figure 4.4 – Mushy layer equilibrium thickness vs. ice shell thickness for variable ocean concentrations. Increasing the ocean salinity slightly decreases the equilibrium mushy layer thickness. This is a result of the solutal contraction of the selected ocean.

4.2.1.3.4 Thermal Gradient

To investigate the effects of ice-ocean thermal gradient on the equilibrium thickness of the mushy layer Equation 4.44 was solved using three surface temperatures; 35 K, 100 K, and 230 K. A terrestrial ocean composition is assumed (Table 3.1), and an ocean temperature of 270.90 K is utilized. The relationship between ice shell thickness (H) and mushy layer equilibrium thickness (h) for all four ocean concentrations can be seen in Figure 4.5. The curves show that decreased thermal gradients at the ice-ocean interface support much thicker equilibrium mushy layer thicknesses. This is a logical consequence of assuming local thermodynamic equilibrium in the mushy layer (See Section 4.2.1.2). If the ice-mush interface salinity is assumed to lie on the liquidus produced by a conductive

thermal profile, a thicker mushy layer must be formed to produce the same local Rayleigh number (Equation 4.41), and thus ice-mush interface velocity, for a smaller thermal gradient than would be needed to produce the same ice-mush interface velocity under a larger thermal gradient. This is important as the large scale of planetary ice shells, along with the potential for ongoing intrashell hydrologic activity, suggests that different regions within the ice shell have been subject to a diverse range of thermal gradients over their long history, leading to potentially disparate ice-ocean/brine interface conditions and likely influencing heterogeneities in the physicochemical characteristics of the ice shell. Such heterogeneities may play a crucial role in driving geophysical processes and geological feature formation as well as producing mechanical boundaries and potentially habitable regions within the ice shell.

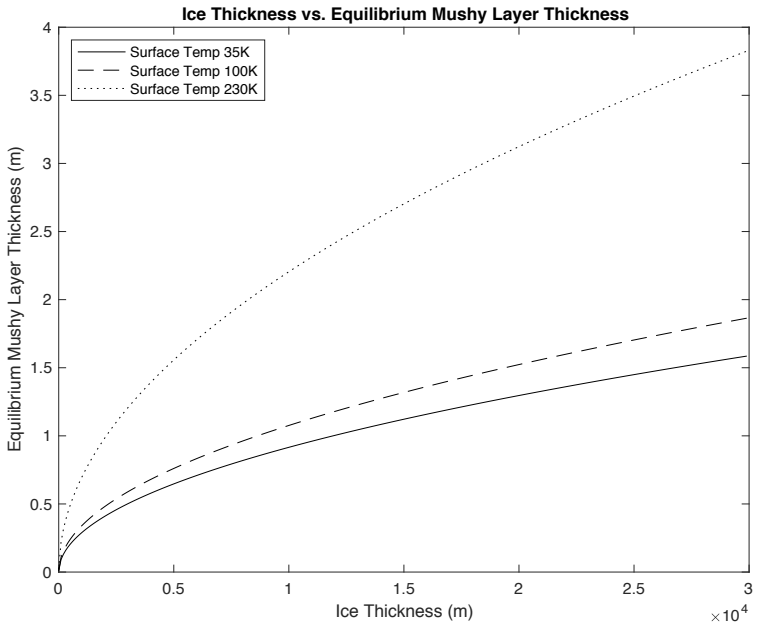

Figure 4.5 – Mushy layer equilibrium thickness vs. ice shell thickness under variable ice-ocean interface thermal gradient. As ice-ocean thermal gradients decrease equilibrium mushy layer thickness

increases. Similar to the terrestrial case (Figure 4.2), this suggests that the ice-ocean interfaces of thick ice shells should be characterized by substantially thick, hydraulically connected, multiphase layers – allowing for ongoing fluid and solute transport. Such a layer could promote the formation and sustenance of interstitial chemical gradients favorable for potential organisms as well as constitute a unique and spatiotemporally variable medium for heat exchange between the ocean and ice shell (e.g. [*Soderlund et al.*, 2014]).

4.2.2 Mushy Layer Stability

It is important to quantify the stability of the ice-ocean interface mushy layer of icy worlds to determine if these boundaries are long-lived and stable components of ice shells or exist as transient features. As evidenced by their terrestrial counterparts, the dynamics and evolution of these boundary layers determine the growth rate and physicochemical composition of the overlying ice [*Eicken*, 1992; *Nakawo and Sinha*, 1981; *Wolfenbarger et al.*, 2018; *Zotikov et al.*, 1980]. The disparity between the material properties of terrestrial ocean-derived ices (e.g. sea ice vs. marine ice), along with global heterogeneities in ocean circulation, ice shell thickness, and surface temperature [*Ojakangas and Stevenson*, 1989; *Soderlund*, 2019; *Soderlund et al.*, 2014], suggests that ice-ocean worlds likely support a spectrum of ice-ocean interface conditions capable of producing diverse ices. Regional heterogeneities in ice properties could facilitate geophysical processes [*Barr and McKinnon*, 2007] and facilitate inhomogeneous ocean-surface material transport. To investigate the stability of the equilibrium mushy layer thickness, h, we will assume the system is at equilibrium, perturb it by a small amount h' ($h \Rightarrow h+h'$), and investigate the effects on the ice-mush interface velocity $v_m^*(t)$. Above we've shown that for the advective regime:

$$v_m^*(t) = br_j^{\downarrow} = \alpha\left(\frac{g\rho_{sw}\beta\Delta S_j\widetilde{\Pi}h}{\kappa\mu} - Ra_c\right) \tag{4.45}$$

$$= \alpha\left(\frac{g\rho_{sw}\beta(15.1106\left(T_{mp} - \left(T_S + (H-h)\frac{(T_{oc}-T_S)}{H}\right)\right) - S_{oc})\widetilde{\Pi}h}{\kappa\mu} - Ra_c\right) \tag{4.46}$$

$$= \frac{\alpha g\rho_{sw}\beta(15.1106\left(T_{mp} - T_S + (h-H)\frac{(T_{oc}-T_S)}{H}\right) - S_{oc})\widetilde{\Pi}h}{\kappa\mu} - \alpha Ra_c \tag{4.47}$$

Let $C_1 = \alpha g\rho_{sw}\beta\widetilde{\Pi}/\kappa\mu$, and introduce the perturbation (h => h+h'), then:

$$v_m^*(t) = C_1(h+h')(15.1106\left(T_{mp} - T_S + ((h+h')-H)\frac{(T_{oc}-T_S)}{H}\right) - S_{oc}) - \alpha Ra_c \tag{4.48}$$

$$= \left[C_1 h 15.1106\left(T_{mp} - T_S + (h-H)\frac{(T_{oc}-T_S)}{H}\right) - S_{oc}) - \alpha Ra_c\right] + \left[C_1 hh' 15.1106\frac{(T_{oc}-T_S)}{H} + C_1 h'(15.1106\left(T_{mp} - T_S + \left((h+h')-H\right)\frac{(T_{oc}-T_S)}{H}\right) - S_{oc})\right] \tag{4.49}$$

Where the terms in the first set of square brackets are just the original interface velocity due to the equilibrium mushy layer thickness h, and the terms in the second set of square brackets are the change in interface velocity due to the perturbation h', we'll call this Δv_m^*:

$$\Delta v_m^* = C_1 hh' 15.1106\frac{(T_{oc}-T_S)}{H} + C_1 h'\left(15.1106\left(T_{mp} - T_S + \left((h+h')-H\right)\frac{(T_{oc}-T_S)}{H}\right) - S_{oc}\right) \tag{4.50}$$

$$= C_1 hh' 15.1106 \frac{(T_{oc} - T_S)}{H} + C_1 h' \left(15.1106 \left(T_{mp} - T_S + (h - H) \frac{(T_{oc} - T_S)}{H} \right) - S_{oc} \right)$$

$$+ C_1 h' h' 15.1106 \frac{(T_{oc} - T_S)}{H} \qquad (4.51)$$

For h' small, the last term can be neglected. So:

$$\Delta v_m^* \approx C_1 hh' 15.1106 \frac{(T_{oc} - T_S)}{H}$$

$$+ C_1 h' \left(15.1106 \left(T_{mp} - T_S + (h - H) \frac{(T_{oc} - T_S)}{H} \right) - S_{oc} \right) \qquad (4.52)$$

For the first term on the right-hand side, $C_1 h 15.1106 \frac{(T_{oc} - T_S)}{H} \geq 0$ for all realistic values of C_1, h, H and assuming the ice is thickening i.e. $T_{oc} > T_S$, which is the case we consider here. For the second term on the right-hand side, $C_1 \left(15.1106 \left(T_{mp} - T_S + (h - H) \frac{(T_{oc} - T_S)}{H} \right) - S_{oc} \right) = C_1 (S_{int} - S_{oc}) \geq 0$ for all realistic values of C_1 and assuming $S_{int} > S_{oc}$, which is reasonable for thickening ice. Therefore:

$$\begin{cases} \Delta v_m^* > 0 & if \quad h' > 0 \\ \Delta v_m^* < 0 & if \quad h' < 0 \end{cases} \qquad (4.53)$$

This suggests that if the mushy layer thickens the ice-mush interface velocity will increase, tending towards the equilibrium thickness h, while if the mushy layer thins the ice-mush velocity will decrease, also tending towards the equilibrium thickness h. This implies that the mushy layer thickness h is a stable equilibrium. Perturbations from this equilibrium thickness will decay (be smoothed out by the system). The existence of a stable

equilibrium suggests that mushy layers are likely a prevalent feature of ice-ocean worlds, persisting for long periods of time and characterizing the ice-ocean/brine interfaces of these systems. Thus, quantifying the multiphase physics that govern these boundary layers and their interactions with both the ocean and ice shell promises to drastically improve our understanding of ice-ocean world geophysical and biogeochemical processes.

4.3 Heterogeneities and Depositional Processes Within Growing Mushy Layers

4.3.1 Fluid Flow and Brine Channel Formation

Mushy layers themselves are not homogeneous media, but support an array of structural, thermal, and compositional heterogeneities [*Buffo et al.*, 2018; *Golden et al.*, 2007; *Wells et al.*, 2011; *Wettlaufer et al.*, 1997a; b; *Worster et al.*, 1990; *Worster and Rees Jones*, 2015]. The complexity and small scale of these heterogenous features leads to their frequent exclusion from numerical models. An archetype example is the formation and dynamics of brine channels. A byproduct of the convective downwelling of concentrated interstitial pore fluid, these dendritic channel structures play a fundamental role in the freshening of the mushy layer [*Griewank and Notz*, 2013; *Rees Jones and Worster*, 2013; *Turner et al.*, 2013; *Wells et al.*, 2010; 2011]. Nearly all models of ice-ocean interface dynamics and evolution are one-dimensional, necessitating parameterization of this inherently two-dimensional process. Frequently the convective flow through these channels is parameterized using optimization arguments, and a number of successful parameterizations exist [*Buffo et al.*, 2018; *Griewank and Notz*, 2013; *Hunke et al.*, 2011; *Turner and Hunke*, 2015; *Turner et al.*, 2013; *Wells et al.*, 2010; 2011]. However, these parameterizations employ isotropy and homogeneity (e.g. brine channel spacing, mushy

layer permeabilities) that may not be representative of a dynamic natural system. In both laboratory and natural environments heterogenous brine channel and brinicle formation and evolution are observed [*Golden et al.*, 2007; *Notz and Worster*, 2008; *Wettlaufer et al.*, 1997b; *Worster and Rees Jones*, 2015]. Such heterogeneities may induce lateral variation in mushy layer physicochemical and transport properties. Constraining the interdependence of environmental parameters and mushy layer heterogeneity is imperative in understanding the dynamics and evolution of these active interfaces. In magmatic systems it is these small-scale heterogeneous drainage processes that determine the structure and composition of the resultant rock [*Fowler*, 1987; *Jordan and Hesse*, 2015; *Reiners*, 1998; *Worster et al.*, 1990]. Contemporary models have begun to simulate mushy layer formation in two dimensions, removing the need for parameterization of pore fluid convection [*Katz and Worster*, 2008; *Oertling and Watts*, 2004; *Wells et al.*, 2019]. These models successfully simulate the onset of density instabilities and convection in the mushy layer, leading to the formation and evolution of brine channels. While the spatiotemporal extent of these models is limited by the substantial computational cost of simulating such detailed multiphase reactive transport processes, they provide an unparalleled method for understanding the role of heterogeneities in the dynamics and evolution of mushy layers as well as a numerical technique that can be extended to include additional physics or tailored to simulate diverse ice-ocean environments.

4.3.2 Current Limitations

The use of reactive transport modeling to simulate ocean-derived ices is an active and ever evolving field spanning ocean, atmosphere, Earth systems, and planetary science.

As such, it is instructive to assess the current limits of our knowledge on the subject and identify key outstanding questions as well as strategies to address them. Here, three of these limitations which are particularly important to the dynamics and evolution of planetary ice-ocean systems are highlighted. The problem is briefly contextualized, its relevance to the current work is outlined, and the broader implications of its solution are discussed.

Two closely related problems were introduced in Chapter 3; identifying if a critical porosity exists and if so, what is its value, and constraining the permeability-porosity relationship of ocean-derived ices. Here, critical porosity is the liquid fraction at which fluid flow in the mushy layer ceases and is akin to the mathematical concept of a percolation threshold. In ice-ocean systems this is physically represented by the solidification of brine pockets and channels until their connectivity with the underlying ocean vanishes, leaving only isolated brine pockets which are incapable of brine drainage. Many models of sea ice implement a critical porosity of 5% [*Buffo et al.*, 2018; *Buffo et al.*, *in review; Wongpan et al.*, 2015]. While this estimate is broadly used by a number of successful models and is based on empirical observations [*Golden et al.*, 1998; *Golden et al.*, 2007], it remains a contentious subject in the community [*Hunke et al.*, 2011; *Turner and Hunke*, 2015; *Turner et al.*, 2013] and it has been shown that minimal variations in its value can appreciably affect estimates of sea ice bulk salinity [*Buffo et al.*, 2018]. In planetary applications some investigators implement a critical porosity [*Buffo et al.*, *in review; Hammond et al.*, 2018] while others allow fluid flow to persist for all non-zero porosities [*Hesse and Castillo-Rogez*, 2019; *Kalousová et al.*, 2014; 2016] suggesting brine can continue to percolate along grain boundaries. One consequence of excluding a critical porosity is the rapid downward transport of any perched water within an ice shell into the

underlying ocean [*Hesse and Castillo-Rogez*, 2019; *Kalousová et al.*, 2014; 2016]. While laboratory experiments have identified brine along grain boundaries in low temperature ices [*Desbois et al.*, 2008; *McCarthy et al.*, 2013], natural terrestrial ices are capable of supporting supraglacial and englacial hydrological systems [*Forster et al.*, 2014; *Koenig et al.*, 2014] suggesting a relative level if impermeability. Additionally, the surface of Europa exhibits numerous features which suggest that endogenic ocean material has been transported across the ice shell. In Chapter 3 it was shown that critical porosity plays a crucial role in determining the extent of impurity entrainment in planetary ices [*Buffo et al.*, *in review*]. Constraining the value of this parameter will improve estimates of ice shell composition and determine the rates of putative ocean-surface material transport.

A similar problem is determining the permeability of the mushy layer. This hurdle is common to all problems involving fluid transport in porous media [*Bear*, 2013]. The permeability is governed by the complex geometry and connectivity of the pore space, a difficult quantity to collect, especially for the fragile ice-ocean interface. Computed tomography imagery of ice cores have begun to elucidate the complex temperature dependent evolution of brine pockets and channels in sea ice [*Golden et al.*, 2007]. In numerical models permeability is typically parameterized as a function of porosity (e.g. [*Griewank and Notz*, 2013; *Katz and Worster*, 2008; *Oertling and Watts*, 2004]). While many of these parameterizations are capable of reproducing certain features of ice-ocean interface dynamics and evolution in Chapter 2 it was shown that the choice of permeability-porosity relationship will affect the rate of impurity entrainment in the overlying ice. For planetary applications, where observations of ice properties will be utilized to infer

characteristics of subsurface water reservoirs, constraining this relationship is of the utmost importance.

Finally, planetary ice-ocean environments are likely subject to thermal, chemical, and physical regimes that are substantially different than those found on Earth. Understanding how variable environmental parameters influence the properties and dynamics of ice-ocean systems is crucial in determining how geophysical processes shape diverse icy worlds. Laboratory experiments have demonstrated that, upon freezing, brines of different compositions produce ices with diverse microstructural properties [*McCarthy et al.*, 2007]. These small-scale structural differences may result in drastically different thermodynamic, mechanical, and fluid transport properties, suggesting that ice-ocean worlds of different compositions may exhibit unique ice shell dynamics. In Section 4.2.1.3 it was shown that variable physical and thermochemical pressures effect the geometry of the ice-ocean interface mushy layer, which may impact energy and material transport rates between the ocean and overlying ice shell. Continued theoretical and laboratory investigations promise to improve our understanding of planetary ice properties and will inform both numerical models and the analysis of future spacecraft observations.

4.3.3 Ice Diagenesis

Ice-ocean interfaces may be additionally modified by depositional processes, wherein ice crystals nucleated in the underlying water column buoyantly sediment onto the basal ice interface. This process has been observed under ice shelves and ice shelf adjacent sea in Antarctica where the accretion of frazil and platelet ice leads to the formation of porous marine ice and sub-ice platelet layers beneath ice shelves and sea ice, respectively

[*Buffo et al.*, 2018; *Craven et al.*, 2009; *Dempsey et al.*, 2010; *Fricker et al.*, 2001; *Langhorne et al.*, 2015; *Robinson et al.*, 2014]. On Earth, these depositional processes are driven by the ice pump mechanism, where ice shelf basal melting and topography drives the formation of buoyant supercooled water plumes – the source of both frazil and platelet ice [*Lewis and Perkin*, 1983]. Similar depositional processes have been theorized to occur on other ice-ocean worlds, potentially driven by ocean currents and/or latitudinal variations in basal ice topography [*Soderlund et al.*, 2014]. The buoyancy driven sedimentation of ice crystals onto the ice-ocean interface will further modify the mushy layer. No longer driven solely by thermodynamic heat loss to the overlying ice, a high porosity layer of deposited crystals begins to form if the advancing ice-mush interface velocity does not match that of the sedimentation rate [*Buffo et al.*, 2018]. In these accreted regions porosity is dependent on the packing efficiency and ensuing buoyancy driven compaction of the deposited ice crystals. Unconsolidated platelet ice layers beneath ice shelf adjacent sea ice can have porosities as high as 25% [*Gough et al.*, 2012; *Wongpan et al.*, 2015] and sub-ice shelf marine ice can remain hydraulically connected to the underlying ocean as far as ~70 m above the ice-ocean interface [*Craven et al.*, 2009]. Under such conditions, the combined depositional, thermal, chemical, and mechanical processes occurring in the layer will govern the evolution of the ice-ocean interface.

An analogous process of deposition, compaction, and thermochemical evolution governs the diagenesis of marine sediments [*Berner*, 1980]. Providing a gradient rich medium for benthic fauna in terrestrial oceans, the ice-ocean interface of worlds like Europa may supply an analogous inverted substrate for potential organisms. This possibility is strengthened by the likelihood that these interfaces exist as persistently

multiphase boundaries, akin to those that support substantial biological communities at the base of sea ice and ice shelves on Earth [*Daly et al.*, 2013; *Krembs et al.*, 2011; *Loose et al.*, 2011; *Vancoppenolle et al.*, 2013]. The formation of brinicles on Europa has been suggested as a process which could produce chemical gradients similar to those observed in chemical gardens and hydrothermal regions of the terrestrial ocean, oases for benthic ecology [*Vance et al.*, 2019]. Additionally, in the case of Europa, it has been suggested that delivery of surface derived oxidants to a reduced ocean may drive redox potentials favorable to the reactions of metabolic processes [*Chyba and Phillips*, 2001; *Hand et al.*, 2007; *Vance et al.*, 2016; *Vance et al.*, 2018]. As the boundary where these oxidants would be introduced into the ocean, the ice-ocean interface could provide a chemical boon for any prospective biosphere in an otherwise potentially oligotrophic water column. In turn, akin to both terrestrial sea ice communities [*Krembs et al.*, 2011] and bioturbation in marine sediments [*Berner*, 1980], any potential biosphere will likely alter the evolution of the host ice-ocean substrate. Understanding how organisms interact with and depend upon the microstructural and chemical evolution of ice-ocean interfaces will help constrain the habitability of these environments and the role biogeochemical processes play in the dynamics of these active boundary layers. Furthermore, quantifying the entrainment of biosignatures within forming ices will aid in predicting the likelihood of ocean-surface transport and surface expression of ocean-derived materials on icy worlds.

While no models of two-dimensional reactive transport or biosignature entrainment currently exist for planetary ices, a number of one-dimensional reactive transport and compaction models [*Buffo et al.*, *in review; Hammond et al.*, 2018] and two-dimensional multiphase models [*Hesse and Castillo-Rogez*, 2019; *Kalousová et al.*, 2014; 2016] have

been used to investigate the thermochemical evolution and dynamics of ice-ocean worlds. These existing models can be leveraged alongside contemporary models of sea ice, which include formalisms for simulating small-scale heterogeneities within the mushy layer [*Katz and Worster*, 2008; *Oertling and Watts*, 2004; *Wells et al.*, 2019] and biogeochemical processes [*Tedesco and Vichi*, 2014; *Vancoppenolle et al.*, 2013; *Vancoppenolle and Tedesco*, 2015], to improve our understanding of the role ice-ocean interfaces play in governing the geophysics and habitability of ice-ocean worlds. Integrative models constraining the thermal, physical, chemical, and biological processes at this important boundary layer would have direct implications for geophysical and biogeochemical models of icy worlds as well as the interpretation of future spacecraft observations.

4.4 Conclusion

As a dynamic physical and thermochemical boundary, the ice-ocean interface of ocean worlds likely plays a crucial role in their geophysics and habitability. Persisting as geophysically thin porous layers governed by multiphase reactive transport processes they dictate the thermochemical evolution of the overlying ice and may provide a gradient rich oasis for potential astrobiology. A number of terrestrial analogs (sea ice, ice shelves, magmatic systems) provide invaluable resources when designing and validating models seeking to simulate planetary ice-ocean systems. With mounting evidence supporting the notion that ice shells are heterogeneous and active structures that may harbor ongoing hydrological processes constraining the effects of multiphase dynamics on their evolution is an imperative progression in simulating ice-ocean world geophysics and biogeochemical cycling. The inclusion of reactive transport processes in models of terrestrial geophysics

has revolutionized our understanding of the Earth system. With enhanced spacecraft observations and advances in computing power a comparable renaissance may be afoot.

Chapter 5: A Sum of Its Parts: A Wholesale Approach to Planetary Ice-Ocean Interfaces

The organization of this thesis was designed to reflect the progressive construction and integration of crucial pieces into a much larger puzzle, answering the questions: what are the physics that govern the properties and evolution of ice-ocean/brine interfaces, how do these dynamic boundaries affect the geophysics and habitability of ice-ocean worlds in our solar system, and what do the observable near surface properties they produce reveal about ice-ocean world interiors? Here, the work presented in Chapters 1-4 is reviewed in the context of these driving questions. Preliminary work investigating the biogeochemistry of novel planetary analog ice-brine systems in central British Columbia's Cariboo Plateau is presented, and its role in the larger project is discussed. The value of the multipronged approach taken throughout this work (involving field work, laboratory analysis, numerical modeling, and theoretical analysis) is demonstrated by the robust validation of the numerical models against both analytic solutions and empirical observations of ice on Earth as well as the production of novel and broadly applicable results that affect a broad range of scientific communities. The specific advances to these fields provided by this work are enumerated, as are the new uncertainties that have been elucidated. Finally, the ongoing evolution of this work is placed in context with the future trajectory of scientific fields it has the potential to impact, which include ocean, climate, cryosphere, Earth systems, and planetary science. Explicit strategies to integrate current and future results into interdisciplinary pursuits is discussed.

5.1 Ice-Ocean Worlds in Our Solar System: Geophysics and Astrobiology

The likely presence of contemporary liquid water has placed ice-ocean worlds as frontrunners in our search for life in the solar system and has spawned the NASA flagship Europa Clipper mission, whose future observations and data products have largely inspired this work. In the first chapter, I introduced the prominent ice-ocean worlds within our solar system, including Earth, and established the motivation for the ensuing work by demonstrating the imperative role impurity entrainment at the ice-ocean interface of terrestrial ices play in the ice's dynamics and evolution and hypothesizing that analogous ice-ocean interface dynamics will dictate the geophysical processes and habitability of icy satellites. Ice-ocean interactions are important components of the Earth system, with impacts on climate, ocean, atmospheric, and biogeochemical processes. The physics of multiphase reactive transport, which has the ability to accurately predict the dynamics occurring at the ice-ocean interface and the material properties of the overlying ice, has been the backbone of contemporary sea ice modeling studies. A major finding is that ice-ocean boundaries are characterized by regions of porous ice saturated with hypersaline brines, supporting fluid and solute transport to and from the underlying ocean, and ultimately dictating the thermochemical evolution of the overlying ice. Given the likely analogous structure of ice-ocean interfaces on icy satellites, it follows that ice shell properties and dynamics will be similarly governed by the hydrosphere-cryosphere boundary and that models hoping to simulate planetary ices should include the effects of multiphase dynamics.

A ubiquitous feature of ocean worlds in our solar system, apart from our own, is that the surfaces of these bodies are characterized by global ice shells that overlay and

insulate their subsurface oceans. Ice shells likely play an imperative role in the dynamics, evolution, habitability, and surface characteristics of these worlds. As both a barrier to and conveyor of energy and mass between the oceans and surfaces of these worlds the physical and thermochemical properties of the ice will not only facilitate the geophysical transport across the shell but also be the primary medium for future spacecraft observations. Since the interfacial dynamics of ices on Earth have been shown to dictate many of the material properties of the overlying ice and that these properties can be correlated with the thermochemical characteristics of the interface at the time of formation, this suggests that variations in observed ice properties on other bodies may correlate to a difference in processing history and/or parent water body. For the complex surface geology of Europa this implies active and spatiotemporally heterogeneous ice shell geophysical processes. What remains to be constrained is the relation between ice-ocean interface dynamics and resultant ice properties in planetary environments. This gap in our understanding of ice-ocean worlds provides a key science driver for the main work presented here which seeks to quantify the effects of the physical, thermal, and chemical environment near the ice-ocean interface on the properties of the overlying ice shell. This will improve our understanding of ice-ocean world geophysics and provide a method for relating spacecraft observations of the surface and near subsurface to interior properties of these icy worlds.

The ice-ocean interface plays a unique role in supporting a rich and diverse ecosystem in Earth's polar environments. The formation and persistence of thermal and chemical gradients in the porous basal layer of ocean-derived ices provides a metabolically advantageous substrate for both micro- and macrofauna. The importance of redox disequilibrium in fueling the metabolisms of any potential Europan organisms is presented,

highlighting the importance of ocean-surface interaction in delivering surface derived oxidants to a putatively reducing ocean. As the interface where oxidants would be introduced into the ocean, the likely porous and dynamic ice-ocean boundary may provide a physicochemical boon for any potential astrobiology. Encouragingly, a number of sources have suggested that ice based thermochemical gardens may characterize the interface, akin to hydrothermal and brinicle systems on Earth, and provide ecological oases in an otherwise potentially oligotrophic ocean.

The need to understand ecosystem and physical dynamics that occur at ice-ocean interfaces in planetary environments through a wholistic approach benchmarked by, and improving upon, known dynamics on Earth forms the strategic approach of this work. The numerical models are built on the foundational theory of multiphase reactive transport in porous media and its immense success in simulating the dynamics and evolution of numerous Earth systems, including terrestrial ocean-derived ices. A driving principal of this theses is understanding the ability of planetary ices to record historical information about their environments. The numerical model of Chapter 2 was designed to investigate the ability of sea ice to record variations in oceanic supercooling through associated depositional processes and validate the ability to simulate ice-ocean interface systems. Its success provided the foundation to extend the model to planetary systems. Chapter 3 reports the results of extending this model to the Europa ice-ocean system, producing the first physically based estimates of ice shell salinity and hydrological feature thermochemical evolution, and providing quantitative predictions of the ice shell's compositional structure that can be tested by the upcoming Europa Clipper mission. The analytical investigations of Chapter 4 extend the work to investigate the effects of diverse

ice-ocean world environments on the structure of the ice-ocean interface and implications this may have on energy and mass transport between the ocean and ice shell, as well as how mushy layers could affect ice-ocean world geophysical processes and habitability. Additionally, I demonstrate the importance of small-scale heterogeneities in the ice-ocean interface mushy layer on its physicochemical evolution and ability to support biogeochemical processes. The effects of diverse ice-ocean world environments on their geophysics and habitability, and our ability to accurately simulate and detect them, has motivated current analog field work (discussed below) which seeks to characterize the physical, thermal and biogeochemical environments of diverse hypersaline ice-brine systems in British Columbia. The ability to simulate the dynamics and evolution of these diverse systems with the numerical models constructed throughout this work will provide a novel tool for investigating these terrestrial systems and will bolster confidence in the models' ability to accommodate an array of potential planetary environments. With this, a comprehensive picture of planetary ice shell thermophysics and biogeochemistry begins to take shape, providing a method to predict the material properties and composition of icy worlds, which will inform both numerical models and aid in the interpretation of spacecraft observations.

5.2 Ice as a Record of Ocean Processes: Antarctic Sea Ice

A compact version of Chapter 2 is published in the Journal of Geophysical Research: Oceans [*Buffo et al.*, 2018]. The goal of this work was to construct a stand-alone one-dimensional finite difference model capable of simulating the multiphase reactive transport processes that govern the formation and evolution of sea ice. The motivation for

including the physics of buoyancy driven platelet ice accretion was twofold. First and foremost, the goal of this work was to devise an efficient method of simulating platelet ice accretion and its effects on the structural and thermochemical properties of ice shelf adjacent sea ice. The ability to relate environmental characteristics (e.g. ocean chemistry, atmospheric forcing, supercooling) to observable ice core properties provides a method to reconstruct the spatiotemporal evolution of the ice-ocean interface from the thermochemical signatures recorded in the stratigraphy of the overlying ice. Accurately including platelet ice accretion into sea ice models has direct implications for identifying the presence and evolution of sub-ice shelf water masses and their interactions with the global oceans, atmosphere and cryosphere – an imperative interrelation to understand in a rapidly changing climate. The secondary goal of this work was to produce and benchmark an approach which has the versatility to accommodate the physics of diverse environments. Verification of the model's efficacy against terrestrial analogues with substantial empirical observations bolsters the model's applicability to more exotic ice-ocean environments in the solar system.

The ability to accurately simulate the annual evolution of growing sea ice subject to the phenomenon of platelet ice accretion allows for the synthesis of a digital ice record (Figures 5.1a and 5.1b). In lieu of the impossible task of continuously field sampling multiple locations, these digital records can reconstruct the entire freezing season over any desired region and be validated with any empirical observations made in the area. This provides a tool to investigate the spatiotemporal evolution and dynamics of large areas of platelet affected sea ice. In Figure 5.1 an entire freezing season is simulated and then simulated ice cores are extracted to investigate the evolution of the ice structure and

composition over time. The results match well with empirical observations made by [*Dempsey et al.*, 2010], suggesting this technique can be used to improve systems models seeking to include the comprehensive dynamics of platelet ice processes.

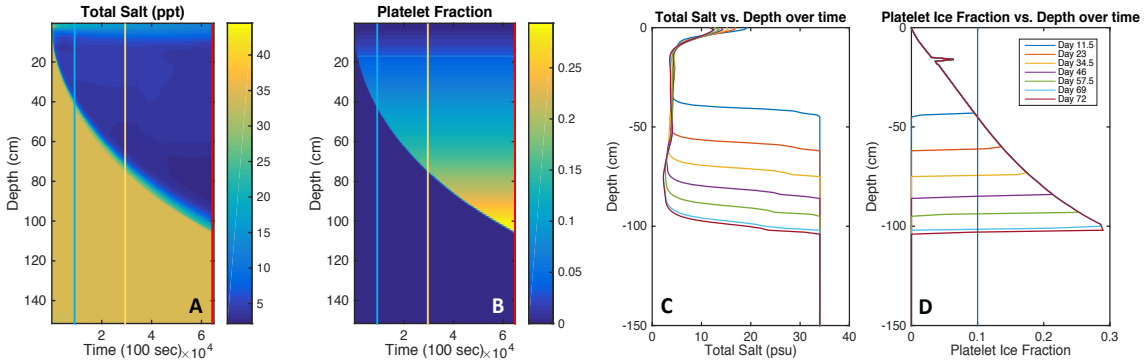

Figure 5.1 – The spatiotemporal evolution of platelet affected sea ice. A) The evolution of bulk salinity in the ice cover during an entire freezing season. B) The platelet fraction in the ice cover during an entire freezing season. (blue, yellow, and red vertical lines of plots A and B correspond to the Day 11.5, Day 34.5, and Day 72 vertical profiles of plots C and D) C) Bulk salinity profiles of digital ice cores extracted from plot A showing the characteristic 'c-shape' of first year sea ice [*Malmgren and Institutt*, 1927]. D) Platelet ice fraction profiles extracted from plot D showing the increase in platelet ice fraction with depth as the overlying ice becomes increasingly insulating and basal growth due to atmospheric heat loss slows.

5.3 Planetary Ices: A Window into Interior Processes

A compact version of Chapter 3 has been submitted to Science Advances [*Buffo et al.*, *in review*]. The goal of this work was to construct a stand-alone one-dimensional finite difference model capable of simulating the multiphase reactive transport processes and diverse thermochemical environments that govern the formation and evolution of planetary ices. The numerical model of sea ice described in Chapter 2 was extended to accommodate putative Europan ocean compositions and a wide range of potential ice-ocean interface

thermal gradients. The motivation for constructing such a model was to provide a physically realistic simulation of planetary ice-ocean interfaces capable of predicting the physical and thermochemical properties of ices formed under environments relevant to ice-ocean worlds. For while heterogeneities in ice characteristics have been invoked as a potential driver of ice shell geophysical processes and impurity entrainment at the ice-ocean interface likely influences ocean-surface material transport, which has been lauded as a crucial control on the moon's habitability, the thermochemical structure of the ice shell remains largely unconstrained. The model was used to derive constitutive relationships between ocean chemistry, ice-ocean interface thermal gradients, and ice composition – providing a method to quantify the thermochemical evolution of Europa's ice shell and hydrological features contained within and link observable ice characteristics to properties of its parent water body and thermal environment at the time of formation. These results have direct implications for geophysical and biogeochemical models of Europa, as well as interpreting upcoming spacecraft observations. Moreover, the model was designed to be accessible and easily adapted to accommodate the diverse thermal and physicochemical environments of ocean worlds throughout the solar system, allowing future application and progress in many areas.

Constraints are placed on the total impurity load and bulk salinity profile of the Europan ice shell derived from constitutive relationships between impurity entrainment and local thermal gradient for a variety of ocean compositions, resulting in bulk ice shell salinities that range from 1.053-14.72 ppt. The model shows that the upper ice shell freezes rapidly with high salt content down to ~250 meters and places a permeability dependent upper limit on impurity entrainment into Europa's ice of 5% of the ocean composition for

the bulk of the ice shell over most of Europa's history (Figure 5.2a). These new constraints are applied to geologic features of interest; fractures derived from the ice-ocean interface and shallow lenses within the shell. The results show that water-filled fractures refreeze rapidly, producing high salt content along fracture walls that could promote future sliding (Figure 5.2c). Finally, it is shown show that impurity rejection during the solidification of perched water within the ice shell produces highly concentrated salt layers, over 2 m thick for a 2 km deep lens (Figure 5.2b). This method of quantifying compositional heterogeneities within Europa's ice shell will benefit future geophysical models of ice-ocean worlds and inform the planning and data analysis of the Europa Clipper mission.

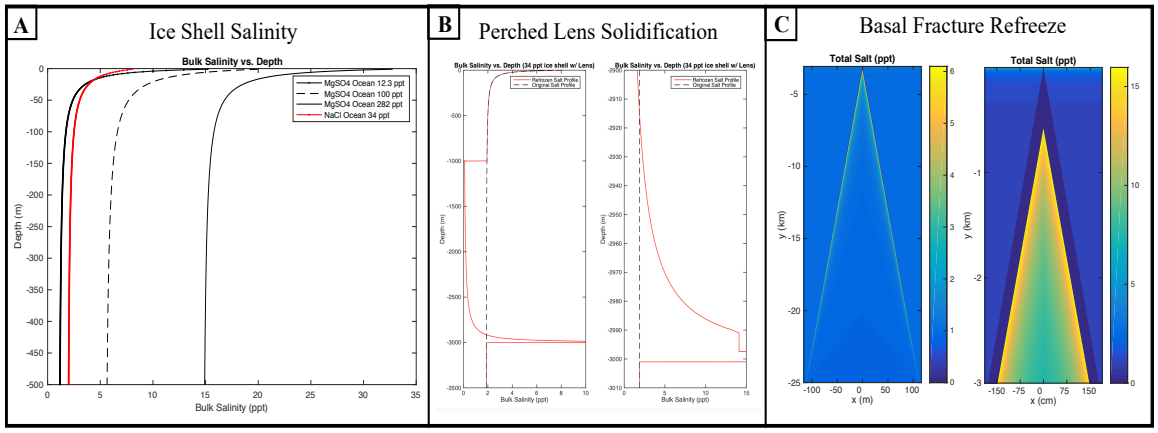

Figure 5.2 – Compositional variations within Europa's ice shell. A) Bulk salinity variations with depth in the upper ice shell (500 m) showing the trend toward the asymptotic salinity limit that characterizes much of the ice shell. B) The bulk salinity profile of a re-solidified perched lens (originally melted from an ice shell that formed from a 34 ppt NaCl ocean) in which an ~2.23 m layer of pure salt forms due to the concentrating process of brine rejection. C) Compositional profiles of refrozen basal fractures at the ice-ocean interface (left) and an ice-lens interface (right) suggesting hydrological processes within the shell may promote compositionally heterogeneous regions that could result in thermomechanical weaknesses.

5.4 Moving Forward: Extending Our Understanding of Planetary Ice-Ocean Interfaces

The goal of Chapter 4 was to further investigate the structure and evolution of ice-ocean interfaces and the implications their presence and characteristics have on the geophysics and habitability of ice-ocean worlds. The dependence of mushy layer geometry and evolution on environmental parameters is explored by analytically solving for the thickness of a simplified ice-ocean mushy layer system. Two dynamic regimes are investigated, one driven by molecular diffusion and one driven by convection of brine within the mushy layer, to investigate the impact of gravity, thermal gradient, and ocean composition on the thickness of mushy layers. Additionally, perturbation analysis shows that there exist stable equilibrium mushy layer thicknesses, suggesting that mushy layers are likely persistent and common features of ice-ocean worlds. Understanding the potential diversity of these multiphase layers across solar system bodies provides insight into the potential rates and mechanisms of heat and solute transport between their respective oceans and ice shells. Variations in mushy layer properties may drive diverse geophysical processes unique to individual bodies or that may vary regionally on an individual icy world. Current limitations to numerical models of multiphase reactive transport in planetary ices highlights the important roles that critical porosity and permeability-porosity relationships play in the dynamics and evolution of ice-ocean interfaces. This was a recurring theme in this work, where in Chapter 2 (Section 2.4.3) variations in critical porosity and permeability-porosity relationships substantially impacted the bulk salinity profiles simulated in sea ice, and in Chapter 3 (Section 3.4.1) critical porosity set the lower limit for impurity entrainment in the ice shell. Contemporary models exploring the two-

dimensional heterogeneities produced during the solidification of sea ice are reviewed as are the diagenetic and biogeochemical processes that characterize a number of terrestrial ice-ocean environments. Environmental conditions and small-scale heterogeneities likely affect the dynamics and properties of planetary ice-ocean interfaces. Drawing parallels to the advances made by reactive transport modelling in our understanding of the Earth system, a shift in our concept of ice-ocean worlds may be underway.

5.5 Ongoing and Future Work

5.5.1 British Columbia's Hypersaline Lakes as Planetary Analogs

While the structure and interface dynamics of sea ice and marine ice are relatively well documented [*Collins et al.*, 2008; *Craven et al.*, 2009; *Galton-Fenzi et al.*, 2012; *Griewank and Notz*, 2013; *Hunke et al.*, 2011; *Khazendar and Jenkins*, 2003; *Turner and Hunke*, 2015; *Wolfenbarger et al.*, 2018], little is known about how other major compounds affect the ice [*McCarthy et al.*, 2007]. The Cariboo Plateau of central British Columbia, Canada houses an array of unique and compositionally diverse hypersaline lakes [*Renaut and Long*, 1989] that have been suggested as terrestrial analogs for putative Martian and icy world hydrological systems [*Buffo et al.*, 2019; *Pontefract et al.*, 2017; *Toner et al.*, 2014]. Additionally, these lakes host an extraordinary ecological assemblage of micro- and macrofauna [*Pontefract et al.*, 2017; *Renaut and Long*, 1989]. Understanding the hydrological, thermal, biological and geochemical characteristics of these environments promises to extend our understanding of halophilic psychrophiles in an understudied ecological niche on Earth as well as provide an accessible analog laboratory to investigate biosignature production, distribution, and detectability in hypersaline ice-brine systems

that mirror high priority astrobiology targets elsewhere in our solar system. During February of 2019, one week of exploratory field work was conducted to collect ice samples at three hypersaline lake systems for later ion chromatography and microbial ecology (cell counting and 16S rRNA) analysis. The goal of this campaign is to produce novel quantitative thermal, chemical, and biological profiles of the ice in conjunction with summer and winter biogeochemical assays of the brine, sediment, and salt crusts of the lakes (collaborative effort with Dr. Alexandra Pontefract (MIT)), with the overarching goal of understanding how biosignatures interact with and shape the physicochemical and thermal environment of this unique analog system and what implications this has for biosignature distribution, preservation, and detection on Mars and ice-ocean worlds. Future work will utilize successors of the multiphase reactive transport models of Chapters 2 and 3, adapted to include biogeochemical processes, to simulate the dynamics and evolution of these ice-brine systems with the aim of validating their applicability to diverse ice-ocean world environments. These new biogeochemical data sets will substantially expand the diversity and number of existing ice-ocean/brine system biogeochemical measurements (e.g. sea ice [*Collins et al.*, 2008], subglacial lakes [*Christner et al.*, 2001], Antarctic dry valley lakes [*Doran et al.*, 2003; *Priscu et al.*, 1998]). By ensuring that the models simulating biogeochemical processes and entrainment in ice-ocean/brine systems can reproduce the empirical observations made across a broad range of terrestrial ices will strengthen the validity of their application to planetary ices, providing a predictive model of biosignature entrainment and expression on ice-ocean worlds.

While sea ice is by far the most well studied terrestrial ice-ocean/brine analog, much about the complexities of its biogeochemistry are only beginning to be understood

[*Collins et al.*, 2008; *Loose et al.*, 2011]. Furthermore, with the diverse chemistries proposed for oceans and brines throughout the solar system [*Nimmo and Pappalardo*, 2016; *Zolotov and Shock*, 2001], constraining how variable environmental pressures (brine chemistry, water activity, pH, chao-/kosmotropicity) impact the habitability of ice-ocean/brine systems is imperative in identifying and understanding astrobiological regions of interest [*Oren*, 2013]. The hypersaline lakes of central British Columbia's semi-arid Cariboo plateau (See Figure 5.3) offer a unique laboratory to carry out such investigations. These shallow endorheic basins seasonally fill, evaporate, and freeze forming tens to hundreds of individual brine pools, giving them their characteristic 'spotted' appearance [*Renaut and Long*, 1989] (See Figure 5.4). In addition to lake to lake compositional diversity, adjacent pools in a single lake have been observed to have drastically variable chemistry [*Pontefract et al.*, 2017; *Renaut and Long*, 1989], providing a novel environment to investigate the influence of an array of thermochemical stressors on the composition and local microbial ecology of the wintertime ice cover.

A unique and important feature of certain lakes is the magnesium sulfate ($MgSO_4$) dominated chemistry, which may more closely mirror Europa's ocean composition than our sodium chloride dominated ocean, as evidenced by the spectral detection of magnesium and sulfide salts on the moon's surface [*Brown and Hand*, 2013; *Fox-Powell and Cockell*, 2018; *Zolotov and Shock*, 2001]. During winter months, these lakes form an ice cover, providing a new analog environment for exploring the ice chemistry of Europa. This site provides a unique laboratory within which to investigate the biosignature dynamics of a $MgSO_4$ dominated system. To date, no compositional, structural, or biological measurements of this ice exists, and carrying out these measurements will constrain the

effects diverse brine chemistry has on biosignature entrainment dynamics. In February 2019, three diverse lake sites were visited (Basque Lake [50°36'00.0"N 121°21'30.9"W], Last Chance Lake (a sodium sulfate dominated system and alternate analog for Europa) [51°19'39.7"N 121°38'01.7"W], and Salt Lake [51°04'27.7"N 121°35'05.4"W] (Figure 5.3)). The focus of this field work was to 1) characterize the ice (thickness, porosity, textures, temperature), 2) experiment with preliminary field techniques (coring, fluorescein dispersion, ice core cutting and sampling, UV autofluorescence [See Figure 5.5]) to optimize measurement techniques for the following field season (February 2020), and 3) collect samples to establish biogeochemical profiles of the ice through ion and bioburden analysis (ion chromatography [28 ice samples, 5 brine samples], cell counting [28 ice samples], 16s rRNA [9 ice samples, 5 brine samples]).

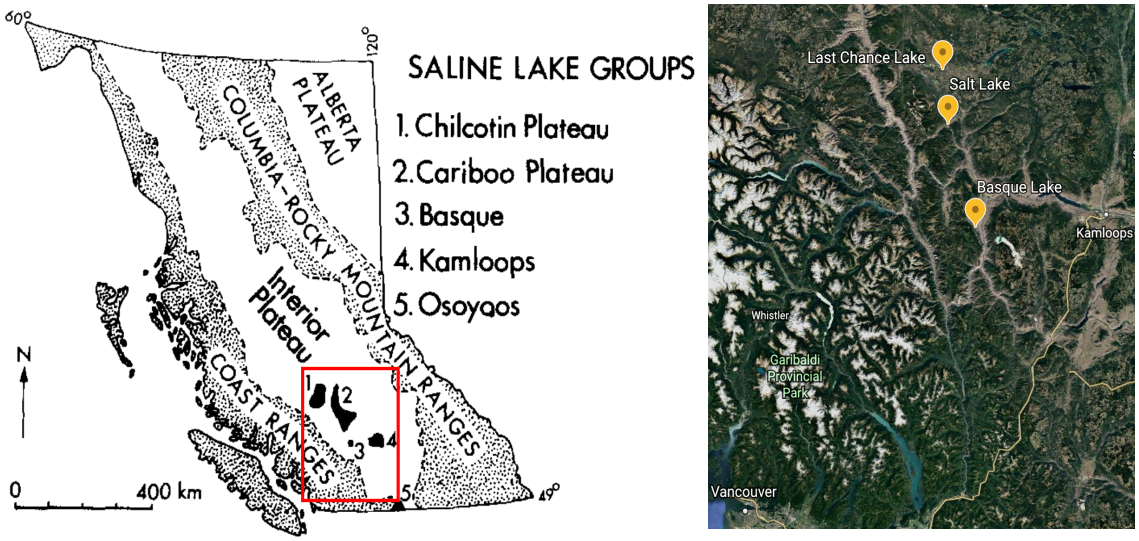

Figure 5.3 – Hypersaline lake locations. Left) Map of the hypersaline lake groups of central British Columbia (modified from [*Renaut and Long*, 1989]) Last Chance Lake and Salt Lake are members of the Cariboo Plateau group while Basque Lake is a member of the Basque group. Right) Enlarged view of the region outlined in red showing the lake locations visited during February 2019.

Figure 5.4 – Spotted textures of Last Chance Lake and Basque Lake. The cyclic evaporative, freezing, and thawing cycles of these hypersaline lakes give rise to their characteristic 'spotted' texture. These spots can be subaqueous (Left – Last Chance Lake) or form discrete chemically distinct brine pools (Right – Basque Lake [Photo Credit: Peter Doran (2019)])

5.5.2 Methods and Preliminary Results

5.5.2.1 Methods

At each lake, three of the frozen over pools were sampled. A total ice thickness measurement was taken by boring through the ice cover with a 4" Forstner bit. At both Last Chance Lake and Basque Lake two of the sample sites were frozen to the underlying bed while one site had an ice layer overlying a brine layer overlying saturated sediments. At Salt Lake there was a brine layer present at all sample sites. Subsequently, holes were bored to acquire samples from discrete layers of the ice. At each layer a coring bit was used to take enough 1" long cores of the ice to fill a 250ml sterilized Nalgene sample bottle. A probe thermometer was used to measure the temperature of the ice at each layer (See Figure 5.5a). The samples were returned from the field and melted prior to preparation and analysis. For cell counts, 45ml of the melt was combined with 4.5ml of 2.5%

glutaraldehyde solution (a fixative) and incubated for at least 24 hours before being filtered through a 0.2-micron polyethersulfone (PES) membrane filter which will be stained using 4',6-diamidino-2-phenylindole (DAPI) and counted under microscope. Anion and cation concentrations will be identified using ion chromatography at the Georgia Institute of Technology. Ion samples were filtered prior to analysis and the PES filters were sent to Dr. Alexandra Pontefract (MIT) for Illumina 16s rRNA sequencing. The temperature measurements will be used alongside the ion analysis to determine ice porosity by assuming ions are excluded from the ice phase and any remaining brine must lie on the liquidus, a common practice in sea ice research [*Hunke et al.*, 2011]. Together, this will provide novel and complete physicochemical, thermal, and biological stratigraphy for nine different pools, which will allow us to compare how a variety of environmental stressors affect the distribution of biosignatures within, and ecology of, these unique ice-brine systems.

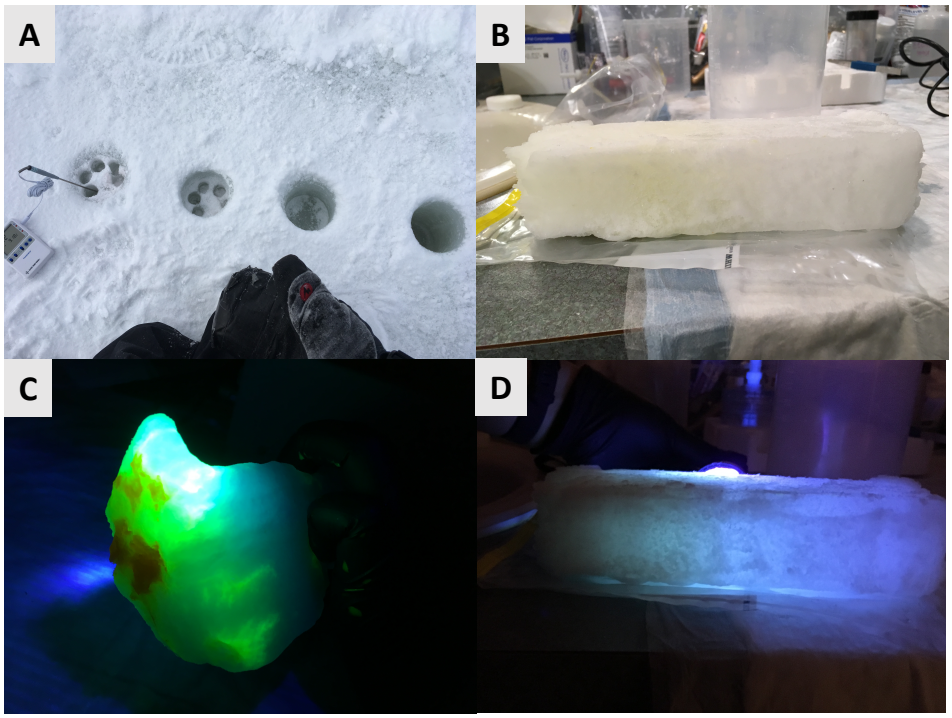

Figure 5.5 – Sampling techniques and experimental procedures. A) The coring technique used to acquire ice samples and thermal profiles within the ice. Left to Right – Shallow sample depth with probe thermometer. Middle sample depth with cores extracted. Bottom sample depth before cores are taken. Fully bored through hole to acquire ice thickness. B) Ice core extracted from Salt Lake, showing visible signs variable composition from bottom (left end) to top (right end). C) Fluorescein stained brine channels at the bottom of the core from panel (B), demonstrating the multiphase nature of the basal ice-brine interface. D) UV induced autofluorescence of biologic material entrained in the ice core from panel (B), suggesting a higher bioburden near the ice-brine interface.

5.5.2.2 Thermal Profiles

Vertical temperature profiles of the ice cover and underlying brine were taken at each lake site visited using a probe thermometer, the results of which can be seen in Figure 5.6. All of the sites exhibit an increasing temperature with depth. The sites that were frozen to the bed were substantially cooler than those which possessed a brine layer. There are

two potential explanations for this. The first explanation is that the amplified temperatures and the existence of brine layers seen at Last Chance Lake (Site 3) and Basque Lake (Site 3) correspond to diurnal warming, as these sites were samples later in the day than Sites 1 and 2 for both lakes. It is possible that thermal conduction could warm the ice and in turn allow for melting of the basal layer of the ice. Earlier sites were not revisited later in the day and obtaining temporally varying samples for the same site could elucidate whether surface warming is capable of reactivating a basal brine layer. Alternatively, the sites containing brine layers typically had thicker ice covers which may insulate the underlying liquid, allowing it to avoid diurnal freezing. Furthermore, any residual brine may provide an oasis for resident microbiology, which could in turn affect the evolution of the overlying ice.

The presence of super cold brines beneath a number of sample sites suggests substantial solute content in these ice-brine system (to be quantified by future ion chromatography results). This is bolstered by the discovery of precipitated salt veins in the sediments of all sites that were frozen to the bed and a precipitated salt layer (~2 cm of pure epsomite) at all three Salt Lake sites which existed between the brine and underlying sediment. These lakes provide unique, frigid, hypersaline environments to investigate the biogeochemical processes of halophilic psychrophiles and compose a diverse and rigorous set of benchmarks for validating the physics of numerical models hoping to simulate these and analogous planetary systems.

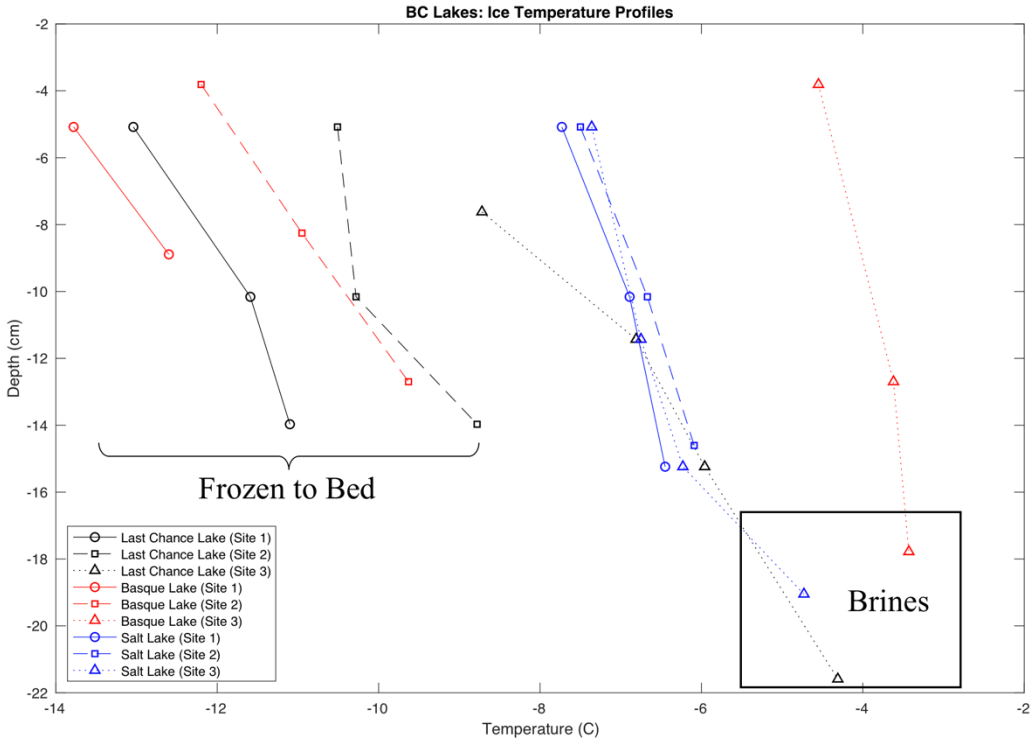

Figure 5.6 – Thermal profiles of hypersaline lakes. Temperature vs depth measurements for the nine sample sites visited during February 2019. Additionally, sites which were frozen to the underlying bed are labeled accordingly, and the box labeled 'brines' represents the temperatures of the underlying brine layers (only the measurement for Salt Lake site 3 is included as the brines at site 1 and 2 had comparable temperature).

5.5.3 Future Work and Relevance to Astrobiology

In addition to the completion of the ion chromatography analysis, cell counting, and 16s rRNA survey, which will round out the biogeochemical profiles of these hypersaline systems during February 2019, another field season is scheduled for February 2020. This return trip will allow for resampling of the sites visited in 2019 to investigate the annual evolution of the biogeochemistry of these systems. Variable environmental pressures (e.g. precipitation, lake level, temperature) may affect the ecology and evolution

of these ice-brine systems and carrying out an additional field season will allow the relationship between biosignature expression and the physicochemical environment to begin to be quantified and constrained. Additionally, preliminary experiments performed during the 2019 field season investigating the presence and extent of brine channels at the ice-brine interfaces of extracted ice cores through fluorescein dying (See Figure 5.5c) has spurred an effort to create a methodology for quantifying the permeability of the ice using spectrophotometric measurements of fluorescein concentration. Constraining brine dynamics in ice-ocean/brine environments is a fundamental hurdle in improving multiphase models of these systems (See Section 4.3.2) as the small-scale fluid processes likely play a critical role in governing their physicochemical evolution and in facilitating biogeochemical cycles. In sea ice, biology is concentrated in interstitial melts and depends on fluid flow to transport nutrients and waste through its porous habitat [*Loose et al.*, 2011; *Tedesco and Vichi*, 2014; *Thomas and Dieckmann*, 2003; *Vancoppenolle et al.*, 2013]. Additionally, some organisms produce substances capable of altering the ice microstructure [*Krembs et al.*, 2011]. Constraining heterogenous reactive solute transport in ice-ocean/brine mushy layers is imperative for understanding the evolutionary strategies used by psychrophiles to thrive in these environments. Moreover, determining the extent to which the dynamics of these hypersaline lake systems differ from those of sea ice provides insight into the role physicochemical pressures play in governing ice-ocean interface processes and characteristics (e.g. the dependence of mushy layer thickness on ocean composition [Figure 4.4]).

Composing spatiotemporal biogeochemical profiles of these hypersaline lake systems improves our understanding of how terrestrial habitats support extremophiles and

provides novel analog laboratories to investigate how ice-ocean/brine processes may operate in diverse physicochemical systems on other planetary bodies. The unique compositions of a number of these lakes and their similarity to putative Martian brine and Europan ocean chemistries makes understanding their dynamics directly applicable to these two astrobiology targets. Specifically, constraining how the thermochemical environment impacts solute and biosignature entrainment in the overlying ice provides a novel endmember to juxtapose sea ice. Possessing diverse datasets with which to validate the multiphase model of solute and biosignature entrainment in planetary ices ensures the model's ability to accommodate the physics of distinct ice-ocean/brine systems. Such a model will provide a tool to investigate potential biogeochemical processes and biosignature entrainment in planetary ices that is broadly applicable to any ice-ocean world. By providing a modular and adaptable model, the effects of ice-ocean world biogeochemistry can be included in larger geophysical models of oceans and ice shells, providing improved constraints on ice-ocean world habitability estimates and producing testable predictions of biosignature expression in planetary ices. These results will have direct implications for both planetary protection and exploration, as quantifying ocean-surface interaction and bioburden plays imperative roles in mitigating contamination and identifying detection limits, respectively.

5.6 Frozen Fingerprints: A Song of Ice and Brine

The goal of this work has been to create a comprehensive picture of planetary ice shells given the fact that ocean derived ices behave as multiphase reactive porous media. Furthermore, it seeks to assess the implications this has on the geophysics and habitability

of ice-ocean worlds such that testable predictions can be made that relate observable features to interior properties and processes. The progressive and multipronged approach taken throughout this work builds from first principles a novel finite difference model of planetary ices which has been validated against both analytical solutions and empirical observations of diverse terrestrial ice-ocean and -brine environments. The model accounts for the multiphase evolution of ice-ocean/brine systems subject to planetary environmental conditions and produces estimates of ice shell physicochemical evolution and material properties. The model has been designed in such a way that it can be easily adapted and tailored to accommodate diverse thermochemical environments and additional physics. Thus, the model provides a flexible and ever-evolving tool for simulating the two-phase geophysical processes that govern icy satellites. It can provide predictive estimates of ice shell properties useful for the interpretation of upcoming spacecraft observations (i.e. Europa Clipper) and will be able to actively integrate new information and science goals as the mission progresses.

This work has demonstrated the complex nature of ocean-derived planetary ices as well as the crucial role they play in governing the dynamics and evolution of their respective world's cryosphere. With the ubiquity and astrobiological relevance of ice-ocean worlds in our solar system understanding the physics that govern their dynamics, evolution, and habitability has substantial implications across a broad range of disciplines. Moreover, this work highlights the unique ability of planetary ices to record information about the thermochemical environment in which they formed through the entrainment of solutes and other impurities. This work demonstrates the importance of this phenomenon in both Earth and icy satellite systems and constructs a model capable of simulating the

associated dynamics. In the terrestrial system both sea ice and congelation growth marine ice are investigated, providing end members for observable growth rates. It is shown that the properties of the resulting ice contain unique identifiers about the thermal and chemical environment in which the ice formed, including the level of supercooling present in the water column, the ice-ocean interface thermal gradient, and ocean chemistry. The ability to reconstruct the thermochemical history of ice-ocean interactions from material properties of the resulting ice provides an invaluable tool for Earth science and suggests that the ice shells of moons like Europa may provide an accessible and observable record of their interior processes. What remained was to quantify the relationship between observable ice properties and the thermal and chemical processes and characteristics of the interior. This was the motivation for, and ultimate product of, the multiphase reactive transport model of planetary ices.

Applying the model to Europa, an archetype for ice-ocean worlds and a high priority astrobiology target, a synthetic picture of the moon's ice shell was produced (See Figure 5.7). Predictions of the bulk ice shell composition were made, and the physicochemical structures associated with hydrological processes (e.g. lenses, fractures) within the shell were predicted. These structures and compositional profiles are explicitly and uniquely related to the ice-ocean/brine interfacial processes which form them, providing a method to investigate interior geophysical processes through spacecraft observations. Specifically, the ice penetrating radar REASON, part of the Europa Clipper instrument suite, will rely on the dielectric properties, electrical conductivity, and compositional contrasts of the ice shell to investigate the interior structure of Europa [*Grima et al.*, 2016; *Kalousová et al.*, 2017; *Schroeder et al.*, 2016]. As these properties

depend critically on the ionic concentration within the ice, knowledge of the compositional structure of the ice shell and heterogeneities produced by geological features of interest will be imperative to interpreting the resultant radargrams and identifying any subsurface liquid water bodies (e.g. Figure 5.8). Ongoing work presented in Chapter 4 constrains the effects of environmental parameters on ice-ocean/brine interface evolution and identifies implications this may have on ice shell properties and dynamics. Chapter 5 outlines continued analog work and modeling efforts to understand and simulate biogeochemical processes in planetary ices and the observable biosignatures they may produce. The integration of these advances with the successful multiphase reactive transport models of Chapter 2 and 3 constitutes a novel and versatile tool to investigate the geophysics and biogeochemical processes of planetary ices with an improved realism that promises to substantially impact upcoming missions and our understanding of ice-ocean worlds.

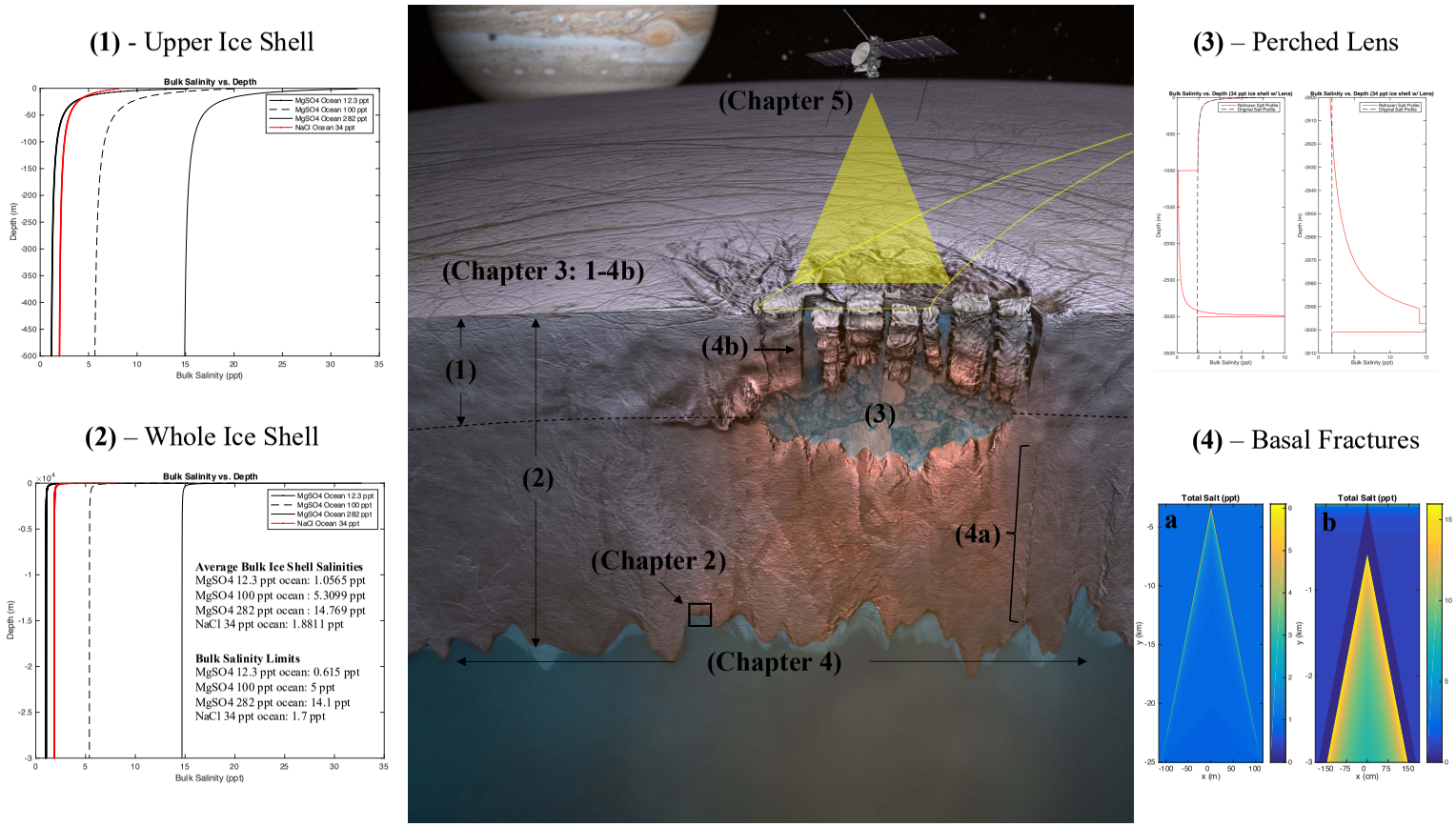

Figure 5.7 – A comprehensive picture of Europa's ice shell. Europa's ice shell is likely a dynamic and heterogeneous entity. Here, the processes and properties investigated throughout this work are summarized. **Chapter 2)** Formulated the foundational multiphase model of ice-ocean interface dynamics. **Chapter 3): 1)** Composition of the upper ice shell and its dependence on ocean chemistry. **2)** Composition of the entire ice shell, highlighting the lower limit set by critical porosity and the average bulk salinity of ice shells derived from diverse ocean chemistries. **3)** The compositional profile produced by the solidification of a 2 km thick perched water lens – resulting in the precipitation of ~2.23 m of salt. **4)** The compositional profile of solidified basal fractures (a: ice-ocean interface fracture, b: ice-lens interface fracture) **Chapter 4)** Investigated the effects of environmental parameters on the geometry and dynamics of the ice-ocean interface mushy layer and its implication on ice-ocean world geophysics and habitability. **Chapter 5)** Highlighted the progressive and multipronged approach of the project and the resultant ability to provide quantitative predictions that can be tested by the upcoming Europa Clipper Mission [*Pappalardo et al.*, 2017]. (Central image adapted from Britney Schmidt/Dead Pixel FX, UT Austin)

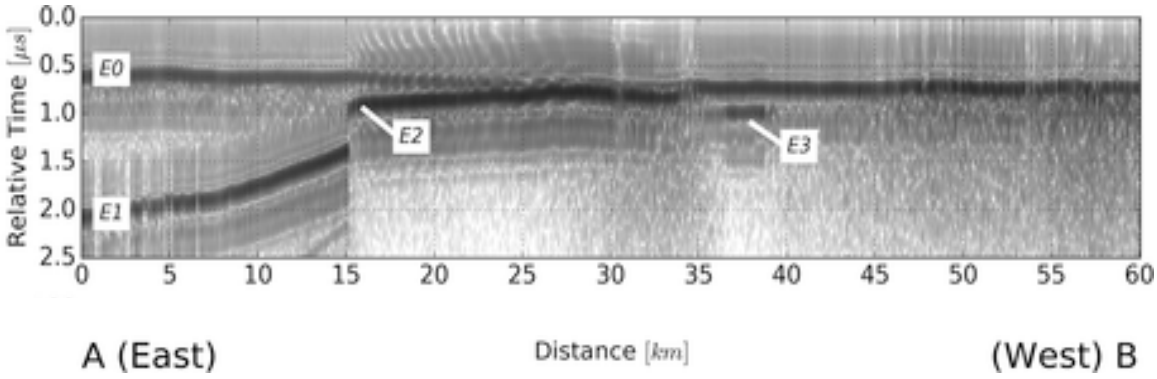

Figure 5.8 – Ice penetrating radar interactions with subsurface water. A radargram of the brine layer in McMurdo Ice Shelf (modified from [*Grima et al.*, 2016]) demonstrating the ability of radar to identify subsurface water bodies and the attenuation effects they induce. E0 is the ice shelf surface, E1 and E3 are the ice-ocean interface, and E2 is the brine layer.

References

Aagaard, K., and E. C. Carmack (1989), The role of sea ice and other fresh water in the Arctic circulation, *Journal of Geophysical Research: Oceans*, *94*(C10), 14485-14498.

Abdalati, W., H. J. Zwally, R. Bindschadler, B. Csatho, S. L. Farrell, H. A. Fricker, D. Harding, R. Kwok, M. Lefsky, and T. Markus (2010), The ICESat-2 laser altimetry mission, *Proceedings of the IEEE*, *98*(5), 735-751.

Ackley, S. F., and C. Sullivan (1994), Physical controls on the development and characteristics of Antarctic sea ice biological communities—a review and synthesis, *Deep Sea Research Part I: Oceanographic Research Papers*, *41*(10), 1583-1604.

Allu Peddinti, D., and A. K. McNamara (2015), Material transport across Europa's ice shell, *Geophysical Research Letters*, *42*(11), 4288-4293.

Anderson, J., E. Lau, W. Sjogren, G. Schubert, and W. Moore (1997), Gravitational evidence for an undifferentiated Callisto, *Nature*, *387*(6630), 264.

Anderson, J., G. Schubert, R. Jacobson, E. Lau, W. Moore, and W. Sjogren (1998), Europa's differentiated internal structure: Inferences from four Galileo encounters, *Science*, *281*(5385), 2019-2022.

Arrigo, K. R., G. Dieckmann, M. Gosselin, D. H. Robinson, C. H. Fritsen, and C. W. Sullivan (1995), High resolution study of the platelet ice ecosystem in McMurdo Sound, Antarctica: biomass, nutrient, and production profiles within a dense microalgal bloom, *Marine Ecology Progress Series*, *127*, 255-268.

Assur, A. (1958), Composition of sea ice and its tensile strength, *Arctic sea ice*, *598*, 106-138.

Baker, V., R. Strom, V. Gulick, J. Kargel, G. Komatsu, and V. Kale (1991), Ancient oceans, ice sheets and the hydrological cycle on Mars, *Nature*, *352*(6336), 589.

Barge, L. M., and L. M. White (2017), Experimentally testing hydrothermal vent origin of life on Enceladus and other icy/ocean worlds, *Astrobiology*, *17*(9), 820-833.

Barr, A. C., and W. B. McKinnon (2007), Convection in ice I shells and mantles with self-consistent grain size, *Journal of Geophysical Research: Planets*, *112*(E2).

Barry, R., M. Serreze, J. Maslanik, and R. Preller (1993), The Arctic sea ice-climate system: Observations and modeling, *Reviews of Geophysics*, *31*(4), 397-422.

Bassis, J., and C. Walker (2011), Upper and lower limits on the stability of calving glaciers from the yield strength envelope of ice, *Proc. R. Soc. A*, rspa20110422.

Bauer, J. M., B. J. Buratti, J.-Y. Li, J. A. Mosher, M. D. Hicks, B. E. Schmidt, and J. D. Goguen (2010), Direct detection of seasonal changes on Triton with Hubble Space Telescope, *The Astrophysical Journal Letters*, *723*(1), L49.

Bear, J. (2013), *Dynamics of fluids in porous media*, Courier Corporation.

Berner, R. A. (1980), *Early diagenesis: a theoretical approach*, Princeton University Press.

Billings, S. E., and S. A. Kattenhorn (2005), The great thickness debate: Ice shell thickness models for Europa and comparisons with estimates based on flexure at ridges, *Icarus*, *177*(2), 397-412.

Bintanja, R., G. Van Oldenborgh, S. Drijfhout, B. Wouters, and C. Katsman (2013), Important role for ocean warming and increased ice-shelf melt in Antarctic sea-ice expansion, *Nature Geoscience*, *6*(5), 376.

Bitz, C. M., and W. H. Lipscomb (1999), An energy-conserving thermodynamic model of sea ice, *Journal of Geophysical Research: Oceans*, *104*(C7), 15669-15677.

Blankenship, D. D., D. A. Young, W. B. Moore, and J. C. Moore (2009), Radar sounding of Europa's subsurface properties and processes: The view from Earth, *Europa. University of Arizona Press, Tucson, AZ*.

Board, S. S., and N. R. Council (2012), *Vision and voyages for planetary science in the decade 2013-2022*, National Academies Press.

Braun, J. (2010), The many surface expressions of mantle dynamics, *Nature Geoscience*, *3*(12), 825.

Brown, M., and K. Hand (2013), Salts and radiation products on the surface of Europa, *The Astronomical Journal*, *145*(4), 110.

Brown, R. H., R. N. Clark, B. J. Buratti, D. P. Cruikshank, J. W. Barnes, R. M. Mastrapa, J. Bauer, S. Newman, T. Momary, and K. Baines (2006), Composition and physical properties of Enceladus' surface, *Science*, *311*(5766), 1425-1428.

Brown, R. H., R. L. Kirk, T. Johnson, and L. A. Soderblom (1990), Energy sources for Triton's geyser-like plumes, *Science*, *250*(4979), 431-435.

Brown, R. H., L. Soderblom, J. Soderblom, R. Clark, R. Jaumann, J. Barnes, C. Sotin, B. Buratti, K. Baines, and P. Nicholson (2008), The identification of liquid ethane in Titan's Ontario Lacus, *Nature*, *454*(7204), 607.

Buczkowski, D., B. Schmidt, D. Williams, S. Mest, J. Scully, A. Ermakov, F. Preusker, P. Schenk, K. Otto, and H. Hiesinger (2016), The geomorphology of Ceres, *Science*, *353*(6303), aaf4332.

Buffo, J., and B. Schmidt (2017), Biomarker Production and Preservation on Europa, paper presented at AGU Fall Meeting Abstracts.

Buffo, J., B. Schmidt, and C. Huber (2018), Multiphase reactive transport and platelet ice accretion in the sea ice of McMurdo sound, Antarctica, *Journal of Geophysical Research: Oceans*, *123*(1), 324-345.

Buffo, J., B. Schmidt, C. Huber, and C. Walker (*in review*), Entrainment and dynamics of ocean-derived impurities within Europa's ice shell, *Science Advances*.

Buffo, J., B. Schmidt, A. Pontefract, and J. Lawrence (2019), Frozen Fingerprints: Chemical and Biological Entrainment in Planetary Ices, in *Astrobiology Science Conference*, edited, Bellevue, Washington.

Buratti, B., and J. Veverka (1983), Voyager photometry of Europa, *Icarus*, *55*(1), 93-110.

Burke, K., B. Steinberger, T. H. Torsvik, and M. A. Smethurst (2008), Plume generation zones at the margins of large low shear velocity provinces on the core–mantle boundary, *Earth and Planetary Science Letters*, *265*(1-2), 49-60.

Byrne, S., C. M. Dundas, M. R. Kennedy, M. T. Mellon, A. S. McEwen, S. C. Cull, I. J. Daubar, D. E. Shean, K. D. Seelos, and S. L. Murchie (2009), Distribution of mid-latitude ground ice on Mars from new impact craters, *science*, *325*(5948), 1674-1676.

Čadek, O., G. Tobie, T. Van Hoolst, M. Massé, G. Choblet, A. Lefèvre, G. Mitri, R. M. Baland, M. Běhounková, and O. Bourgeois (2016), Enceladus's internal ocean and ice shell constrained from Cassini gravity, shape, and libration data, *Geophysical Research Letters*, *43*(11), 5653-5660.

Canup, R. M., and W. R. Ward (2002), Formation of the Galilean satellites: Conditions of accretion, *The Astronomical Journal*, *124*(6), 3404.

Carns, R. C., R. E. Brandt, and S. G. Warren (2015), Salt precipitation in sea ice and its effect on albedo, with application to Snowball Earth, *Journal of Geophysical Research: Oceans*, *120*(11), 7400-7412.
Carr, M. H. (1987), Water on Mars, *Nature*, *326*(6108), 30.
Carr, M. H., M. J. Belton, C. R. Chapman, M. E. Davies, P. Geissler, R. Greenberg, A. S. McEwen, B. R. Tufts, R. Greeley, and R. Sullivan (1998), Evidence for a subsurface ocean on Europa, *Nature*, *391*(6665), 363.
Cassen, P., R. T. Reynolds, and S. Peale (1979), Is there liquid water on Europa?, *Geophysical Research Letters*, *6*(9), 731-734.
Castillo-Rogez, J. C., and T. B. McCord (2010), Ceres' evolution and present state constrained by shape data, *Icarus*, *205*(2), 443-459.
Castillo-Rogez, J. C., and J. I. Lunine (2010), Evolution of Titan's rocky core constrained by Cassini observations, *Geophysical Research Letters*, *37*(20).
Cavalieri, D., and C. Parkinson (2008), Antarctic sea ice variability and trends, 1979–2006, *Journal of Geophysical Research: Oceans*, *113*(C7).
Cavalieri, D., C. Parkinson, and K. Y. Vinnikov (2003), 30-Year satellite record reveals contrasting Arctic and Antarctic decadal sea ice variability, *Geophysical Research Letters*, *30*(18).
Cavalieri, D. J., P. Gloersen, C. L. Parkinson, J. C. Comiso, and H. J. Zwally (1997), Observed hemispheric asymmetry in global sea ice changes, *Science*, *278*(5340), 1104-1106.
Chaplin, M. (2006), Do we underestimate the importance of water in cell biology?, *Nature Reviews Molecular Cell Biology*, *7*(11), 861.
Chaplin, M. F. (2001), Water: its importance to life, *Biochemistry and Molecular Biology Education*, *29*(2), 54-59.
Charette, M. A., and W. H. Smith (2010), The volume of Earth's ocean, *Oceanography*, *23*(2), 112-114.
Chistyakova, S., and R. Latypov (2010), On the development of internal chemical zonation in small mafic dykes, *Geological Magazine*, *147*(1), 1-12.
Choblet, G., G. Tobie, C. Sotin, M. Běhounková, O. Čadek, F. Postberg, and O. Souček (2017), Powering prolonged hydrothermal activity inside Enceladus, *Nature Astronomy*, *1*(12), 841.
Christner, B. C., E. Mosley-Thompson, L. G. Thompson, and J. N. Reeve (2001), Isolation of bacteria and 16S rDNAs from Lake Vostok accretion ice, *Environmental Microbiology*, *3*(9), 570-577.
Chyba, C. F., and C. B. Phillips (2001), Possible ecosystems and the search for life on Europa, *Proceedings of the National Academy of Sciences*, *98*(3), 801-804.
Collins, G., and F. Nimmo (2009), Chaotic terrain on Europa, in *Europa*, edited, pp. 259-281, University of Arizona Press Tucson.
Collins, G. C., and J. C. Goodman (2007), Enceladus' south polar sea, *Icarus*, *189*(1), 72-82.
Collins, R. E., S. D. Carpenter, and J. W. Deming (2008), Spatial heterogeneity and temporal dynamics of particles, bacteria, and pEPS in Arctic winter sea ice, *Journal of Marine Systems*, *74*(3-4), 902-917.

Commission, I. O. (2010), The International thermodynamic equation of seawater–2010: calculation and use of thermodynamic properties.[includes corrections up to 31st October 2015].

Consolmagno, G. J., and J. S. Lewis (1978), The evolution of icy satellite interiors and surfaces, *Icarus*, *34*(2), 280-293.

Cottier, F., H. Eicken, and P. Wadhams (1999), Linkages between salinity and brine channel distribution in young sea ice, *Journal of Geophysical Research: Oceans*, *104*(C7), 15859-15871.

Cox, G. F., and W. F. Weeks (1974), Salinity variations in sea ice, *Journal of Glaciology*, *13*(67), 109-120.

Craven, M., I. Allison, R. Brand, A. Elcheikh, J. Hunter, M. Hemer, and S. Donoghue (2004), Initial borehole results from the Amery Ice Shelf hot-water drilling project, *Annals of Glaciology*, *39*, 531-539.

Craven, M., I. Allison, H. A. Fricker, and R. Warner (2009), Properties of a marine ice layer under the Amery Ice Shelf, East Antarctica, *Journal of Glaciology*, *55*(192), 717-728.

Craven, M., F. Carsey, A. Behar, J. Matthews, R. Brand, A. Elcheikh, S. Hall, and A. Treverrow (2005), Borehole imagery of meteoric and marine ice layers in the Amery Ice Shelf, East Antarctica, *Journal of Glaciology*, *51*(172), 75-84.

Cruikshank, D. P. (2005), Triton, Pluto, Centaurs, and trans-neptunian bodies, *Space science reviews*, *116*(1-2), 421-439.

Curry, J. A., J. L. Schramm, and E. E. Ebert (1995), Sea ice-albedo climate feedback mechanism, *Journal of Climate*, *8*(2), 240-247.

Daly, M., F. Rack, and R. Zook (2013), Edwardsiella andrillae, a new species of sea anemone from Antarctic Ice, *PloS one*, *8*(12), e83476.

Daly, S. F. (1984), Frazil ice dynamics*Rep.*, COLD REGIONS RESEARCH AND ENGINEERING LAB HANOVER NH.

Davis, N., and P. Wadhams (1995), A statistical analysis of Arctic pressure ridge morphology, *Journal of Geophysical Research: Oceans*, *100*(C6), 10915-10925.

Dayton, P. K., G. A. Robilliard, and A. L. Devries (1969), Anchor ice formation in McMurdo Sound, Antarctica, and its biological effects, *Science*, *163*(3864), 273-274.

De Sanctis, M., A. Raponi, E. Ammannito, M. Ciarniello, M. Toplis, H. McSween, J. Castillo-Rogez, B. Ehlmann, F. Carrozzo, and S. Marchi (2016), Bright carbonate deposits as evidence of aqueous alteration on (1) Ceres, *Nature*, *536*(7614), 54.

Dempsey, D. (2008), Observation and modeling of platelet ice in McMurdo Sound, Antarctica, Master's thesis, University of Otago.

Dempsey, D., and P. Langhorne (2012), Geometric properties of platelet ice crystals, *Cold Regions Science and Technology*, *78*, 1-13.

Dempsey, D., P. Langhorne, N. Robinson, M. Williams, T. Haskell, and R. Frew (2010), Observation and modeling of platelet ice fabric in McMurdo Sound, Antarctica, *Journal of Geophysical Research: Oceans*, *115*(C1).

Depoorter, M. A., J. Bamber, J. Griggs, J. Lenaerts, S. R. Ligtenberg, M. Van den Broeke, and G. Moholdt (2013), Calving fluxes and basal melt rates of Antarctic ice shelves, *Nature*, *502*(7469), 89.

Des Marais, D. J., J. A. Nuth III, L. J. Allamandola, A. P. Boss, J. D. Farmer, T. M. Hoehler, B. M. Jakosky, V. S. Meadows, A. Pohorille, and B. Runnegar (2008), The NASA astrobiology roadmap, *Astrobiology*, *8*(4), 715-730.

Desbois, G., J. Urai, C. Burkhardt, M. Drury, M. Hayles, and B. Humbel (2008), Cryogenic vitrification and 3D serial sectioning using high resolution cryo-FIB SEM technology for brine-filled grain boundaries in halite: first results, *Geofluids*, *8*(1), 60-72.

Dickson, R. R., and J. Brown (1994), The production of North Atlantic Deep Water: sources, rates, and pathways, *Journal of Geophysical Research: Oceans*, *99*(C6), 12319-12341.

Doggett, T., R. Greeley, P. Figueredo, and K. Tanaka (2009), Geologic stratigraphy and evolution of Europa's surface, in *Europa*, edited, pp. 137-160, University of Arizona Press Tucson, AZ.

Dombard, A. J., G. W. Patterson, A. P. Lederer, and L. M. Prockter (2013), Flanking fractures and the formation of double ridges on Europa, *Icarus*, *223*(1), 74-81.

Doran, P. T., C. H. Fritsen, C. P. McKay, J. C. Priscu, and E. E. Adams (2003), Formation and character of an ancient 19-m ice cover and underlying trapped brine in an "ice-sealed" east Antarctic lake, *Proceedings of the National Academy of Sciences*, *100*(1), 26-31.

Dougherty, M., K. Khurana, F. Neubauer, C. Russell, J. Saur, J. Leisner, and M. Burton (2006), Identification of a dynamic atmosphere at Enceladus with the Cassini magnetometer, *Science*, *311*(5766), 1406-1409.

Douté, S., B. Schmitt, Y. Langevin, J. Bibring, F. Altieri, G. Bellucci, B. Gondet, and F. Poulet (2007), South pole of Mars: Nature and composition of the icy terrains from Mars Express OMEGA observations, *Planetary and Space Science*, *55*(1-2), 113-133.

Durham, W., O. Prieto-Ballesteros, D. Goldsby, and J. Kargel (2010), Rheological and thermal properties of icy materials, *Space Science Reviews*, *153*(1-4), 273-298.

Ebert, E. E., and J. A. Curry (1993), An intermediate one-dimensional thermodynamic sea ice model for investigating ice-atmosphere interactions, *Journal of Geophysical Research: Oceans*, *98*(C6), 10085-10109.

Eicken, H. (1992), Salinity profiles of Antarctic sea ice: field data and model results, *Journal of Geophysical Research: Oceans*, *97*(C10), 15545-15557.

Eicken, H. (2002), Studies of Earth analogs of potential Europan habitats: opportunities and limitations, paper presented at Europa Focus Group Workshop.

Eicken, H. (2003), From the microscopic, to the macroscopic, to the regional scale: growth, microstructure and properties of sea ice, *Sea ice: an introduction to its physics, chemistry, biology and geology*, 22-81.

Eicken, H., H. Krouse, D. Kadko, and D. Perovich (2002), Tracer studies of pathways and rates of meltwater transport through Arctic summer sea ice, *Journal of Geophysical Research: Oceans*, *107*(C10), SHE 22-21-SHE 22-20.

Eicken, H., and M. A. Lange (1989), Development and properties of sea ice in the coastal regime of the southeastern Weddell Sea, *Journal of Geophysical Research: Oceans*, *94*(C6), 8193-8206.

Eicken, H., J. Weissenberger, I. Bussmann, J. Freitag, W. Schuster, F. V. Delgado, K. Evers, P. Jochmann, C. Krembs, and R. Gradinger (1998), Ice tank studies of

physical and biological sea-ice processes, paper presented at Ice in surface waters. Proceedings of the 14th International Symposium on Ice. AA Balkema, Rotterdam, The Netherlands.

Emms, P., and A. Fowler (1994), Compositional convection in the solidification of binary alloys, *Journal of Fluid Mechanics*, *262*, 111-139.

Fagents, S. A., R. Greeley, R. J. Sullivan, R. T. Pappalardo, L. M. Prockter, and G. S. Team (2000), Cryomagmatic mechanisms for the formation of Rhadamanthys Linea, triple band margins, and other low-albedo features on Europa, *Icarus*, *144*(1), 54-88.

Fanale, F. P., J. C. Granahan, T. B. McCord, G. Hansen, C. A. Hibbitts, R. Carlson, D. Matson, A. Ocampo, L. Kamp, and W. Smythe (1999), Galileo's multiinstrument spectral view of Europa's surface composition, *Icarus*, *139*(2), 179-188.

Feltham, D., N. Untersteiner, J. Wettlaufer, and M. Worster (2006), Sea ice is a mushy layer, *Geophysical Research Letters*, *33*(14).

Figueredo, P. H., R. Greeley, S. Neuer, L. Irwin, and D. Schulze-Makuch (2003), Locating potential biosignatures on Europa from surface geology observations, *Astrobiology*, *3*(4), 851-861.

Fischer, P. D., M. E. Brown, and K. P. Hand (2015), Spatially resolved spectroscopy of Europa: The distinct spectrum of large-scale chaos, *The Astronomical Journal*, *150*(5), 164.

Foley, B. J., and T. W. Becker (2009), Generation of plate-like behavior and mantle heterogeneity from a spherical, viscoplastic convection model, *Geochemistry, Geophysics, Geosystems*, *10*(8).

Forster, R. R., J. E. Box, M. R. Van Den Broeke, C. Miège, E. W. Burgess, J. H. Van Angelen, J. T. Lenaerts, L. S. Koenig, J. Paden, and C. Lewis (2014), Extensive liquid meltwater storage in firn within the Greenland ice sheet, *Nature Geoscience*, *7*(2), 95.

Fortes, A. (2000), Exobiological implications of a possible ammonia–water ocean inside Titan, *Icarus*, *146*(2), 444-452.

Fowler, A. (1987), Theories of mushy zones: applications to alloy solidification, magma transport, frost heave and igneous intrusions, in *Structure and Dynamics of Partially Solidified Systems*, edited, pp. 159-199, Springer.

Fox-Powell, M. G., and C. S. Cockell (2018), Building a Geochemical View of Microbial Salt Tolerance: Halophilic Adaptation of Marinococcus in a Natural Magnesium Sulfate Brine, *Frontiers in microbiology*, *9*, 739.

Freitag, J. (1999), The hydraulic properties of Arctic sea ice-Implications for the small-scale particle transport, *Ber. Polarforsch*, *325*, 150.

Fretwell, P., H. D. Pritchard, D. G. Vaughan, J. L. Bamber, N. Barrand, R. Bell, C. Bianchi, R. Bingham, D. D. Blankenship, and G. Casassa (2013), Bedmap2: improved ice bed, surface and thickness datasets for Antarctica.

Fricker, H. A., S. Popov, I. Allison, and N. Young (2001), Distribution of marine ice beneath the Amery Ice Shelf, *Geophysical Research Letters*, *28*(11), 2241-2244.

Gaeman, J., S. Hier-Majumder, and J. H. Roberts (2012), Sustainability of a subsurface ocean within Triton's interior, *Icarus*, *220*(2), 339-347.

Gaidos, E. J. (2001), Cryovolcanism and the recent flow of liquid water on Mars, *Icarus*, *153*(1), 218-223.

Galley, R., M. Trachtenberg, A. Langlois, D. Barber, and L. Shafai (2009), Observations of geophysical and dielectric properties and ground penetrating radar signatures for discrimination of snow, sea ice and freshwater ice thickness, *Cold Regions Science and Technology*, *57*(1), 29-38.

Galton-Fenzi, B., J. Hunter, R. Coleman, S. Marsland, and R. Warner (2012), Modeling the basal melting and marine ice accretion of the Amery Ice Shelf, *Journal of Geophysical Research: Oceans*, *117*(C9).

Gleeson, D. F., R. Pappalardo, M. Anderson, S. Grasby, R. Mielke, K. Wright, and A. Templeton (2012), Biosignature detection at an Arctic analog to Europa, *Astrobiology*, *12*(2), 135-150.

Glein, C. R., J. A. Baross, and J. H. Waite Jr (2015), The pH of Enceladus' ocean, *Geochimica et Cosmochimica Acta*, *162*, 202-219.

Glein, C. R., and E. L. Shock (2010), Sodium chloride as a geophysical probe of a subsurface ocean on Enceladus, *Geophysical Research Letters*, *37*(9).

Glover, P. W., M. J. Hole, and J. Pous (2000), A modified Archie's law for two conducting phases, *Earth and Planetary Science Letters*, *180*(3-4), 369-383.

Golden, K., S. Ackley, and V. Lytle (1998), The percolation phase transition in sea ice, *Science*, *282*(5397), 2238-2241.

Golden, K. M., H. Eicken, A. Heaton, J. Miner, D. Pringle, and J. Zhu (2007), Thermal evolution of permeability and microstructure in sea ice, *Geophysical Research Letters*, *34*(16).

Goosse, H., and T. Fichefet (1999), Importance of ice-ocean interactions for the global ocean circulation: A model study, *Journal of Geophysical Research: Oceans*, *104*(C10), 23337-23355.

Gough, A. J., A. R. Mahoney, P. J. Langhorne, M. J. Williams, N. J. Robinson, and T. G. Haskell (2012), Signatures of supercooling: McMurdo Sound platelet ice, *Journal of Glaciology*, *58*(207), 38-50.

Gow, A., S. Ackley, W. Weeks, and J. Govoni (1982), Physical and structural characteristics of Antarctic sea ice, *Annals of Glaciology*, *3*, 113-117.

Grasset, O., M. Dougherty, A. Coustenis, E. Bunce, C. Erd, D. Titov, M. Blanc, A. Coates, P. Drossart, and L. Fletcher (2013), JUpiter ICy moons Explorer (JUICE): An ESA mission to orbit Ganymede and to characterise the Jupiter system, *Planetary and Space Science*, *78*, 1-21.

Greeley, R., C. F. Chyba, J. Head, T. McCord, W. B. McKinnon, R. T. Pappalardo, and P. H. Figueredo (2004), Geology of Europa, *Jupiter: The Planet, Satellites and Magnetosphere*, 329-362.

Greeley, R., R. Sullivan, M. D. Coon, P. E. Geissler, B. R. Tufts, J. W. Head III, R. T. Pappalardo, and J. M. Moore (1998a), Terrestrial sea ice morphology: Considerations for Europa, *Icarus*, *135*(1), 25-40.

Greeley, R., R. Sullivan, J. Klemaszewski, K. Homan, J. W. Head III, R. T. Pappalardo, J. Veverka, B. E. Clark, T. V. Johnson, and K. P. Klaasen (1998b), Europa: initial Galileo geological observations, *Icarus*, *135*(1), 4-24.

Griewank, P., and D. Notz (2015), A 1-D modelling study of Arctic sea-ice salinity, *The Cryosphere*, *9*(1), 305-329.

Griewank, P. J., and D. Notz (2013), Insights into brine dynamics and sea ice desalination from a 1-D model study of gravity drainage, *Journal of Geophysical Research: Oceans*, *118*(7), 3370-3386.

Grima, C., J. S. Greenbaum, E. J. Lopez Garcia, K. M. Soderlund, A. Rosales, D. D. Blankenship, and D. A. Young (2016), Radar detection of the brine extent at McMurdo Ice Shelf, Antarctica, and its control by snow accumulation, *Geophysical Research Letters*, *43*(13), 7011-7018.

Grumbine, R. W. (1991), A model of the formation of high-salinity shelf water on polar continental shelves, *Journal of Geophysical Research: Oceans*, *96*(C12), 22049-22062.

Haas, C., S. Gerland, H. Eicken, and H. Miller (1997), Comparison of sea-ice thickness measurements under summer and winter conditions in the Arctic using a small electromagnetic induction device, *Geophysics*, *62*(3), 749-757.

Hammond, N. P., E. Parmenteir, and A. C. Barr (2018), Compaction and Melt Transport in Ammonia-Rich Ice Shells: Implications for the Evolution of Triton, *Journal of Geophysical Research: Planets*, *123*(12), 3105-3118.

Han, L., and A. P. Showman (2005), Thermo-compositional convection in Europa's icy shell with salinity, *Geophysical research letters*, *32*(20).

Hand, E. (2015), Dawn probe to look for a habitable ocean on Ceres, edited, American Association for the Advancement of Science.

Hand, K., C. Chyba, J. Priscu, R. Carlson, and K. Nealson (2009), Astrobiology and the potential for life on Europa, *Europa*, 589-629.

Hand, K. P., R. W. Carlson, and C. F. Chyba (2007), Energy, chemical disequilibrium, and geological constraints on Europa, *Astrobiology*, *7*(6), 1006-1022.

Hand, K. P., and C. F. Chyba (2007), Empirical constraints on the salinity of the europan ocean and implications for a thin ice shell, *Icarus*, *189*(2), 424-438.

Head, J., R. Pappalardo, R. Greeley, R. Sullivan, C. Pilcher, G. Schubert, W. Moore, M. Carr, J. Moore, and M. Belton (1997), Evidence for recent solid-state convection on Europa: The nature of pits, domes, spots, and ridges, paper presented at Bulletin of the American Astronomical Society.

Head, J. W., R. T. Pappalardo, and R. Sullivan (1999), Europa: Morphological characteristics of ridges and triple bands from Galileo data (E4 and E6) and assessment of a linear diapirism model, *Journal of Geophysical Research: Planets*, *104*(E10), 24223-24236.

Helfenstein, P., and E. Parmentier (1983), Patterns of fracture and tidal stresses on Europa, *Icarus*, *53*(3), 415-430.

Hellmer, H. H. (2004), Impact of Antarctic ice shelf basal melting on sea ice and deep ocean properties, *Geophysical Research Letters*, *31*(10).

Hesse, M., and J. Castillo-Rogez (2019), Thermal Evolution of the Impact-Induced Cryomagma Chamber Beneath Occator Crater on Ceres, *Geophysical Research Letters*, *46*(3), 1213-1221.

Holland, M. M., and C. M. Bitz (2003), Polar amplification of climate change in coupled models, *Climate Dynamics*, *21*(3-4), 221-232.

Holland, P. R., H. F. Corr, D. G. Vaughan, A. Jenkins, and P. Skvarca (2009), Marine ice in Larsen ice shelf, *Geophysical Research Letters*, *36*(11).

Holland, P. R., and D. L. Feltham (2005), Frazil dynamics and precipitation in a water column with depth-dependent supercooling, *Journal of Fluid Mechanics*, *530*, 101-124.

Hoppa, G., R. Greenberg, B. R. Tufts, P. Geissler, C. Phillips, and M. Milazzo (2000), Distribution of strike-slip faults on Europa, *Journal of Geophysical Research: Planets*, *105*(E9), 22617-22627.

Hoppa, G., B. R. Tufts, R. Greenberg, and P. Geissler (1999), Strike–slip faults on Europa: Global shear patterns driven by tidal stress, *Icarus*, *141*(2), 287-298.

Hoppmann, M., M. Nicolaus, S. Paul, P. A. Hunkeler, G. Heinemann, S. Willmes, R. Timmermann, O. Boebel, T. Schmidt, and M. Kühnel (2015), Ice platelets below Weddell Sea landfast sea ice, *Annals of Glaciology*, *56*(69), 175-190.

Howell, S. M., and R. T. Pappalardo (2018), Band formation and ocean-surface interaction on Europa and Ganymede, *Geophysical Research Letters*, *45*(10), 4701-4709.

Howell, S. M., and R. T. Pappalardo (2019), Can Earth-like plate tectonics occur in ocean world ice shells?, *Icarus*, *322*, 69-79.

Huber, C., A. Parmigiani, B. Chopard, M. Manga, and O. Bachmann (2008), Lattice Boltzmann model for melting with natural convection, *International Journal of Heat and Fluid Flow*, *29*(5), 1469-1480.

Hughes, K., P. Langhorne, G. Leonard, and C. Stevens (2014), Extension of an Ice Shelf Water plume model beneath sea ice with application in McMurdo Sound, Antarctica, *Journal of Geophysical Research: Oceans*, *119*(12), 8662-8687.

Hunke, E., D. Notz, A. Turner, and M. Vancoppenolle (2011), The multiphase physics of sea ice: a review for model developers, *The Cryosphere*, *5*(4), 989-1009.

Hunkeler, P. A., M. Hoppmann, S. Hendricks, T. Kalscheuer, and R. Gerdes (2016), A glimpse beneath Antarctic sea ice: Platelet layer volume from multifrequency electromagnetic induction sounding, *Geophysical Research Letters*, *43*(1), 222-231.

Huppert, H. E., and M. G. Worster (1985), Dynamic solidification of a binary melt, *Nature*, *314*(6013), 703.

Hussmann, H., F. Sohl, and T. Spohn (2006), Subsurface oceans and deep interiors of medium-sized outer planet satellites and large trans-neptunian objects, *Icarus*, *185*(1), 258-273.

Hussmann, H., and T. Spohn (2004), Thermal-orbital evolution of Io and Europa, *Icarus*, *171*(2), 391-410.

Hussmann, H., T. Spohn, and K. Wieczerkowski (2002), Thermal equilibrium states of Europa's ice shell: Implications for internal ocean thickness and surface heat flow, *Icarus*, *156*(1), 143-151.

Imanaka, H. (2019), Astrobiology on Titan: Geophysics to Organic Chemistry, in *Astrobiology*, edited, pp. 409-418, Springer.

Jacobs, S. S., A. L. Gordon, and J. Ardai (1979), Circulation and melting beneath the Ross Ice Shelf, *Science*, *203*(4379), 439-443.

Jaumann, R., R. N. Clark, F. Nimmo, A. R. Hendrix, B. J. Buratti, T. Denk, J. M. Moore, P. M. Schenk, S. J. Ostro, and R. Srama (2009), Icy satellites: Geological evolution and surface processes, in *Saturn from Cassini-Huygens*, edited, pp. 637-681, Springer.

Jeffries, M., and W. Weeks (1993), Structural characteristics and development of sea ice in the western Ross Sea, *Antarctic Science*, *5*(1), 63-75.

Jenkins, A., and A. Bombosch (1995), Modeling the effects of frazil ice crystals on the dynamics and thermodynamics of ice shelf water plumes, *Journal of Geophysical Research: Oceans*, *100*(C4), 6967-6981.

Johannessen, O. M., L. Bengtsson, M. W. Miles, S. I. Kuzmina, V. A. Semenov, G. V. Alekseev, A. P. Nagurnyi, V. F. Zakharov, L. P. Bobylev, and L. H. Pettersson (2004), Arctic climate change: observed and modelled temperature and sea-ice variability, *Tellus A: Dynamic Meteorology and Oceanography*, *56*(4), 328-341.

Johnson, B. C., T. J. Bowling, A. J. Trowbridge, and A. M. Freed (2016), Formation of the Sputnik Planum basin and the thickness of Pluto's subsurface ocean, *Geophysical Research Letters*, *43*(19), 10,068-010,077.

Johnson, B. C., R. Y. Sheppard, A. C. Pascuzzo, E. A. Fisher, and S. E. Wiggins (2017a), Porosity and Salt Content Determine if Subduction Can Occur in Europa's Ice Shell, *Journal of Geophysical Research: Planets*.

Johnson, B. C., R. Y. Sheppard, A. C. Pascuzzo, E. A. Fisher, and S. E. Wiggins (2017b), Porosity and Salt Content Determine if Subduction Can Occur in Europa's Ice Shell, *Journal of Geophysical Research: Planets*, *122*(12), 2765-2778.

Jordan, J. S., and M. A. Hesse (2015), Reactive transport in a partially molten system with binary solid solution, *Geochemistry, Geophysics, Geosystems*, *16*(12), 4153-4177.

Joughin, I., and R. B. Alley (2011), Stability of the West Antarctic ice sheet in a warming world, *Nature Geoscience*, *4*(8), 506.

Kalousová, K., D. M. Schroeder, and K. M. Soderlund (2017), Radar attenuation in Europa's ice shell: Obstacles and opportunities for constraining the shell thickness and its thermal structure, *Journal of Geophysical Research: Planets*, *122*(3), 524-545.

Kalousová, K., O. Souček, G. Tobie, G. Choblet, and O. Čadek (2014), Ice melting and downward transport of meltwater by two-phase flow in Europa's ice shell, *Journal of Geophysical Research: Planets*, *119*(3), 532-549.

Kalousová, K., O. Souček, G. Tobie, G. Choblet, and O. Čadek (2016), Water generation and transport below Europa's strike-slip faults, *Journal of Geophysical Research: Planets*, *121*(12), 2444-2462.

Kargel, J. S., J. Z. Kaye, J. W. Head III, G. M. Marion, R. Sassen, J. K. Crowley, O. P. Ballesteros, S. A. Grant, and D. L. Hogenboom (2000), Europa's crust and ocean: origin, composition, and the prospects for life, *Icarus*, *148*(1), 226-265.

Kattenhorn, S. A. (2018), Commentary: The Feasibility of Subduction and Implications for Plate Tectonics on Jupiter’s moon Europa.

Kattenhorn, S. A., and T. Hurford (2009), Tectonics of Europa, in *Europa*, edited, pp. 199-236, University of Arizona Press Tucson.

Kattenhorn, S. A., and L. M. Prockter (2014), Evidence for subduction in the ice shell of Europa, *Nature Geoscience*, *7*(10), 762.

Katz, R. F., and M. G. Worster (2008), Simulation of directional solidification, thermochemical convection, and chimney formation in a Hele-Shaw cell, *Journal of Computational Physics*, *227*(23), 9823-9840.

Kauffeld, M., M. Kawaji, and P. W. Egolf (2005), Handbook on ice slurries, *International Institute of Refrigeration, Paris*, *359*.

Kawano, Y., and T. Ohashi (2008), Effect of salinity diffusion and heat flux on the growth of sea ice microstructure.

Khazendar, A., and A. Jenkins (2003), A model of marine ice formation within Antarctic ice shelf rifts, *Journal of Geophysical Research: Oceans*, *108*(C7).

Khazendar, A., E. Rignot, and E. Larour (2009), Roles of marine ice, rheology, and fracture in the flow and stability of the Brunt/Stancomb-Wills Ice Shelf, *Journal of Geophysical Research: Earth Surface*, *114*(F4).

Khurana, K., M. Kivelson, D. Stevenson, G. Schubert, C. Russell, R. Walker, and C. Polanskey (1998), Induced magnetic fields as evidence for subsurface oceans in Europa and Callisto, *Nature*, *395*(6704), 777.

Kivelson, M. G., K. K. Khurana, C. T. Russell, M. Volwerk, R. J. Walker, and C. Zimmer (2000), Galileo magnetometer measurements: A stronger case for a subsurface ocean at Europa, *Science*, *289*(5483), 1340-1343.

Koenig, L. S., C. Miège, R. R. Forster, and L. Brucker (2014), Initial in situ measurements of perennial meltwater storage in the Greenland firn aquifer, *Geophysical Research Letters*, *41*(1), 81-85.

Korosov, A. A., P. Rampal, L. T. Pedersen, R. Saldo, Y. Ye, G. Heygster, T. Lavergne, S. Aaboe, and F. Girard-Ardhuin (2018), A new tracking algorithm for sea ice age distribution estimation, *Cryosphere*, *12*(6), 2073-2085.

Krembs, C., H. Eicken, and J. W. Deming (2011), Exopolymer alteration of physical properties of sea ice and implications for ice habitability and biogeochemistry in a warmer Arctic, *Proceedings of the National Academy of Sciences*, *108*(9), 3653-3658.

Kurtz, N., and T. Markus (2012), Satellite observations of Antarctic sea ice thickness and volume, *Journal of Geophysical Research: Oceans*, *117*(C8).

Kuskov, O., and V. Kronrod (2005), Internal structure of Europa and Callisto, *Icarus*, *177*(2), 550-569.

Lake, R., and E. Lewis (1970), Salt rejection by sea ice during growth, *Journal of Geophysical Research*, *75*(3), 583-597.

Langhorne, P., K. Hughes, A. Gough, I. Smith, M. Williams, N. Robinson, C. Stevens, W. Rack, D. Price, and G. Leonard (2015), Observed platelet ice distributions in Antarctic sea ice: An index for ocean-ice shelf heat flux, *Geophysical Research Letters*, *42*(13), 5442-5451.

Lawrence, J., B. E. Schmidt, L. Winslow, P. Doran, S. Kim, C. Walker, J. Buffo, M. Skidmore, K. Soderlund, and D. Blankenship (2016), Insights Into Ice-Ocean Interactions on Earth and Europa, paper presented at AGU Fall Meeting Abstracts.

Laxon, S. W., K. A. Giles, A. L. Ridout, D. J. Wingham, R. Willatt, R. Cullen, R. Kwok, A. Schweiger, J. Zhang, and C. Haas (2013), CryoSat-2 estimates of Arctic sea ice thickness and volume, *Geophysical Research Letters*, *40*(4), 732-737.

Lay, T., J. Hernlund, and B. A. Buffett (2008), Core–mantle boundary heat flow, *Nature geoscience*, *1*(1), 25.

Leonard, G., C. Purdie, P. Langhorne, T. Haskell, M. Williams, and R. Frew (2006), Observations of platelet ice growth and oceanographic conditions during the winter of 2003 in McMurdo Sound, Antarctica, *Journal of Geophysical Research: Oceans*, *111*(C4).

Lewis, E., and R. Perkin (1983), Supercooling and energy exchange near the Arctic Ocean surface, *Journal of Geophysical Research: Oceans*, *88*(C12), 7681-7685.
Lewis, J. S. (1971), Satellites of the outer planets: Their physical and chemical nature, *Icarus*, *15*(2), 174-185.
Light, B., G. Maykut, and T. Grenfell (2003), Effects of temperature on the microstructure of first-year Arctic sea ice, *Journal of Geophysical Research: Oceans*, *108*(C2).
Lipps, J. H., and S. Rieboldt (2005), Habitats and taphonomy of Europa, *Icarus*, *177*(2), 515-527.
Loose, B., W. McGillis, P. Schlosser, D. Perovich, and T. Takahashi (2009), Effects of freezing, growth, and ice cover on gas transport processes in laboratory seawater experiments, *Geophysical Research Letters*, *36*(5).
Loose, B., L. A. Miller, S. Elliott, and T. Papakyriakou (2011), Sea ice biogeochemistry and material transport across the frozen interface, *Oceanography*, *24*(3), 202-218.
Lorenz, R. D., and S. E. Shandera (2001), Physical properties of ammonia-rich ice: Application to Titan, *Geophysical research letters*, *28*(2), 215-218.
Lowell, R. P., and M. DuBose (2005), Hydrothermal systems on Europa, *Geophysical research letters*, *32*(5).
Lucchitta, B. K., and L. A. Soderblom (1982), The geology of Europa, paper presented at Satellites of Jupiter.
Luckman, A., D. Jansen, B. Kulessa, E. King, P. Sammonds, and D. Benn (2012), Basal crevasses in Larsen C Ice Shelf and implications for their global abundance, *The Cryosphere*, *6*(1), 113-123.
Lunine, J. I., and S. K. Atreya (2008), The methane cycle on Titan, *nature geoscience*, *1*(3), 159.
Lunine, J. I., D. J. Stevenson, and Y. L. Yung (1983), Ethane ocean on Titan, *Science*, *222*(4629), 1229-1230.
Lyon, W. (1961), DIVISION OF OCEANOGRAPHY AND METEOROLOGY: OCEAN AND SEA-ICE RESEARCH IN THE ARCTIC OCEAN VIA SUBMARINE, *Transactions of the New York Academy of Sciences*, *23*(8 Series II), 662-674.
Lyubetskaya, T., and J. Korenaga (2007), Chemical composition of Earth's primitive mantle and its variance: 2. Implications for global geodynamics, *Journal of Geophysical Research: Solid Earth*, *112*(B3).
Malmgren, F., and G. Institutt (1927), *On the properties of sea-ice*, AS John Griegs Boktrykkeri.
Manga, M., and C. Michaut (2017), Formation of lenticulae on Europa by saucer-shaped sills, *Icarus*, *286*, 261-269.
Manga, M., and A. Sinton (2004), Formation of bands and ridges on Europa by cyclic deformation: Insights from analogue wax experiments, *Journal of Geophysical Research: Planets*, *109*(E9).
Manga, M., and C. Y. Wang (2007), Pressurized oceans and the eruption of liquid water on Europa and Enceladus, *Geophysical Research Letters*, *34*(7).
Marion, G. M., C. H. Fritsen, H. Eicken, and M. C. Payne (2003), The search for life on Europa: limiting environmental factors, potential habitats, and Earth analogues, *Astrobiology*, *3*(4), 785-811.
Martin, S. (1981), Frazil ice in rivers and oceans, *Annual Review of Fluid Mechanics*, *13*(1), 379-397.

Martorano, M., J. F. Neto, T. Oliveira, and T. Tsubaki (2011), Macrosegregation of impurities in directionally solidified silicon, *Metallurgical and Materials Transactions A*, *42*(7), 1870-1886.

Maruyama, S., M. Santosh, and D. Zhao (2007), Superplume, supercontinent, and post-perovskite: mantle dynamics and anti-plate tectonics on the core–mantle boundary, *Gondwana Research*, *11*(1-2), 7-37.

Massom, R. A., T. A. Scambos, L. G. Bennetts, P. Reid, V. A. Squire, and S. E. Stammerjohn (2018), Antarctic ice shelf disintegration triggered by sea ice loss and ocean swell, *Nature*, *558*(7710), 383.

Matson, D. L., J. C. Castillo, J. Lunine, and T. V. Johnson (2007), Enceladus' plume: Compositional evidence for a hot interior, *Icarus*, *187*(2), 569-573.

Mawson, D. (1914), Australasian Antarctic Expedition, 1911-1914, *The Geographical Journal*, *44*(3), 257-284.

McCarthy, C., J. Blackford, and C. Jeffree (2013), Low-temperature-SEM study of dihedral angles in the ice-I/sulfuric acid partially molten system, *Journal of microscopy*, *249*(2), 150-157.

McCarthy, C., R. F. Cooper, S. H. Kirby, K. D. Rieck, and L. A. Stern (2007), Solidification and microstructures of binary ice-I/hydrate eutectic aggregates, *American Mineralogist*, *92*(10), 1550-1560.

McCord, T. B., G. B. Hansen, D. L. Matson, T. V. Johnson, J. K. Crowley, F. P. Fanale, R. W. Carlson, W. D. Smythe, P. D. Martin, and C. A. Hibbitts (1999), Hydrated salt minerals on Europa's surface from the Galileo near-infrared mapping spectrometer (NIMS) investigation, *Journal of Geophysical Research: Planets*, *104*(E5), 11827-11851.

McCord, T. B., G. Teeter, G. B. Hansen, M. T. Sieger, and T. M. Orlando (2002), Brines exposed to Europa surface conditions, *Journal of Geophysical Research: Planets*, *107*(E1), 4-1-4-6.

McFarlane, V., M. Loewen, and F. Hicks (2014), Laboratory measurements of the rise velocity of frazil ice particles, *Cold Regions Science and Technology*, *106*, 120-130.

McGRATH, D., K. Steffen, T. Scambos, H. Rajaram, G. Casassa, and J. L. R. Lagos (2012), Basal crevasses and associated surface crevassing on the Larsen C ice shelf, Antarctica, and their role in ice-shelf instability, *Annals of Glaciology*, *53*(60), 10-18.

McGuinness, M., M. Williams, P. Langhorne, C. Purdie, and J. Crook (2009), Frazil deposition under growing sea ice, *Journal of Geophysical Research: Oceans*, *114*(C7).

McKenzie, D. (1984), The generation and compaction of partially molten rock, *Journal of petrology*, *25*(3), 713-765.

McKinnon, W. B. (1999), Convective instability in Europa's floating ice shell, *Geophysical Research Letters*, *26*(7), 951-954.

Mellor, M. (1986), Mechanical behavior of sea ice, in *The geophysics of sea ice*, edited, pp. 165-281, Springer.

Meredith, M. P., and M. A. Brandon (2017), Oceanography and sea ice in the Southern Ocean, *Sea ice*, 216-238.

Michaut, C., and M. Manga (2014), Domes, pits, and small chaos on Europa produced by water sills, *Journal of Geophysical Research: Planets*, *119*(3), 550-573.
Miles, B. W., C. R. Stokes, and S. S. Jamieson (2017), Simultaneous disintegration of outlet glaciers in Porpoise Bay (Wilkes Land), East Antarctica, driven by sea ice break-up, *The Cryosphere.*, *11*, 427-442.
Mitri, G., and A. P. Showman (2005), Convective–conductive transitions and sensitivity of a convecting ice shell to perturbations in heat flux and tidal-heating rate: Implications for Europa, *Icarus*, *177*(2), 447-460.
Mitri, G., A. P. Showman, J. I. Lunine, and R. D. Lorenz (2007), Hydrocarbon lakes on Titan, *Icarus*, *186*(2), 385-394.
Moore, J. C. (2000), Models of radar absorption in Europan ice, *Icarus*, *147*(1), 292-300.
Mottl, M. J., B. T. Glazer, R. I. Kaiser, and K. J. Meech (2007), Water and astrobiology, *Chemie der Erde-Geochemistry*, *67*(4), 253-282.
Mustard, J. F., C. D. Cooper, and M. K. Rifkin (2001), Evidence for recent climate change on Mars from the identification of youthful near-surface ground ice, *Nature*, *412*(6845), 411.
Nagel, K., D. Breuer, and T. Spohn (2004), A model for the interior structure, evolution, and differentiation of Callisto, *Icarus*, *169*(2), 402-412.
Nakagawa, T., and P. J. Tackley (2004), Effects of a perovskite-post perovskite phase change near core-mantle boundary in compressible mantle convection, *Geophysical Research Letters*, *31*(16).
Nakawo, M., and N. K. Sinha (1981), Growth rate and salinity profile of first-year sea ice in the high Arctic, *Journal of Glaciology*, *27*(96), 315-330.
Nakawo, M., and N. K. Sinha (1984), A note on brine layer spacing of first-year sea ice, *Atmosphere-ocean*, *22*(2), 193-206.
Nansen, F. (1897), *Farthest North: Being the Record of a Voyage of Exploration of the Ship "Fram" 1893–96 and of a Fifteen Months' Sleigh Journey by Dr. Nansen and Lieut. Johansen (Complete)*, Library of Alexandria.
Neveu, M., S. J. Desch, and J. C. Castillo-Rogez (2017), Aqueous geochemistry in icy world interiors: Equilibrium fluid, rock, and gas compositions, and fate of antifreezes and radionuclides, *Geochimica et Cosmochimica Acta*, *212*, 324-371.
Nimmo, F., and E. Gaidos (2002), Strike-slip motion and double ridge formation on Europa, *Journal of Geophysical Research: Planets*, *107*(E4), 5-1-5-8.
Nimmo, F., B. Giese, and R. Pappalardo (2003), Estimates of Europa's ice shell thickness from elastically-supported topography, *Geophysical Research Letters*, *30*(5).
Nimmo, F., D. Hamilton, W. McKinnon, P. Schenk, R. Binzel, C. Bierson, R. Beyer, J. Moore, S. Stern, and H. Weaver (2016), Reorientation of Sputnik Planitia implies a subsurface ocean on Pluto, *Nature*, *540*(7631), 94.
Nimmo, F., and R. Pappalardo (2016), Ocean worlds in the outer solar system, *Journal of Geophysical Research: Planets*, *121*(8), 1378-1399.
Nimmo, F., and P. Schenk (2006), Normal faulting on Europa: Implications for ice shell properties, *Journal of structural geology*, *28*(12), 2194-2203.
Notz, D. (2012), Challenges in simulating sea ice in Earth System Models, *Wiley Interdisciplinary Reviews: Climate Change*, *3*(6), 509-526.
Notz, D., and C. M. Bitz (2017), Sea ice in Earth system models, *Sea ice*, 304-325.

Notz, D., and M. G. Worster (2008), In situ measurements of the evolution of young sea ice, *Journal of Geophysical Research: Oceans*, *113*(C3).
Notz, D., and M. G. Worster (2009), Desalination processes of sea ice revisited, *Journal of Geophysical Research: Oceans*, *114*(C5).
Oertling, A. B., and R. G. Watts (2004), Growth of and brine drainage from NaCl-H2O freezing: A simulation of young sea ice, *Journal of Geophysical Research: Oceans*, *109*(C4).
Ohashi, T. (2004), A numerical simulation of the development of ice-microstructres, paper presented at Proceedings of the 19th international symposium on Okhotsk sea & sea ice, 2004.
Ohashi, T. (2007), Numerical simulation of salinity diffusion and growth instability in the microstructure evolution of sea ice, paper presented at Proceedings of the 22th international symposium on Okhotsk sea & sea ice, 2007.
Ojakangas, G. W., and D. J. Stevenson (1989), Thermal state of an ice shell on Europa, *Icarus*, *81*(2), 220-241.
Ojha, L., M. B. Wilhelm, S. L. Murchie, A. S. McEwen, J. J. Wray, J. Hanley, M. Massé, and M. Chojnacki (2015), Spectral evidence for hydrated salts in recurring slope lineae on Mars, *Nature Geoscience*, *8*(11), 829.
Olson, P., G. Schubert, and C. Anderson (1987), Plume formation in the D ″-layer and the roughness of the core–mantle boundary, *Nature*, *327*(6121), 409.
Olson, P. L., R. S. Coe, P. E. Driscoll, G. A. Glatzmaier, and P. H. Roberts (2010), Geodynamo reversal frequency and heterogeneous core–mantle boundary heat flow, *Physics of the Earth and Planetary Interiors*, *180*(1-2), 66-79.
Oren, A. (2013), Life in magnesium-and calcium-rich hypersaline environments: salt stress by chaotropic ions, in *Polyextremophiles*, edited, pp. 215-232, Springer.
Orosei, R., S. Lauro, E. Pettinelli, A. Cicchetti, M. Coradini, B. Cosciotti, F. Di Paolo, E. Flamini, E. Mattei, and M. Pajola (2018), Radar evidence of subglacial liquid water on Mars, *Science*, *361*(6401), 490-493.
Orsi, A. H., G. C. Johnson, and J. L. Bullister (1999), Circulation, mixing, and production of Antarctic Bottom Water, *Progress in Oceanography*, *43*(1), 55-109.
Paolo, F. S., H. A. Fricker, and L. Padman (2015), Volume loss from Antarctic ice shelves is accelerating, *Science*, *348*(6232), 327-331.
Pappalardo, R., M. Belton, H. Breneman, M. Carr, C. Chapman, G. Collins, T. Denk, S. Fagents, P. Geissler, and B. Giese (1999), Does Europa have a subsurface ocean? Evaluation of the geological evidence, *Journal of Geophysical Research: Planets*, *104*(E10), 24015-24055.
Pappalardo, R., and M. Coon (1996), A sea ice analog for the surface of Europa, paper presented at Lunar and Planetary Science Conference.
Pappalardo, R., J. Head, R. Greeley, R. Sullivan, C. Pilcher, G. Schubert, W. Moore, M. Carr, J. Moore, and M. Belton (1998), Geological evidence for solid-state convection in Europa's ice shell, *Nature*, *391*(6665), 365.
Pappalardo, R., D. Senske, H. Korth, R. Klima, S. Vance, and K. Craft (2017), The Europa Clipper Mission: Exploring The Habilatbility of A Unique Icy World, paper presented at European Planetary Science Congress.
Pappalardo, R. T., and A. C. Barr (2004), The origin of domes on Europa: The role of thermally induced compositional diapirism, *Geophysical Research Letters*, *31*(1).

Parkinson, C. D., M.-C. Liang, Y. L. Yung, and J. L. Kirschivnk (2008), Habitability of Enceladus: planetary conditions for life, *Origins of Life and Evolution of Biospheres*, *38*(4), 355-369.

Parmentier, F.-J. W., T. R. Christensen, L. L. Sørensen, S. Rysgaard, A. D. McGuire, P. A. Miller, and D. A. Walker (2013), The impact of lower sea-ice extent on Arctic greenhouse-gas exchange, *Nature climate change*, *3*(3), 195.

Perovich, D. K., B. C. Elder, and J. A. Richter-Menge (1997), Observations of the annual cycle of sea ice temperature and mass balance, *Geophysical research letters*, *24*(5), 555-558.

Perovich, D. K., T. C. Grenfell, B. Light, B. C. Elder, J. Harbeck, C. Polashenski, W. B. Tucker, and C. Stelmach (2009), Transpolar observations of the morphological properties of Arctic sea ice, *Journal of Geophysical Research: Oceans*, *114*(C1).

Petrich, C., and H. Eicken (2010), Growth, structure and properties of sea ice, *Sea ice*, *2*, 23-77.

Petrich, C., and H. Eicken (2017), Overview of sea ice growth and properties, *Sea ice*, 1-41.

Phillips, C. B., and R. T. Pappalardo (2014), Europa Clipper mission concept: Exploring Jupiter's ocean moon, *Eos, Transactions American Geophysical Union*, *95*(20), 165-167.

Pieri, D. C. (1981), Lineament and polygon patterns on Europa, *Nature*, *289*, 17-21.

Plescia, J., and J. Boyce (1983), Crater numbers and geological histories of Iapetus, Enceladus, Tethys and Hyperion, *Nature*, *301*(5902), 666.

Pontefract, A., T. F. Zhu, V. K. Walker, H. Hepburn, C. Lui, M. T. Zuber, G. Ruvkun, and C. E. Carr (2017), Microbial diversity in a hypersaline sulfate lake: a terrestrial analog of ancient Mars, *Frontiers in microbiology*, *8*, 1819.

Porco, C., P. Helfenstein, P. Thomas, A. Ingersoll, J. Wisdom, R. West, G. Neukum, T. Denk, R. Wagner, and T. Roatsch (2006), Cassini observes the active south pole of Enceladus, *science*, *311*(5766), 1393-1401.

Postberg, F., S. Kempf, J. Schmidt, N. Brilliantov, A. Beinsen, B. Abel, U. Buck, and R. Srama (2009), Sodium salts in E-ring ice grains from an ocean below the surface of Enceladus, *Nature*, *459*(7250), 1098.

Poulet, F., J.-P. Bibring, J. Mustard, A. Gendrin, N. Mangold, Y. Langevin, R. Arvidson, B. Gondet, C. Gomez, and T. O. Team (2005), Phyllosilicates on Mars and implications for early Martian climate, *Nature*, *438*(7068), 623.

Priscu, J. C., C. H. Fritsen, E. E. Adams, S. J. Giovannoni, H. W. Paerl, C. P. McKay, P. T. Doran, D. A. Gordon, B. D. Lanoil, and J. L. Pinckney (1998), Perennial Antarctic lake ice: an oasis for life in a polar desert, *Science*, *280*(5372), 2095-2098.

Priscu, J. C., and K. P. Hand (2012), Microbial habitability of icy worlds, *Microbe*, *7*(4), 167-172.

Pritchard, M. S., A. B. Bush, and S. J. Marshall (2008), Neglecting ice-atmosphere interactions underestimates ice sheet melt in millennial-scale deglaciation simulations, *Geophysical Research Letters*, *35*(1).

Prockter, L. M. (2005), Ice in the solar system, *Johns Hopkins APL technical digest*, *26*(2), 175-188.

Prockter, L. M. (2017), The Structure and Thickness of Europa's Ice Shell, paper presented at Accessing the Subsurface Oceans of Icy Worlds, California Institute of Technology, October 9-12.

Prockter, L. M., J. W. Head, R. T. Pappalardo, R. J. Sullivan, A. E. Clifton, B. Giese, R. Wagner, and G. Neukum (2002), Morphology of Europan bands at high resolution: A mid-ocean ridge-type rift mechanism, *Journal of Geophysical Research: Planets*, *107*(E5).

Quick, L. C., D. L. Buczkowski, O. Ruesch, J. E. Scully, J. Castillo-Rogez, C. A. Raymond, P. M. Schenk, H. G. Sizemore, and M. V. Sykes (2019), A possible brine reservoir beneath Occator crater: Thermal and compositional evolution and formation of the Cerealia Dome and Vinalia Faculae, *Icarus*, *320*, 119-135.

Rees Jones, D. W., and M. G. Worster (2013), A simple dynamical model for gravity drainage of brine from growing sea ice, *Geophysical Research Letters*, *40*(2), 307-311.

Rees Jones, D. W., and M. G. Worster (2014), A physically based parameterization of gravity drainage for sea-ice modeling, *Journal of Geophysical Research: Oceans*, *119*(9), 5599-5621.

Reiners, P. W. (1998), Reactive melt transport in the mantle and geochemical signatures of mantle-derived magmas, *Journal of Petrology*, *39*(5), 1039-1061.

Renaut, R. W., and P. R. Long (1989), Sedimentology of the saline lakes of the Cariboo plateau, Interior British Columbia, Canada, *Sedimentary Geology*, *64*(4), 239-264.

Reynolds, R. T., C. P. McKay, and J. F. Kasting (1987), Europa, tidally heated oceans, and habitable zones around giant planets, *Advances in Space Research*, *7*(5), 125-132.

Reynolds, R. T., S. W. Squyres, D. S. Colburn, and C. P. McKay (1983), On the habitability of Europa, *Icarus*, *56*(2), 246-254.

Rignot, E., and K. Steffen (2008), Channelized bottom melting and stability of floating ice shelves, *Geophysical Research Letters*, *35*(2).

Rist, M., P. Sammonds, S. Murrell, P. Meredith, C. Doake, H. Oerter, and K. Matsuki (1999), Experimental and theoretical fracture mechanics applied to Antarctic ice fracture and surface crevassing, *Journal of Geophysical Research: Solid Earth*, *104*(B2), 2973-2987.

Robinson, N. J., M. J. Williams, C. L. Stevens, P. J. Langhorne, and T. G. Haskell (2014), Evolution of a supercooled Ice Shelf Water plume with an actively growing subice platelet matrix, *Journal of Geophysical Research: Oceans*, *119*(6), 3425-3446.

Robuchon, G., and F. Nimmo (2011), Thermal evolution of Pluto and implications for surface tectonics and a subsurface ocean, *Icarus*, *216*(2), 426-439.

Ross, M., and G. Schubert (1987), Tidal heating in an internal ocean model of Europa, *Nature*, *325*(6100), 133-134.

Rubinšteĭn, L. (2000), *The stefan problem*, American Mathematical Soc.

Rudolph, M. L., and M. Manga (2009), Fracture penetration in planetary ice shells, *Icarus*, *199*(2), 536-541.

Ruesch, O., T. Platz, P. Schenk, L. McFadden, J. Castillo-Rogez, L. Quick, S. Byrne, F. Preusker, D. O'Brien, and N. Schmedemann (2016), Cryovolcanism on Ceres, *Science*, *353*(6303), aaf4286.

Russell, C., C. Raymond, E. Ammannito, D. Buczkowski, M. De Sanctis, H. Hiesinger, R. Jaumann, A. Konopliv, H. McSween, and A. Nathues (2016), Dawn arrives at Ceres: Exploration of a small, volatile-rich world, *Science*, *353*(6303), 1008-1010.

Russell, M. J., A. E. Murray, and K. P. Hand (2017), The possible emergence of life and differentiation of a shallow biosphere on irradiated icy worlds: the example of Europa, *Astrobiology*, *17*(12), 1265-1273.

Rysgaard, S., R. N. Glud, M. Sejr, J. Bendtsen, and P. Christensen (2007), Inorganic carbon transport during sea ice growth and decay: A carbon pump in polar seas, *Journal of Geophysical Research: Oceans*, *112*(C3).

Sarmiento, J. á., N. Gruber, M. Brzezinski, and J. Dunne (2004), High-latitude controls of thermocline nutrients and low latitude biological productivity, *Nature*, *427*(6969), 56.

Schenk, P., H. Sizemore, B. Schmidt, J. Castillo-Rogez, M. De Sanctis, T. Bowling, J. Scully, D. Buczkowski, L. Quick, and F. Preusker (2019), The central pit and dome at Cerealia Facula bright deposit and floor deposits in Occator crater, Ceres: Morphology, comparisons and formation, *Icarus*, *320*, 159-187.

Schenk, P. M., and W. B. McKinnon (2009), One-hundred-km-scale basins on Enceladus: Evidence for an active ice shell, *Geophysical Research Letters*, *36*(16).

Schmidt, B., D. Blankenship, G. Patterson, and P. Schenk (2011a), Active formation of ‘chaos terrain’over shallow subsurface water on Europa, *Nature*, *479*(7374), 502.

Schmidt, B. E., D. D. Blankenship, G. W. Patterson, and P. M. Schenk (2011b), Active formation of 'chaos terrain' over shallow subsurface water on Europa, *Nature*, *479*(7374), 502-505, doi:10.1038/nature10608.

Schmidt, B. E., J. Buffo, and A. Main Campus (2017a), Biomarker Production and Preservation on Europa, paper presented at European Planetary Science Congress.

Schmidt, B. E., K. H. Hughson, H. T. Chilton, J. E. Scully, T. Platz, A. Nathues, H. Sizemore, M. T. Bland, S. Byrne, and S. Marchi (2017b), Geomorphological evidence for ground ice on dwarf planet Ceres, *Nature Geoscience*, *10*(5), 338.

Schroeder, D. M., A. Romero-Wolf, L. Carrer, C. Grima, B. A. Campbell, W. Kofman, L. Bruzzone, and D. D. Blankenship (2016), Assessing the potential for passive radio sounding of Europa and Ganymede with RIME and REASON, *Planetary and Space Science*, *134*, 52-60.

Schubert, G., J. Anderson, T. Spohn, and W. McKinnon (2004), Interior composition, structure and dynamics of the Galilean satellites, *Jupiter: The planet, satellites and magnetosphere*, *1*, 281-306.

Schwerdtfecer, P. (1963), The thermal properties of sea ice, *Journal of Glaciology*, *4*(36), 789-807.

Scully, J. E., D. L. Buczkowski, C. A. Raymond, T. Bowling, D. A. Williams, A. Neesemann, P. M. Schenk, J. C. Castillo-Rogez, and C. T. Russell (2019), Ceres’ Occator crater and its faculae explored through geologic mapping, *Icarus*, *320*, 7-23.

Shimada, K., T. Kamoshida, M. Itoh, S. Nishino, E. Carmack, F. McLaughlin, S. Zimmermann, and A. Proshutinsky (2006), Pacific Ocean inflow: Influence on catastrophic reduction of sea ice cover in the Arctic Ocean, *Geophysical Research Letters*, *33*(8).

Sinha, N. K. (1977), Technique for studying structure of sea ice, *Journal of Glaciology*, *18*(79), 315-324.
Smedsrud, L. H., and A. Jenkins (2004), Frazil ice formation in an ice shelf water plume, *Journal of Geophysical Research: Oceans*, *109*(C3).
Smith, I. J., P. J. Langhorne, T. G. Haskell, H. J. Trodahl, R. Frew, and M. R. Vennell (2001), Platelet ice and the land-fast sea ice of McMurdo Sound, Antarctica, *Annals of Glaciology*, *33*, 21-27.
Soderlund, K. (2019), Ocean dynamics of outer solar system satellites, *arXiv preprint arXiv:1901.04093*.
Soderlund, K., B. Schmidt, J. Wicht, and D. Blankenship (2014), Ocean-driven heating of Europa's icy shell at low latitudes, *Nature Geoscience*, *7*(1), 16.
Sohl, F., H. Hussmann, B. Schwentker, T. Spohn, and R. Lorenz (2003), Interior structure models and tidal Love numbers of Titan, *Journal of Geophysical Research: Planets*, *108*(E12).
Sotin, C., and D. Prieur (2007), Jupiter's moon Europa: geology and habitability, *Complete course in astrobiology*, 253-271.
Sotin, C., and G. Tobie (2004), Internal structure and dynamics of the large icy satellites, *Comptes Rendus Physique*, *5*(7), 769-780.
Sparks, W., K. Hand, M. McGrath, E. Bergeron, M. Cracraft, and S. Deustua (2016), Probing for evidence of plumes on Europa with HST/STIS, *The Astrophysical Journal*, *829*(2), 121.
Sparks, W. B., B. E. Schmidt, M. A. McGrath, K. P. Hand, J. Spencer, M. Cracraft, and S. E. Deustua (2017), Active cryovolcanism on Europa?, *The Astrophysical Journal Letters*, *839*(2), L18.
Spaun, N., J. Head, G. Collins, L. Prockter, and R. Pappalardo (1998), Conamara Chaos region, Europa: Reconstruction of mobile polygonal ice blocks, *Geophysical research letters*, *25*(23), 4277-4280.
Spencer, J. R. (1987), THE SURFACES OF EUROPA, GANYMEDE, AND CALLISTO: AN INVESTIGATION USING VOYAGER IRIS THERMAL INFRARED SPECTRA (JUPITER).
Squyres, S., R. Arvidson, J. F. Bell, J. Brückner, N. Cabrol, W. Calvin, M. Carr, P. Christensen, B. Clark, and L. Crumpler (2004), The Opportunity Rover's Athena science investigation at Meridiani Planum, Mars, *science*, *306*(5702), 1698-1703.
Squyres, S. W., R. T. Reynolds, P. M. Cassen, and S. J. Peale (1983), Liquid water and active resurfacing on Europa, *Nature*, *301*(5897), 225-226.
Steefel, C. I., D. J. DePaolo, and P. C. Lichtner (2005), Reactive transport modeling: An essential tool and a new research approach for the Earth sciences, *Earth and Planetary Science Letters*, *240*(3-4), 539-558.
Stroeve, J., M. M. Holland, W. Meier, T. Scambos, and M. Serreze (2007), Arctic sea ice decline: Faster than forecast, *Geophysical research letters*, *34*(9).
Svensson, U., and A. Omstedt (1994), Simulation of supercooling and size distribution in frazil ice dynamics, *Cold regions science and technology*, *22*(3), 221-233.
Tait, M., and F. Franks (1971), Water in biological systems, *Nature*, *230*(5289), 91.
Tedesco, L., and M. Vichi (2014), Sea ice biogeochemistry: A guide for modellers, *PloS one*, *9*(2), e89217.
Thomas, D. N. (2017), *Sea ice*, John Wiley & Sons.

Thomas, D. N., and G. S. Dieckmann (2003), Biogeochemistry of Antarctic sea ice, in *Oceanography and Marine Biology, An Annual Review, Volume 40*, edited, pp. 151-156, CRC Press.

Thomas, D. N., and G. S. Dieckmann (2008), *Sea ice: an introduction to its physics, chemistry, biology and geology*, John Wiley & Sons.

Thomas, P., R. Tajeddine, M. Tiscareno, J. Burns, J. Joseph, T. Loredo, P. Helfenstein, and C. Porco (2016), Enceladus's measured physical libration requires a global subsurface ocean, *Icarus*, *264*, 37-47.

Thomson, R. E., and J. R. Delaney (2001), Evidence for a weakly stratified Europan ocean sustained by seafloor heat flux, *Journal of Geophysical Research: Planets*, *106*(E6), 12355-12365.

Tobie, G., G. Choblet, and C. Sotin (2003), Tidally heated convection: Constraints on Europa's ice shell thickness, *Journal of Geophysical Research: Planets*, *108*(E11).

Toner, J., D. Catling, and B. Light (2014), The formation of supercooled brines, viscous liquids, and low-temperature perchlorate glasses in aqueous solutions relevant to Mars, *Icarus*, *233*, 36-47.

Travis, B., J. Palguta, and G. Schubert (2012), A whole-moon thermal history model of Europa: Impact of hydrothermal circulation and salt transport, *Icarus*, *218*(2), 1006-1019.

Turcotte, D., and G. Schubert (2014), *Geodynamics*, Cambridge University Press.

Turner, A. K., and E. C. Hunke (2015), Impacts of a mushy-layer thermodynamic approach in global sea-ice simulations using the CICE sea-ice model, *Journal of Geophysical Research: Oceans*, *120*(2), 1253-1275.

Turner, A. K., E. C. Hunke, and C. M. Bitz (2013), Two modes of sea-ice gravity drainage: A parameterization for large-scale modeling, *Journal of Geophysical Research: Oceans*, *118*(5), 2279-2294.

Van der Veen, C. (1998a), Fracture mechanics approach to penetration of bottom crevasses on glaciers, *Cold Regions Science and Technology*, *27*(3), 213-223.

Van der Veen, C. (1998b), Fracture mechanics approach to penetration of surface crevasses on glaciers, *Cold Regions Science and Technology*, *27*(1), 31-47.

Vance, S., M. Bouffard, M. Choukroun, and C. Sotin (2014), Ganymede′ s internal structure including thermodynamics of magnesium sulfate oceans in contact with ice, *Planetary and Space Science*, *96*, 62-70.

Vance, S., K. Hand, and R. Pappalardo (2016), Geophysical controls of chemical disequilibria in Europa, *Geophysical Research Letters*, *43*(10), 4871-4879.

Vance, S., J. Harnmeijer, J. Kimura, H. Hussmann, B. DeMartin, and J. M. Brown (2007), Hydrothermal systems in small ocean planets, *Astrobiology*, *7*(6), 987-1005.

Vance, S. D., L. M. Barge, S. S. Cardoso, and J. H. Cartwright (2019), Self-Assembling Ice Membranes on Europa: Brinicle Properties, Field Examples, and Possible Energetic Systems in Icy Ocean Worlds, *arXiv preprint arXiv:1903.01584*.

Vance, S. D., M. P. Panning, S. Stähler, F. Cammarano, B. G. Bills, G. Tobie, S. Kamata, S. Kedar, C. Sotin, and W. T. Pike (2018), Geophysical investigations of habitability in ice-covered ocean worlds, *Journal of Geophysical Research: Planets*, *123*(1), 180-205.

Vancoppenolle, M., C. M. Bitz, and T. Fichefet (2007), Summer landfast sea ice desalination at Point Barrow, Alaska: Modeling and observations, *Journal of Geophysical Research: Oceans*, *112*(C4).

Vancoppenolle, M., K. M. Meiners, C. Michel, L. Bopp, F. Brabant, G. Carnat, B. Delille, D. Lannuzel, G. Madec, and S. Moreau (2013), Role of sea ice in global biogeochemical cycles: emerging views and challenges, *Quaternary science reviews*, *79*, 207-230.

Vancoppenolle, M., and L. Tedesco (2015), Numerical modelling of sea ice biogeochemistry, *Sea Ice*.

Villanueva, G., M. Mumma, R. Novak, H. Käufl, P. Hartogh, T. Encrenaz, A. Tokunaga, A. Khayat, and M. Smith (2015), Strong water isotopic anomalies in the martian atmosphere: Probing current and ancient reservoirs, *Science*, *348*(6231), 218-221.

Waite, J. H., M. R. Combi, W.-H. Ip, T. E. Cravens, R. L. McNutt, W. Kasprzak, R. Yelle, J. Luhmann, H. Niemann, and D. Gell (2006), Cassini ion and neutral mass spectrometer: Enceladus plume composition and structure, *science*, *311*(5766), 1419-1422.

Waite, J. H., C. R. Glein, R. S. Perryman, B. D. Teolis, B. A. Magee, G. Miller, J. Grimes, M. E. Perry, K. E. Miller, and A. Bouquet (2017), Cassini finds molecular hydrogen in the Enceladus plume: evidence for hydrothermal processes, *Science*, *356*(6334), 155-159.

Walker, C., and B. Schmidt (2015), Ice collapse over trapped water bodies on Enceladus and Europa, *Geophysical Research Letters*, *42*(3), 712-719.

Walker, C. C., J. N. Bassis, and B. E. Schmidt ((in revision)), Propagation of vertical fractures through planetary ice shells and the role of basal cracks at the ice-ocean interface, *Earth and Planetary Science Letters*.

Weeks, W. (2010), *On sea ice*, University of Alaska Press.

Weeks, W., and G. Lofgren (1967), The effective solute distribution coefficient during the freezing of NaCl solutions, *Physics of Snow and Ice: proceedings= 雪氷の物理学 : 論文集*, *1*(1), 579-597.

Weeks, W. F., and S. F. Ackley (1986), The growth, structure, and properties of sea ice, in *The geophysics of sea ice*, edited, pp. 9-164, Springer.

Wells, A., J. Wettlaufer, and S. Orszag (2010), Maximal potential energy transport: A variational principle for solidification problems, *Physical review letters*, *105*(25), 254502.

Wells, A., J. Wettlaufer, and S. Orszag (2011), Brine fluxes from growing sea ice, *Geophysical Research Letters*, *38*(4).

Wells, A. J., J. R. Hitchen, and J. R. Parkinson (2019), Mushy-layer growth and convection, with application to sea ice, *Philosophical Transactions of the Royal Society A*, *377*(2146), 20180165.

Wettlaufer, J., M. G. Worster, and H. E. Huppert (1997a), Natural convection during solidification of an alloy from above with application to the evolution of sea ice, *Journal of fluid mechanics*, *344*, 291-316.

Wettlaufer, J., M. G. Worster, and H. E. Huppert (1997b), The phase evolution of young sea ice, *Geophysical research letters*, *24*(10), 1251-1254.

Wettlaufer, J. S. (2010), Sea ice and astrobiology, in *Sea ice*, edited.

Winton, M. (2008), Sea ice-albedo feedback and nonlinear Arctic climate change, *Arctic Sea ice decline: observations, projections, mechanisms, and implications, Geophys. Monogr. Ser*, *180*, 111-131.

Wolfenbarger, N., D. Blankenship, K. Soderlund, D. Young, and C. Grima (2018), Leveraging Terrestrial Marine Ice Cores to Constrain the Composition of Ice on Europa, *LPI Contributions*, *2100*.

Wongpan, P., P. J. Langhorne, D. E. Dempsey, L. Hahn-Woernle, and Z. Sun (2015), Simulation of the crystal growth of platelet sea ice with diffusive heat and mass transfer, *Annals of Glaciology*, *56*(69), 127-136.

Worster, M. (1992), The dynamics of mushy layers, in *Interactive dynamics of convection and solidification*, edited, pp. 113-138, Springer.

Worster, M. G. (1991), Natural convection in a mushy layer, *Journal of fluid mechanics*, *224*, 335-359.

Worster, M. G. (1997), Convection in mushy layers, *Annual Review of Fluid Mechanics*, *29*(1), 91-122.

Worster, M. G., H. E. Huppert, and R. S. J. Sparks (1990), Convection and crystallization in magma cooled from above, *Earth and Planetary Science Letters*, *101*(1), 78-89.

Worster, M. G., and D. W. Rees Jones (2015), Sea-ice thermodynamics and brine drainage, *Philosophical Transactions of the Royal Society A: Mathematical, Physical and Engineering Sciences*, *373*(2045), 20140166.

Zhong, S., A. McNamara, E. Tan, L. Moresi, and M. Gurnis (2008), A benchmark study on mantle convection in a 3-D spherical shell using CitcomS, *Geochemistry, Geophysics, Geosystems*, *9*(10).

Zolotov, M. Y. (2007), An oceanic composition on early and today's Enceladus, *Geophysical Research Letters*, *34*(23).

Zolotov, M. Y., and J. Kargel (2009), *On the chemical composition of Europa's icy shell, ocean, and underlying rocks*, University of Arizona Press Tucson, AZ.

Zolotov, M. Y., and E. L. Shock (2001), Composition and stability of salts on the surface of Europa and their oceanic origin, *Journal of Geophysical Research: Planets*, *106*(E12), 32815-32827.

Zotikov, I. A., V. S. Zagorodnov, and J. V. Raikovsky (1980), Core drilling through the Ross Ice Shelf (Antarctica) confirmed basal freezing, *Science*, *207*(4438), 1463-1465.

Zwally, H. J., J. Comiso, and A. Gordon (1985), Antarctic offshore leads and polynyas and oceanographic effects, *Oceanology of the Antarctic continental shelf*, *43*, 203-226.